UNIVERSITY OF SOUTHAMPTON

HYDRODYNAMICS AND SEDIMENT TRANSPORT ON A MACRO-TIDAL, MIXED (SAND AND SHINGLE) BEACH

Travis Mason, BSc

Submitted in fulfilment of the requirements for the degree of
Doctor of Philosophy

DEPARTMENT OF OCEANOGRAPHY
FACULTY OF SCIENCE

September 1997

UNIVERSITY OF SOUTHAMPTON

ABSTRACT

FACULTY OF SCIENCE
OCEANOGRAPHY

Doctor of Philosophy

HYDRODYNAMICS AND SEDIMENT TRANSPORT ON A MACRO-TIDAL, MIXED (SAND AND SHINGLE) BEACH

Travis Mason

A field investigation of a macro-tidal, ridge and runnel beach at Morfa Dyffryn, North Wales, is described, which examines the distinctive characteristics of a mixed (sand and shingle) beach.

The moments of the velocity field and wave reflection at Morfa Dyffryn are compared with those from a similarly macro-tidal, sandy beach at Nieuwpoort-aan-Zee, Belgium. Strong, wind-enhanced, mean longshore currents persist into shallow water. Results of the velocity moment analysis indicate that the mean flows dominate the sediment transport patterns, particularly in shallow water, early in the flood and late in the ebb phases of the tide. The mean longshore current can be responsible for mobilising (in addition to transporting) sediment, when in excess of 0.3 m s^{-1}. Mean fluxes dominate the measured suspended sediment transport patterns, in common with other macro-tidal beaches. Suspended sediment fluxes are generally at their highest in shallow water, although extremely high fluxes were observed just after High Water. These patterns are attributed to increased re-suspension due to wind/resolved mean current interaction. Therefore, high transport rates can occur, even in the absence of storm conditions. The relict sand/shingle ridge has little influence on reflection of wind wave energy. However, reflection of swell waves is enhanced, once the swash zone inundates the sand/shingle berm, due to its steeper gradient.

Fluctuations in the beach water table due to tidal inundation are compared to groundwater behaviour on a sandy beach at Canford Cliffs, Dorset. The GRIST I model (which was derived for sandy beaches) predicts well both the location and translation of a seepage face across the sand/shingle profile. The sand fraction of the sediment determines the response of the water table. Laboratory hydraulic conductivity tests undertaken on sand/shingle mixtures indicate that the shingle content of a beach should be in excess of 80% to 90%, before increased dissipation of energy through percolation can occur.

The main significance of the sand/shingle mixture, in relation to the morphodynamic response of the ridge, is through its ability to maintain a steeper slope than would be supported by a sandy beach. The change in gradient across the mixed beach profile has more influence on the hydrodynamics, than does the sediment composition.

List of Figures

List of Tables

List of Plates

List of Symbols

c	Suspended sediment concentration (ML^{-3})
g	Acceleration due to gravity (LT^{-2})
h	Mean water depth (L)
i	Immersed weight sediment transport rate (FT^{-1}) *or* hydraulic gradient (dimensionless)
k	Wave number (L^{-1}) *or* intrinsic permeability (L^{-2}) *or* coefficient
n	Porosity (dimensionless)
q	Flux through a saturated sediment (M^3L^{-1})
s	Specific yield (dimensionless)
t	Time (T)
u, v	Cross-shore, longshore oscillatory velocity (LT^{-1})
$\bar{u}$,$\bar{v}$	Mean cross-shore, mean longshore current (LT^{-1})
u_b	Significant orbital velocity (LT^{-1})
u_m	Maximum orbital velocity (LT^{-1})
x	Cross-shore distance (L) or vector
y	Longshore distance (L) or vector
z	Height above sediment surface or datum (L)
A	Wave asymmetry *or* area (L^2)
D	Grain size diameter (L) *or* aquifer depth (L)
E	Spectral energy density (various)
H	Wave height (L), Hydraulic head (L) *or* Hilbert transform of a time-series
K	Hydraulic conductivity (LT^{-1})
L	Wave length (L)
M	Number of segments
N	Number of observations
Q	Volume of discharge (M^3)
S	Spectral estimate *or* skewness term
T	Period (T)
V	Voltage
W	Fall velocity of sediment (LT^{-1})
X	An observation
Z	Elevation of the water table (L)
df	Bandwidth of spectral frequency (T^{-1})
C_f	Drag coefficient (dimensionless)
Q_p	Peakedness parameter (dimensionless)
R_t	Correction factor for influence of temperature on viscosity of water (dimensionless)
R_T	Tidal range (L)
$\vec{U}_t$	Total instantaneous cross-shore velocity vector (LT^{-1})
V_{ep}	Exit point critical velocity (LT^{-1})

α	Angle of oscillatory current *or* a constant
β	Bed slope
ϵ	Spectral width parameter (dimensionless)
ϵ_b, ϵ_s	Bedload, suspended load efficiency factors (dimensionless)
η	Sea surface elevation (L)
μ	Dynamic coefficient of viscosity
ρ	Fluid density (ML^{-3})
θ	Angle of steady current
ϕ	Angle of internal friction of sediment *or* total potential ($ML^{-1}T^{-2}$) *or* power spectra
Ψ	Velocity moment
Σ	Irribarren Number *or* seepage face parameter

Acknowledgements

I should like to express my thanks to my supervisors; Professor Michael Collins for his support and encouragement (and, not least, for taking me on in the first place); and Dr George Voulgaris of Wood's Hole Oceanographic Institution for his knowledge, enthusiasm and guidance, even at a distance of 5000 miles. I am grateful also to my "honorary" supervisor, Dr Andrew Baird, Department of Geography, University of Sheffield, for his advice about beach groundwater.

It is a pleasure to acknowledge, with many thanks:
Mike Wilkin (now at Oregon Graduate Institute), whose contribution was considerable, whatever I have learnt of fieldwork and instrumentation being almost entirely due to him; John Cross, for such generous access to his extensive knowledge of the Hampshire and Dorset coastline and for transforming my rudimentary surveying into something approaching a useful skill; John Davis, for assistance with fieldwork and instrumentation together with his rapid response to panic phone calls from various field sites; Kate Davis, for preparation of several diagrams; Dr Molland and colleagues, Department of Ship Science, for use of their Towing Tank; Professor Tanton and Stephen Wake, Institute of Irrigation Studies, Department of Civil & Environmental Engineering, for use of the geotechnical laboratory and equipment.

The Countryside Council for Wales, Snowdonia National Park Authority and Meirionnydd District Council, to whom I am greatly indebted, not only for permission to carry out research at Morfa Dyffryn, but also for the encouragement, enthusiasm and practical assistance of Dr Rod Jones and Jonathon Neale (CCW), Islwyn Pritchard-Jones and Gareth "Mutley" Pierce-Jones (SNPA) and Huw Davies (MDC); Ian Lisk and staff at the Meteorological Office, Aberporth, for information cheerfully supplied, at all hours of the day and night.

David Simmonds and Karen Stapleton of the Institute of Marine Studies, University of Plymouth and their erstwhile colleagues Jonathan Miles, Paul Fisher and Pauline Framingham, with whom I experienced my introduction to large-scale fieldwork and surveying in the snow. To Dave Simmonds, in particular, I owe untold thanks for his generous advice and patience (and indeed his computer programmes). His fortuitous move to the School of Civil & Structural Engineering led me to valuable new sources of collaboration, discussion and idle chatter, notably from Erik Van Wellen (with whom I shared my introduction to surveying in driving rain, at night, in a Force 9) and Suzana Ilic. I thank them all greatly for their pleasant company and sense of humour, particularly whilst on fieldwork.

Diane Horn of the Department of Geography, Birkbeck College, University of London, for the loan of equipment, introduction to the field of beach groundwater and, more importantly, without whom I might well have ended up a periglacial geomorphologist; Keith Powell and Tom Coates at HR, for access to their library and an enlightening conversation about the morphodynamic continuum, respectively; Andrew Bradbury of

New Forest District Council, for advice and his engineering perspective; Nigel Pontee (now of ABP Research) for being interested in mixed beaches; Kevin Mawdesley, who is managing an RGS/ODA research project in Nepal, for lots of things but primarily for feigning some interest in matters coastal these past four years.

My colleagues in Sediment Dynamics, both current and former; in particular, Steve Wallbridge, Les Whitcombe and Mark Lee, who have given freely and generously of both their time and expertise, and latterly, Craig Brand and Magali Lecouturier. I count myself fortunate to have spent the past four years in such friendly and lively company.

My special thanks also to my mother and husband for their support (any semblance of domesticity in the household during the past year being entirely to them) and particularly to my two sons, David and John, who have endured their mother's distraction with fortitude.

Finally, I should like to acknowledge Rosemary Lovelock. Her infectious optimism in life and her determined cheerfulness when facing her death continue to inspire me; I hope she would have been proud of me, as I was indeed proud to call her a friend.

CHAPTER 1: INTRODUCTION

The vast majority of research into coastal hydrodynamics and the resultant sediment transport has been concerned with sandy, micro-tidal beaches, with some recent interest in macro-tidal and ridge and runnel beaches. Research into processes on shingle beaches lags considerably behind that for sandy beaches (McKay & Terich, 1992). Meanwhile, beaches which contain a mixture of sand and shingle have aroused only sporadic interest; this is despite their being morphologically distinct from, and more complex than either sand or shingle beaches (Kirk, 1980). Although comparatively rare on a worldwide basis (Zenkovich, 1967), mixed beaches occur commonly around the shores of Great Britain and Eire. Similarly, they are found in other regions where the effects of glaciation have provided an abundant source of sands and gravels, for subsequent re-working by Holocene rising sea levels; these include Canada (*e.g.* Carter *et al.*, 1990), New Zealand (*e.g.* Kirk, 1969), Greenland (Nielsen, 1991), the Arctic Sea coast (Finkelstein, 1982; Hill, 1990) and Tierra del Fuego (Bujalesky & González-Bonorino, 1991).

The terminology used for beaches containing sediment sizes larger than sand is somewhat ambiguous (Carter & Orford, 1993). Despite their suggestion that the term *shingle* is " ... rarely heard outside England ... and is ... arcane and should be avoided", it is a term recognised instantly and used widely in Great Britain, at least, by engineers and non-engineers alike. It also has an all-inclusive size implication, in contrast to the alternatives referred to by Carter & Orford (*op. cit.*) *e.g.* pebble, gravel, cobble and coarse-grained. Accordingly, throughout this research programme, the term *shingle* will be used to represent beach sediment with a mean diameter greater than 2 mm (hence, including granules) whatever its geology or shape; this is in preference to the more logical perhaps, but distinctly prosaic, *coarse clastic*. However, when referring to previous research, the term used by the appropriate author will be used.

Mixed beaches fall into one of two categories. Firstly, that inferred from McLean & Kirk (1969) of a generally homogenous mixture of shingle and sand, with varying proportions of each, both cross-shore and longshore. The low water sandy region is exposed only during spring tides, if at all. Secondly, beaches with a broadly shingle ridge towards the high tide region, with a sandy inter-tidal terrace *i.e.* a sand beach with fringing shingle, which is referred to hereafter as a composite beach. Both types of beach may have a noticeable break of slope between the mixed/shingle and sand sections; both

are found commonly in the UK. Hayling Island (Hampshire) and Shoreham-by-Sea (West Sussex) are examples of the homogeneous type; Morfa Dyffryn (Meirionnydd) is an example of a composite beach (Plates 1.1 and 1.2). These examples illustrate another interesting feature of mixed beaches in macro-tidal environments, namely that the low-tide beach is almost invariably of a dissipative nature, with an abrupt switch to reflective conditions at mid- or high tide (Wright & Short 1984).

Interest in the sediment characteristics and processes of development of mixed beaches *per se* originates almost entirely from work undertaken in New Zealand by McLean, Kirk and co-workers in the late 1960's and 1970's. Concurrent work was being carried out in the UK, but under the auspices of gravel beaches, notably by Bluck (1967) and Orford (1975). The important recognition by the latter authors, of the differential transport of varying particle shapes (both through and across the profile) was not translated into recognition, at the time, that whilst a sand and gravel barrier may have "... affinities with its pure gravel and pure sand counterparts ... it is this very mix which imbues the structure with its own idiosyncracies" (Orford & Carter 1982).

The absence of research into coarse-grained beaches is related to a number of factors; one of these may be that few such systems exist in the USA. Undoubtedly, a major limitation to such research is the difficulty in using expensive and comparatively fragile equipment in the harsh conditions which actually mobilise shingle. Shingle beaches, are known to be an efficient form of natural sea defence, capable of dissipating over 90% of incident wave energy (Powell, 1990; Diserens & Coates, 1993). In addition, swash zone processes dominate on shingle beaches yet, even on sandy beaches, such processes and associated sediment transport are poorly understood in comparison with the surf zone. Once again, this is due mainly to the lack of suitably rugged, high-frequency electronic instruments which can measure the shallow, reversing, high velocity flows which are present in the swash. If such instruments are available, it is understandable that they would seldom be risked during conditions when shingle is mobile; these are the very conditions which need investigating. Consequently, research into shingle and mixed beaches has tended to concentrate upon the sediment and profile changes, inferring evolutionary and dynamic behaviour directly from sediment characteristics and sorting processes (*e.g.* McLean & Kirk, 1969; Caldwell & Williams, 1985; Hill, 1990; Bujalesky & Gonzáles-Bonorino, 1991 and Carter & Orford, 1991).

Plate 1.1 Hayling Island

Plate 1.2 Morfa Dyffryn

Recent interest by engineers in the coastal defence properties of shingle beaches has revived and spurred both laboratory-based and field research into the response of shingle beach profiles under monochromatic and random wave attack (*e.g.* Powell, 1986, 1988; Quick, 1991; Bradbury & Powell, 1992; Powell *et al.*, 1992 and Bradbury, 1995). It is to be hoped that the complementary laboratory study undertaken by Quick & Dyksterhuis (1994) will herald a similar resurgence of interest in mixed beaches, since there has been little progress since an earlier review (Kirk, 1980).

One of the most important reasons why shingle beaches are effective dissipators of wave energy is that their high hydraulic conductivity permits rapid and, sometimes, turbulent infiltration into the bed. Accordingly, the hydraulic conductivity of the beach sediment and fluctuations of the water table are important controls on the capacity of the beach to absorb and store infiltrating water. Beach groundwater and its rôle in sediment transport has been largely neglected since the pioneering work, some 50 years ago, of Grant (1946, 1948) and Emery & Foster (1948). However, two unrelated factors have led to a recent revival of interest. The first factor concerns the introduction of large-scale beach pumping schemes, as a method of "soft" engineering. Grant's earlier observations (*op. cit.*) were the foundation for these newly-developed shoreline protection schemes in Denmark (*e.g.* Hansen, 1986; Vesterby & Parks, 1988), the USA (Parks, 1989; Terchunian, 1990) and most recently, at Restormel in Cornwall. In such systems, the level of beach groundwater is retained artificially low by sub-surface draining. The second factor is the increasing concentration of interest into sediment transport processes within the inner surf and swash zones of the beach, combined with the realisation that the tidally-varying location of a seepage zone can influence sediment transport in the swash zone.

The position of the water table is also an important factor to be taken into consideration in the design of foundations of buildings and structures near the coastline, to assess the dangers of saltwater intrusion into shallow coastal aquifers, and for coastal agricultural land in general (Nielsen, 1990; Turner, 1995*a*). On a smaller scale, the water table controls interstitial oxygenation within the beach sediment, with subsequent influence on beach microfauna (McLachlan, 1989). There are also wider implications. For example, sewage was discovered discharging into a lagoon behind a sand barrier, rather than out to sea, due to the unappreciated effects of groundwater flow across the barrier (Nielsen & Kang, 1994).

Beach groundwater research has been confined, generally, to sand beaches. There has been only a single field study undertaken into groundwater fluctuations on a shingle beach/barrier system (Nicholls, 1985); however, the link between sediment mixture and permeability is not only of academic interest. A number of recent shingle beach replenishment schemes have utilised material dredged from offshore, which inevitably contains a proportion of sands and fines. The effects of the presence of such material may be unexpected such as, for example, the notably higher *in-situ* bulk density of the beach (replenishment) material and cliffing at Whitstable and Hayling Island (McFarland *et al.*, 1996).

1.1 The Present Study

The research programme examines the hydrodynamic regime across a mixed beach, from the deepwater sand region, through the surf and swash zones, by infiltration into the beach sediment, as storage as groundwater and subsequent exfiltration during an ebbing tide. Interaction between the sand and shingle sections of the beach is examined. Similarly, the effect of the presence of interstitial sand (within the shingle) is investigated in relation to the permeability/porosity of the sediment and its ability to change the transport behaviour compared to that on a sandy beach. By this means, it will be possible to establish if a composite mixed beach responds more like a sand than a shingle beach, or whether its behaviour differs substantially from either type of beach.

The implications of understanding the various interacting processes (at various temporal and spatial scales) for the subsequent modelling of sediment transport on mixed beaches, are important. For example, if each part of a composite beach behaves in essentially the same manner as its sand or shingle counterpart, with little interaction between them, then the relevant transport models can be linked without substantial modification. It is by no means impossible however, that even net sediment transport directions may vary over different sections of the beach.

There are three main areas of investigation, as outlined below:

(a) Cross-shore and longshore wave and current modifications across the macro-tidal ridge and runnel profile. This component will include an examination of the temporally-varying moments of the velocity field, combined with a comparison

with data obtained from a macro-tidal sand beach with an extensive ridge and runnel system in Nieuwpoort, Belgium (using data from the MAST II C-STAB project [O'Connor, 1996]). Such inter-comparison will assist in examining the more general applicability of the velocity moments methods, for the prediction of sediment transport.

(b) Wave interaction with the mixed beach profile, which involves: (i) decomposition of the current and wave data into incoming and reflected components; and (ii) investigating changes brought about by the break of slope between the sand and shingle sections of the beach. The consequences of the presence of a sand/shingle ridge, for suspended sediment transport, will be discussed.

(c) Fluctuations in the water table across the profile, in response to tidal inundation, and a comparison with modelled water table elevation, in order to assess the importance of varying sediment composition on seepage face development.

The structure of the thesis is here summarised. Previous research into mixed beaches together with the particular aspects in which the response of such beaches will be compared to a sandy beach (*i.e.* velocity moments, wave reflection and beach groundwater) are reviewed in Chapter 2. Chapters 3 and 4 incorporate details on the instrumentation, the location of the field experiments and the methods used for data analysis. The results from the field experiment, together with some discussion of the results, are included in Chapters 5 to 9 for: tides, waves and currents; velocity moments; wave reflection; sediment transport and beach groundwater respectively. Finally, in Chapter 10, the results are integrated, to assess how the particular characteristics of a mixed beach affect their morphodynamic behaviour. Similarly, some possible consequences for engineering schemes for beach replenishment with mixed shingle/sand sediments are considered.

CHAPTER 2: LITERATURE REVIEW

The first Section of this Chapter consists of a review of previous research into mixed beaches, including studies of their groundwater. The review is concerned then with two indicators of the hydrodynamic behaviour of a mixed beach: the velocity moments of the current field; and wave reflection characteristics. Finally, the general literature on beach groundwater is summarised. Within each Section, the relevant theories are considered followed, where relevant, by a review of field and laboratory experiments.

2.1 Mixed Beaches

The published literature on mixed beaches is somewhat limited. A proportion of research regarded (by various authors) as being concerned with shingle beaches, however, contains evidence to suggest that the beaches were of a type which could be considered mixed. However, any distinctive differences between a shingle beach and mixed beach were seldom acknowledged. Included in this Section is a brief review of relevant papers relating to the study of gravel and sand-and-gravel barrier beaches, particularly in Ireland and Canada.

2.1.1 Sediments

The plan shape, profiles and sediments of mixed beaches in New Zealand were characterised in a series of papers by McLean (1967, 1970), Kirk (1969, 1975*a*), McLean & Kirk (1969). Two theories which sought to explain the link between sediment sorting and grain size were examined by McLean & Kirk (1969): the "hydraulics theory", that sorting patterns result from a combination of bed roughness, settling velocity and thresholds for sediment transport (Inman, 1949); and the theory of Folk & Ward (1957), who considered that sorting patterns were the result of the mixing of two end members of the sediment population *i.e.* sediment source is the primary influence, with hydraulic action only a secondary factor. Beaches were found with similar sorting patterns and similar form yet with different bi-modal grain size distributions; this led to the conclusion that hydraulic factors were responsible for the variability of size/sorting patterns and were secondary, therefore, to the "source area effect" (McLean & Kirk, *op. cit.*; Kirk, 1970).

The first detailed study undertaken in the UK, of the sedimentary characteristics of a mixed beach, was Bluck's (1967) examination of particle size and shape on 6 South Wales gravel beaches. However, the distinctive nature of the beach was not recognised at the time. Differential transport of particles of different shapes, both across and through the beach profile was identified; hence, the differential transport of sand and gravel is inherent. Infiltrating backwash transports preferentially finer spherical grains to seaward, through the gravel framework, this acts as a form of sieve although, presumably, infiltrating swash creates the same mechanism but to a lesser extent.

A notable feature of this early research was the "sand run" (Bluck, *op. cit.*) which separated the landward zone of imbricated disc-shaped particles from the seaward large cobble frame (infilled with spherical and rod shaped grains). Particles moved across the sand rapidly; this is a process referred to as overpassing and observed in other mixed sediment environments (*e.g.* Ferguson *et al.*, 1989; Carter *et al.*, 1990; Isla 1993).

Short-term changes in bi-modal sediment distribution across an estuarine beach, with a covering of small pebbles, were reported elsewhere by Nordstrom & Jackson (1993). Here, wave energy was linked with simultaneous measurements of beach profiles, sediment changes, and groundwater movement. These investigators identified a conceptual model, whereby all beach sediment is re-worked by waves during "high energy" conditions (wave height > 0.2 m); this led to net erosion across the beachface and subsequent burial of pebbles near the low-tide terrace. During the post-storm recovery phase, sand covering the pebbles is moved to landward by low-energy waves; fines are carried offshore by exfiltrating beach groundwater, leading to a surface lag of pebbles. Nordstrom & Jackson (*op. cit.*) observed that there may be no direct comparison with either gravel or mixed beaches, given the small proportion of pebbles and the overall low-level energy on their meso-tidal, estuarine beach. Nonetheless, their study has identified a set of threshold conditions during which the sub-population of pebbles was transported separately from the sand fraction; hence, the minimum conditions for gravel overpassing. This particular research demonstrated also that even small fluctuations in wave energy could have a noticeable effect on the distribution of surface sediments, on low-energy beaches.

Support for the Nordstrom & Jackson's (1993) conceptual model has been provided by Miller (1997), who examined the transport rates of sand and pebbles on an

unusual mixed beach at Wemyss, South Fife, Scotland. If a high proportion of sand was present on the beach, the sand was preferentially transported by the backwash; this created "sand runs" in front of pebble bands. Once the pebbles were mobilised, they slid and rolled across these sand runs and either remained on the surface or became buried lower down the beach. When only small quantities of sand were present, fine pebbles were transported preferentially under low energy conditions; however, they could be trapped within the interstities of the coarser-grained framework of the beach. In higher energy conditions, larger pebbles overpassed sections of the beach containing finer pebbles; consequently they had higher transport rates than the finer pebble fraction.

The sediments at Wemyss Beach consisted of indigenous sandstone pebbles and industrial placers including ironstone and coal waste material. The specific gravity of the sediment was identified as a crucial factor controlling sediment transport (Miller, 1997). Sandstone particles were transported at up to twice the velocity of the ironstone, whilst the transport velocity of the low density coal tracers was 10 times that of both the iron and sandstone particles.

The proportion of sand mixed with gravel has been linked variously with wave exposure, with the most exposed beach having the lowest proportion of sand (Bluck, 1967). Nevertheless, it has been argued subsequently (Orford, 1975) that the two facies types discriminated by Bluck (*op. cit.*) as representing high energy and low energy environments, were not exclusive indicators of wave regime. Seasonal changes in the sand content at 3 sites along a lengthy section of complex beach/barriers in Washington State, USA, have been noted (McKay & Terich, 1992). These were attributed to offshore movement of sand, during winter storms. The winter profiles at the Queets/South Beach sites (Washington) contained no sand whilst, in contrast, the summer profiles all contained at least 25% sand at their low water positions and no sand at the crests. However, at the South Rock View Beach sites, the low water position contained between 13 and 53 % of sand during summer, *increasing* to between 76 and 100 % during the winter. No reason for this difference in behaviour was offered.

Mixed beaches along the Suffolk coastline were investigated, with field measurements obtained over tidal and seasonal cycles and historical data for longer-term trends (Pontee, 1995). The average sand content at all the sites was around 30%, with the active regions of the beachface containing finer and more poorly sorted gravel than

the upper foreshore. There was a concentration of gravel above the high water mark, due to wave asymmetry and increased particle exposure. A further concentration, near the low water mark step, was attributed to seaward transport during the ebb tide. However, it was observed that one of the most noticeable features of the beaches was the great variability in sediment composition over a range of time scales (from days to months) under what might be considered similar wave conditions. It was concluded, albeit tentatively, that increasing wave height and period reduced the mean gravel size and increased the sand content.

The erosional/accretionary nature of a beach has been considered also to be a factor in determining the proportion of sand and gravel. For example, the result of 10 years rapid erosion at Canterbury Bight was considerable steepening of the foreshore, with an associated halving of the sand content (Kirk, 1980).

Finally, as a precautionary note, the usual particle size distribution parameters (sorting, skewness and kurtosis) must be used with caution on mixed beaches, which have effectively bi-modal distributions (Bluck, 1967; Kirk, 1980).

2.1.2 Beach profile response

The general relationship between sediment size and foreshore slope is similar to that found on sandy beaches, although not as linear a character. More importantly, well sorted sediments were found to have steeper slopes than corresponding poorly sorted sediments of similar mean grain size (Kirk, 1969; McLean & Kirk, 1969). The effects of grain shape were considered predominant only for mean grain sizes greater than -3ϕ (8mm), when imbrication of discoidal particles was the primary control on slope.

Seasonal changes in the profile shape of mixed beaches, similar to those occurring on sandy beaches, were observed by McKay & Terich (1992). At all sites studied, with the exception of one, a fair weather berm formed the entire length of the barrier during summer. During winter, this berm was absent. Profiles at the other site (the Rialto Beach barrier) behaved in no systematic seasonal manner; this was due mainly to the lack of sediment supply combined with barrier breakdown by frequent overwashing. The investigators concluded that differences in profile shape, together with their consistency, represented barriers in different stages of evolution.

Elsewhere, Pontee (1995) found that the only clear, seasonal trend in mixed beach profile was towards a greater variability during winter. Over the time scale of a tidal cycle, the classic landward progression of a step during a flood tide was identified; this was followed by seaward translation during the ebb, common to both sand and shingle beaches (*e.g.* Strahler, 1966; Powell, 1986). Storm conditions at the same location led to the shoreward migration of ridges, often in combination with storm surges, with a relatively planar beach surface to seaward. The development of beach scarps was also observed, particularly where the sediments were well compacted. Overall, the response of the mixed beach profiles, to storm conditions, was found to be similar to that of pure gravel beaches (Pontee, *op. cit.*). Offshore sediment transport and bar development, which is often the response of sandy beaches to storm conditions, was not observed.

The relationship between storm magnitude and the erosional profile is not, however, straightforward. Nonetheless, Orford & Carter (1982, 1985) reconstructed the hydrodynamic conditions required to create the sedimentary sequences found in a series of pits through a ramp which had built up to seaward of a dune complex in southeast Ireland. Fair-weather conditions had led to the development of a 40 m wide terrace on a mixed sand-and-gravel barrier in southwestern Ireland, in just 15 months; this was a result of the seaward addition of small swash ridges. The terrace formed above MHWS, protecting the dunes during moderate storms. If the storms were sufficiently severe to elevate SWL above the terrace, energy was dissipated across the terrace; this led, subsequently, to depositional conditions and the build-up of a ramp of wave-lain sediments at the foot of the dunes.

A further problem arises in the interpretation of facies from individual cross-sections, particularly in relation to antecedent conditions. Hence, berms high up the profile need not necessarily indicate higher energy conditions; they may have formed simply during spring tidal conditions (Caldwell & Williams, 1985). Hence the macro-tidal nature of many British mixed beaches makes the complex processes difficult to investigate. Elsewhere, the single breaker position under most wave conditions and at all states of the tide on the South Island, New Zealand beaches simplifies the problem (Kirk, 1980), as does the absence of any cross-shore sediment transport between the subaerial beach and the nearshore zone.

The Holocene evolution of sand-and-gravel fringing beaches and barriers, over time scales ranging from months to decades has been examined in a major series of publications by Carter, Orford and co-authors. Sedimentary structures associated with different depositionary processes, such as overwashing and overtopping, were identified. At the same time, the mechanisms by which such beaches transgress/migrate shorewards have been discussed (Orford & Carter, 1982; Carter *et al.*, 1990 and Orford *et al.*, 1991*a*). These investigators have developed models of barrier evolution, which differentiate between swash- and drift-aligned barriers, based upon their sedimentary characteristics (Carter & Orford, 1991; Orford *et al.*, 1991*b* and Carter *et al.*, 1992). The degree to which Holocene barrier morphology can be attributed to changes in sea level, rather than variations in sediment supply or wave climate has been assessed (*e.g.* Carter *et al.*, 1989; Orford *et al.*, 1995).

2.1.3 Hydrodynamics and sediment transport rates on mixed beaches

There are only limited measurements of the hydrodynamics associated with mixed beaches. However, those which do exist have identified the importance of the high permeability of coarse-grained sediments. A rare example of swash measurements in the field has been reported by Kirk (1975*b*). Velocities of 1.68 ms^{-1} over 2.98 seconds with a maximum of 2.5 ms^{-1}, were measured on Kaikoura Beach, New Zealand, whilst backwash velocities extended over a longer period of time, but were slower and more variable (averaging 1.4 ms^{-1} for 4.25 seconds). Such velocities exceeded the thresholds for all the sediment sizes on the foreshore; this was sufficient to permit high transport rates. Backwash became increasingly dominant with higher wave energy levels, in response to reduced infiltration as the foreshore became saturated with the large volumes of water carried forward in the swash. Deceleration in the swash velocities was distinctive, once the swash reached a particular level above the water table.

When a mixed shingle-sand barrier in southern California was breached artificially, the observed threshold velocities were about 1.6 ms^{-1} for shingle sizes of 5 to 200 mm (Walker *et al.*, 1991). The whole range of shingle sizes was in transport, with neither smaller or larger clasts being preferentially moved. Transport was confined generally to the uprush and backwash, rather than by longshore currents and accordingly, the longshore transport rate for the shingle was less than 1 or 2 % of the mean longshore current. These observations led to the conclusion that the shingle and sand transport

systems were effectively de-coupled; there was no net longshore shingle movement, yet sand was transported towards the south.

Recently, Miller (1997) found also that sand and pebble fractions could be transported in different directions, at different rates. Under low energy conditions, sand was found to be mobile whilst the pebbles were not; hence the latter became buried. Pebbles became mobile only in response to higher energy conditions and were transported only in the direction of the dominant waves. As the wave height increased, the sand was transported offshore; at the same time, the longshore transport of the exposed layer of pebbles increased. In general, the rate of longshore transport was lower when a high proportion of sand was present. Where conditions were conducive to the overpassing phenomenon, pebbles were transported more easily, but this tended to be confined to cross-shore transport and hence, the potential for longshore transport is low (Carter *et al.*, 1990; Miller, 1997). Latterly, it was concluded that higher sand content increased the stability of the beach sediments (Miller, *op. cit.*).

2.1.4 Groundwater on mixed beaches

The influence of beach groundwater levels on the net sediment transport budget of mixed beaches was identified by Kirk (1975*b*), in a similar manner to sand beaches, as discussed later. At Nash beach (South Wales), with impermeable sediments below the beach and a backing cliff, the presence of a high water table was considered to reduce the capacity for beach drainage both to landward and seaward (Caldwell & Williams, 1985).

In a study of water seepage through gravel and sand barriers in southeastern Ireland, Carter *et al.* (1984) established the conditions whereby streams discharged through a barrier; this was either by seepage or in a surface channel, based upon sediment type and barrier morphology. Seepage velocities and discharge volumes were calculated using Darcy's Law and theoretical coefficients of permeability. Hydraulic head was defined as the difference between the tidal elevation and the level of the lagoon, to landward of the barrier. Although seaward stream flow through the barrier was investigated, Carter *et al.* (*op. cit.*) noted the possibility of landward seepage, particularly during storms, and the erosion of the leeward side of the barrier (caused by seepage fans).

2.1.5 Laboratory experiments on shingle/mixed beach profiles

The response of a restrained laboratory "shingle" beach to monochromatic and, later, random waves has been described by a series of empirical equations (Powell, 1986, 1988, 1990). This research was developed subsequently to establish threshold conditions on a shingle barrier for overtopping and crest lowering, leading to subsequent failure and breaching (Bradbury & Powell, 1992). Unusually, the model was calibrated and validated, using both physical models and field data (beach profile and hydrographic data with concurrent on-site wave monitoring). This data set included the dramatic response of the Hurst Castle Spit to the December 1989 storm. Here, the barrier crest was lowered 3 m in places, and the barrier as a whole rolled landward, by over 60 metres. Bradbury & Powell (*op. cit.*) noted also the outflow of groundwater on the lee side of the model spit and in the field, at Hurst Castle Spit. Such water movement is clearly of sufficent speed to transport sediment and form outwash fans, presumably of a similar form to those recorded elsewhere (*e.g.* Carter *et al.*, 1984).

An interesting conclusion from the laboratory work with random waves was that energy dissipation across the model shingle beaches may have occurred primarily through wave breaking and frictional losses across the surface layers of the beach. Hence, flow within the body of the beach produced little additional dissipation (Powell, 1988).

Only two series of experiments have exposed mixed sediment laboratory beaches to differing wave energy regimes (Quick & Dyksterhuis, 1994; Holmes *et al.*, 1996). the former investigators have suggested that waves breaking on a permeable beach should produce a net onshore shear stress, during swash and backwash; this leads to net onshore sediment transport and profile steepening, until equilibrium is reached. The observation that beaches of low permeability will have lower equilibrium slopes than beaches of high permeability, agrees qualitatively with field observations (*e.g.* Komar, 1976; Finkelstein, 1982). This characteristic has been attributed to the permeability of the sediment (Quick & Dyksterhuis, *op. cit.*), although Carter *et al.* (1990) considered that the outer boulder frame (common on mixed beaches) produces large bed roughness and hence greater energy dissipation. This interpretation agrees with the conclusions of Powell (1988) referred to previously. Quick & Dyksterhuis (*op. cit.*) identified that low energy waves had no effect on a profile of 50:50 sand and gravel (D_{50} = 3.4 mm), whilst medium waves led to the formation of a small offshore bar and slight profile lowering. High waves led

to major offshore transport of both the sand and gravel; the profile was similar to that formed by sand, when subjected to the same wave energy conditions. Meanwhile, an all-gravel profile responded, once a threshold wave height was reached, with step formation at the breakpoint and some onshore transport, but there was little change in overall slope. It was concluded that *the sand fraction* was the controlling factor for profile reduction under high waves. For example, when under high energy conditions, a beach containing 25% sand responds in the same manner as a sandy beach. This interpretation is in direct contrast, however, to the profile response observed elsewhere (Pontee, 1995). In the latter sutdy, beaches containing an average 30% sand responded to storm conditions in a similar manner to gravel beaches (Section 2.1.2).

The response of fine, coarse and bimodal sand laboratory beaches to wave action has been compared by Holmes *et al.* (1996). It was concluded that profile response of the bimodal beach was similar to that of the fine sand beach, which is in agreement with the findings of Quick & Dyksterhuis (1994). On the coarse sand bed, infiltration was greater; this led to lower backwash volume and, hence, increased wave asymmetry in the swash zone (as predicted by Grant [1946]). Also, the higher threshold velocities for the larger grain sizes produced a net onshore transport and berm formation.

However, it has been suggested that the finer sand in the bimodal sediment de-stabilised the coarser fraction (Holmes *et al.*, 1996). The relative exposure of the larger particles is increased with friction reduced, when the finer particles are present. Hence, the mobility of the coarse sediment is increased. It was concluded that the permeability of the finest fraction controls profile behaviour. However, the bimodal beach consisted of 50:50 coarse and fine sand; therefore, it was not established what threshold proportion of sand is required to induce behaviour similar to that of a fine sand beach.

2.1.6 Influence of permeability

Further indications of the influence of the permeability of sediments on waves and wave transmission through the beach are provided by publications in the engineering literature, in particular, the research undertaken with wave reflection and transmission through permeable structures, such as berms and breakwaters. For example, increased permeability has been found to reduce wave run-up and swash height, increasingly for high values of the surf similarity parameter (Kobayashi *et al.*, 1991). An increase in the

permeability of the core material of a rubble mound breakwater was found to increase the stability of the armour layer; this was because a greater proportion of wave energy was dissipated within the core (Timco *et al.*, 1984). Decreasing permeability increases the internal set-up within the structure (van Gent, 1994).

Comparisons undertaken between a laboratory model impermeable breakwater, an homogeneous permeable berm breakwater and a permeable berm breakwater with impermeable core, showed that waves incident upon the impermeable structure were more extreme in terms of velocity and elevation; this was in comparison to those incident on the permeable structures, for which the model incorporated a measure of wave transmission (van Gent, 1994). Surface elevation excursion, wave run-up and offshore velocities were reduced across the permeable breakwaters, particularly for the homogeneous structure. Reflection and subsequent increase in wave height, close to the structure, were also considerably weaker in the case of the permeable breakwaters. van Gent (1994) concluded, from these results, that the porous flow through the structures was an important component in the modelling of wave action on coastal stuctures. this consideration applies for infiltration and seepage, and in its influence on external waves and currents. Further details concerning the influence of permeability on wave reflection, are included in Section 2.3.4.

It should be noted, in summary, that many of the field sites referred to in this review, are broadly homogeneous-type beaches or barriers. In such environments, sand and shingle are mixed in varying proportions across the majority of the intertidal zone (*e.g.* McLean, 1967; Kirk, 1969; McLean, 1970; Kirk, 1975*b*; Orford & Carter, 1982; Pontee, 1995 and Miller, 1997). These are the type of beaches which are referred to as "morphologically distinct and dynamically complex" (Kirk, 1980). Research into processes on composite-type sand beaches, with a fringing gravel ridge, has progressed minimally since Orford (1975) examined the shape sorting of pebbles at Llanrhystyd (Cardigan Bay, Wales). Further, with the exception of Walker *et al.* (1991), no detailed hydrodynamic measurements have been obtained for composite-type mixed beaches.

2.2 Velocity Moments

It has long been recognised that sediment transport nearshore is inextricably linked to small asymmetries in the velocity field. A purely sinusoidal flow would produce no *net* sediment transport, in itself; the only such movement would result from gravity-aided transport downslope and, hence, generally offshore. The implication of asymmetric oscillatory velocities has been noted by Cornish (1898) and, subsequently, sediment transport has been linked to some power of the oscillatory velocity, u^n (for example $n = 3$ [Inman & Bagnold, 1963] and $n = 6$ (Madsen & Grant, [1976]).

2.2.1 Definition of velocity moments

These are statistical properties derived from a series of observations, representing the deviation of each observation from the mean then raised to a power and averaged:

1st Moment	$\frac{\sum (X - X_o)}{N}$	
2nd Moment	$\frac{\sum (X - X_o)^2}{N}$	Variance
3rd Moment	$\frac{\sum (X - X_o)^3}{N}$	Skewness
4th Moment	$\frac{\sum (X - X_o)^4}{N}$	Asymmetry

(2.1 *a, b, c* and *d*)

where X is the observation, X_0 is a given value and N is the number of observations. When X_o is the mean of all the observations, the first moment is zero and the second moment is referred to as the variance (WMO, 1988). Translated into wave parameters, the mean value provides both the direction and magnitude of the residual flows, such as the longshore current or undertow. The variance is a measure of wave energy and, for cross-shore velocities, is defined as $< u^2 >$ (the angled brackets refer to time-averaged value), where u is the detrended and de-meaned cross-shore time series.

The higher-order terms are essentially a measure of the non-linearity of the nearshore velocity field. The skewness is a measure of the horizontal asymmetry of a wave; this occurs, for example, in a Stokes-type wave with a high peaked crest and a

flatter, longer trough. The skewness term is usually normalized (Doering & Bowen 1987) as:

$$\frac{<u^3>}{<u^2>^{3/2}} \tag{2.2}$$

but it is often referred to as wave asymmetry. Asymmetry in the statistical sense refers to the wave's vertical asymmetry, such as the saw-tooth profile of a wave with a steep front face but a shallow slope on its rear face. Such a wave may be asymmetric, but is not necessarily skewed since it may have a crest and trough of equal height. Elgar *et al.* (1988) defined wave asymmetry, A, using the Hilbert transform of the cross-shore velocity time series:

$$A(u) = -S(H[u]) \tag{2.3}$$

where u is the detrended and de-meaned cross-shore velocity time series (as before) and H its Hilbert transform. S is the normalised skewness, as given by (2.2). For a deep water, linear wave, $S = A = 0$, whilst for a Stokes-type wave, $S \neq 0$, $A = 0$ and a "saw-tooth" wave has $S = 0$, $A \neq 0$. Asymmetry terms do not appear in the Bailard-type sediment transport models (see below), but their higher-order terms become important if the acceleration field is of interest.

2.2.2 Bailard's (1981) model for total load sediment transport

The energetics-based theory for sediment transport stems from Bagnold's stream flow model (1966), which predicts an immersed weight sediment transport rate, i, as the sum of sediment transported in two different modes: (i) supported by the bed in grain-to-grain collisions (bedload); or (ii) suspended above the bed, supported by turbulence within the fluid (suspended load). Other transport models have been based either directly or indirectly on Bagnold (1963, 1966), but will not be discussed here.

The Bailard (1981) energetics model is regarded as one of the best theoretical models for time-dependent total load sediment transport (Schoonees & Theron 1995) and is used widely (*e.g.* Roelvink & Stive, 1989; Nairn,1990; Scott *et al.*, 1991; Gillott & Southgate, 1996). Bailard (1981) developed Bagnold's uni-directional model to produce

a total load, time-averaged, immersed weight sediment transport rate across an arbitrarily sloping bed. The model consisted of a component in the direction of the instantaneous velocity vector, together with a secondary component directed downslope:

$$\begin{aligned} <\vec{i}_t> = \rho C_f \frac{\epsilon_b}{\tan\phi} [<|\vec{u}_t|^2 \vec{u}_t> - \frac{\tan\beta}{\tan\phi} <|\vec{u}_t|^3> \hat{i}] \\ + \rho C_f \frac{\epsilon_s}{W} [<|\vec{u}_t|^3 \vec{u}_t> - \frac{\epsilon_s}{W} \tan\beta <|\vec{u}_t|^5> \hat{i}] \end{aligned} \quad (2.4)$$

where ρ is fluid density, C_f is a drag coefficient, ϵ_b and ϵ_s are bedload and suspended load efficiency factors (which represent the proportion of stream energy used in transporting sediment), ϕ is the angle of internal friction of the sediment, β is local bedslope, W is the sediment fall velocity, $\hat{i}$ is the unit vector and $\vec{u}_t$ is the total instantaneous near-bed velocity vector. Angled brackets, < >, represent time-averaging. The right hand side of the first line of (2.4) represents transport by bedload; the second line, the suspended load.

2.2.3 Sediment transport rates - Guza & Thornton's (1985) equations

An important development of the Bailard (1981) approach was its adaption for a random wave field by Guza & Thornton (1985), since the odd moments of random (or Gaussian) waves will be notably different from those for an equivalent monochromatic field. The differences are shown in Table 2.1, where it can be seen that the odd moments of oscillatory velocity $<\tilde{u}^3>$ and $<|\tilde{u}^3|\tilde{u}>$ are not zero. This conclusion was confirmed by Huntley (1976) whose field data demonstrated clearly that the wave-induced velocity is oscillatory, but is not distributed symmetrically through time.

Moment	Monochromatic waves		Random waves	
	Sign	Magnitude	Sign	Magnitude
Mean		0	±	≠ 0
Variance	+	+	+	+
Skewness		0	±	≠ 0
Asymmetry	+	+	+	+

Table 2.1 Comparison of moments for random and monochromatic waves

Even moments are not dependant critically on asymmetries in nearshore velocities, since they are even powers; neither are those moments which are odd powers of absolute values $|\tilde{u}|^3$ and $|\tilde{u}|^5$. However Guza & Thornton (1985) demonstrated that a random sea will produce considerably higher values for even moments than an "equivalent monochromatic wave" *i.e.* having the same total variance as the random waves. Clearly then, the extension of Bailard's general equations, for random seas, was a major advance in energetics-based predictions of nearshore sediment transport rates; it forms the basis of the analyses of velocity moments, in this research project.

Guza & Thornton produced a generalized form of transport equation:

$$\langle i_x \rangle = \rho C_f u_m^3 \left[\frac{\epsilon_b}{\tan\phi} \left[\psi_1 \cos\alpha_1 + \delta_u^3 + \delta_u \left(\frac{1}{2} + \cos^2\alpha_2 + \delta_v^2 \right) + \delta_v \sin\alpha_3 \cos\alpha_3 + \frac{\tan\beta}{\tan\phi} (u3)' \right] + \frac{u_m}{W} \epsilon_s \left[\psi_2 \cos\alpha_5 + \delta_u (u3)' \right] + \frac{u_m^2}{W^2} \epsilon_s^2 \tan\beta \, (u5)' \right] \tag{2.5}$$

$$\langle i_y \rangle = \rho C_f u_m^3 \left[\frac{\epsilon_b}{\tan\phi} \left[\psi_1 \sin\alpha_1 + \delta_v^3 + \delta_v \left(\frac{1}{2} + \sin^2\alpha_2 + \delta_u^2 \right) + \delta_u \sin\alpha_3 \cos\alpha_3 \right] + \frac{u_m}{W} \epsilon_s \left[\psi_2 \sin\alpha_5 + \delta_v (u3)' \right] \right] \tag{2.6}$$

where i_x and i_y are the immersed weight sediment transport rates in the cross-shore and longshore direction respectively and $\vec{u}_t$ is the total velocity field. u_m, the former magnitude of wave orbital velocity, is now derived from the total oscillatory variance, ψ_1 and ψ_2 are velocity moments, δ is the relative steady current strength at an angle θ, and α is an oscillatory current angle (with remaining terms as defined for eqn. 2.4):

$$|\vec{u}_t| = \sqrt{\tilde{u}^2 + \tilde{v}^2 + \bar{u}^2 + \bar{v}^2 + 2(\tilde{u}\bar{u} + \tilde{v}\bar{v})} \tag{2.7}$$

$$u_m = \sqrt{2\left(\langle \tilde{u}^2 \rangle + \langle \tilde{v}^2 \rangle\right)} \tag{2.8}$$

$$\psi_1 = \frac{\langle \tilde{u}(\tilde{u}^2 + \tilde{v}^2) \rangle^2 + \langle \tilde{v}(\tilde{u}^2 + \tilde{v}^2) \rangle^2}{u_m^3} \tag{2.9}$$

$$\psi_2 = \frac{\sqrt{\left(<|\vec{u}_t|^3\tilde{u}>^2 + <|\vec{u}_t|^3\tilde{v}>^2\right)}}{u_m^4} \tag{2.10}$$

$$u3^* = \frac{<|\vec{u}_t|^3>}{u_m^3} \tag{2.11}$$

$$u5^* = \frac{<|\vec{u}_t|^5>}{u_m^5} \tag{2.12}$$

$$\tan\alpha_1 = \frac{<\tilde{v}^3 + \tilde{u}^2\tilde{v}>}{<\tilde{u}^3 + \tilde{u}\tilde{v}^2>} \tag{2.13}$$

$$\tan\alpha_2 = \left(\frac{<\tilde{v}^2>}{<\tilde{u}^2>}\right)^{1/2} \tag{2.14}$$

$$\sin 2\alpha_3 = \frac{4<\tilde{u}\tilde{v}>}{u_m^2} \tag{2.15}$$

$$\tan\alpha_5 = \frac{<|\vec{u}_t|^3\tilde{v}>}{<|\vec{u}_t|^3\tilde{u}>} \tag{2.16}$$

$$\delta_u = \left(\frac{(\bar{u}^2 + \bar{v}^2)^{1/2}}{u_m}\right)\cos\theta \tag{2.17}$$

$$\delta_v = \left(\frac{(\bar{u}^2 + \bar{v}^2)^{1/2}}{u_m}\right)\sin\theta \tag{2.18}$$

$$\tan\theta = \frac{\bar{v}}{\bar{u}} \tag{2.19}$$

Eqns. (2.5) and (2.6) will be used, together with field data from Morfa Dyffryn, to predict a net sediment transport rate for cross- and longshore. These are compared then with the actual transport rates, as measured by co-located OBS's and EMCM's (Section 8.4).

2.2.4 Velocity moment terms

Guza & Thornton's (1985) field data suggested that the two most important terms in (2.4) were $< | u_t |^2 u_t >$ for bedload, and $< | u_t |^3 u_t >$ for suspended load. Previous studies have examined the contributions of the individual components of these two moments, namely the gravity (or short) wave, infragravity (long) wave and mean cross-shore flow components (both in the laboratory and using field data).

Theoretical calculations of velocity moments have been formulated for inclusion in a model (referred to as COSMOS) for nearshore hydrodynamics, sediment transport and profile evolution (Southgate & Nairn, 1993; Nairn & Southgate, 1993). Nairn & Southgate (*op. cit.*) used only the short wave and mean flow component in their laboratory study. This work was later expanded upon by Gillott & Southgate (1996) to include long waves and, in particular, the interaction between short and long waves, represented by the terms $<u_s^2 u_l>$ and $<| u_s |^3 u_l>$. However, the importance of the mean cross-shore current was not assessed. Both these studies assumed that the magnitude of the long wave component is much smaller than that for the short waves. A similar approach was adopted by Roelvink & Stive (1989) who, in addition, assumed that the mean cross-shore velocity was smaller than the amplitude of the oscillatory component. However, inclusion of the longwave contributions was necessary, to predict with accuracy the measured laboratory moments. Roelvink & Stive (*op. cit.*) extended (2.4) to include the additional stirring of the sediment by wave breaking-induced turbulence, which penetrated to the seabed.

Field data from a macro-tidal beach, at Spurn Head, were decomposed into short, long and mean cross-shore flow components (Foote, 1994). Bedload and suspended load moments followed distinctive patterns in relation to mean water depth; from these, a series of "shape functions" was derived. Bedload functions produced a pattern of onshore transport outside the surf zone, but offshore transport inside the surf zone (when the combination of wave stirring at gravity and infragravity frequencies with mean offshore

flows predominated over the onshore nature of incident wave skewness). Foote (1994) found that the moment terms predicted accurately the direction of short wave, long wave and mean flow components both inside and outside the surf zone during the flood tide. Nonetheless, the relative magnitude of their contribution was inaccurate. However, the short wave component predictions were noticeably inaccurate for the ebb tide. Hence it was concluded that the energetics model could not predict accurately sediment transport on the macro-tidal beach (although no account was taken of the strong wave-induced and tidally-induced lonshore currents). Tidal asymmetry in sand transport on this macro-tidal beach was attributed to the destruction of a ripple field, which had formed around high water. Exfiltrating groundwater was offered as a further possible reason (Davidson *et al.*, 1993).

Recently, Thornton *et al.* (1996) have assessed the ability of Bailard's model to predict sediment transport in the presence of strong longshore currents. Results from the model were compared to measured daily beach profile changes.

Foote (*op. cit.*) and Thornton *et al.* (*op. cit.*) made different assumptions about the most important of the components of the suspended velocity moment, ψ_2 *i.e.* they decomposed (2.4) in a different manner. The former study used only cross-shore data, whilst the latter considered that mean longshore currents >> short waves. The decomposition of (2.4), used by these authors, is given in Chapter 6, where the implications of the different assumptions will be discussed.

Neither of these derivations of velocity moment terms is entirely applicable to conditions at Morfa Dyffryn within the context of the present investigation. At Morfa Dyffryn, the macro-tidal regime and extensive ridge and runnel inter-tidal zone produced strong longshore currents; these were tidally-induced, rather than wave-induced. Consequently, the mean currents and short waves are of similar importance. Accordingly, this research programme uses a method of decomposion of the velocity moments which takes into account gravity waves, infragravity waves and mean currents in both the cross- and longshore directions. The method of decomposition was derived for a macro-tidal, sandy beach at Nieuwpoort-aan-Zee, Belgium (Voulgaris & Collins, 1996), where strong, tidally-induced longshore currents were also present. Further details about this method are given in Chapter 6.

2.3 Wave Reflection

Recent interest in wave reflection from beaches and nearshore structures has been concerned with the differential reflection of the whole wave spectrum, rather than of the incident (gravity) waves. This approach has followed the realisation that reflection of lower frequency waves can lead to cross- and alongshore standing wave structure (Huntley, 1996). On sufficiently steep-sided structures or beaches, almost complete reflection of long waves can be recorded. Higher frequency waves tend to be dissipated near the shoreline through breaking wave processes and, hence, have a lower reflectivity. On natural beaches, reflection is strongly dependent upon frequency, for a given beach slope. Therefore, the beach acts as a selective absorber/reflector, although significant reflection of small amplitude wind wave frequencies can occur (Tatavarti, 1989). However, this selection is not related simply to frequency; it is also a function of wave height, with reflection generally increasing with decreasing wave amplitude.

The calculation of reflection coefficients, from measured field data, is based upon either:

(a) a cross-shore transect of pressure transducers (*e.g.* Nelson & Gonsalves, 1990; Davidson *et al.*, 1994; Elgar *et al.*, 1994; Bird *et al.*, 1996), or an array of wave staffs (*e.g.* Chadwick *et al.*, 1995; Van Wellen *et al.*, 1997); or

(b) a co-located pressure sensor and current meter (*e.g.* Guza & Bowen, 1976; Guza *et al.*, 1984; Takezawa *et al.*, 1988; Tatavarti, 1989; Walton, 1992*a*; Raubenheimer *et al.*, 1995 and Miles *et al.*, 1996).

The advantages and disadvantages of both methods of predicting reflection coefficients are discussed in Section 2.3.4.

2.3.1 Reflection coefficients from pressure sensors

Reflection coefficients derived from an array of pressure sensors or wave staffs calculate a directional energy spectrum, using a variety of methods in either the frequency domain (*e.g.* Goda & Suzuki, 1976; Mansard & Funke, 1980) or the time domain (*e.g.* Frigård & Brorsen, 1995). The components of the directional spectrum can be summed

over the appropriate 180°, which represent onshore-directed energy; the reciprocal 180° represents the off-shore directed component of wave energy *(e.g.* Elgar *et al.*, 1994). Reviews of these techniques can be found in Isaacson (1991) and Hughes (1993); they will not be discussed further, since reflection coefficients for the field experiment at Morfa Dyffryn will be derived from a co-located current meter and pressure sensor.

2.3.2 Reflection coefficients from pressure and velocity time series

The theory behind the method which uses a co-located pressure and current meter (after Guza *et al.*, 1984) assumes that the sea surface is the net result of the linear superposition of incoming and outgoing components. The velocity time-series represents the instantaneous slope of the water surface, through its pressure potential; hence, the instantaneous direction of each component. Linear wave theory correlates a sinusoidal incoming wave with cross-shore velocity, which allows the velocity time-series to be scaled. At the crest of an incoming wave, the sea surface is at its maximum elevation and the onshore orbital velocities are at their (positive) maximum; an outgoing wave crest has maximum elevation and maximum offshore-directed (negative) orbital velocity. Hence, the net sea surface represents an addition of amplitudes, but a difference of velocities. Therefore, the incoming component is represented by the addition of the sea surface elevation time-series and the scaled velocity time-series:

$$\eta_t + u_t = (\eta_i + \eta_r) + (\eta_i - \eta_r) = 2\,\eta_i \tag{2.20}$$

whilst the outgoing component is the difference between the elevation and scaled velocity time-series:

$$\eta_t - u_t = (\eta_i + \eta_r) - (\eta_i - \eta_r) = 2\,\eta_r \tag{2.21}$$

The shallow water derivation of linear wave theory is used for the scaling procedure and hence, (2.20) and (2.21) are represented generally as:

$$\eta_{in}(t) = \frac{\eta_{(t)} + \alpha \sqrt{\frac{h}{g}}\, u_{(t)}}{2} \tag{2.22}$$

$$\eta_{out}(t) = \frac{\eta_{(t)} - \alpha \sqrt{\frac{h}{g}}\, u_{(t)}}{2} \tag{2.23}$$

where η is the (de-meaned and detrended) sea surface elevation, η_{in}, and η_{out}, are the incident and reflected wave trains, h is mean water depth, g is acceleration due to gravity and u is the oscillatory component of the cross-shore velocity (positive values representing the onshore direction). The constant, α, is taken usually as unity. However, it represents the vertical distribution of the current velocity (Takezawa *et al.*, 1988) and, therefore, may be influenced by strong longshore currents (Kubota *et al.*, 1993)*a*. Eqns (2.22) and (2.23) have been used to derive incident and reflected time series by Nagata, 1964; Guza & Bowen, 1976, Guza *et al.*, 1984; Masselink, 1995; Raubenheimer *et al.*, 1995 and Miles *et al.*, 1996.

To examine the influence of using linear wave theory, Kubota *et al.* (1990*a*) compared the results produced by (2.22) and (2.23) with separation based on: (i) small-amplitude wave theory, with u expressed using its Fourier coefficients; and (ii) a quasi-nonlinear long wave theory based on the Shallow Water Equations where:

$$\eta_{in} = (1/2)\left[\eta + \alpha u \sqrt{h/g} \cdot h/(h - \eta)\right] \tag{2.24}$$

$$\eta_{out} = (1/2)\left[\eta - \alpha u \sqrt{h/g} \cdot h/(h - \eta)\right] \tag{2.25}$$

A value for α was derived from the ratio of the measured:

$$\left(\overline{\eta^2}/\overline{u^2}\right)^{0.5} \tag{2.26}$$

with that calculated using the small-amplitude wave theory; this was 1.26 for a gentle sandy beach and 1.54 for a steep beach. These investigators concluded that the quasi-nonlinear method was the most appropriate for separation in the time domain, with the difference being more pronounced on the gently sloping beach. However, the incident and reflected time-series given in Kubota *et al.* (1990*a*) are remarkably similar except for one or two isolated perturbations; these could not always be explained. The consequences of using these different methods of separation on the spectra of the decomposed time-series and, hence, on the reflection coefficient were not discussed.

The methods described above decompose the sea surface elevation in the time domain, but the pressure and velocity time-series can also be combined in the frequency domain (*e.g.* Tatavarti *et al.*, 1988; Walton, 1992*a*). A third method involves principal component analysis (PCA) *e.g.* Tatavarti *et al.*, (1998); Huntley *et al.*, (1995), which assumes that the correlated parts of the elevation and current signals are contained in their first eigenfunction (the first principal component); similarly, that signal noise is confined mainly within the remaining higher eigenfunctions. A comparison of the reflection coefficients, produced by these three methods, is discussed in Section 2.3.3.

Hughes (1993) has described a method for obtaining reflection coefficients from co-located horizontal and vertical velocity measurements (using methods similar to the frequency domain velocity/sea surface decomposition). The derivations have been compared with the results from a wave gauge array. The results obtained using both methods were comparable for a gently sloping laboratory (impermeable) beach. The vertical velocities method was not recommended for shallow water, but in any case, it does not appear to have been used for field data and, therefore, will not be discussed further.

2.3.3 Frequency-Dependent Reflection Coefficients (FDRF)

Once the spectra of the incident and reflected waves are determined (by whichever method) the reflection coefficient, r, is derived from the square root of the ratio of the spectra of the outgoing component of the sea surface elevation, E_{out}, at frequency f, to that of the incoming component E_{in} (Kajima, 1969):

$$r(f) = \sqrt{\frac{E_{out}(f)}{E_{in}(f)}} \tag{2.27}$$

Hence, the reflection coefficient is determined across the whole frequency range, unlike the empirical formulation of an average value (*e.g.* Seelig, 1983); it is referred to, henceforth, as a Frequency Dependent Reflection Function (FDRF).

Huntley *et al.* (1995) compared frequency-dependent coefficients for reflection (FRDF) using time domain, frequency domain and PCA methods. This investigation showed that PCA offered the most reliable results, since bias due to signal noise was reduced greatly (in comparison to the time domain and frequency domain methods). The time domain method tended to overestimate FDRF, particularly if there was any significant noise in the current and elevation signals As an example, any component of longshore wave structure (edge waves) would produce uncorrelated noise between the pressure and velocity signals; this is because it would be present in the sea surface but not in the cross-shore velocity. Huntley *et al.* (1995) assessed the effect of signal noise using a series of simulated wave and current time-series with known levels of Gaussian-distributed white noise (which is independent of frequency) and with given values of reflection coefficient. From this, these investigators were able to estimate the bias due to signal noise (as represented by the coherence between the incoming and outgoing components) and the required correction to the FDRF (Huntley *et al.*, 1995, Figure 2).

Providing the coherence between the pressure and velocity signals is high, the improvement in FDRF estimates given by the PCA method, over the time domain method, is "reassuringly small" (Miles *et al.*, 1996). However, a more serious problem is any time lag between the instantaneous pressure and velocity readings. Such a delay may be caused either by the filter characteristics of the instruments and/or the instruments not being exactly co-located in a cross-shore direction. This time delay leads to overestimates of FDRF, if not applied as a correction to the times series prior to the analysis. The instrumental time delay can be determined electronically, or if necessary empirically, by calculating the FDRF for a range of possible time lags. Modelling has shown that the correct time lag provides the lowest FDRF value and the flattest response across the spectrum (Simmonds, pers. comm.).

2.3.4 Comparison between co-located current meter/pressure sensor and wave transect array methods, for calculating reflection coefficients

The main advantage in using a co-located pressure sensor and current meter, to derive reflection coefficients, is the avoidance of the two major potential problems with using a transect or array of pressure sensors: (i) the risk of spacing the sensors at integrals of half the wavelength; and (ii) the assumption that the wave field remains homogeneous across the length of the transect (Huntley *et al.*, 1995). The second assumption, especially, is likely to be invalid for the shoaling and surf zones of a beach.

Raubenheimer *et al.* (1995) considered that the relative proportion of reflected energy should increase towards the shoreline, due to energy dissipation of the incident waves through breaking. Whilst this is likely to be the case across a dissipative shoreline, it may not apply outside the surf zone or on a steep beach where, for example, wave breaking is confined to a narrow region of plunging breakers. Under such conditions, the cross-shore location of the sensor should not affect the reflection coefficient, since the ratio of the variance of the outgoing and incoming components remains the same. Hence, a further advantage of the velocity/pressure method is that, in the absence of edge waves, reliable reflection coefficients can be obtained from a single sensor location (Tatavarti, 1989).

The disadvantage in the derivation is that most of the methods for decomposing the concurrent sea surface and current time-series, require the wave field to be broadly orthogonal to the beach. It should be noted that new methods of analysis for incident waves, with an angle of approach to the beach greater than 10°, are under development *e.g.* the Modified Maximum Likelihood Estimator (Huntley *et al.*, 1995). Interestingly, Benoit & Teisson (1994) found reflection from a laboratory breakwater to be only weakly dependent upon wave direction from 0 to 60°, with minimum and maximum values at 15° and 45°, respectively. Other problems in the calculation are those referred to in Section 2.3.3 above, namely that results can be distorted due to the presence of noise (in either or both of the time-series), or by a time delay between the time-series caused by the current meter and pressure sensor not being exactly co-located in the cross-shore direction (Tatavarti *et al.*, 1988; Huntley *et al.*, 1995).

2.3.5 Influence of sediment composition on wave reflection (laboratory experiments/structures)

Most research into the inter-relationship between wave reflection and sediment type (as characterised by its porosity and permeability) involves experiments on permeable berms, or breakwaters. The effects of permeability on run-up and wave reflection are known to be important factors in the design of permeable coastal structures. However, as recently as 1992, Kobayashi & Wurjanto wrote that "our quantitative understanding of the hydrodynamic processes involved with irregular wave interaction with permeable slopes is still rudimentary, although extensive hydraulic model tests have been performed"

In fact, Kobayashi *et al.*'s (1991) laboratory experiments found that the presence of a thick permeable layer of gravel on a 1:3 sloping beach, reduced wave reflection with a corresponding reduction in wave height; it was impossible to generate exactly the same wave train, as for an impermeable slope, because of this effect. Reflection coefficients were generally lower across most of the spectrum for the permeable slope, although the values reduced systematically across the normalised frequency range; this represented wind-wave frequencies, for both the permeable and impermeable beds. Reflection of the lower normalised frequencies was almost total for the impermeable slope and > 90% for the permeable structure. The surface of both structures was "rough"; therefore, it is implicit that reduced reflection coefficient represented energy dissipation through infiltration, rather than through bed friction.

Kobayashi & Wurjanto (1992) achieved similar results from their numerical model results of wave propagation over a 1:3 slope with a thick permeable underlayer in comparison with an impermeable bed. Lower reflection coefficients were derived for the slope with a thick permeable underlayer, with increasingly lower reflection in the higher frequency range, than from the impermeable slope. The model predicted an offshore mean cross-shore flow (undertow) for waves incident upon the impermeable slope, but the time-averaged flow was onshore on the permeable structure. This was evidence, the authors suggested, that permeability can affect the net cross-shore transport of sand and gravel; they concluded also that a thick permeable layer can reduce wave reflection and run-up.

2.3.6 Effect of slope upon wave reflection (laboratory experiments/structures)

Once again, most research is engineering-based but recent experiments on permeable breakwaters, berms and seawall are of interest for the insight they may provide into wave reflection (particularly from steep, mixed or shingle beaches). Bulk wave reflection (*i.e.* reflection coefficients weighted and averaged across the spectrum) is expected to increase with increasing slope; for example, from 20 - 24 % for a laboratory breakwater slope of 1:2, 30 - 35 % from a 2:3 slope, to 34 - 38 % reflection from a 3:4 slope (Benoit & Teisson, 1994). At Elmer, West Sussex, reflection from a porous, rock island breakwater was considerably higher around high water; this was when the effective slope of the breakwater increased. In contrast, towards low water, the shallow water depths and lower slope of the structure led to a reduction in the reflection coefficient (Bird *et al.*, 1994; Davidson *et al.*, 1994). A later, comprehensive, study of wave reflection at the same location demonstrated that reducing the seaward gradient of the structure from 1:1 to 1:2 led to a 15% reduction in the reflection coefficient, depending upon the prevailing wave conditions (Bird *et al.*, 1996). Low values for the reflection coefficient on gentle beach slopes have also been observed in laboratory data and are attributed to dissipation of energy, across a wide surf zone (Guza & Bowen, 1976).

2.3.7 Influence of wave steepness

Davidson *et al.* (1994) considered that FDRF was related directly to the steepness of the incident waves, but only when the waves broke directly adjacent to a berm breakwater structure; if a surf zone of breaking waves was present, wave reflection became minimal. Benoit & Teisson (1994) found also that wave steepness affected the reflection coefficient, which they attributed tentatively to the nature of reflection from the permeable model breakwater. Waves of low steepness were considered to dissipate their energy within the core of the breakwater, through percolation; in comparison, the energy of steep waves is dissipated through plunging. Consequently, the reflection coefficient for both wave types is lower than for waves of medium steepness; these were reflected from the outer armoured layer, with less dissipation through percolation or wave breaking. In contrast, Sakakiyama & Kajima's (1992) experiments of wave reflection and transmission through a rubble-mound breakwater showed that the reflection coefficient remained essentially constant for waves of increasing steepness; however, wave transmission decreased markedly.

2.3.8 Wave reflection from beaches (field experiments)

Field data have confirmed that preferential reflection of low frequency waves occurs also from beaches as well as from structures (*e.g.* Tatavarti, 1989, whose thesis represented some of the earliest, detailed, research into wave reflection from beaches). This particular study will be described in more detail in Section 7.4, since it forms the basis of a comparison with the wave reflection data at Morfa Dyffryn.

More recently, waves of different periods have been found to reflect differently according to the beach slope (Kubota *et al.*, 1993). Reflection of waves from three sandy beaches have been described; one of these was backed by a steep sea wall. Only long period waves reflected from slopes of less than 1:20 (2.8°), whilst individual swell waves were observed to reflect from gradients steeper than 1:10 (5.7°).

Detailed analysis of the data obtained from the steep sand beach (Oarai Beach, Japan) identified that waves of lower frequency than 0.065 Hz reflected almost completely to form two-dimensional non-breaking standing waves; those in the frequency range $0.065 < f < 0.09$ Hz (swell waves) formed partially standing waves, some of which were breaking. The remaining energy in the reflected component at these frequencies (which was not dissipated during breaking) was reflected offshore. Hence, the η_{out} component contained long period waves which had not been identified in the incident wave series (Takezawa *et al.*, 1990). On a more gently sloping sand beach (Hazaki Beach, Japan), the energy from wind-waves was dissipated through breaking. There was no significant reflection, but low period waves ($f < 0.03$ Hz) formed perfect standing waves; those in the frequency range $0.03 < f < 0.06$ Hz were partially standing, in the cross-shore direction (Kubota *et al.*, 1990*b*)

Chadwick *et al.* (1995) have observed also the reflection of swell waves (~ 0.11 Hz), with some minor reflection at the higher harmonic frequency (at Elmer, West Sussex) during Storm Force 10 winds from the southwest. Only a small amount of low frequency energy was present.

A systematic increase in the reflection coefficient, with decreasing frequency from a macro-tidal, ridge and runnel beach at Nieuwpoort-aan-Zee, Belgium, has been reported (Huntley, 1996). This produced up to 90% reflection at very low frequencies of 0.08 Hz

and lower. There was some, possibly significant, reflection from incident frequencies between 0.1 and 0.3 Hz, but reflection at higher frequencies was insignificant.

2.3.9 Tidal variation in wave reflection

Few wave reflection results from meso- or macro-tidal natural beaches have been published (the Japanese beaches were micro-tidal and therefore any tidal signature in reflection cannot be assessed). However, those which do exist suggest a tendency towards higher reflection coefficients at high water, with the inevitable link to steeper beach gradients. For example, tidal stage had an important influence on the reflection coefficient at Felpham, West Sussex, where reflection generally increased with increasing shoreface gradient (Davidson *et al.*,1994). This beach is possibly the closest comparison with Morfa Dyffryn, since the area is macro-tidal and the beach consists of mixed sediments.

Elgar *et al.* (1994) derived reflection coefficients on the basis of a directional analysis of the energy spectrum, using a cross-shore transect of pressure sensors in 13 m of water (at the CERC Research Facility at Duck, NC, USA). Incident wave energy was derived as the sum of the energy from 180 to 360°, with offshore-propagating energy from 0 to 180°. These investigators found that swell and sea wave reflection ($0.044 < f < 0.2$) was greatest at high water, with reflection occuring from the steepest section of the beachface. For swell and sea waves, the reflection coefficient was approximately proportional to β^5.

Reflection coefficients have been derived also for the beach at Duck, using co-located current meter and pressure sensor in 6.5 m of water and at a second site at Ocean City, where the sandy beach had a nearshore slope of 0.06 (3.8°) (Walton, 1992). The co-located pressure sensor and current meter were located in just under 11 m of water. The analysis concentrated upon storm data from Duck, with dominantly swell waves (7 to 12 s peak period and 2 to 3 m H_{m0}). At Ocean City, the waves were shorter but were still substantial (1.6 m H_{m0}, offshore). At neither site was there any significant reflected energy at the major swell wave frequencies. Three days of records, at intervals of 3 hours, were examined. Therefore, the effect of the steeper beachface towards high water which was observed at Duck (Elgar *et al.*, 1994) may not have been discernable. However, the low level of reflected energy from the steep beach at Ocean City is

surprising; it suggests that the influence of wave energy (for the swell waves) overrides that of beach slope.

Reflection coefficients from a high energy, dissipative surf zone, using 4 cross-shore pressure transducers have been examined (Nelson & Gonsalves, 1990). Only the low frequency part of the spectrum was used to estimate reflection coefficients, since they considered that the assumption of linear wave motion between the cross-shore array of pressure transducers renders their method of analysis (*cf.* Mansard & Funke, 1980) invalid for wind wave frequencies. Consequently, the results were concerned with only low frequency waves. A consistent trend towards higher reflection coefficients around high water was noted, with greater variability at low water. The steeper beach gradient (maximum 0.04) at high water, together with increased turbulence across the wider surf zone at low water (and, hence, greater interference and suppression of reflected waves) were the possible explanations offered.

2.3.10 Implications of wave reflection from a composite beach

With the exception of the studies of Davidson *et al.* (1994) and Chadwick *et al.* (1995), all field data concerning wave reflection from beaches have been derived from sandy beaches. Hence, there are no published data for wave reflection from a composite-type mixed beach. Tidal variation in reflection is of particular interest for a composite beach such as Morfa Dyffryn, for a number of reasons, as outlined below:

(a) Wave reflection should vary systematically with tidal stage, in accordance with the change in shoreface gradient from which the waves are reflected. Hence, the link between reflection and beach gradient should be particularly distinctive at Morfa Dyffryn, given the marked break of slope between the sand and mixed sediment region of the composite beach;

(b) Tidal variation in the reflection from the sand/ shingle ridge will influence sediment transport across the profile which, in turn, suggests the importance of integrating sediment transport throughout the entire tidal cycle. In a macro-tidal region, this will vary throughout spring-neap tidal phases;

(c) Laboratory studies and field data obtained from porous breakwaters have shown that an increase in permeability leads to a reduction in wave reflection. Therefore, reflection coefficients from a mixed beach should be higher than from a shingle beach, of similar gradient, since less energy is dissipated through percolation.

Hence, the reflective signature of the relict sand/shingle bank at Morfa Dyffryn may enhance sediment transport. However, wave reflection is only one factor in the complex morphodynamic response of a beach, rather than an instinctive morphodynamic continuum of the type:

dissipative	<==>	intermediate	<==>	reflective
sand	<==>	mixed	<==>	shingle

the relationship between sand, composite and shingle beaches might be well be triangular.

2.4 Beach Groundwater

2.4.1 Introduction

The possible link between beach groundwater and sediment transport was first suggested by the pioneering work of Grant (1946, 1948); it hinges upon the state of saturation of the beach sediments. When the swash zone advances over an unsaturated beach (on a flooding tide), a proportion of the swash volume infiltrates into the bed, depositing its sediment load, particularly where the swash flow changes from turbulent to laminar (near the run-up maximum). The volume of the backwash is diminished considerably, compared to that of the swash, as its velocity in the early stages reduces the competence of the flow and, hence, the likelihood of sediment entrainment. Since the swash water depth is relatively shallow near the run-up limit, even a minor loss of volume (due to infiltration) can produce a significant decrease in the available energy of the backwash (Waddell 1976). The smaller the waves or the lower the beach slope, the more critical the losses caused by infiltration (Nelson & Miller 1974). On balance, less sediment is transported to seaward by the backwash, than is transported landwards and deposited by the swash. Conversely, during the ebb phase of the tide, the backwash

volume is not reduced by swash infiltration (and, indeed, may be augmented by water from seepage lower down the profile). Hence, entrainment thresholds are more likely to be reached during the backwash. Overall, the relative balance of sediment transport in the swash zone in response to the infiltration theory, is for deposition during the flood phase of the tide and erosion during the ebb.

The beach groundwater table fluctuates in response to tidal inundation, but also in response to wave action (for a detailed review of groundwater behaviour on beaches, see Baird & Horn [1996]). The rate of the rise and fall of the water table depends upon tidal range, beach geometry and sediment composition (which determines its hydraulic conductivity and specific yield). On sandy beaches, the water table rises rapidly with the flooding tide. However, the rate of fall of the ebbing tide can exceed that of the water table. This process results in the tidal elevation and the water table becoming decoupled; this leads to the development of a seepage face.

Further research on beach groundwater, over the last decade, has concentrated upon establishing, then modelling, the external controls on the level and the fluctuations in the water table and prediction of seepage zone development, rather than the direct influence of the water table on the transport of sand. The implications for sediment transport were recognised by Chappell *et al.* (1979), who maintained that the passage of pressure waves through the beach below the water table can induce liquefaction; this leads to slumping of the beachface, during storms. However, only now is research addressing the mechanisms by which beach groundwater interacts with swash/backwash, to affect the stability of the sediment and, hence, to address the fundamental influence of groundwater on sediment mobility, on beaches.

The inherently logical conceptual model, whereby infiltration of swash and backwash into unsaturated sand, is seen as the principal mechanism for beach erosion/accretion above the still water level (Grant, 1946, 1948), has been invoked for example, by Isaacs & Bascom (1949), Longuet-Higgins & Parkin (1962), Duncan (1964), Strahler (1966), Heathershaw *et al.* (1981), Lanyon *et al.* (1982*a*), Carter & Orford (1993) and Turner (1993*a*). However, the major limitations to the model are the time and space scales over which it is applicable. During a flood tide, across a medium to fine sand beach, only a few swashes are generally required to saturate the sediment; after this

the volume of water which can infiltrate a saturated sand bed becomes minimal. Therefore, the potential for enhanced deposition is limited to: (i) the first few swashes across unsaturated sand *i.e.* towards the run-up limit; and (ii) the section of beach profile to landward of the seepage face. Depending upon the tidal range, beach profile and sediment size, there may be phases of the tide when the infiltration theory (*sensu stricto*) is important for enhanced deposition. Other mechanisms must be found to account for interaction between beach groundwater and sediment transport, for the remaining stages of the tide; at such times, the swash advances over a saturated beachface.

Fluidisation of sand, due to seepage forces, is a another mechanism through which groundwater can affect sediment transport; this was also recognised previously (Grant, 1946) where it was suggested that dilation of the sand fabric (when saturated) may reduce the entrainment threshold. More recently, Baird *et al.* (1996, 1997) proposed that fluidisation is generally possible only in the presence of swash and it is limited temporally to the latter stages of backwash. These investigators suggested that fluidisation of the saturated sediment results from reversing pressure gradients, due to the loading/unloading cycle of a swash/backwash. Pressure can propagate rapidly through the saturated sediment, since the potential for infiltration is somewhat limited. Hence, when swash advances over a saturated sediment, the pressure acting on the sediment surface (*i.e.* the hydrostatic pressure of the wave) propagates downwards through the surface layers. During the backwash cycle, the pressure at the surface is released; this leads to the generation of large, upward-acting hydraulic gradients. Baird *et al.* (1996) reported that preliminary model tests indicate that this pressure reversal is a mechanism for potentially- enhanced sediment transport, under swash action. In contrast to the earlier (Grant) conceptual model, this process occurs potentially on the flood tide, in addition to the ebb. However, the relative importance of infiltration and fluidisation, to sediment transport, remains to be established (Weisman *et al.*, 1995; Turner & Leatherman, 1997).

Another unresolved problem relates to the influence of beach groundwater on flood/ebb asymmetry, in terms of suspended sediment transport; this has been noted previously for a macro-tidal beach, but attributed to bedform destruction by the ebbing tide (Davidson *et al.*, 1993). However, it was speculated also that exfiltrating groundwater may increase the turbulence levels in the backwash and dilate the sediment,

leading to enhanced entrainment. Certainly rilling can be observed in effluent zones, indicating an overland flow of about 1 ms^{-1}. Exfiltrating groundwater may also contribute to mean seaward flows.

2.4.2 Theory of groundwater movement [1]

This area of research incorporates two scientific disciplines, hydrodynamics and groundwater hydrology, each with its own well-established terminology. Inevitably, there is some overlap in the terms used, examples of which are given in Table 2.2; however, the context within which each term is used should be clarified.

Symbol	Groundwater	Hydrodynamics
H	hydraulic head (L)	wave height (L)
z	height above datum (gravitational head) (L)	height above sediment surface (L)
v	specific discharge through medium (LT^{-1})	longshore mean/ oscillatory current velocity (LT^{-1})
ψ	pressure head (L)	velocity moment
ϕ	(total) potential ($ML^{-1}T^{-2}$)	angle of repose of sediment
k	intrinsic/specific permeability (L^2)	wave number (L^{-1})
D	aquifer depth (L)	grain size diameter (L)

Table 2.2 Definition of terms used in this research programme, in relation to groundwater and hydrodynamics.

[1] Strictly, "groundwater" refers to water at or below the water table, with pore water pressures equal to, or greater than, atmospheric; any water present above the water table being termed "soil water". In reality, there is a continuum between the two types and, in so dynamic an environment as a beach, the division is probably arbitrary. For the purposes of this research, therefore, the term "groundwater" is used to refer to all interstitial water within the beach sediment, whether below or above the water table.

2.4.3 Energy potential of sub-surface water

The total potential energy of sub-surface water is expressed generally with reference to a hypothetical body of pure water, at atmospheric pressure and at a similar elevation and temperature. Accordingly, the relative potential energy can be assessed at different locations within a body of sediment. Then, patterns of groundwater flow can be predicted, since groundwater will flow in the direction of decreasing energy potential, at a rate proportional to the negative potential gradient ($-\partial\phi/\partial x$ or $-\partial\phi/\partial z$).

A number of factors contribute to the total energy potential of groundwater, ϕ_t, which at any location is expressed as (Hillel 1982):

$$\phi_t = \phi_g + \phi_p + \phi \ldots \quad (2.28)$$

ϕ_g is the potential due to gravity and ϕ_p that due to pressure (also known as matric potential). Other potentials can occur *(e.g.* the potential due to osmotic forces) but are sufficiently small, in comparison to the other two forces to be disregarded. Pressure potential is the sum of several parts. However, for measurements below the water table on beaches, the dominant component is the hydrostatic pressure of water below the water table:

$$\phi_p = \rho g h \quad (2.29)$$

where ρ is the mass density of the fluid, g is the acceleration due to gravity and h is the depth between the free-water surface and point of measurement. Since the reference potential is at atmospheric pressure (therefore zero potential), the pressure potential below the water table is positive and increases with depth. Above the water table, the pressure potential may be negative (sub-atmospheric) due primarily to capillary forces. Capillary forces result from surface tension of water in contact with sediment particles; they are of considerable importance for flow through unsaturated sediments.

Total potential is difficult to measure and for convenience, many measurements of groundwater are made in terms of energy per unit weight *i.e.* the height of a vertical

column of liquid corresponding to the given pressure, referred to as hydraulic head (H). Eqn (2.28) could also be represented as:

$$H = H_z + H_p \tag{2.30}$$

H_z (elevation or gravitational head) is expressed, usually, relative to a base level; it is, therefore, the height between the measurement point and this arbitrary datum (Figure 2.1). As explained in Section 2.4.6 (below), Chart Datum is used in this research to represent the reference level for beach groundwater calculations. H_p (pressure head, ψ) is the length of the column of water above the point of measurement. Hence, in the present study, the data from dipwells fitted with pressure sensors are readings of pressure head; the elevation head being the distance from Chart Datum to the sensor, as illustrated by Figure 2.1.

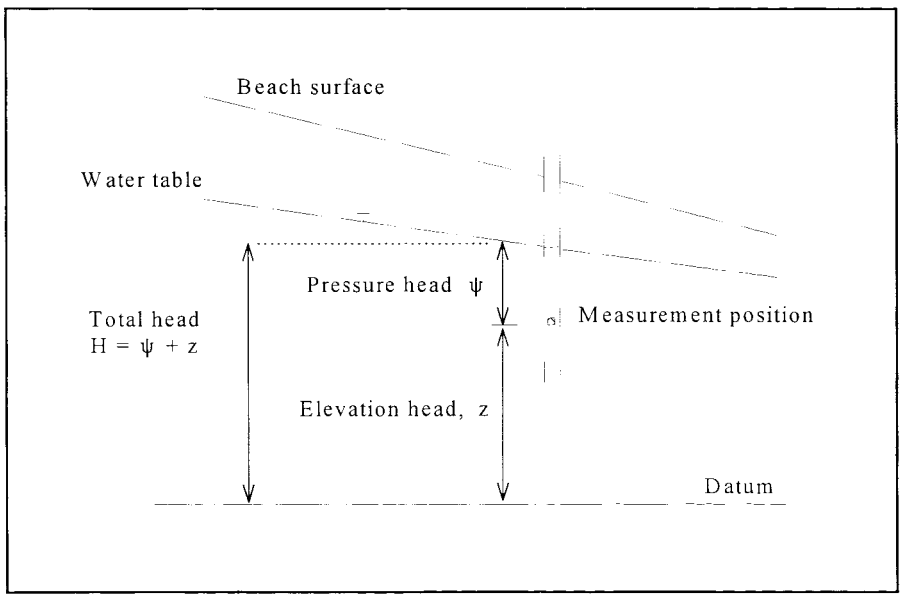

Figure 2.1 Definition of components of hydraulic head (after Ward & Robinson 1991)

There is some confusion in beach groundwater literature concerning the terms dipwell/stilling well/standpipe piezometer and piezometer; these have been usedsomewhat indiscriminately and interchangeably (*e.g.* Dominick *et al.*, 1971; Nicholls, 1985; Nielsen, 1990*a*; Hegge & Masselink, 1991; Aseervatham *et al.*, 1993;

Turner, 1993*b*; Kang & Nielsen, 1994). A well open to the atmosphere and perforated throughout its length measures the elevation of the water table. Such an observation may be quite different from the water level measured by a piezometer (perforated over only a small region, at the bottom of the pipe), which measures the hydraulic head at the position of the perforations. *Only* if groundwater flow is essentially hydrostatic (*i.e.* horizontal, gravity-driven) will the two readings be the same.

2.4.4 Darcy's Law

Groundwater movement is described usually on a macroscopic basis *i.e.* it is assumed the volume of sediment is sufficiently great relative to the size of pores and small heterogeneities, so that an "average" velocity of water through the sediment can be considered (Hillel, 1982). The flux, q, through a saturated sediment is proportional to the hydraulic gradient across the flow and is described by Darcy's Law:

$$q = \frac{Q}{A} = -Ki \tag{2.31}$$

where Q/A is the volume of water flowing through a unit cross-sectional area of sediment, A, in unit time and i is the hydraulic gradient. K is the constant of proportionality referred to as hydraulic conductivity and has units of LT^{-1}. Darcy's Law is valid only for laminar flow through the sediment since the relationship between hydraulic gradient and flux discharge become non-linear when flow is turbulent (Shaw, 1988).

2.4.5 Equations for groundwater flow

Groundwater flow through an unconfined aquifer to a river, where the surface permeable bed overlies a horizontal impermeable layer, is shown in Figure 2.2. This situation is not dissimilar to that relating to a beach, with the river replaced by mean sea level. Apart from the area close to the seepage zone, the total hydraulic head (or potential) does not change with depth.

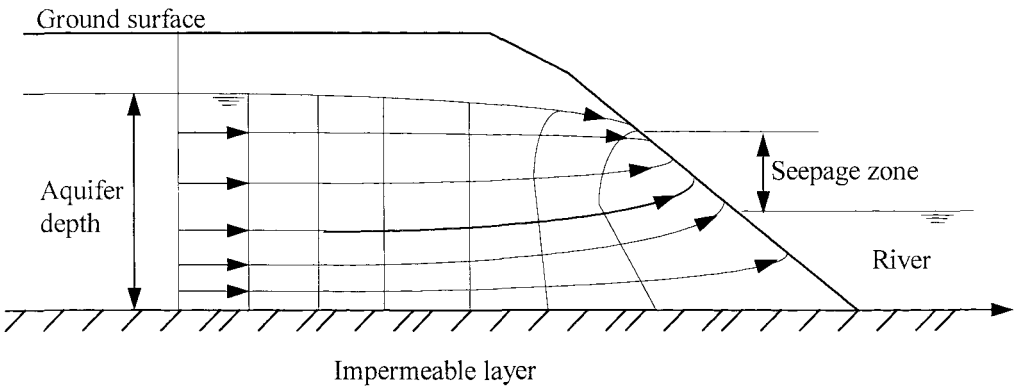

Figure 2.2 Schematic diagram of unconfined flow from an aquifer (after Shaw, 1988)

Therefore, there is no vertical flow component *i.e.* pressures are hydrostatic, the lines of equal hydraulic head (equipotential lines) are vertical and groundwater flow is essentially horizontal. The water table is, in effect, the upper boundary of the saturated aquifer and its slope represents the hydraulic gradient at that point. In order to calculate groundwater flow towards the river, as shown in Figure 2.2, the following assumptions are made:

(a) the hydraulic gradient ($\partial h/\partial x$) equals the slope of the water table; and
(b) specific discharge is constant with depth.

These assumptions of horizontal groundwater flow through a shallow aquifer are known at the Dupuit-Forchheimer approximation; they are used widely for the solution of unconfined groundwater flow into a shallow sink (Hillel, 1982). Providing the assumptions are valid, two-dimensional groundwater flow can be represented adequately by a one-dimensional version of Darcy's Law:

$$q = -Kh\frac{\partial h}{\partial x} \tag{2.32}$$

where q is the groundwater discharge per unit width, h is the elevation of the water table above a given datum (the aquifer depth), K is hydraulic conductivity and x is the horizontal distance over which ∂h is measured. The approximations cease to be valid

immediately adjacent to the seepage zone. However, providing the variation in the aquifer depth is small compared to its overall depth and the slope of the water table is low, (2.32) has been found to provide satisfactory predictions of q (Shaw, 1988).

Strictly, Darcy's Law is applicable only to describe steady flow processes. The expression must be combined with the mass-conservation law, to provide a general equation for non-steady or transient flows, when potential and fluxes vary throughout time (Hillel, 1982). In situations where the Dupuit-Forchheimer assumptions may be considered valid, (2.32) is combined with a one-dimensional form of the continuity equation:

$$\frac{\partial h}{\partial t} = -\frac{1}{s}\frac{\partial q}{\partial x} \tag{2.33}$$

to provide the one-dimensional form of the Boussinesq equation (Boussinesq [1904] as given by Fetter [1994]):

$$\frac{\partial h}{\partial t} = \frac{1}{s}\frac{\partial}{\partial x}\left(Kh\frac{\partial h}{\partial x}\right) \tag{2.34}$$

For eqns (2.33) and (2.34), s is specific yield, t is time and the remaining variables are as for (2.32). In this format, the Boussinesq equation is applicable to saturated flow. An additional term was added by Parlange & Brutsaert (1987), to account for mass transfer of water between the water table and capillary fringe due to capillarity effects (after Barry *et al.*, 1996):

$$n_e\frac{\partial \eta}{\partial t} = K\frac{\partial}{\partial x}\left(\eta\frac{\partial \eta}{\partial x}\right) + B\frac{\partial^2}{\partial t\,\partial x}\left(\eta\frac{\partial \eta}{\partial x}\right) \tag{2.35}$$

where n_e is the effective porosity of the sand, B is the thickness of the capillary fringe, η is the height of the free surface of the aquifer (*i.e.* the water table) and the remaining terms are as for (2.34). Barry *et al.* (1996) confirmed that the need to include capillarity effects is likely to be confined to beaches with small-grained sediments of relatively low hydraulic conductivity. The effect of capillarity is unlikely, therefore, to be of importance

on shingle beaches or on mixed beaches where the sand component consists of coarse or medium sand.

2.4.6 Hydraulic conductivity

Hydraulic conductivity, K, is a function of both the sediment properties and the fluid flowing through it. The controlling factors for K are porosity, sediment size and grading (which, together, determine the distribution of pores and the path through which the fluid is conducted, called tortuosity) and the density and viscosity of the fluid (Hillel 1982). Typical values of K are presented in Table 2.3. Although it has units of velocity, K represents an average value for the flux through a cross-sectional area. Since the flux is transmitted only through the pore spaces of the sediment, the actual flow velocity through the sediment is greater than the flux, q by approximately a factor of the porosity.

Sediment	K (ms^{-1})
Gravel	0.16 to 0.04
Coarse sand	0.01 to 0.0065
Medium sand	0.001
Fine sand	0.0001

Table 2.3 Typical values of hydraulic conductivity (British Standards Institution, 1990)

Some confusion can exist over use of the term *permeability*, which is not the same as hydraulic conductivity. Attempts have been made to apportion hydraulic conductivity into a component due to the sediment properties alone (*i.e.* the intrinsic permeability of the sediment, k) and that due to the fluid, f. The relationship between hydraulic conductivity, K, and intrinsic permeability, k is:

$$k = \frac{K\mu}{\rho g} \tag{2.36}$$

where μ and ρ are, respectively, the dynamic viscosity and density of the fluid and g is the acceleration due to gravity. Although fluidity will change with varying temperature,

in particular, for this research the temperature and density of groundwater within the beach will be considered constant during the period under investigation. Laboratory calculations of K will be corrected for temperature effects.

2.4.7 Forces driving beach groundwater fluctuations

The elevation of the water table within a beach at any time, $Z_{\eta(t)}$, can be defined as the sum of three elements, which will be examined separately in relation to their individual forcing mechanisms:

$$Z_{\eta(t)} = Z_o + Z_{tide} + Z_{wave} \quad (2.37)$$

It should be noted that other contributions to groundwater fluctuations may originate from very long period waves *i.e.* longer than 100 seconds (Lewandowski & Zeidler, 1978), shelf waves or bay seiches (Lanyon *et al.*, 1982*b*); however, these will not be considered further, since the record length of the field data collected is insufficiently long to resolve these very long period waves.

Z_o marks a level about which oscillations of the water table are described. Classical drainage theory for tidal groundwater fluctuations places the mean elevation of the water table at the shoreline at Mean Sea Level (Jacob, 1940, quoted in Turner, 1995*a*). Although recent research has shown that the water table can remain elevated above MSL, this remains a commonly used datum (*e.g.* Nielsen 1990*a*, Hegge & Masselink 1991). However, nearly all published fieldwork on these fluctuations has taken place on micro-tidal beaches (Table 2.4), where the super-elevation can be up to 1.5 m (Turner, 1993*a*). MSL has less physical meaning on a macro-tidal beach, given the rapidly-varying residence time of the swash zone across the beachface.

Although, ideally, the existence and location of an impermeable barrier should be established, for this study the elevation of the Lowest Astronomical Tide (LAT) will be used to represent Z_o and provides, consequently, both seaward and lower boundaries. The LAT is defined, in the UK, as the lowest sea level which can be predicted to occur under average meteorological conditions and under any combination of astronomical conditions

Beach Groundwater Field Experiments					
Author	Location	Tidal range/ Sediment type	Instruments	Sampling Frequency	Comments
Emery & Foster (1948)	El Segundo Beach and Marine St Beach, La Jolla, California	Sand	1" diameter perforated wells	30 - 60 minutes, for 12 hours	Measured water table 20 - 40 ft from shoreline
Duncan (1964)	Manhattan Beach, USA	Sand	Holes	30 minutes, for 1 tidal cycle	Primarily study of sediment lenses transported by swash
Ericksen (1970)	New Zealand	Fine sand Coarse sand			
Dominick *et al.* (1971)	Galleon Beach, Grand Cayman Is.	Sand Md 3.03 ϕ	3.2 cm diameter piezometers	Hourly, for 48 hours	Data to calibrate mathematical model, for groundwater fluctuations in water table (vertical beachface) over tidal scale
Harrison & Boon (1972)	Virginia Beach, USA	1 m / Sand	13 wells with Potentiometers	10 - 15 minutes, for 31 days	New equipment for automatic recording of groundwater fluctuations
Waddell (1976, 1980)	Little Talbot Is, Florida, USA	1.3 m / Medium sand	Wells with capacitance sensors	10 minutes to 1 hour +	
Lewandowski & Zeidler (1978)	Lubiatowo Beach, Poland		Piezometers		
Chappell et al (1979)	Durras Beach, Australia	Sand	"Spear-point wells" (Piezometers)		Early experimental field tests for beach pumping schemes
Lanyon *et al.* (1982*a, b*) Eliot & Clarke (1988)	South Beach, Wollongong, Australia	0.9 to 1.3 m / Sand (D_{50} 0.35 mm)	3 wells each on 2 profiles	30 minutes, for 50 hours	

Author	Location	Tidal range/ Sediment type	Instruments	Sampling Frequency	Comments
Nicholls (1985)	Hurst Castle Spit, UK	1.1 m, 2.4 m / Shingle barrier	6 Standpipe piezometers	Manually, every 20 minutes, 3 tides (2 spring, 1 neap)	Examined seepage across a shingle barrier
Clarke & Eliot (1987)	City Beach, W. Australia		Well 500 m landward of shoreline	7 year record, at monthly intervals	Linked annual groundwater fluctuations with annual shoreline changes
Nielsen *et al.* (1988)	Dee Why Beach, Australia	Sand (0.3 mm)	8 Stilling Wells (dipmeter)	30 minutes, for 2 x 24 hours (plus landward well hourly for 3 months)	Used manometers to link water table changes to variations in set-up *etc* due to changing wave conditions
Nielsen (1990)	Barrenjoey Beach, Australia	c. 1 m / Sand	11 Stilling Wells	30 minutes, for 25 hours	Used harmonic analysis to examine lags in water table response to tide
Hegge & Masselink (1991)	South City Beach, W. Aus.	0.6 m / Sand (0.35 mm)	1 Piezometer (with capacitance wire probe).	4 Hz, for 35 minutes	Resistance wires for run-up. First high-frequency measurements to assess contribution of waves to water table changes
McArdle & McLachlan (1991)	Southern Africa & west coast USA	2.1 m / sand 3.6 m / sand	Swash poles	15 minutes, for 12 hours	Manual recording of "effluent line" crossings on dissipative, intermediate and reflective beaches
Vanek (1991)	Laholm Bay, Sweden Little Pond, Cape Cod, USA	Both 0.1 to 0.5 m	Piezometers		

Author	Location	Tidal range/ Sediment type	Instruments	Sampling Frequency	Comments
Turner (1993*a*)	Pearl Beach, Ocean Beach, NSW, Aus	1.2 m / Sand (0.3 mm) Fine sand	Neutron probe Stilling wells	Low, mid and high tide	Saturation levels through beach profile
Turner (1993*b*)	North Harbour Beach, Queensland, Aus	up to 6 m Sand	14 stilling wells with capacitance probes	1.15 Hz, for 18 hours	Field data for testing of model to predict position of seepage face
Kang *et al.* (1994*a*)	Palm Beach, Pittwater Beach, NSW, Aus	1.5 m		Variations over 5 days	Comparison of water table overheight due to waves
Kang *et al.* (1994*b*)	5 beaches, Australia	Sand	Stilling wells	Manual measurements at 15-30 minute intervals, 2 tidal cycles	
Turner (1995*a*)	Lennox Head, NSW, Australia		Seven wells (1m intake), with PT	15 minutes	FFT of well data (10 to 160 hours)
Baird *et al.* (1996*a*)	Canford Cliffs, UK	< 2 m / Sand	10 dipwells (PT's) 10 piezometers, 4 with PT's	18 minutes, at 4 Hz every 20 minutes for 3 days (2 deployments)	Data used for validation of GRIST model
Turner & Nielsen (1997)	Assateague Is, Maryland, USA	1 m / Sand	PT's buried in sand	17 minutes, at 8 Hz	Measured pore water pressures in swash zone

Table 2.4 Beach groundwater field experiments, abstracted from the publications of various authors

(Hydrographer of the Navy 1996). The use of LAT to represent Z_o has a number of advantages, as outlined below:

(a) The avoidance in defining MSL, which may prove unreliable in areas with asymmetric tides or a large tidal range; also additional definitions of Mean Water Surface (MWS) or Still Water Level (SWL), which will not necessarily correspond to MSL due to the effects of set-up and set-down. In addition, the datum is fixed; it will not vary either fortnightly or seasonally, as may be the case with MSL. Therefore, clear comparisons can be undertaken between spring and neap tides.

(b) In the UK, survey data used to record beach profiles and instrument locations can be adjusted readily to the elevation of Chart Datum, on Admiralty charts), since the relationship of CD to Ordnance Datum is established at various locations. Hence, predictions of Z_{tide} at the beachface can be derived directly from Admiralty Tide Tables.

(c) The beach water table is unlikely to be lower than CD, even during Extreme Low Water Spring Tides; hence, all water table elevations will be positive.

(d) This approach provides the required (arbitrary) base level for head calculations and the construction of flow nets.

$\boldsymbol{Z_{tide}}$ represents the fluctuations in the water table elevation, above Z_o, due to tidal forcing. The amplitude of tidally-forced groundwater fluctuation attenuates to shoreward of the beachface (Emery & Foster, 1948; Erickson, 1970). Such landward dampening can be identified within 10 m (Nielsen, 1990*a*; Turner, 1993*a*), but can extend up to 30 m (Turner *et al.*, 1997). The inland position, where oscillations of the water table due to tidal forcing are negligible, is used as the landward boundary in some analytical models for tidally-forced groundwater oscillations (e.g. Dominick *et al.*, 1971; Nielsen, 1990*a*).

The tidal response of the water table is not sinusoidal, but asymmetrical; it rises steeply with a flooding tide, but falls more slowly during the ebb (due to the capacity of the beach sediment to store seawater). For example, on a flooding tide the entire beach

profile up to the high water mark becomes sequentially available for infiltration. In contrast, during the ebb, drainage can take place only from the seepage zone seawards *i.e.* there is a smaller surface area through which the beach can drain. This pattern leads to a non-linear lag between the rate of fall of the tide and the corresponding fall in water table (Erickson, 1970; Dominick *et al.*, 1971; Nielsen, 1990*a*). Hence, the water table and the tidal level may become de-coupled during the ebb. Such de-coupling, with the subsequent development of a seepage zone, has important consequences for sediment transport; this will be discussed further in Section 2.4.6 (below). A further consequence of the asymmetric response of beach groundwater to tidal inundation is that the water table slopes in a landward direction during the flood, but seawards during the ebb (Emery & Foster, 1948; Erickson, 1970). The asymmetric response means also that the water table can extend above the mean sea level. Nielsen (1990*a*) approximated this over-height using:

$$h_{\infty} = \frac{h_o^2}{4d} \tag{2.38}$$

where h_{∞} is the inland over-height of the water table above MSL, h_o is the amplitude of the tide and d is the aquifer depth (after Turner & Nielsen, 1997). Eqn (2.38) predicts that the over-height can be up to 25% higher than MSL, in the case of a shallow aquifer of a similar depth to the tidal amplitude. However, (2.38) was derived for a vertical beachface; even second-order solutions have not been able to compensate adequately for the non-linear effects of the sloping beach (Turner *et al.*, 1997).

Z_{wave} is the oscillation of the water table, due to individual waves or groups of waves, in the swash zone. In 1988, Eliot & Clarke reported that the existence of Z_{wave} remained unresolved. Since then, it has been established that groundwater fluctuations can occur on a shorter time scale than Z_{tide} ; however, the mechanisms of generation and the period of the oscillations remain in doubt.

Some earlier field studies concluded that waves did not materially influence the water table. For example, Lanyon *et al.* (1982*a*) analysed the varying groundwater level in wells at 30 min intervals for 2 days; they concluded that swash run-up and infiltration had no effect on the groundwater levels to landward of the berm crest. However,

groundwater measurements obtained at 30 min intervals would not identify any such effect. More recently, a comparison of the water table response, on two nearby beaches in Australia, has suggested that wave action influenced the water table (Kang *et al.*, 1994*a*). Both beaches were subject to the same tidal regime, but one was open to ocean waves; the other was protected. Wave activity raised the water table by up to 0.7 m on the exposed beach, compared with the sheltered beach. Wave action, through swash excursion, was held to be responsible for elevated groundwater levels on a micro-tidal beach in the UK (Baird *et al.*, 1996).

In the absence of any tidal variation, the contribution of wave run-up to the inland over-height of the water table (*i.e.* the mean height of the water table above mean sea level) was correlated with the surf similarity parameter ξ (Battjes, 1974). The calculations were based upon from laboratory studies, using the relationship:

$$\overline{\eta}_{\infty} = 0.62 \tan \beta_F \sqrt{H_i L_o} \qquad (2.39)$$

where $\overline{\eta}_{\infty}$ is the asymptotic inland watertable over-height, β_F is the slope of the beachface, H_i is wave period and L_o is deep water wave length (Aseervatham *et al.*, 1993; Kang *et al.*, 1994*a*). When calibrated for field conditions, H_i was replaced by the deep water rms wave height and the coefficient in (2.39) is reduced to 0.55 (Kang *et al.*, 1994*a*; Nielsen & Kang, 1995). Laboratory experiments undertaken on an equilibrium beach profile identified that the higher the permeability of the sediment, the lower the wave-induced over-height of the water table (Gourlay, 1992). However, (2.39) implies that the over-height due to waves is dependent solely on the prevailing wave conditions (height and period) and beach slope, rather than being dependent directly on the hydraulic conductivity. Hence, the effect of permeability may be "more apparent than real" (Gourlay, 1992). However, since beach slope and sediment size are intimately linked, it remains difficult to attribute the over-height to one or the other controlling factors.

High-frequency measurements have suggested that the beach groundwater level can respond to individual waves; several mechanisms have been identified as being responsible for these rapid changes in water table elevation. Waddell (1976) referred to fluctuations of the water table over periods of 8 to 11 s in a well located just to landward

of the highest swash. The oscillations were attributed to pressure forces created by breaking waves and transmitted through the saturated sediments, rather than the addition of infiltrating water. A similar conclusion was reached by Chappell *et al.* (1979), who recorded high frequency water table fluctuations near the swash limit; these were of longer period than the primary waves, since swash interference meant that only the larger swash run-up influenced the water table at the measuring position. The rising phase of the groundwater oscillation was found to precede the arrival of the swash wave at the measuring position, by up to several seconds; this suggested that pressure propagation influenced high-frequency groundwater oscillations more than infiltration.

Hegge & Masselink (1991) considered that the beach water table responds to a combination of pressure forces and water input. Resistance wire measurements of swash run-up were compared to fluctuations in groundwater, measured using a piezometer; it was found that the "groundwater" maxima lagged the swash maxima by an average of 4s. However, the fluctuations recorded by a piezometer, as described by Hegge & Masselink (*op. cit.*), do not necessarily represent the response of the water table (Section 2.4.3). *Only* if groundwater flow through the beach is shown to be hydrostatic (horizontal) will the records produced by a piezometer and dipwell be the same. It is likely that hydrostatic conditions do prevail on sandy beaches (Baird *et al.*, 1996), except within the seepage zone. However, they remain unproven for shingle or mixed beaches. The use of a single piezometer by Hegge & Masselink (1991) means that the fluctuations cannot be partitioned into those due to pressure transmission or infiltrating groundwater.

However, infiltrating water can lead to rapid fluctuations of the water table due to the reversed Wieringermeer Effect, as follows: the effect results from the presence of a capillary fringe above the water table (Turner & Nielsen, 1997). Within this fringe, although the sediment pores approach 100% saturation, the moisture is held by capillary forces. Thus, the pore water pressures in the capillary fringe are lower than atmospheric pressure; in contrast, the pressures at and below the water table, are at atmospheric pressure and greater than atmospheric pressure, respectively (by definition). A field experiment has demonstrated that with the addition of only a small quantity of infiltrating water, the potential surface (the water table) can "rise" through the sand sediment by 0.3m in 15 s (Gillham, 1984). However, the response time was considered to be longer than anticipated, due to air entrapment. Conversely, laboratory experiments have shown that

a rapid fall in the water table can follow a small amount of drainage (Nielsen *et al.*, 1988). The capillary fringe, in fine and coarse sands, can be of the order of ~0.5 to ~0.15 m, respectively; it is only ~0.015 m for fine gravel (Fetter, 1994). Turner's (1993*a*) neutron probe measurements have confirmed the existence of a capillary fringe in a sandy beach. Field evidence of rapid water table rise through the capillary zone on a sandy beach refuted a prevailing (but erroneous) idea that somehow the rising water table was caused, or accompanied, by high upward flow velocities (of ~ 0.1 ms^{-1}); these were deemed responsible then for liquefaction (*e.g.* Chappell *et al.*, 1979).

Although groundwater has been shown to respond to individual waves, it may not necessarily be at the same frequency. Despite the rapidity of the groundwater fluctuations observed by Turner & Nielsen (1997), spectral analysis of the time-series showed that the oscillation was not at the frequency of either the gravity or infragravity waves; it was at a considerably longer time scale, of around 0.006 Hz, (167 s). Hence, fluctuations were not a direct response to the ambient waves measured only 20 m to seaward.

In contrast to the results above, Waddell (1976) observed that the water table responded instantaneously to the waves. This discrepancy has been explained in terms of the balance between two different mechanisms, causing the high-frequency response of the groundwater (Li *et al.*, 1996*a*) . The first mechanism is the horizontal mass transport of water from the beach face, landwards through the saturated sediment. The rise in the water table results from mass conservation of the flux of water. The amplitude and phase lag of the oscillations, forced by this mechanism, are attenuated landwards at a rate determined by the magnitude of the oscillation at the beachface and the hydraulic properties of the sediment. The second mechanism is related to changing pressure within the capillary fringe due to a local mass transfer of water across the water table. Pressure at the top of the capillary fringe remains generally static (over the time-scales for waves, under consideration here). Therefore, a change in pressure within the capillary fringe (which is, by definition, at sub-atmospheric pressure) will result in an instantaneous change in position of the water table (by definition, the level of zero pressure). Thus, there is no phase shift between the sea level oscillation and the groundwater response, although there is landward attenuation.

Accordingly, Li *et al.* (1996*a*) attributed instantaneous fluctuations in groundwater at wave frequencies (such as those observed by Waddell [1976]) to pressure forces, which operate through the effect of capillarity.[2] Similarly, fluctuations at tidal frequencies were considered to be due to the horizontal mass transfer of water, with attendant increasing phase lags and attenuation to landward.

Hegge & Masselink (1991) observed that pressure forces are likely to dominate to seaward of the seepage zone, whilst infiltration is of more importance to landward; the reversed Wieringermeer Effect may be significant, just to landward of the water table outcrop. Clearly the interpretation of field results is very sensitive to the measuring position relative to the swash run-up and the tidal stage (ebb or flood). Furthermore, establishing exact correlations between wave and groundwater fluctuations can be hampered by the response time of the measuring instruments.

2.4.8 Factors controlling water table oscillations

There are three major factors which control the response of the water table to tidal/wave forcing; these are summarised below:

(a) Tidal range determines the proportion of the beach face which is inundated each tide, and the time of coverage/exposure (which, in turn, will vary according to the Spring-Neap cycle) and any local flood/ebb tide asymmetry. Harmonic analysis of water level fluctuations in a groundwater well can enable an assessment of the contribution of each tidal constituent, to groundwater fluctuations (Lanyon *et al.*, 1982*b*).

(b) Sediment composition, on the basis of the relationship between hydraulic conductivity and sediment size (less well established for mixed/poorly graded sediments). Overall, the hydraulic conductivity for mixed/layered sediments is controlled by the 10% finest fraction of the grain size distribution. The grain size defines the likely height of the capillary fringe. There is also an important link

[2] Note that this should not be confused with the the reversed Wieringermeer Effect, which also operates through the capillary zone, but which entails downward infiltration of water.

with the antecedent moisture characteristics. Once saturated, finer sediments hold water longer and release it more slowly than for coarser materials. Similarly, perched water tables may be present, particularly on beaches consisting of mixed sediment.

(c) The beach profile has been shown to be of great importance by the early analytical models for tidally-forced groundwater changes. These were based upon a vertical beachface solution, which was found to be unsatisfactory (Nielsen *et al.*, 1988). Only when equations for a sloping beach face were developed, did the models begin to reproduce field conditions adequately. As suggested by Turner *et al.* (1995*a*), water can "fill" the beach vertically during the flood, but must drain more or less horizontally during the ebb, and similarly, on the scale of swash (Hegge & Masselink, 1991).

Together, the above factors determine the flood/ebb tide asymmetry in the water table response to the tidal translation *i.e.* whether/where the water table and the tide will become de-coupled, with subsequent development of a seepage zone. The occurrence of this de-coupling is reasonably well documented for sandy beaches; its relevance to mixed/shingle beaches remains to be resolved.

Recently, the importance of the seepage zone for sediment transport has been recognised. The location and cross-shore translation of the seepage zone influence swash zone sediment transport in three ways (Turner, 1995*a*): (i) net loss/addition of swash/backwash water volume, through infiltration/exfiltration; (ii) de-stabilisation and fluidisation of the sediment surface, due to seepage forces (Nielsen, 1992, Baird *et al.*, 1996); and (iii) changes in horizontal shear stresses at the bed, due to changes in boundary layer flow. At present, none of these controlling factors has been incorporated into a complete description of sediment transport.

2.4.9 Modelling beach groundwater

Despite early attempts to model analytically groundwater fluctuations, due to tidal oscillations alone (Dominick *et al.*, 1971; Harrison *et al.*, 1971; Fang *et al.*, 1972; Nielsen, 1990*a*), the following complications have prevented the provision of an

analytical solution of groundwater to combined wave/tidal fluctuations (Turner *et al.*, 1997): a sloping beachface; seepage zone development; state of saturation of sediment within the swash zone.

Two models have been developed recently, to predict the location and timing of the seepage zone on a sand beach. Turner's SEEP model (1993*b*, *c*, 1995*a*, *b*) is an analytical solution, which predicts the critical rate of fall of the tide for de-coupling of the tide and water table:

$$V_{ep} = -\frac{K}{n}\sin^2\beta \qquad (2.40)$$

where V_{ep} is the exit point critical velocity, K is the hydraulic conductivity, n here is the specific yield and β is the beach slope. When the rate of fall of the tide, V_{tide}, exceeds V_{ep} then de-coupling occurs. Eqn (2.40) was used to derive a seepage face parameter, Σ:

$$\Sigma = \frac{\pi R_T}{T}\frac{n}{K\sin^2\beta} \qquad (2.41)$$

where R_T and T are the tidal range and period, respectively (with the remaining variables as for 2.40). A seepage face is predicted to develop where $\Sigma > 1$. Output from the SEEP model was found to replicate well the seepage face development on a macro-tidal beach, once a correction factor for wave run-up was incorporated (Turner 1995*b*).

In contrast, Baird uses a finite difference scheme (Baird & Horn, 1996; Baird *et al.*, 1996, 1997) based upon the one-dimensional Boussinesq equation (2.35) and a simple de-coupling criterion, to model the response of groundwater to tidal forcing. The model (GRIST) predicted well both the water table fluctuations and the development of a seepage zone, over several tides on a micro-tidal sand beach. Given that the model has been validated for a sandy beach, an early version of GRIST will be used in this research; it will examine the response of groundwater to tidal forcing on a mixed beach, in comparison to that on a sandy beach. The GRIST I model will be described in more detail in Chapter 9. The GRIST model was modified subsequently to consider two-dimensional flow where the water table is considered as a free surface. This approach

permits the prediction of radial flow and represents more realistically the physical reality of seepage face development. Further work is ongoing elsewhere, to include swash waves superimposed upon tidal oscillations (Baird, pers. comm.).

Li *et al.* (1996*b*) developed a comprehensive Boundary Element Model, to simulate groundwater fluctuations due to tides; it incorporates seepage face dynamics. This model was modified subsequently to include the mass transfer of water through the capillary fringe and to account for the high-frequency oscillations due to waves (Section 2.4.7) but without the reversed Wieringermeer Effect (Li *et al.*, 1996*a*). As yet, the model remains to be tested against field data. A further development of the model was to simulate the effect of beach drainage (Li *et al.*, 1996*c*).

2.4.10 Beach groundwater numerical and laboratory experiments

Despite the prevailing view that erosion/accretion above the still water level is due to relative infiltration losses (Section 2.4.1), there have been few experiments to validate this theory by modelling swash and backwash infiltration. Packwood (1983) modelled numerically the effect on wave run-up of infiltration into a sandy bed, on a plane laboratory sand beach. Run-up on a fine sand beach was found to be very similar to that on a roughened impermeable slope *i.e.* infiltration was almost negligible. In contrast, on a medium sand beach, maximum run-up was reduced slightly, whilst the depth of the backwash was reduced considerably. Hence, Packwood (*op. cit.*) concluded that the effects on infiltration are more significant for backwash, than for swash. It was acknowledged also that the effect is only likely to occur during the latter stages of the rising tide, when the water table is at a reasonable distance below the sediment surface.

Results of laboratory experiments to examine the over-height of the water table in a sand beach, due to run-up of regular and irregular waves (Aseervatham *et al.*, 1993; Kang & Nielsen, 1994; Kang *et al.*, 1994*a*), have been discussed in Section 2.4.7. The remaining laboratory experiments, discussed below, were conducted mainly for beach pumping schemes; they can help to isolate the response of the beach profile, to varying levels of groundwater. However, at present, these results shed little light on the mechanisms by which these profile changes are achieved.

Ogden & Weisman's (1991) and Weisman *et al.*'s (1995) laboratory tests included the influence of tidal range and the flow rate from the beach drain. With a constant SWL (*i.e.* no tide) and under an erosive wave regime, the beach developed a steeper upper beach face with more pronounced berm when the beach drain was in operation, but erosion was greater below the SWL. During accretive conditions, the beach drain made little difference to the behaviour of the profile. In general, the effect of the drain should be noticeable also in the record of swash run-up *i.e.* there should be more swashes when the drain is operating, since the weaker backwash should interfere less with the subsequent swash. The laboratory tests undertaken found that the period of the uprush, under erosive wave conditions, does decrease with the beach drain; however, this occurs only until the developing berm becomes sufficiently steep for the gravity-aided backwash to cause, once again, swash/backwash interference. Under all other wave conditions, the drain made little difference to the period of the swash.

Under laboratory tidal cycles and accretive conditions, the tidal influence on the profile response was clear. Once again, the beach drain made little difference other than causing a slightly steeper berm near the swash limit. For the slightly erosive regime, the beach drain produced a more pronounced berm at the swash limit, but also showed enhanced erosion (particularly between the MWL and low tide levels).

In contrast to the results above, Sato *et al.*'s (1994) laboratory simulation of a drainage system was found to enhance deposition under an accretional wave regime. Even under erosive wave conditions, accretion occurred on the beach face; less erosion took place offshore, than occurred without pumping. These investigators suggested that the drainage system induced a shoreward flow, which could overcome the wave-induced offshore flow (such as undertow); this lead to lower erosion rates, even during erosive wave conditions.

The impact on the beach profile of a variable groundwater level, within a laboratory sandy beach, was examined by Oh & Dean (1994). When the water table was maintained at the level of mean sea level, sediment was transported both onshore and offshore, leading to bar and berm formation. However, a high water table combined with wave-induced set-up led to strong onshore transport at the berm and to landward of the offshore bar. Minor erosion was confined to the trough and to seaward of the bar.

Hence it was concluded that transport was confined to areas of pre-existing marginal stability only. These results are in direct contrast to the notion that a high water table should lead to offshore transport and net erosion. Subsequent lowering of the water table, to a level below mean sea level, led to little overall change in the profile.

Another interesting, but unexpected, conclusion was that the effect of the higher water table seemed to extend far offshore. The zone of influence of the lower water table was much more restricted, since the downward flow of water stabilised the sediment. Oh & Dean's (*op. cit.*) numerical modelling of flow within the beach suggested that high groundwater levels enhanced flow within the beach and produced maximum outflow velocities of 0.4 cm s^{-1}. However, the effect of upward flow within the beach was of minor importance, compared with the effect of steep beach slope.

2.4.11 Rôle of groundwater in sediment transport

It has been speculated that the widely-observed intertidal break of slope on macro-tidal beaches is due to emerging groundwater, creating different swash zone sediment transport regimes to landward and seaward of the break (Turner, 1993*b, c*, 1995*a, b*) (Section 2.4.8). There was a tendency for the location of the intertidal break of slope to translate seawards, as the hydraulic conductivity of the sand beach increased. However, at present, the mechanisms by which sediment is transported differentially across a saturated and unsaturated zone of a beach remain unproven. It may be that the break of slope determines the outcrop of the water table (since hydraulic gradients will be markedly lower to seaward of the break of slope), rather than the converse.

It is within the swash zone that the impact of beach groundwater is of most importance, both for net infiltration (Grant, 1946; Emery & Foster, 1948) and for the pressure gradient reversals and subsequent impact on fluidisation of sediment (Baird *et al.*, 1996). In addition, the water table oscillations caused by the reversed Wieringermeer Effect can influence sediment transport only where the water table is reasonably close to the surface and where the sediment is in receipt of small quantities of water; by implication, the sediment is draining in between swashes *i.e.* it is limited to when the swash zone crosses the region just to landward of the seepage face.

It has long been realized that high sediment loads can be transported within the swash zone (*e.g.* Beach & Sternberg, 1991), although research has been hampered by absence of suitable instrumentation to measure waves, currents and mobile sediments here. Recent measurements obtained from a macro-tidal beach have suggested that sediment transport should be integrated over the whole tidal cycle, for adequate predictions of net transport direction (Voulgaris *et al.*, 1997). This relates to the fact that sediment transport in the swash zone may have a different net direction from that of the outer surf zone.

Ultimately, there is a need to elucidate the mechanisms by which groundwater interacts with swash/backwash and the subsequent consequences for sediment transport in the swash zone. The processes are likely to be different for saturated and unsaturated regions of the beach, which will vary according to the tidal progression. A numerical model which incorporates waves (including swash/backwash and run-up), infiltration into unsaturated and saturated sediment, groundwater fluctuations and resultant swash zone sediment transport remains the future objective. GRIST II, which integrates groundwater oscillations over a tidal cycle with superimposed waves (including swash, backwash, and set-up), is under development (Baird, pers. comm.).

However, with the exception of Nicholls (1985), all research into beach groundwater has been undertaken on sandy beaches (Table 2.4). Nicholls (*op. cit.*) compared the water table elevation across Hurst Castle Spit, over a neap and spring tidal cycle. Wave activity caused higher levels of set-up and swash excursion across the more permeable shingle at higher elevations of the Spit; this resulted in more percolation into the beach. An asymmetric variation in the water table, due to tidal inundation, was observed. However, there are a number of features specific to Hurst Castle Spit which may influence the water table response; (i) the complications of cross-barrier seepage, due to differential tidal (water) levels on either side of the Spit; (ii) artesian conditions at a particular location; (iii) perched water table above the clay basement 4 m below the crest of the Spit. The volume of seepage was reported to be sufficient to cause erosion of the back crest of the Spit under extreme conditions. It was concluded that the water table fluctuations across the shingle barrier had an important influence on sediment transport,

There are no high-frequency field measurements available of water table fluctuations on shingle or sand/shingle beaches and, likewise, no measurements (at any frequency) from mixed beaches. The importance and effect of the seepage zone on swash zone sediment transport (Section 2.4.8) is uncertain for beach sediments with high hydraulic conductivity. On the one hand, development of a seepage zone is likely to be spatially and temporally restricted, in comparison with a sand beach; on the other, backwash is likely to be enhanced by larger volumes of exfiltrating water (at higher seepage velocities) resulting from steeper beach gradients and, possibly, non-Darcian flow.

A first stage in assessing the importance of groundwater on a mixed beach is to determine whether the water table responds to tidal inundation, in a similar manner to a sand beach. In the present study, this will be achieved by comparing field measurements of tidally-induced groundwater fluctuations across the mixed beach profile at Morfa Dyffryn, North Wales. These results will be compared with the predictions of the GRIST I model, which was validated using measurements from a micro-tidal sandy beach at Canford Cliffs, Dorset.

CHAPTER 3: INSTRUMENTATION AND CALIBRATION

This chapter describes the instrumentation used during the field deployment, the data-recording system, calibration procedures and the calibration equations used for subsequent data analysis. Further details about the deployment of the instruments and sampling schedule are given in Chapter 4.

3.1 Instruments

3.1.1 Pressure sensors

Two different types of pressure sensors were used during the field experiments. Miniature pressure sensors of less than 0.03 m diameter were needed to measure the level of the water table inside dipwells, and larger, more rugged sensors were used to record time series of water surface elevation. The principle of a pressure sensor is to measure an externally applied pressure with reference to another pressure; absolute sensors (*e.g.* barometric pressure sensors) compare the applied pressure to that of a vacuum inside the sensor chamber, whilst differential pressure sensors measure the difference between the pressure applied to both sides of a diaphragm. The voltage output of the sensor is linearly proportional to the input pressure and is later calibrated to the required units of measurement (*e.g.* metres of water).

The miniature pressure sensors (referred to hereafter as Px 1, Px 2 *etc.*) were designed in the Department of Oceanography by Bertrand Herruel (1994) using an MPX5050DP gauge pressure sensor with the following operational specifications (Motorola, 1994):

Pressure Range	0 to 50 kPa
Sensitivity	90 mV/kPa
Response time	1ms
Temperature-compensation range	-40 to +125 °C

The gauge pressure sensor used here is a special type of differential sensor which uses ambient atmospheric pressure as the reference side of the diaphragm via a second port, which was attached to a 3 metre long, thin-walled plastic tube. The sensors were mounted on a small circuit board, fitted with a 5 V voltage regulator and an electric cable.

The pressure housing consisted of a length of finger-shaped nitrile rubber around a small length of 25 mm rigid tubing which, together with the sensor and circuit board was encased by a protective semi-rigid plastic sheath (Figure 3.1 and Plate 3.1). The entire unit was filled with castor oil and sealed once all air bubbles were excluded.

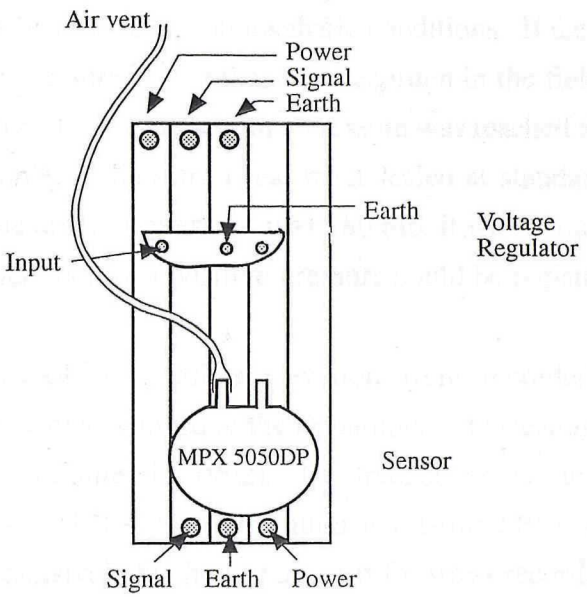

Figure 3.1 PT sensor connectors

Plate 3.1 PT sensor unit (mounted on board) and completed sensor.

In the field, the Px was inserted inside a dipwell and held in place by a rubber bung. The plastic tubing was positioned so that it was open to the atmosphere, but no rain or spray could enter the tube. Once the tide reached each dipwell and the sediment became saturated, the plastic tubing was sealed off, and unsealed once the tide had receded again. The main advantage of having the vents open to the atmosphere is that the instrument can be used in any atmospheric conditions. If the sensors had been sealed at an atmospheric pressure higher than that recorded in the field, the instrument would not begin to register a true reading until a pressure was reached equal to that when it was sealed. For example, if the sensor had been sealed at standard atmospheric pressure (1015 mb), and the ambient pressure was 980 mb, it would need 0.35 metres of water above the instrument before a positive pressure could be registered.

Time-series of sea surface elevation were recorded using three Pressure Transducers previously developed in the Department of Oceanography and referred to as PT3, PT4 and PT5 (Voulgaris, 1992). The transducers are temperature-compensated gauge-type sensors, sealed and housed within an oil-filled PVC cylinder. These sensors have been used extensively by the Department for wave recording on beaches.

3.1.2 Optical Backscatter Sensors (OBS)

OBS's are used increasingly to produce a high frequency time series of the volume of particles suspended in the water column (Downing *et al.*, 1981) which, when combined with information from co-located current meters, can provide suspended sediment fluxes. The instrument is a type of nephelometer, which emits infrared radiation within a limited beamwidth, and subsequently detects any radiation backscattered by particles in the water column, which is then calibrated to give a concentration of suspended sediment. OBS's are considered relatively insensitive to bubbles and plankton (D & A Instruments, 1988; Downing & Beach, 1988) and have been widely used in field studies, both inside and outside the surf zone (*e.g.* Hanes & Huntley, 1986; Beach & Sternberg, 1991; Russell *et al.*, 1991).

3.1.3 Electro-Magnetic Current Meters (EMCM)

EMCM's are used extensively to measure nearshore velocity fields, since they can monitor instantaneous fluctuations of water movement at high frequencies in 2 directions

normal to each other. A magnetic field is produced by and perpendicular to the coil. When water flows through this vertical magnetic field, a voltage is induced at 90° to the direction of flow. Four (paired) electrodes are situated at right angles to each other near the edges of the head. These detect and record the induced voltage in proportion with the x and y components of the water motion. The recorded voltages are converted to units of velocity through an empirical calibration.

Four EMCM's were cantilevered from one of the uprights of the H frame, at varying heights from the bed and so as to minimise flow interference. Heads A and B were 11.5 cm diameter annular meters (Model 800-4, Valeport Marine Scientific) and Heads C and D were 5.5 cm spherical heads (Model 800-5). Heads A, C and D were used to measure cross-shore and longshore velocities at approximately 0.3 m, 0.8 m and 0.12 m from the sea bed respectively, although the configuration was altered slightly during the course of the deployment. Head B was orientated vertically to measure vertical velocities at 0.54 m. A further 5.5 cm spherical EMCM (Valeport Model 800), kindly lent by the Department of Geography, Birkbeck College, University of London, was used in stand-alone configuration.

3.2 Data Recording Procedures

Throughout the field deployment, all electronically-recorded data were sampled and stored on one of two data collection systems. The dipwell and piezometer Px's, PT's, and stand-alone EMCM were sampled simultaneously at 2 Hz and recorded onto the hard disk of a computer at the top of the beach via 2 x 12 bit A/D cards with voltage range ± 5 Volts, giving a resolution of 0.0014 Volts. Data were sampled using the "Digiscope" data-collection software programme written in the Department of Oceanography by Mr M. P. Wilkin. Recorded digital values were converted to voltage by:

$$Voltage = \frac{AD - 2043}{409.8} \tag{3.1}$$

where AD is the recorded digital value.

The remaining instruments (4 EMCM's, 3 OBS's and PT) were integrated as part of the TOSCA instrumentation platform (Voulgaris & Collins, 1994); the data were

sampled at 4 Hz, digitized and stored on the on-board hard disk. Both logging systems were powered from a petrol-driven generator via cables dug into the beach. The systems were programmed to begin sampling on the hour and half hour, 24 hours a day, timed using the internal clock of each recording system. These two clocks became slightly out of phase as the deployment progressed and the consequences will be discussed in the relevant sections below.

3.3 Instrument Calibration

3.3.1 Pressure sensors

Calibration of PT3 and PT5 was carried out in the field, whilst PT4 and all the Px's were calibrated in the laboratory, using the same method. The transducers were lowered into a column of seawater at intervals of 0.25 metres, and the mean voltage for each depth was recorded. The offset voltage was removed and calibration equations were derived using first-order regressions, as given in Table 3.1.

The offset value is partly due to the electronics and partly a result of the atmospheric pressure. Since the calibrations were carried out using the same electronic equipment, connectors, power source and filters as when the data were collected, the electronic component of the offset can be regarded as constant. The Px's were vented to the atmosphere, therefore their offset is due to electronics only and the value given in Table 3.1 was from the field data, and was used for all subsequent calibration of field data. The offset for the PT's includes a component for atmospheric pressure, which will be variable. The atmospheric offset for field data was obtained from the mean voltage reading of the sensor immediately before and after being covered with water. Where the atmospheric pressure had changed appreciably between consecutive low waters, the difference between readings was averaged across the number of data files during coverage.

3.3.2 Optical Backscatter Sensors

Sand from the experimental site was used for the OBS calibration, since the instruments are known to be sensitive to the local sand characteristics (D & A Instruments, 1988). A sample of the sediment was washed, dried and sieved at ¼ ϕ

Sensor	Calibration equation for depth (m)	Sensor	Calibration equation for depth (m)
Px 1	1.0998 * voltage + 0.1170	Px 13	1.1999 * voltage + 0.0809
Px 2	1.1272 * voltage + 0.1184	Px 14	1.1468 * voltage + 0.0356
Px 3	1.1272 * voltage + 0.0647	Px 15	1.1421 * voltage + 0.0128
Px 4	1.0940 * voltage + 0.0690	Px 16	1.1023 * voltage + 0.0659
Px 5	1.1285 * voltage + 0.0927	Px 17	1.1834 * voltage + 0.0398
Px 6	1.1546 * voltage + 0.0446	PT 3	1.0545 * voltage - 0.0158
Px 7	1.1108 * voltage + 0.0318	PT 4	1.4464 * voltage - 0.1068
Px 8	1.1646 * voltage + 0.0394	PT 5	0.6974 * voltage + 0.0194
Px 12	1.1444 * voltage + 0.0439		

Table 3.1 Calibration equations for pressure sensors

intervals, and subsequently classified as fine sand, with D_{50} of 0.22 mm.

The instruments were calibrated in a re-circulating tank containing 10 litres of water, which was kept in constant motion. Offset readings were taken in both still and moving water, then a known quantity of sand was added. The calculated measurements were the mean and standard deviation of 250 voltage readings. The procedure was repeated using progressive additions of 0.5, 1, 2, 5 and 10 g up to a total concentration of 23 gl^{-1}. The calibration equations are presented in Table 3.2.

Sensor	Calibration equation for sediment concentration (gl^{-1} or kgm^{-3})
OBS 1	13.2 * Voltage
OBS 2	13.3 * Voltage
OBS 3	13.6 * Voltage

Table 3.2 Calibration equations for Optical Backscatter Sensors

Offsets for the OBS's were those obtained from the field experiment, when the sensors were placed in a container of still seawater. However, it was noticed that the

offset was unexpectedly high (though steady) at nearly 0.5 Volts. This was later attributed to a fault in the A/D card (see Section 3.6.4 below) and offsets for files recorded prior to Tide 17 are those from the "Belgica" deployment in early September 1994, courtesy of the late and sadly missed Nicolas Grochowski.

3.3.3 Electro Magnetic Current Meters

The EMCM's were calibrated shortly after the field deployment, with the same recording equipment as that used whilst collecting the field data. The calibration was conducted in the 30 metre towing tank of the Department of Ship Science, University of Southampton. Calibration results for each sensor channel are illustrated at Figure 3.2. First order regression equations are given for Heads A and B. However, the linear relationship ceases to be valid for velocities above 1 ms^{-1} for Heads C and D (the spherical heads), which have been fitted with a third order polynomial curve of the type:

$$Velocity = aV^3 + bV^2 + cV + d \qquad (3.2)$$

where V is the voltage output by the sensor. The resultant coefficients are listed inTable 3.3. These calibrations are similar to those produced by the calibration 2 years previously (Voulgaris & Collins, 1994) which indicates that the gain of the instruments is stable.

Channel	a	b	c	d	r^2
A x			1.0487	0.0056	0.9995
A y			1.0329	-0.0065	0.9993
B x			2.0739	-0.0091	0.9993
B y			2.0317	-0.0028	0.9991
C x	-0.0282	-0.0020	1.0052	-0.0101	0.9996
C y	-0.0381	-0.0028	1.0272	0.0040	0.9989
D x	-0.0250	0.0041	0.9942	0.0064	0.9995
D y	-0.0321	-0.0070	0.9963	-0.0037	0.9990

Table 3.3 EMCM coefficients for use in calibration equations.

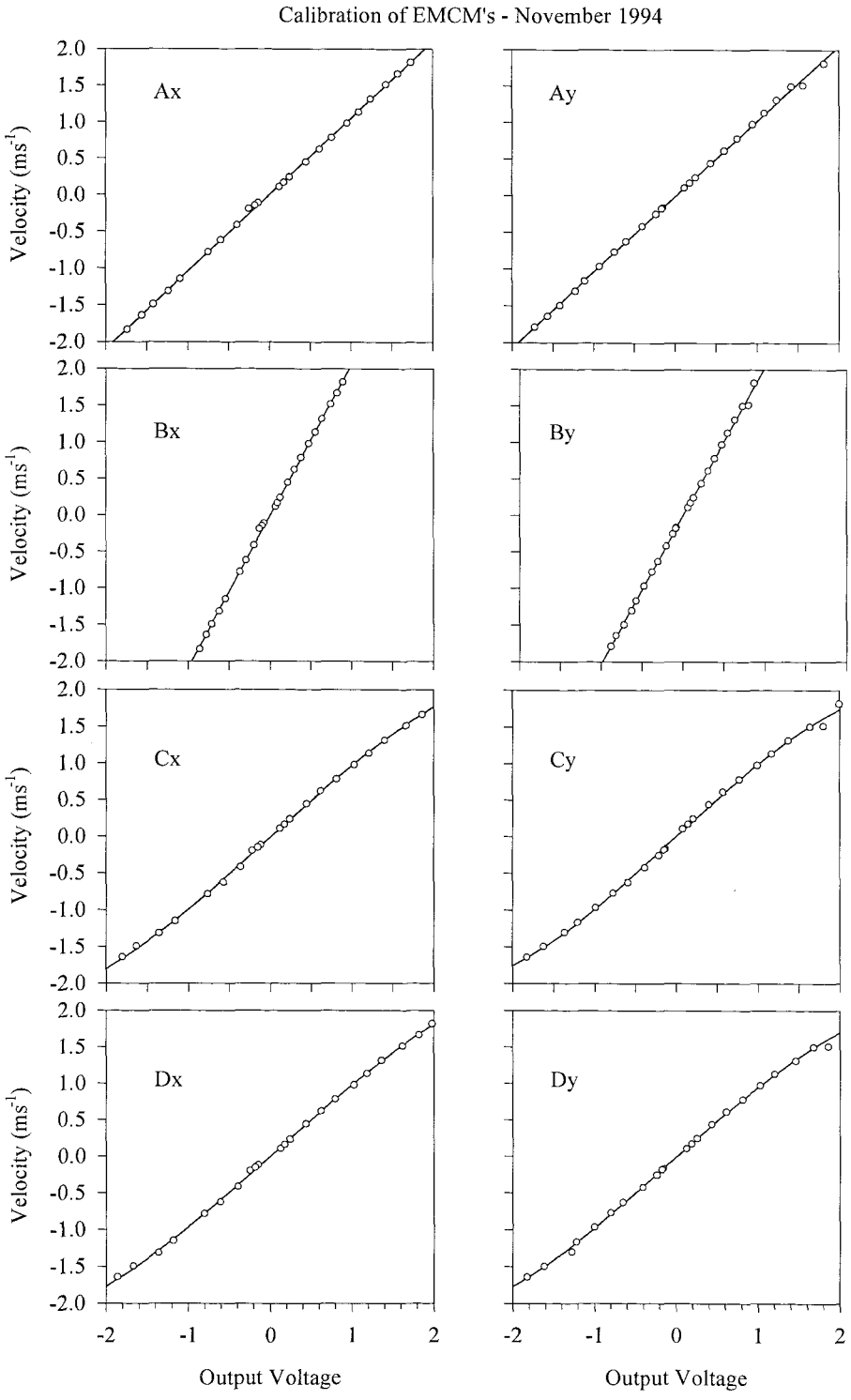

Figure 3.2 Calibration of EMCM's

Calibrations for the stand-alone EMCM were those supplied by the manufacturer (Valeport Marine Ltd):

X Channel:

Voltage < 0.098:	velocity = 1.055 * Voltage
0.098 < Voltage < 0.365:	velocity = 1.057 * Voltage + 0.01
0.365 < Voltage < 0.541:	velocity = 0.837 * Voltage + 0.083
Voltage > 0.541:	velocity = 0.944 * Voltage + 0.026

Y Channel:

Voltage < 0.079:	velocity = 1.070 * Voltage
0.079 < Voltage < 0.352:	velocity = 1.073 * Voltage - 0.007
0.052 < Voltage < 0.548:	velocity = 0.851 * Voltage + 0.072
Voltage > 0.548:	velocity = 0.957 * Voltage + 0.097

3.3.4 EMCM offsets

Several problems were encountered with the EMCM offsets, the most important being an anomalously high voltage recorded during the field offset files, when the EMCM's were placed in a container of still sea water. During the subsequent laboratory calibration of both EMCM's and OBS's, the A/D card onboard TOSCA was found to have acquired an offset of about 0.5 Volts. In addition, of the four sets of field offsets, those for the stand-alone EMCM and to a lesser extent Head A, were particularly variable. During Tides 9 to 27 (excepting Tide 17) the TOSCA logging-system switched off approximately 1.5 minutes before the recording system for the stand-alone EMCM, which suffered an instantaneous voltage drop. The offsets obtained are given in Table 3.4, and include offsets after the voltage drop for the stand-alone EMCM.

Mean current values, for TOSCA data were derived for Tides 8 to 33 using the Tide 19 offset, as shown at Figure 3.3. The sudden decrease in values between Tides 16 and 17 suggest that the A/D card acquired its additional offset voltage during that time. Accordingly, currents for earlier tides were derived using the offset values from the "Belgica" deployment in September 1994 (Grochowski, 1995). Subsequent tides use the Tide 26 offsets, which were found to be the most stable.

EMCM Offsets (Volts)					
	Tide 19	Tide 26	Tide 32	Tide 34	Laboratory
A x	0.62	0.61	0.50	0.61	0.61
A y	0.50	0.52	0.69	0.61	0.56
C x	0.54	0.54	0.53	0.54	0.56
C y	0.50	0.47	0.51	0.52	0.58
D x	0.53	0.52	0.52	0.54	0.55
D y	0.58	0.59	0.58	0.57	0.60
X (end)	0.67 0.13	2.74 0.47		3.13	
Y (end)	0.36 -0.06	2.39 0.16		3.17	

Table 3.4 Field offsets for EMCM's

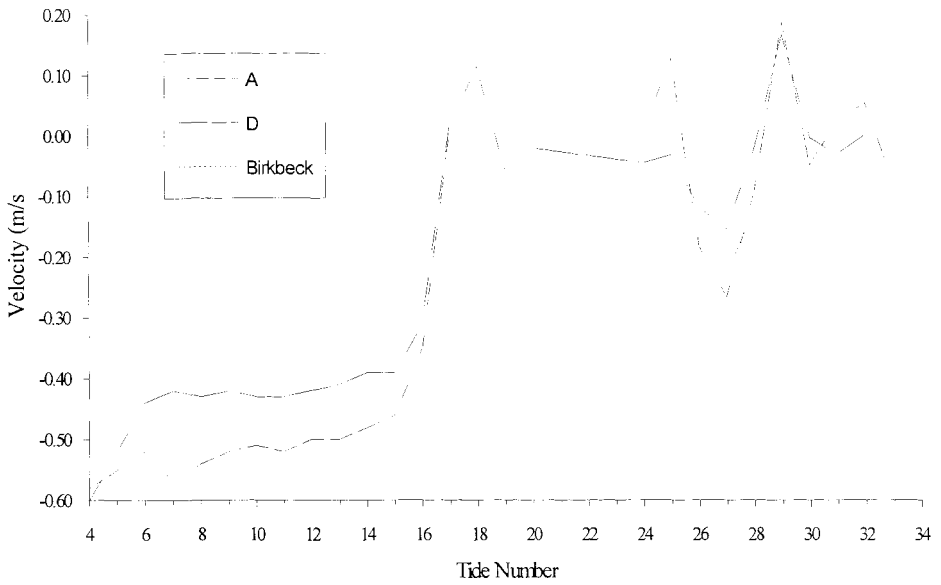

Figure 3.3 Mean cross-shore current velocities

Given such widely varying offsets for the stand-alone EM, currents were calculated for each High Water using every offset. Resulting mean currents of greater than 0.5 ms^{-1} were eliminated as being unrealistically high. Interestingly, there was no clear jump in velocities between Tides 16 and 17, as in the TOSCA data. However, for

both cross-shore and longshore data, the only feasible mean current speeds for Tides 9 to 27 were those obtained using the offset at the end of Tide 19 (*i.e.* the offset after the voltage drop). Tides 6 to 9 and 28 to 33 did not record a drop in voltage at the end of the file, and although the Tide 26 offset produced similar results for the cross-shore velocities, it gave considerably higher longshore velocities (nearly -0.5 ms^{-1}) than the Tide 19 offset (less than -0.1 ms^{-1}). Accordingly, when a voltage drop was recorded, each data file was adjusted by the difference in mean values between the major part of the record (Part 1) and the remaining section after TOSCA had switched off (Part 2) and the Tide 19 end offset was used. The main offset of Tide 19 was used for those files which did not experience a voltage drop.

CHAPTER 4: LOCATION OF FIELD EXPERIMENT AND METHODS

4.1 Location of Experiment

The field site at Morfa Dyffryn, Meirionnydd, is a macro-tidal, composite beach on the Cardigan Bay coast and forms part of a wide sand spit with a narrow, linear, shingle ridge, backed by an extensive sand dune system (Figure 4.1 and Plates 4.1 and 4.2). It was selected as a region without groynes, sea defences, engineering works or replenishment schemes *i.e.* as "natural" a system as is likely to be encountered in southern Britain. The harbour wall at Barmouth 10 kms to the south is the nearest man-made structure, but the most recent engineering works were over 10 years ago, so that any resulting changes in the sediment transport system are likely to have stablized.

The area is within Snowdonia National Park (1951), is also part of a National Nature Reserve (1962), a Site of Special Scientific Interest (1982) and has been listed as a geomorphological Single Interest Locality (Evans, 1995). However, despite its scientific importance, there have been no studies at all in the nearshore region.

4.1.1 Geological setting - onshore

The geological sequence in the area was established by the Mochras Farm BGS borehole in 1967-1969. It revealed nearly 80 metres of Quaternary sediments, with almost 2000 metres of Tertiary and Jurassic sediments below. The top 6.5 metres of Holocene sediments were found to consist of sand, shingle, silt and shells. The present shingle ridge extends several kilometres along the coastline and contains local and exotic boulders and cobbles. Wind blown sand has accumulated into well-developed dune systems up to nearly 15 metres in height at Morfa Dyffryn and Morfa Harlech (Allen & Jackson, 1985). Approximately 1.5 kms inland of the field site, steep cliffs of Cambrian grits and shales mark a major structural fault (Mochras Fault), and may indicate a former coastline.

4.1.2 Offshore

Most of northern Cardigan Bay is shallow and gently sloping, with an overall depth of less than 20 metres. However, a notable feature is the series of 5 offshore ridges (sarnau, or causeways) perpendicular to the coast, which can dry at extreme low waters.

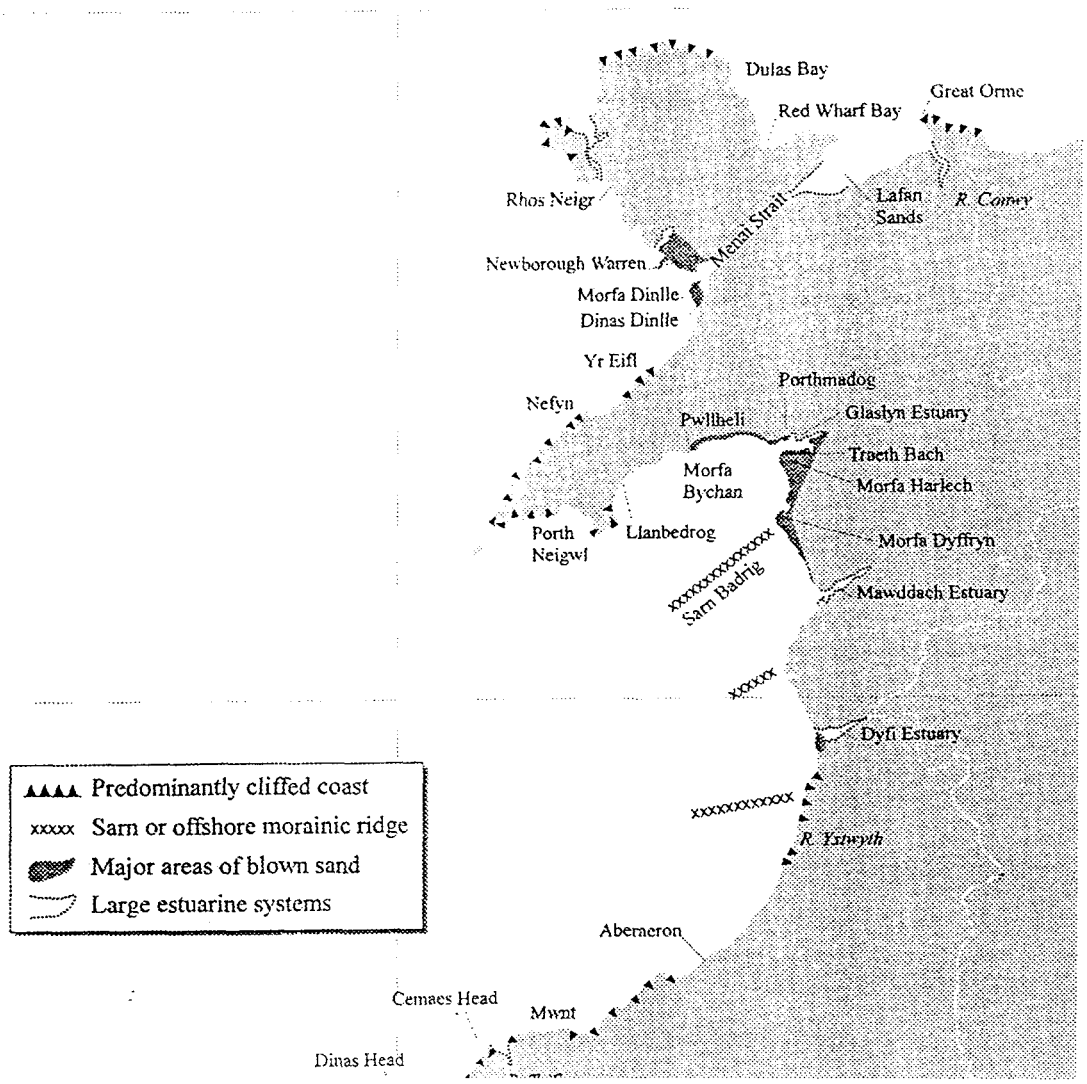

Figure 4.1 Location of field site (JNCC 1995, source British Geological Survey)

Plate 4.1 Morfa Dyffryn

Plate 4.2 Morfa Dyffryn

They have been identified previously as terminal or medial moraines (Bowen, 1977; Garrard, 1977) but more recently are thought to be Late-Glacial sandar (Tappin *et al.*, 1994). Sarn Badrig, at 34 kms long, is the largest and is named from the local legend that St Patrick used the causeway to reach Ireland.

The Pleistocene sediments show a complexity resulting from inundation during the Devensian by both Welsh Ice and Irish Sea Ice, which together have left a cover of 10 metres of glacial tills and glacio-marine sediments. Strong tidal currents in the outer part of Cardigan Bay have winnowed out most of the fine sediments leaving a gravelly sea bed, and transported the finer sands landwards leading to extensive sand accumulation at the former cliff line (Evans, 1995). The position of Harlech Castle, built on the coast in the 12th Century and now nearly a kilometre inland provides an indication of the volume of accretion at Morfa Harlech since then.

4.1.3 Winds, tides, wave climate and sediment transport patterns

The Admiralty Pilot reports that the dominant winds at Milford Haven, considered representative for Cardigan Bay, in September and October are from the west and south-west, with a mean velocity of 15 knots (7.5 ms^{-1}) and an average of 2 days per month with gales. Significant wave height exceedance of 75 % in summer (July/August/September) is 0 to 0.5 m, and 25 % exceedence between 1 and 1.5 m. Autumn values (October/ November/December) are 0 to 0.5 m and 1.5 to 2.0 m respectively (Draper, 1991). Average sea level atmospheric pressure is 1014 mb.

The pattern of offshore tidal currents, listed at Table 4.1, is abstracted from the Tidal Stream Atlas (Hydrographer of the Navy, 1992) in the absence of nearby tidal diamond information. Tidal currents are at their maximum at Barmouth around High Water (-0305 hours relative to HW Dover) and Low Water, with slack water mid-tide at HW -3, indicating a progressive tidal wave (Carter, 1988). Currents are in a southerly direction for 2 hours before and after HW Barmouth, reversing direction to a weak northerly current by HW +3[3]. The strongest northerly currents occur at HW +6 and HW -6. Maximum spring rate is 0.5 to 1 knot in both directions, increasing to 1 knot across

[3] All further references to times before or after High Water, will be in the format HW +(-)2, representing 2 hours after (before) local High Water.

Hours relative to HW Barmouth	Tidal Stream	
	Strength	Direction
- 6	Strong	Northerly
- 5	Moderate	Northerly
-4	Weak	Northerly
-3	Slack	
-2	Moderate	Southerly
-1	Moderate	Southerly
HW	Strong	Southerly
+1	Moderate	Southerly
+2	Moderate	Southerly
+3	Weak	Northerly
+4	Weak	Northerly
+5	Moderate	Northerly
+6	Strong	Northerly

Table 4.1 Tidal regime offshore from Barmouth

Sarn Badrig, over which seas break at all stages of the tide in heavy weather (Hydrographer of the Navy, 1996). Morfa Dyffryn is within Coastal Cell 9a, which extends from St David's Head to Glaslyn estuary and is characterised by general northerly sediment transport, with local reversal at some estuary mouths (Motyka & Brampton, 1993). Despite extensive sand accretion just to the north, Morfa Dyffryn has suffered periods of severe erosion when high waves combined with a storm surge have led to serious flooding of farmland and damage to the dunes. Regular topographic surveying of the coastline by Meirionnydd District Council has begun only within the last 3 years. North-westerly winds, though less frequent, have led to major erosion at Llwyngwyrl to the south of the Mawddach estuary.

4.2 Data Acquisition

All instrumentation was located along one cross-shore transect, referred to as the Main Transect, as shown in Figure 4.2 and illustrated by Plate 4.3. One pressure

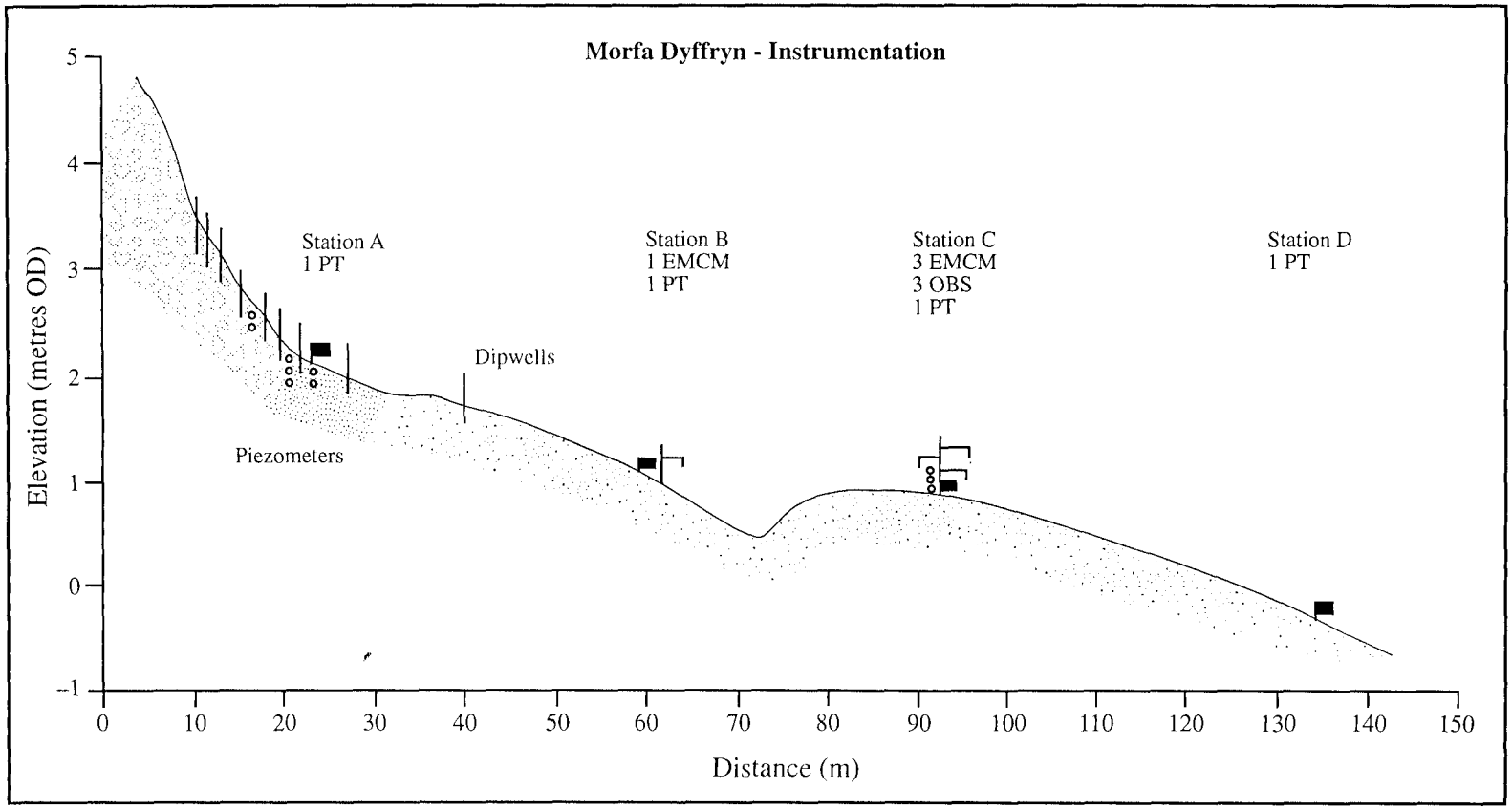

Figure 4.2 Instrument location at Morfa Dyffryn

Plate 4.3 Instrument location along Main Transect

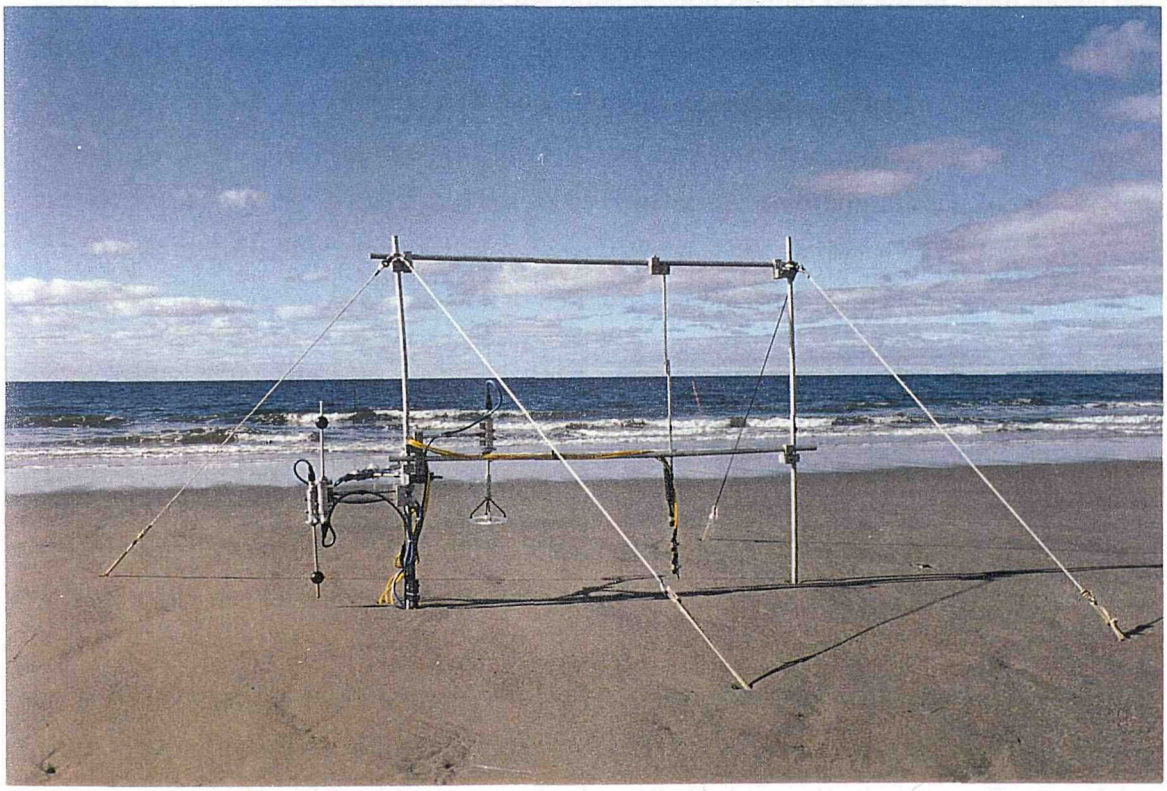

Plate 4.4 TOSCA configuration at Morfa Dyffryn

transducer was placed near the sand/shingle border (Station A). Station B consisted of one EMCM, situated on the inner sand ridge, with an adjacent pressure transducer. Station C on the main sand ridge comprised an instrumented platform (TOSCA), modified for installation in the inter-tidal zone (Voulgaris & Collins, 1996). It contained 3 EMCM's at approximately 0.13, 0.36 and 0.7 m from the seabed, with a further EMCM measuring vertical currents at 0.55 m (Plate 4.4). The current meters were cantilevered from a single steel pipe, to reduce flow interference. Three OBS's measuring suspended sediment concentration were attached to a small steel rod which was suspended below the main steel crossbar. The sensors were 0.09, 0.2 and 0.3 m from the seabed and facing the longshore direction, again to keep flow disturbance to a minimum. A pressure transducer 0.1 m above the bed recorded the sea surface elevation. The most seaward pressure transducer at Station D was used to obtain the representative "deep water" wave conditions outside the surf zone.

A series of 10 dipwells was inserted across the sand/shingle interface region. On the steep shingle ridge, the wells were spaced at approximately 2 metre (horizontal distance) intervals, but were between 7 and 13 metres apart on the flatter sand region (see Figure 4.2). One well was placed in the dune system behind the beach, well above the High Water mark, to act as a control. The wells were open to the atmosphere, and each was fitted with a miniature pressure sensor (Px) to measure the height of water above the sensor inside the well *i.e.* the phreatic surface, or water table. A further 5 wells with pressure sensors were inserted, but the tubes were sealed throughout their length except for 10 cms at the bottom, thus acting as piezometers. They were placed in 2 groups, each at a different elevation in the beach, to measure the pressure head changes with depth.

Various static equipment was inserted, including up to 13 graduated rods which were used as control points for video recording, to observe the position of maximum wave run-up, swash zone sea surface elevation and infiltration volumes. Wave Staffs consisted of 3 groups of 3 rods in triangular formation and were used for visual estimates of angle of wave approach. The schedule of instrumentation is shown in Table 4.2.

The Main Transect was surveyed at least once each day using a total station, with additional profiles surveyed at two to three day intervals. A site-specific grid of control points was laid out and used for survey checks. The Ordnance Survey co-ordinates of the main set-up position were obtained subsequently by Meirionnydd District Council, which

Morfa Dyffryn Field Deployment - September/October 1994													
	TOSCA			Birkbeck				Dipwell	Piezo	Swash			
Day	EMCM	OBS	PT	EMCM	PT4	PT3	PT5	Px's	Px's	rods	Notes	Date	Tides
261	+	+									2 files only	18 Sep	1
262	+	+								1 to 9		19 Sep	2 & 3
263	+	+								+		20 Sep	4 & 5
264	+	+		+	+					+		21 Sep	6 & 7
265	+	+		+	+			1 to 6		+		22 Sep	8 & 9
266	+	+		+	+			+		+		23 Sep	10 & 11
267	+	+		+	+			+		0 to 9		24 Sep	12 & 13
268	+	+		+	+			+		+		25 Sep	14
269	+	+		+	+			+		+	no LW files	26 Sep	15 & 16
270	+	+		+	+	+		1 to 9		+	no LW files	27 Sep	17 & 18
271	+	+		+	+	+		+		+	no LW files	28 Sep	19 & 20
272	+	+	+	+	+	+		+*		+	Px 6 repaired	29 Sep	21 & 22
273	+	+	+	+	+	+		+		+		30 Sep	23 & 24
274	+	+	+	+	+	+		+	+	+		1 Oct	25 & 26
275	+	+	+	+	+*	+		+	+	+	new filter	2 Oct	27 & 28
276	+	+	+	+	+*	+*	+	+	+	+	buried	3 Oct	29 & 30
277	+	+	+	+	+	+	+	+	+	+		4 Oct	31 & 32
278	+	+	+	+	+	+	+	+	+*	0 to 13	1-C 2-C removed	5 Oct	33 & 34
279					+*	+	+	+	+	+	buried	6 Oct	35 & 36
280					+	+	+	+	+	+		7 Oct	37 & 38
281					+	+	+	+	+	+		8 Oct	39

Table 4.2 Instrumentation during field deployment

allowed conversion of the local grid co-ordinates to OS positions and, where needed, elevations relative to Chart Datum.

4.3 Methods of Data Analysis

The right-handed convention for signs will be followed *i.e.* x represents cross-shore, y the longshore and z the vertical directions. Positive values of x indicate onshore velocities or transport (Figure 4.3) with positive z values representing distance upwards. At Morfa Dyffryn, positive values of y represent transport or motion towards the north.

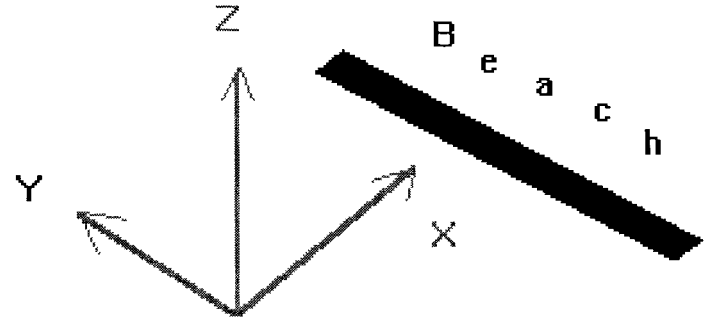

Figure 4.3 Sign convention used at Morfa Dyffryn

All electronic instruments were sampled simultaneously at half-hourly intervals in bursts of 17.07 minutes, which is a compromise between providing a record length suitable for inclusion of infragravity wave energy whilst ensuring reasonable stationarity of the processes on a macro-tidal beach (Davidson *et al.*, 1993). Thus, each file consisted of 4096 data points (TOSCA) or 2048 points, for sampling rates of 4 Hz and 2 Hz respectively. Subsequent wave and current statistics are for the start time of each burst, in Julian Days and decimal days for 1994 *i.e.* Julian Day 261.5 refers to 18 September 1994, at 1200 local time.

4.3.1 Wave statistics

Statistics for the sea surface elevation data were obtained for each file as follows:

a. The mean water level was calculated as the mean of the record length.

b. The mean was then removed and the data de-trended, since stationarity is a primary requirement for spectral analysis (Diggle, 1990).

c. If required, the detrended data could be high-pass filtered to remove noise, using a designed (8th order) zero-phased elliptical filter with specifications:

Stopband loss	=	34 dB
Ripple in the passband	=	0.5 dB
Transition width	=	0.01
Cut-off frequency	=	0.75 Hz

An elliptic filter was chosen for its sharp transition at the chosen cut off frequency, in comparison with the Butterworth filter of the same order, which, despite no ripple in either the pass- or stopbands, has a much wider transition band. Figure 4.4 illustrates the response of the digital filters given the specifications above.

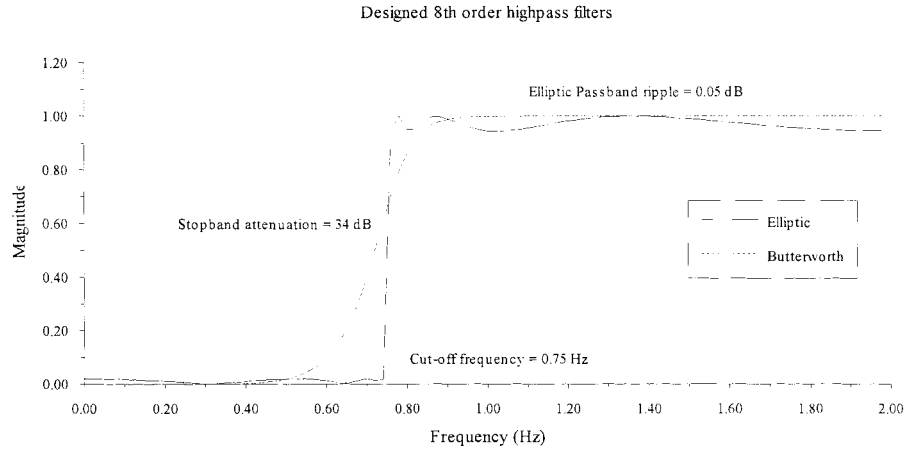

Figure 4.4 Filter response

d. The power spectrum was computed using Welch's averaged periodogram method: the files were divided into 15 blocks, consisting of 8 sequential segments, *M* (of 512 or 256 data points for the 4 Hz and 2 Hz files respectively) each overlapped by 50%. Each block is detrended and windowed (using a Hanning window of the same length as each segment). The magnitude of the Discrete Fourier Transform is squared, and the results of each segment are averaged to give the Power Spectral Density (PSD) estimate for the whole file. The sea surface

elevation spectra were then derived from this wave-induced PSD, after correction for depth attenuation using linear theory (Bishop & Donelan, 1987):

$$S_n(f) = S_p(f)\frac{\cosh^2(k.h)}{\cosh^2 k(h+z)} \tag{4.1}$$

where $S_n(f)$ is the spectral estimate at frequency (f) corrected for pressure attenuation, $S_p(f)$ is the uncorrected variance, k is the wave number, h the water depth and z, in this case, is the height of the sensor above the still water level (*i.e.* a negative number). The wave number, k, was calculated for each of the 256 frequency bands using a sub-routine written by Dr G. Voulgaris, from a polynomial solution using Padé approximations (Hunt, 1979). The correction was applied to each frequency band below 0.25 Hz, to avoid amplifying noise above that frequency (Pawka, 1982).

e. Wave parameters were derived from the moments of the corrected spectrum, using:

$$m_n = \int_0^{0.75Hz} S_n(f)\ f^n\ df \tag{4.2}$$

where m_n is the nth moment and df is the bandwidth of the spectral frequency:

$$df = \frac{Sampling\ frequency * M}{2 * N} \tag{4.3}$$

when M here is the number of segments, N is the record length and where (WMO 1988):

$$H_s = 4\sqrt{m_0} \tag{4.4}$$

$$H_{rms} = \sqrt{8m_0} \tag{4.5}$$

$$T_z = \sqrt{\frac{m_0}{m_2}} \tag{4.6}$$

$$T_{mean} = \frac{m_0}{m_1} \tag{4.7}$$

$$\epsilon = \sqrt{\frac{m_0 m_4 - m_2^2}{m_0 m_4}} \tag{4.8}$$

$$Q_p = \frac{2}{m_0^2} \int_0^{0.75} f[S_n(f)]^2 \, df \tag{4.9}$$

H_s is the significant wave height and H_{rms} is the single wave height which represents the energy of the whole spectrum. T_z is the spectrally-derived value equivalent of the mean zero-downcrossing period, and T_{mean} is the period which corresponds to the mean frequency of the spectrum. The spectral width parameter, ϵ is a measure of the type of spectrum, and varies from 0 (regular waves with a narrow spectrum) to 1 (broad spectrum with a range of wave periods). However, ϵ is a sensitive parameter, since it involves a fourth order moment, and the peakedness parameter Q_p is recommended as an alternative (WMO, 1988). Q_p = 1 represents a broad spectrum, with larger numbers suggesting narrow spectra. Wave period (T_{zero}) was also calculated from the time series, by the zero-upcrossing method.

Davidson (1992) suggested that for studies in very shallow water, H_s should be obtained only from the gravity component of the spectrum, since long waves can influence the outcome unduly. Hence a value for H_s can be derived also from the spectral component above 0.05 Hz.

The degrees of freedom for the spectral analysis is given by (Carter, 1973):

$$d.o.f. = 3.82 \frac{N}{M - 3.24} \quad (4.10)$$

where N is the number of data points (4096 or 2048) and M here is the length of segment (512 or 256). Hence the 4 Hz files (current meter and pressure transducer data at Station C) have approximately 27 degrees of freedom, with approximately 12 degrees of freedom for all remaining EM and pressure sensor data, including dipwell px's.

The sea surface elevation records were also decomposed into incident and long wave components, using an elliptic filter similar to that described above, but with a cut-off frequency of 0.05 Hz (20 s), which was the main location of the trough between high and low frequency energy. The record is low pass filtered to create a low frequency time-series, which is then subtracted from the original filtered, detrended time-series, thus producing a short wave time-series. The resulting long wave and short wave time series are considered to represent the infragravity and gravity wave components. Note that hereafter, the terms *long* waves and *infragravity* waves may be considered synonomous in this study, and similarly for *short* and *gravity* waves.

4.3.2 Current statistics

Mean cross-shore and longshore currents were derived as the mean of each calibrated record length (from which the electronic offset had been removed). The data were then de-meaned and detrended. The standard deviation and covariance of the record were calculated, and the following parameters calculated (Guza & Thornton, 1985):

$$U_m = \sqrt{2 * (\langle u^2 \rangle + \langle v^2 \rangle)} \quad (4.11)$$

$$U_b = 2 * \langle u^2 \rangle \quad (4.12)$$

$$V_b = 2 * \langle v^2 \rangle \tag{4.13}$$

$$\cup_b = \sqrt{U_b^2 + V_b^2} \tag{4.14}$$

$$\theta = atan\left(\frac{mean(v)}{mean(u)} \right) \tag{4.15}$$

$$\delta = \frac{mean(x)}{U_m} \sin\theta \tag{4.16}$$

where u and v are the instantaneous cross- and longshore current velocities respectively. U_m is the maximum wave orbital velocity and U_b V_b and $\cup_b$ are significant cross-shore, longshore and resultant orbital velocities. θ and δ are the resultant current direction and strength.

The velocity records were decomposed into long and short wave components in a similar manner to the sea surface elevation data described above, in order to calculate velocity moments. Derivation of the individual moment terms used in subsequent analysis will be fully described in Chapter 6. The method for deriving Frequency Dependent Reflection coefficents was given in Sections 2.3.2 and 2.3.3.

4.3.3 Local sediment fluxes and transport rates

The time-average of a suspended sediment concentration (SSC) time-series is made up of a mean component and a component fluctuating about that mean, in a similar manner to cross-shore velocity (this is described more fully in Chapter 6):

$$\begin{aligned} c &= \bar{c} + \tilde{c} \\ u &= \bar{u} + \tilde{u} \end{aligned} \tag{4.17}$$

where c represents instantaneous SSC, u represents instantaneous cross-shore velocity and the overbar and tilde symbols represent the mean and fluctuating components respectively. Assuming that net sediment flux is the product of instantaneous cross-shore velocity and SSC, (4.17) becomes:

$$< uc > = < \bar{u}\,\bar{c} > + < \bar{u}\,\tilde{c} > + < \tilde{u}\,\bar{c} > + < \tilde{u}\,\tilde{c} > \tag{4.18}$$

where $< u\,c >$is the net sediment flux. Since by definition, $< \bar{u}\,\tilde{c} >$ and $< \tilde{u}\,\bar{c} >$ are zero, (4.18) reduces to:

$$< uc > = < \bar{u}\,\bar{c} > + < \tilde{u}\,\tilde{c} > \tag{4.19}$$

where $< \bar{u}\,\bar{c} >$and $< \tilde{u}\,\tilde{c} >$are the mean and oscillatory components. The oscillatory component of SSC was divided into gravity and infragravity sections, using the same filtering techniques as for velocity time-series (Section 4.3.1) and then combined with the relevant short and long components of the oscillatory velocity, to give the local flux due to gravity and infragravity waves. Eqn (4.19) then becomes:

$$< uc > = < \bar{u}\,\bar{c} > + < u_s c_s > + < u_l c_l > \tag{4.20}$$

The term $< \tilde{u}\,\tilde{c} >$is referred to as the "flux coupling" (Jaffe *et al.*, 1984) and is an important factor in determining local fluxes cross-shore. In contrast, the longshore local fluxes may be represented adequately by the product of the mean longshore velocity and mean SSC, since the oscillatory component of longshore flow is considered unimportant (Beach, 1989).

Cross-shore oscillatory motion is predicted by linear theory to be constant through the water column, and therefore the flux at a given depth can be given as the suspended sediment concentration at that depth multiplied by the oscillatory velocity at approximately 0.1 m from the seabed (Hanes, 1990). However, at Morfa Dyffryn, the SSC was combined with velocities from the closest EMCM *i.e.*OBS1 and OBS2 (at 0.09 and 0.19 m from the seabed) were combined with the EMCM (at 0.12 m) and OBS3

(0.31 m) with the EMCM at 0.31 m.

In a similar manner to (4.20), the fluctuating component of the SSC may be combined instead with an oscillatory velocity which has been decomposed into incoming, u_{in} and outgoing, u_{out}, components (Miles *et al.*, 1996):

$$< \tilde{u}\,\tilde{c} > \; = \; < u_{in}\,\tilde{c} > + < u_{out}\,\tilde{c} > \qquad (4.21)$$

Decomposition of the velocity time series into incoming and outgoing components is in accordance with the procedures given in Section 4.3.6 dealing with wave reflection.

4.3.4 Calculation of sediment transport rates

The results derived from (4.20) are fluxes at a single point (kg m^{-3}) , which must be integrated over the water column. The box-integration method is used (Voulgaris, 1992):

$$< uc_{tot} > \; = \; \left(< uc >_{z1} * f_1 \right) + \left(< uc >_{z2} * f_2 \right) + \left(< uc >_{z3} * f_3 \right) \qquad (4.22)$$

where $< uc >_z$ is the local flux at z m from the seabed of the relevant mode (gravity, infragravity, mean or net), h is the mean water depth, *z1, z2* and *z3* are the heights from the seabed of the lowest, middle and top OBS sensors respectively. The multiplication factors are:

$$f_1 \; = \; z_1 + \left(\frac{z_2 - z_1}{2} \right) \qquad (4.23)$$

$$f_2 \; = \; \left(\frac{z_3 - z_2}{2} \right) + \left(z_2 - f_1 \right) \qquad (4.24)$$

$$f_3 \; = \; h - \left(f_2 + f_1 \right) \qquad (4.25)$$

Hence the sediment flux is integrated over the whole of the water column. Where the water depth was less than 0.4 m, the function $f_2 = h - f_1$ was used for the middle OBS, and for the two shallow water files of Tide 26 data from only the lowest OBS was used and integrated across the whole water column. The depth-integrated flux, $< uc_{tot} >$, is converted to an immersed weight sediment transport rate (N m^{-2} s^{-1}) by multiplying by:

$$\left(1 - \frac{\rho}{\rho_s}\right) g \tag{4.26}$$

where ρ and ρ_s are the density of seawater and sand respectively and g is the acceleration due to gravity (9.81 m s^{-1}).

Oscillatory suspended sediment transport rates can be calculated also using the co-spectrum of the currents and SSC (Huntley & Hanes, 1987). This also illustrates the direction and magnitude of transport at each frequency and when integrated across the entire frequency range, gives the net oscillatory suspended sediment transport rate.

4.3.5 Reflection coefficients (Frequency-Dependent Reflection Function, FDRF)

For Morfa Dyffryn data, reflection coefficients, FRDF, were calculated using a co-located EMCM and pressure sensor, according to the time-domain method of Guza *et al.* (1984), see also Huntley *et al.* (1995). The time series of sea surface elevation is decomposed into incoming and outgoing components:

$$\eta_{in}(t) = \frac{\eta(t) + \sqrt{\frac{h}{g}} \cdot u(t)}{2} \tag{4.27}$$

$$\eta_{out}(t) = \frac{\eta(t) - \sqrt{\frac{h}{g}} \cdot u(t)}{2} \tag{4.28}$$

where h is mean water depth and $\eta(t)$ and $u(t)$ are the detrended sea surface elevation and cross-shore velocity time series respectively.

Since the time domain method of analysis relies on addition of instantaneous values of sea surface elevation and the velocity (converted to units of elevation), it is critical that the two time series are synchronous. Two possible causes of temporal misalignment are that the instruments are not exactly co-located across-shore or that the electronic filters within the instruments cause some differential delay in the signal. Unless the time series are corrected for any time delay, resulting FDRF values may be artificially high, even when coherence between the incoming and outgoing components is good (Huntley *et al.*, 1995). The error becomes increasingly large with frequency above 0.2 Hz, although is less important for lower frequencies. These types of errors can lead to the situation where the energy of the incoming and outgoing components is not conserved.

For the TOSCA instrumentation, the A/D card and data acquisition software have been found to cause no relative delays between the channels (Voulgaris, pers. comm.). The current meter filters do lead to a delay, in comparison with the pressure transducer. Such a delay has been found also for the current meters deployed at Nieuwpoort, and has a significant impact on the calculation of FDRF (Simmonds, pers. comm.).

For the Morfa Dyffryn data, it was not possible to derive the filter delays electronically since the pressure sensor had been replaced in the meantime. However, a relatively straightforward, if empirical, method of determining the time delay is to calculate FDRF with the pressure transducer time series retarded or advanced by a variety of time delays. The correct time delay has been found to produce the lowest FDRF values, and flattest range of FDRF values across the spectrum (Simmonds, pers.comm.).

This method was employed for the Morfa Dyffryn data, since the resulting time delay accounts for the relative delays of the electronic filters and also tries to account for any spatial/phase lag due to cross-shore separation of the instruments. Figure 4.5 shows a contour plot of FRDF for a range of time delays, where a negative time delay indicates that the recorded pressure time series lags the current meter time series. From this figure, a time delay of -0.3 seconds was selected as the optimal value. This was subsequently applied to the pressure transducer time series using Matlab routines adapted from those kindly provided by Dr David Simmonds of the University of Plymouth.

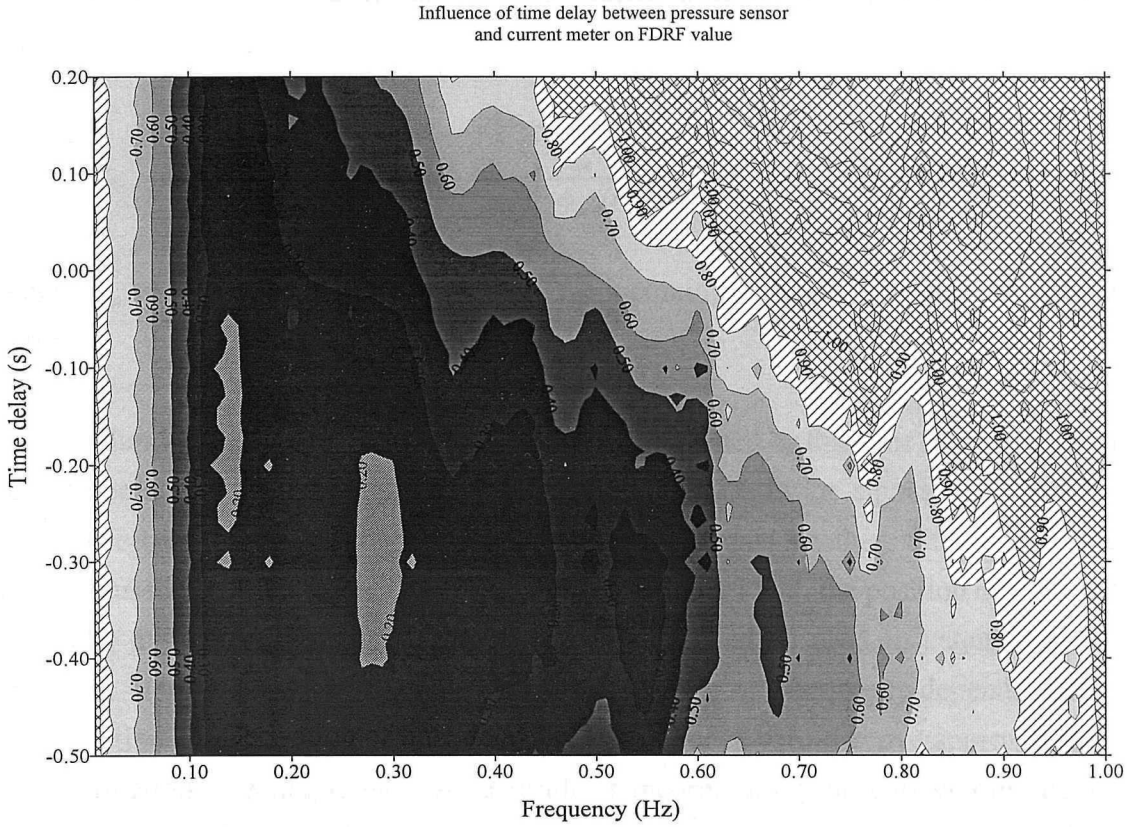

Figure 4.5 Derivation of time delay between EMCM and PT

The time delay due to filters for the instruments used at Nieuwpoort were established using laboratory calibrations at the University of Plymouth. Prior to calculation of FDRF for the Nieuwpoort data, the sea surface elevation time series were shifted to bring them into alignment with the current meter data, using those time delay values provided. Any error in estimating the correct time delay results in a spurious peak in FDRF at frequency of:

$$\frac{1}{4(\tau + \Delta\tau/2)} \tag{4.29}$$

where τ and $\Delta\tau$ are the time delay and time delay error respectively (Tatavarti, 1989). Hence for a time delay of 0.3 s and an error in estimating the delay of 0.1 s, the spurious peak would occur at 1.25 Hz, which is above the frequency range of interest.

Once the incoming and outgoing time series are obtained, the spectra of both components are derived using the method described in Section 4.3.1 and the FDRF calculated:

$$FDRF = \sqrt{\frac{\Phi_{out}(f)}{\Phi_{in}(f)}} \tag{4.30}$$

where ϕ_{in} and ϕ_{out} are the power spectra of the incoming, η_{in}, and outgoing, η_{out}, time series.

Huntley *et al.* (1995) showed that the results obtained by this time domain method tend to be artificially high when there is significant noise in the signal. The level of coherence between between η_{in} and η_{out} is used to provide a value of the bias to the FRDF caused by signal noise. This value is independent of both the position of reflected nodes or antinodes and the number of degrees of freedom used in calculating the spectrum. Hence the bias in FDRF can be removed by use of a frequency-dependent table of correction values (Huntley *et al.*, 1995). For coherence values above approximately 0.7, corrections are negligible. As a result of incorporating the correct time delay, coherence values between the η_{in} and η_{out} time series improved markedly. Of the FDRF figures which fitted the criteria given below, only two values of coherence fell between 0.54 and 0.64 and required correction according to Huntley *et al.* (1995) Figure 2.

An example of the use of the coherence as an indicator of the reliability of the FDRF estimates is values shown at Figure 4.6. The highest FDRF values calculated at Tide 29 HW +0.5 are for the low frequency waves, but the coherence between incoming and outgoing spectra is generally very low. This is probably due to the very low energy levels in the low frequency spectrum. However, there is a high level of coherence between the incoming and outgoing sea surface elevation at the peak incident wave frequency (0.13 Hz, 7.7s) with FDRF and coherence of 0.2 and 0.89 respectively.

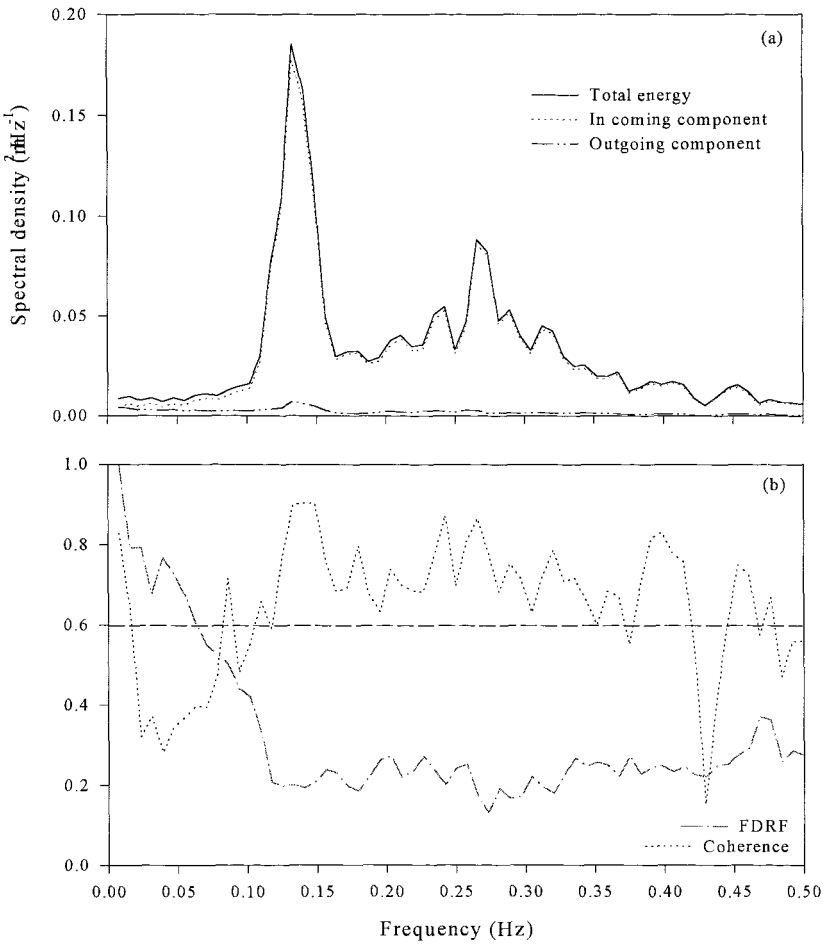

Figure 4.6 Tide 29, HW +0.5: (a) Spectral plot; and (b) FDRF and coherence between η_{in} and η_{out}

Accordingly, reflection coefficients were derived for those frequencies for which the following criteria were fulfilled:

a. The spectral peak of the sea surface elevation was significant (*i.e.* a distinctive peak with confidence values greater than 95%).

b. Coherence between both η_{in} and η_{out} and between the pressure and velocity (P-U) time series was 0.54 or greater. FDRF values with coherence between 0.54 and 0.7 were corrected according to Huntley *et al.* (1995) Figure2.

c. FDRF is less than 1. Although it may be theoretically possible for reflected energy to be greater than incident if, for example, an outgoing free wave is radiated directly from the surf zone (Symonds *et al.*, 1982), FDRF values in this study which were greater than 1 were rejected as representing errors in the method of calculation.

4.3.6 Decomposition of velocity time series

Eqns (4.27) and (4.28) can be re-written to decompose the cross-shore oscillatory velocity time series into incoming and outgoing components:

$$u_{in}(t) = \frac{u(t) + \sqrt{\frac{g}{h}} \cdot \eta(t)}{2} \tag{4.31}$$

$$u_{out}(t) = \frac{u(t) - \sqrt{\frac{g}{h}} \cdot \eta(t)}{2} \tag{4.32}$$

where all variables are as for (4.27). Net sediment transport rates and directions were derived from the co-spectra of the incoming and outgoing cross-shore velocity time series and the suspended sediment concentration time series.

4.3.7 Hydraulic conductivity of sediments

Laboratory tests to estimate the hydraulic conductivity of sand and shingle were conducted on disturbed samples, in accordance with BS 1377 Parts I and V (BSI, 1990) using facilities kindly provided by the Institute of Irrigation Studies, Department of Civil Engineering. The permeameter cell chamber was 7.5 cm diameter with two manometer

tappings spaced 10 cms apart (Plate 4.5). The maximum sediment size permissible with this cell chamber was shingle with D_{50} of 6.25 mm. However, hydraulic conductivity results for 5.7 mm shingle were non-linear, indicating non-Darcian flow and accordingly, shingle of 4 mm mean diameter was used for subsequent tests.

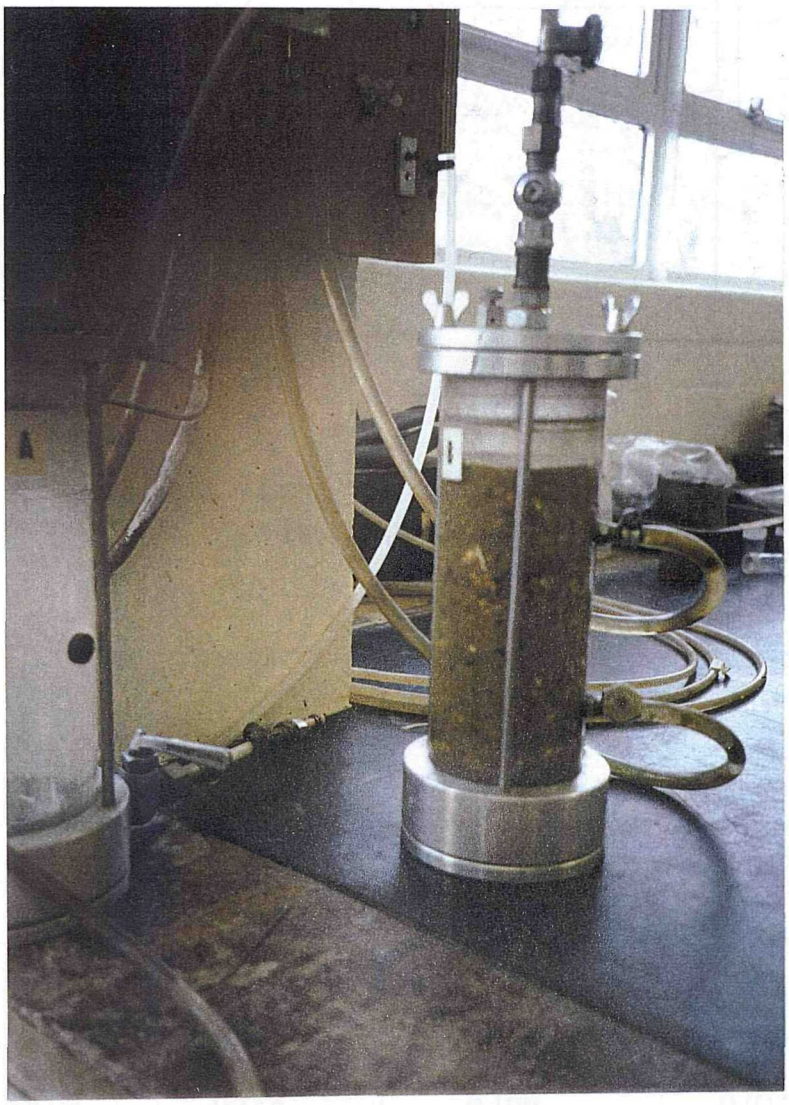

Plate 4.5 Equipment used for hydraulic conductivity tests

Tests were conducted using mixtures of the 4 mm shingle with fine, medium and coarse sands. Particle size characteristics of the sands are given in Table 4.3 and at Figure 4.7. A representative sample of the sands was sieved at 0.25 ϕ intervals and the statistics were calculated using the moments method, with the grading percentages derived graphically. All sands were very well sorted. The fine and medium sands were fine-skewed whilst the coarse sand was near-symmetrical.

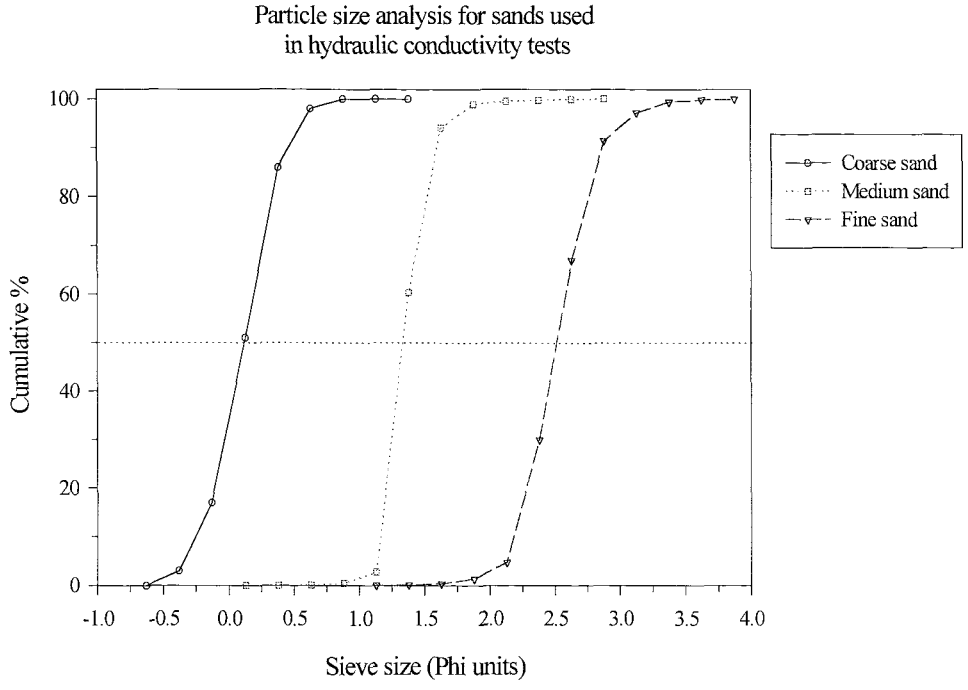

Figure 4.7 Cumulative percentages of sands used in permeameter tests

	Fine Sand		Medium Sand		Coarse Sand	
	Phi	mm	Phi	mm	Phi	mm
Mean	2.651	0.159	1.490	0.356	0.241	0.846
Sorting	0.287	0.820	0.183	0.880	0.260	0.835
Skewness	0.164		0.199		0.041	
Asymmetry	0.419		0.321		0.349	
D10		0.203		0.411		1.086
D50		0.161		0.365		0.847
D90		0.126		0.304		0.669

Table 4.3 Particle size characteristics of sands used for hydraulic conductivity tests

Hydraulic conductivity tests were performed under a constant head of water which had been de-aired. The sample mixtures were placed in the chamber in 4 layers of approximately 5 cms and each layer tamped with 6 blows. Measurements were made by noting the volume of water discharged throught the sediment, V_w , in a given amount of time, t, under a given head of water (h_1 - h_2 , the difference between the water levels in the two manometer tubes). A minimum of 5 measurements were made then the head was increased and the procedure repeated.

Hydraulic conductivity, K, was calculated for each period of constant head:

$$K = \left(\frac{Q}{i}\right) \cdot \left(\frac{R_t}{A}\right) \tag{4.33}$$

where Q is the mean flow rate (V_w / t, ml s^{-1}), i is the hydraulic gradient:

$$i = \frac{(h_1 - h_2)}{y} \tag{4.34}$$

h_1 and h_2 are the two manometer readings (mm) and y is the distance between manometer glands on the cell chamber (mm). A is the cross-sectional area of the sample in the cell chamber (mm^2) and R_t is the correction factor for the influence of temperature on viscosity of water, and which standardises the resulting permeability to 20°C (BS 1377 Part V, BSI, 1990). Results of the tests for a range of sediment mixtures are given in Chapter 9.

CHAPTER 5: RESULTS - METEOROLOGICAL AND HYDRODYNAMIC CONDITIONS

This Chapter presents the results together with some discussion of the wind and hydrodynamic conditions experienced during the field experiment. This initial analysis has concentrated upon a sub-set of 4 consecutive tides (referred to as Tides 26 to 29); these tides included various wind conditions and the change from neaps to springs. No measurements of suspended sediment were available for subsequent tides, but three further spring tides, when the winds were generally calm, were selected to examine the importance of nearshore tidal currents (Tides 31 to 33).

5.1 Weather Conditions

Weather conditions during the field deployment are listed in Table 5.1. Meteorological data from RAE Llanbedr, located adjacent to the field site, were supplied by the Meteorological Office, Aberporth. Wind direction is in degrees (relative to North), wind velocity in knots and atmospheric pressure (at sea level) in mb. Wind data on Julian Days 267, 268, 274, 275 and 281 were obtained from a hand-held anemometer, presented on a Beaufort Scale. Atmospheric pressures on those days were supplied by Aberporth.

A comparison of the wind conditions during the field experiment, with the long-term record for Milford Haven, showed the field conditions to be reasonably typical of average conditions for the season (see Section 4.1.3). An exception was the presence of about 15% more calm days than would be expected (Figure 5.1).

5.2 Tidal Regime

The Admiralty tidal predictions for Barmouth, during the field experiment, encompassed a spring-neap-spring cycle (Figure 5.2). The measured elevation of High Water at Morfa Dyffryn was close to that predicted. The maximum tidal range during the first set of springs was 4.24 m; it was 5.16 m for the second. These data confirm the classification of Morfa Dyffryn as a macro-tidal beach[4] (*cf.* Carter, 1988). The minimum

[4] Masselink & Short (1993) point out that Davies's (1964) original classification does not specify clearly which tidal range should be used (*i.e.* spring, neap or mean). Carter (1988) uses spring tidal range.

Time	0800			1200			1600			
Date	Wind		Pressure (mb)	Wind		Pr	Wind		Pr	Tide No
	Dir (deg)	Velocity (knots)		Dir	Vel		Dir	Vel		
18-9			1027							1
19-9		Calm	1013		Calm	1011	330	5	1010	2 & 3
20-9	350	15	1008	340	15	1008	350	10	1007	4 & 5
21-9	040	15	1015	040	15	1018	070	15	1019	6 & 7
22-9		Calm	1024	Vb	5	1024	270	5	1024	8 & 9
23-9	030	5	1024	030	5	1024				10 & 11
24-9		F 5-6	1015							12 & 13
25-9	ESE	F 5-6	1016							14
26-9	350	7	1018	330	10	1020				15 & 16
27-9		Calm	1021				300	12	1021	17 & 18
28-9	220	7	1022	280	8	1023				19 & 20
29-9	260	6	1022	250	10	1023	240	7	1022	21 & 22
30-9	220	9	1020	220	12	1021				23 & 24
1-10			1022				SW	F 3-4		25 & 26
2-10	SW	F 6-7	1016	SW	F 5-6					27 & 28
3-10	330	10	1008	040	15	1011	040	12	1015	29 & 30
4-10		Calm	1024	010	5	1026	010	8	1026	31 & 32
5-10		Calm	1031	250	8	1033	250	8	1033	33 & 34
6-10	200	15	1032	200	15	1032	220	16	1029	35 & 36
7-10	200	15	1024	190	15	1025				37 & 38
8-10			1020		Calm					39

Table 5.1 Weather conditions at Morfa Dyffryn during the experimental period

tidal range was 1.44 m, during the neap tides (including Tides 26 and 27). Tides 28 and 29 were associated with increasing tidal ranges, mid-way between neaps and springs. During the field deployment, Sarn Badrig was not exposed, but its position was marked regularly by breaking waves.

The percentage of the tidal cycle for which each part of the profile is inundated, during average spring and neap tides is shown in Figure 5.3 (*cf.* Wright *et al.*, 1982). The crest of the main ridge is covered for less than 40% of the spring tidal cycle and only about 5% of the mean neap tidal cycle. When the measured data are examined, there is some asymmetry in the nearshore tidal curve, particularly from HW ±1.5 (Figure 5.4).

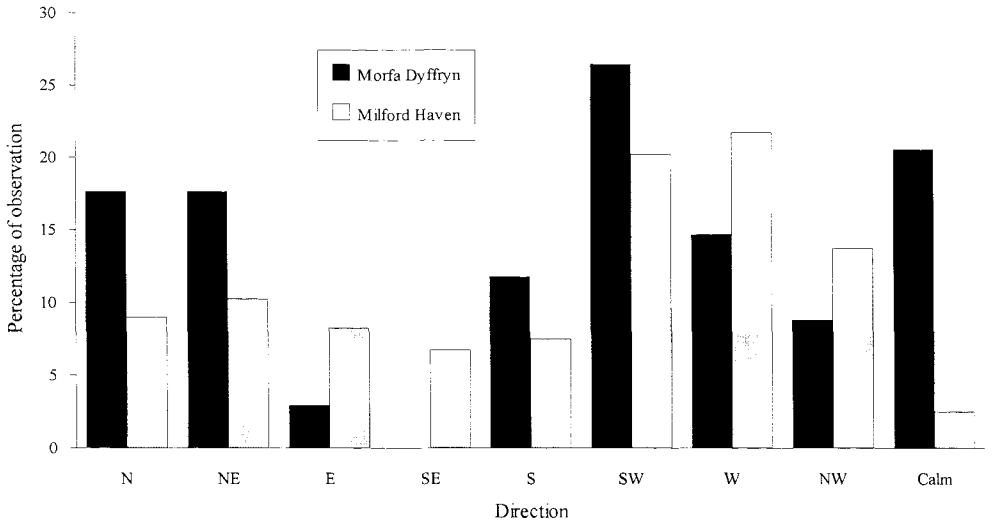

Figure 5.1 Comparison of wind direction occurrence at Morfa Dyffryn, with average conditions (Milford Haven), for September/October

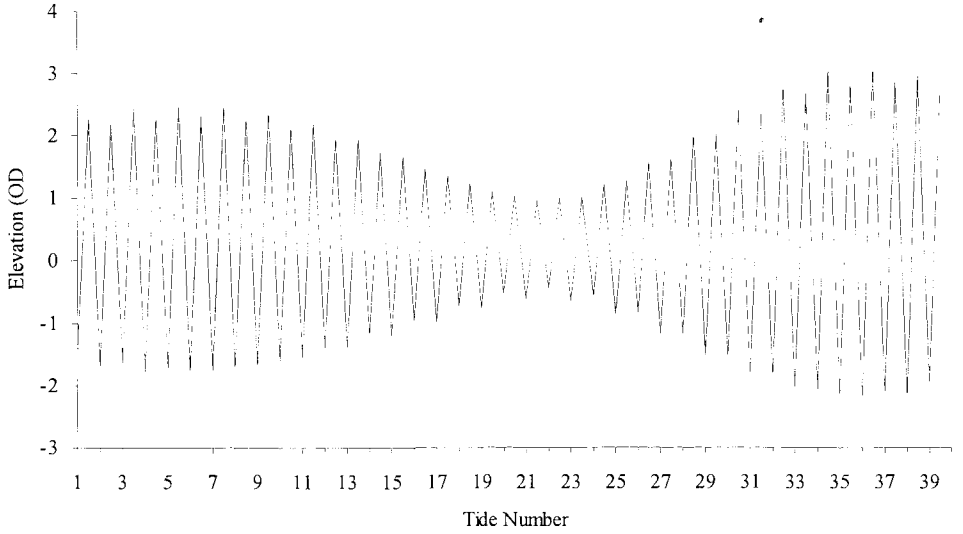

Figure 5.2 Predicted tidal elevation at Barmouth (Tide 1 = 18 September 1994, Julian Day 261), abstracted from Admiralty Tide Tables.

At this time, the ebb tide falls considerably more slowly than the equivalent tidal rise. This pattern is related to frictional effects and the generation of the M_2 sub-harmonics in

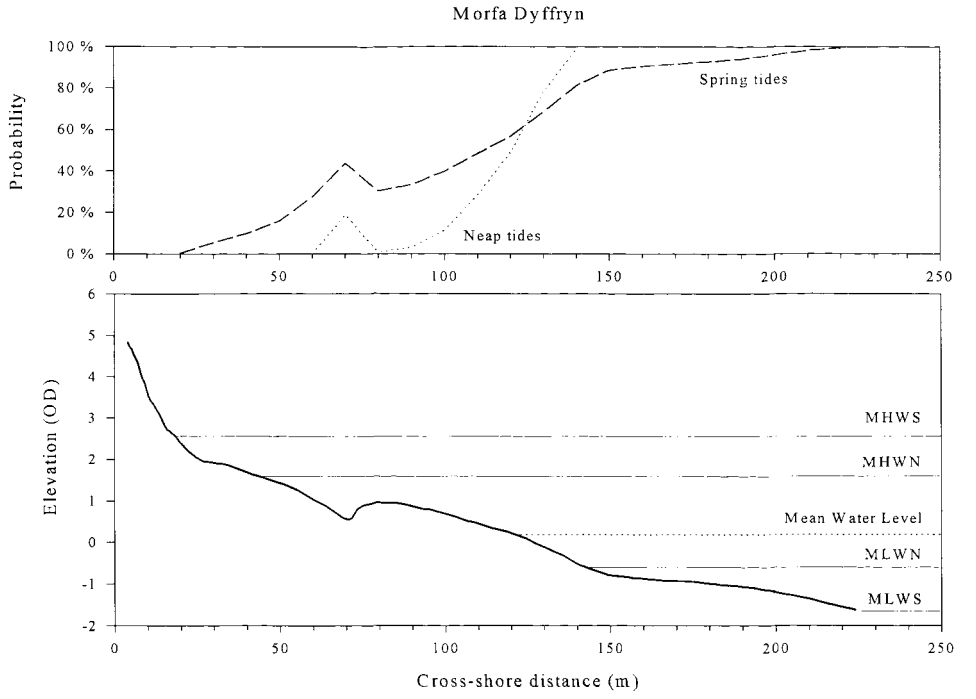

Figure 5.3 Probability of tidal inundation at Morfa Dyffryn, during average spring and neap tidal cycles

shallow water; this resulted in a longer inundation period at Station C (at 93 m) on the ebb, than on the flood during spring tides. For example, during Tide 29, the section of the beachface between about 50 to 100 m along the cross-shore transect was subjected flood currents over 1.5 hours and ebb currents over 2 hours. These observations are of some significance, since the mean currents were also, at times, tidally asymmetric; they were at their highest later in the ebb (Section 5.3.2).

Measurements of currents at Morfa Dyffryn included in general, 2 hrs on either side of High Water (HW). During these hours, offshore tidal currents may be expected to be southerly; strong currents occur at HW with moderate currents 2 hrs on either side, as described previously (Section 4.1.3). Such currents can reach 1 knot (~ 0.5 ms^{-1}), during spring tides. Strong or moderate northerly currents only occur late in the ebb, between HW +5 and HW -6. Only during Tide 29 were the longshore currents in the same direction as the predicted tidal currents, although the strongest recorded current occurred approximately 1.5 hrs after HW. The tidal currents recorded during the experimental period are discussed in more detail later (Section 5.3.2).

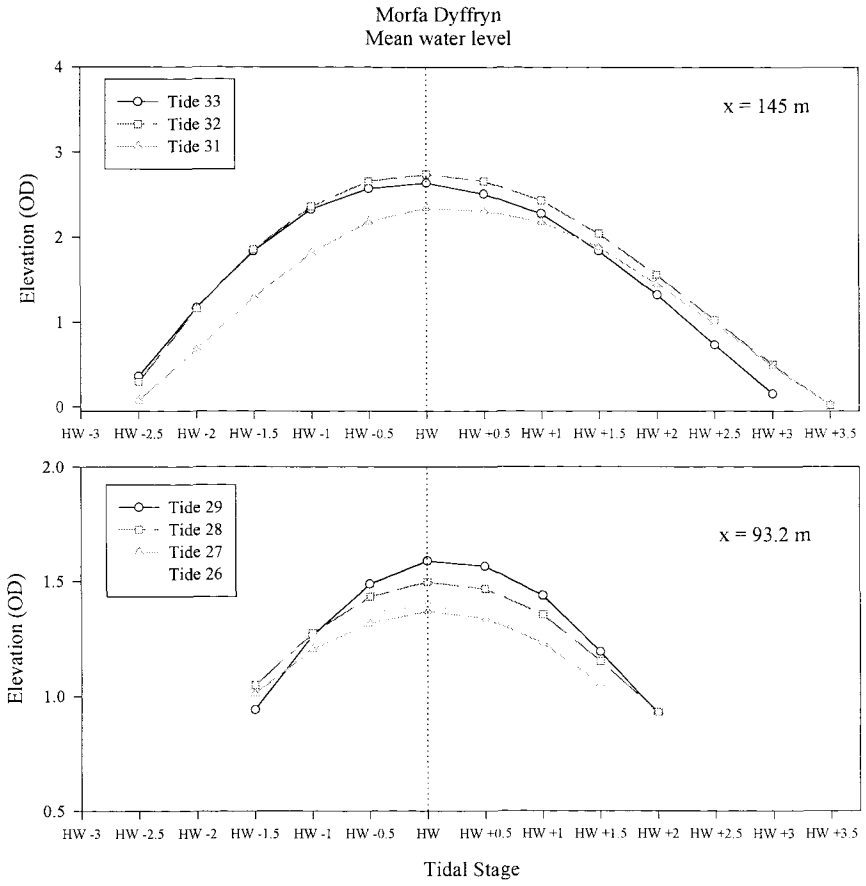

Figure 5.4 Sea surface elevation measured at (a) 145 m and (b) 93 m across the main transect

5.3 Hydrodynamic Conditions: Tides 26 to 29

5.3.1 Waves

H_s and H_{rms} were at their maximum at High Water and at their minimum during the early flood and late ebb phases of the tidal cycle (Figure 5.5). The measuring position was located within the region of breaking waves, throughout all four tides, as shown by the ratio of H_b / h (Figure 5.5 *d*); this was confirmed by visual observations. The

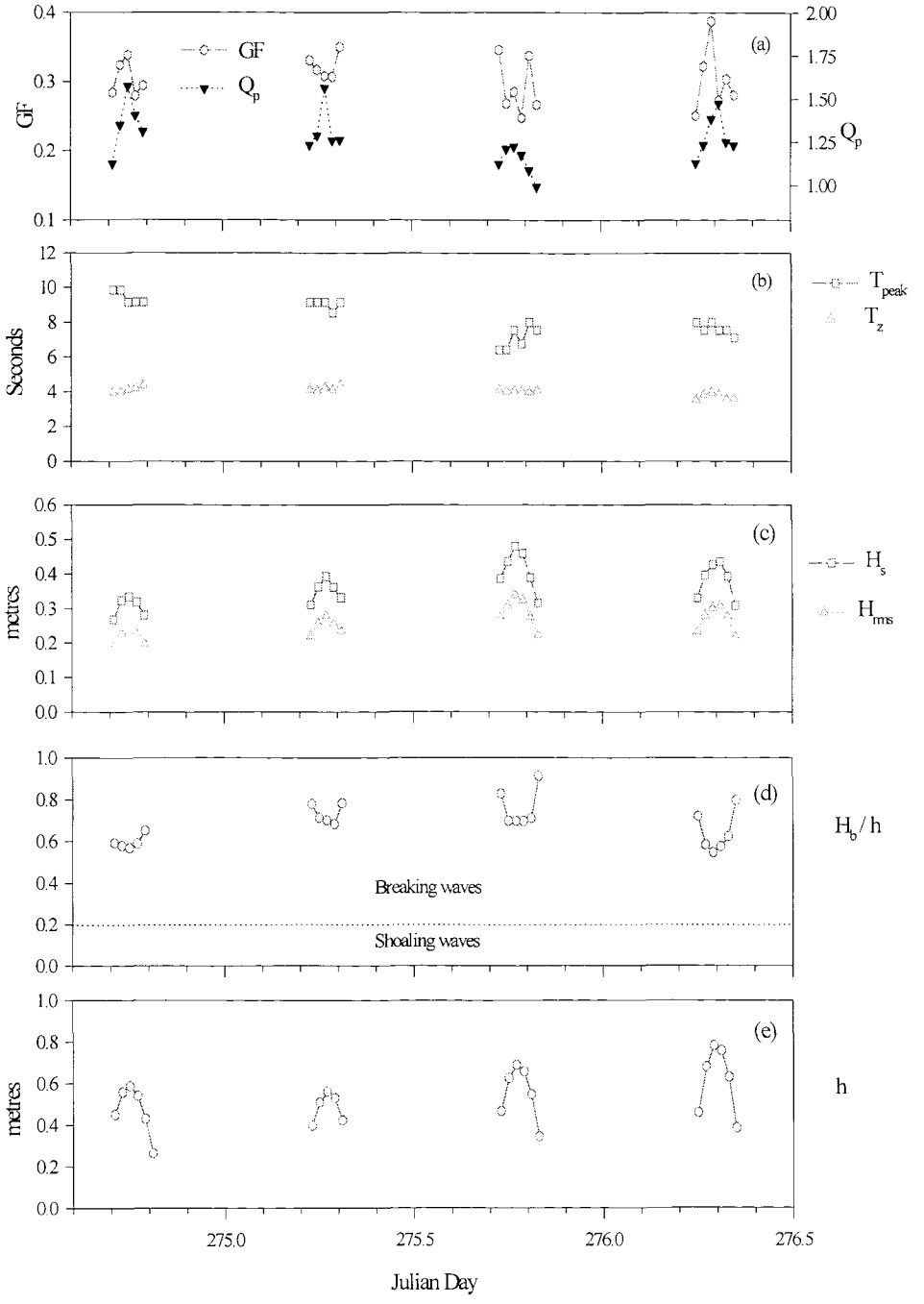

Figure 5.5 Wave characteristics during Tides 26 to 29 (a) Groupiness Factor and spectral width parameter (b) Spectral peak and zero-upcrossing periods (c) Significant and RMS wave height (d) ratio of breaking wave height to water depth (e) mean water depth

prevailing weather conditions included both light winds and moderate breezes; during Tide 26 the winds were (Beaufort) Force 3 - 4 from the southwest (the direction of the maximum fetch) and the breaking waves were spilling in character. The peak wave period, T_p, was around 9 s, whilst the period derived from the zero-crossings of the wave record, T_z, was about 5 s; this suggests that the sea was not fully developed (Figure 5.5*b*). Similar wave periods and wave heights were associated with Tide 27, although the winds had freshened to Force 6 - 7 throughout the flood tide, moderating to Force 5 - 6 by late in the ebb. The surf zone consisted of 5 or 6 lines of spilling breakers, with white horses seen at sea. The wind backed to WNW and moderated further to Force 3 for Tide 28, with 2 or 3 lines of spilling breakers in the surf zone; these were the highest waves of the four tides under consideration. Tide 29 was associated with Force 3 winds from the NNW; this is in the alongshore direction at the field site. Overall, Tide 28 was related to the most fully-developed sea with the broadest spectum, the highest waves and significant cross-shore orbital velocities of all the tides. This occurred some 12 hrs after the strongest winds, from the direction of maximum fetch.

Hence, the distinctive changes in weather conditions during the (4) tides under investigation led to only minor differences in the basic wave statistics; there was less than 0.25 m difference in the nearshore significant wave height, in the surf zone, throughout the period. This observation illustrates also the effectiveness of the wide intertidal terrace, at dissipating wave energy. The similarity of the basic wave descriptors for Tides 26 to 29 illustrates also the perennial problem of inferring nearshore sediment transport from tidally-averaged wave statistics. For example, considerable quantities of sand were transported during Tide 29 (Chapter 8); these washed out the inner runnel, between D1 and D2 (Figure 4.2). Such marked differences in sediment transport would not necessarily be indicated from the results presented in Figure 5.5.

5.3.2 Mean currents

Although the wave parameters did not vary greatly for the (4) tides under investigation, the mean currents were noticeably different[5]. Cross-shore mean currents, during Tides 26 to 28, were generally onshore at low water and offshore around high

[5] All references to currents at Morfa Dyffryn relate to the lowest EMCM (at 0.12 m from the seabed) at Station C, unless indicated otherwise

water. There was a persistant and increasing undertow throughout Tide 29 (Figure 5.6), even when the water was shallower than about 0.45 m.

Not all of the tides included data obtained from very shallow water; this relates to the burst sampling regime, of 17.07 minutes every half hour. The highest EM (at 0.78 m above the bed) was covered for only brief periods during the tides under consideration here; therefore, it is possible to obtain only an indication of vertical structure in the mean current velocity. During Tides 27 to 29, the current at 0.31 m above the bed was generally stronger than, but in the same direction as that at 0.12 m. During the early flood phase of Tide 26, the mean current was onshore at 0.12 m but offshore higher in the water column. The mean flows were measured by EMCM's in the field and these are considered to be reliable only to within about 0.01 to 0.02 ms^{-1} (Huntley, 1991; Beach & Sternberg, 1991). However, of the 24 data files under consideration, only 7 had mean cross-shore flows below 0.02 ms^{-1}; of these, 5 were below 0.01 ms^{-1}. With the exception of High Water of Tide 28, all the longshore currents were considerably higher than 0.02 ms^{-1} ; accordingly, instrumental uncertainties will not affect the resultant current direction.

The longshore currents differed during each of the tides; their direction remained essentially constant, but their magnitude varied considerably. During Tides 26 to 28, the longshore current was highest under shallow water conditions; it was lowest around high water, even reversing direction at HW on Tide 28. This reversal of current was associated with mean currents of less than 0.02 ms^{-1} ; this was the weakest current recorded during all (4) tides and, therefore, was possibly within the error range of the instruments as mentioned above. However, the recorded direction is not caused by a problem of electronic offsets. The mean currents were calculated using all the recorded offsets (Table 3.4) and, although the mean velocity differed in magnitude, the direction remained the same. The reversal occurred only near the seabed, not higher in the water column. The apparent steady increase in longshore current, during Tide 27, may be a product of the burst sampling regime (with only 5 files recorded); however, the consistent increase in longshore current during Tide 29 includes shallow water flood and ebb phases of the tide. This particular current reached velocities of nearly 0.4 ms^{-1}, with no reversal of direction. The surface winds at this time were NNW *(i.e.* parallel to the shoreline), but with a limited fetch (with protection from the Lleyn Peninsula, less than 15 miles to the north) and breaking wave heights of 0.4 m; therefore, it seems unlikely that these high

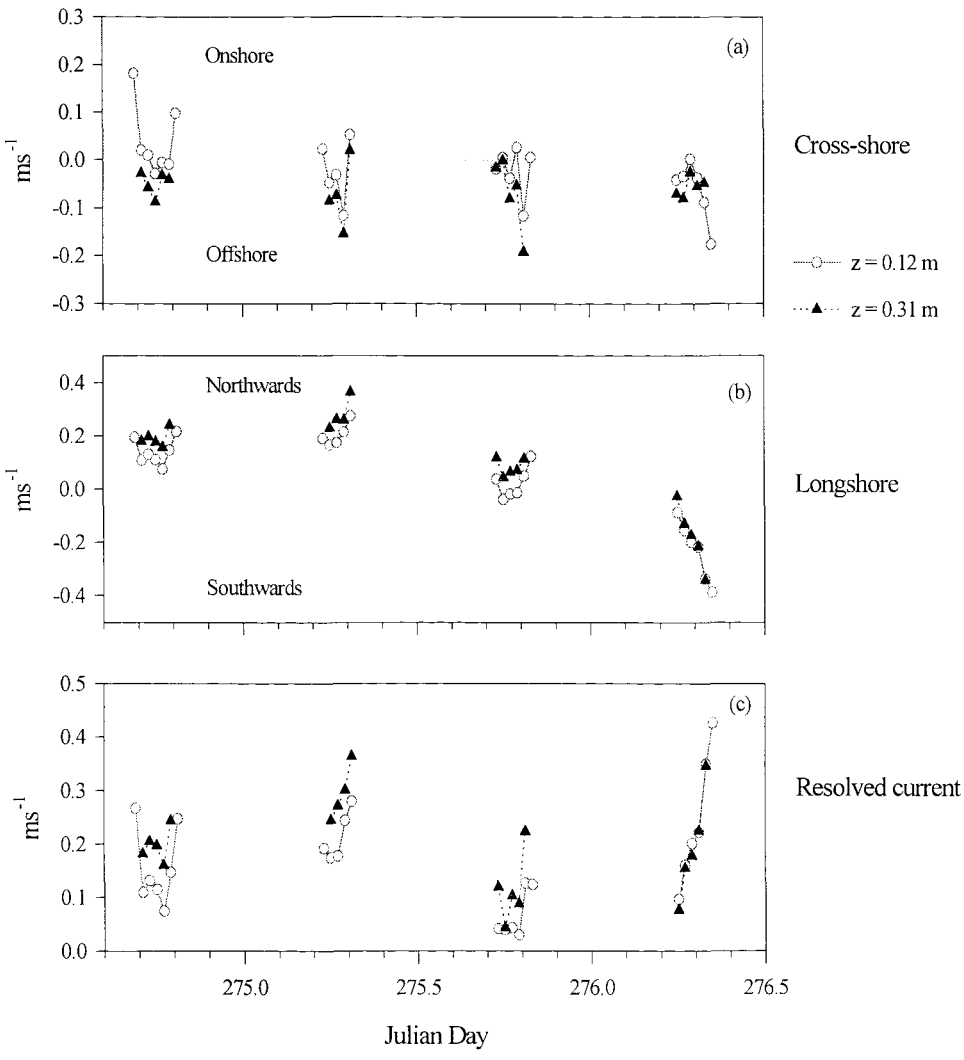

Figure 5.6 Measured mean currents at Station C during Tides 26 to 29 (a) cross-shore (b) longshore and (c) resultant

longshore currents could be generated by wind-wave activity alone.

Although nearshore longshore currents are considered as wave-generated, there is no *a priori* reason why tidally-induced longshore currents should not persist into shallow water areas. Strong, longshore currents of tidal origin have been observed on other beaches associated with a large tidal range. For example, nearshore mean currents

of mainly tidal origin were observed during calm conditions on the macro-tidal beach at Bognor Regis, West Sussex. For this location, it was noted that both the direction and strength of the longshore current could be modified, even reversed, during storms (Voulgaris, 1992). Strong, tidally-induced currents were recorded also at the beginning of the flood phase of the tide at Nieuwpoort-aan-Zee, Belgium (Voulgaris *et al.*, 1997); similarly, just outside the surf zone at Spurn Head (Davidson *et al.*, 1993; Foote, 1994).

With the exception of the data collected during High Water of Tide 28, the mean longshore current *always* exceeded the mean cross-shore current. Such a characteristic was to have an important impact upon the resultant current direction, which was predominantly alongshore. The longshore current also had a notable effect on the resultant current strength and, when combined with a strong undertow in the same quadrant, led to the resultant currents exceeding 0.3 ms^{-1} (see Section 5.3.5). Since the tidal currents might be expected to be southerly throughout the whole of the measurement period (Table 4.1), it is suggested that the longshore current record during Tide 29 (and possibly around the High Water of Tide 28) included a tidal component; this is even though the measurement station was located within the surf zone throughout the period of data collection.

5.3.3 Tidal modification of cross-shore wave-induced currents

In the cross-shore direction, the mean current circulation patterns are attributed generally to wind or wave induction (*e.g.* Svendsen, 1984). However, in macro-tidal regions, an additional cross-shore current component can be generated by the cross-shore migration of the tidal prism. At HW, the component of mean cross-shore current due to translation of the tidal prism is zero; hence, any residual mean current at HW is due to undertow. The mean cross-shore current is presented against the gradient of the water surface ($\partial h/\partial t$) at Station C in Figure 5.7. There remained a persistent undertow of approximately 0.025 ms^{-1} around High Water for all (four) tides. Such a current is in common with the prevailing hydrodynamical conditions on a macro-tidal beach at Nieuwpoort-aan-Zee (Voulgaris *et al.*, 1997); this indicates that it is not related to the tidal conditions, but due to cross-shore water volume circulation. Voulgaris *et al.* (*op. cit.*) have implied that mean cross-shore currents, in excess of this wave-induced value, represent the current component due to tidal influence. At Morfa Dyffryn, the strongest

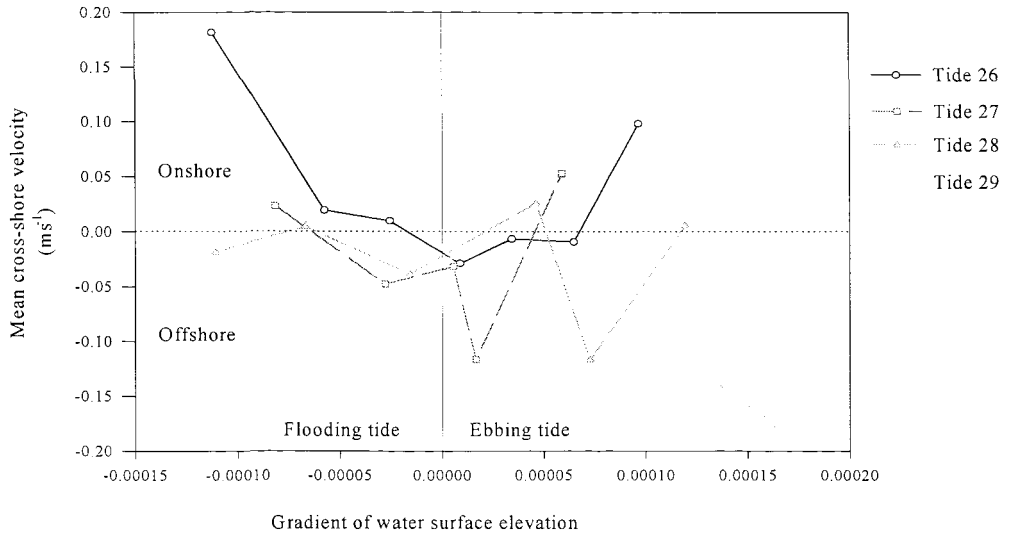

Figure 5.7 Tidal variation in sea surface elevation and mean cross-shore velocity during Tides 26 to 29

offshore flows occurred towards the end of the ebb, during Tide 29; this contained a tidal current component of up to 0.1 ms^{-1}, which was double that due to undertow alone. The tidal component will enhance offshore flow when operating in the same direction as the undertow *i.e.* during the ebb phase of the tide. During the flood, the tidally-induced currents opposed the undertow, so that mean cross-shore currents were lower during the flood than the ebb.

The implication of the observations above is that a tidal asymmetry in mean cross-shore currents will occur in the presence of undertow on all macro-tidal beaches; there will be relatively stronger offshore flows during the ebb, than on the flood. However, there appears to be a threshold tidal range, or volumetric tidal prism, required to generate tidal currents sufficiently strong to affect the wind or wave-induced currents and, thus, to create the tidal asymmetry. If there were no residual tidal influence on the cross-shore mean currents (*i.e.* if the undertow is a function purely of the vertical velocity structure in the water column and the relative height of the EMCM), the variation in the mean cross-shore current throughout the tide would be symmetrical about High Water; this was the case for Tide 26 and, to a lesser extent, Tide 27, but not during Tides 28 and 29 (Figure 5.7). It would appear then, that the tidally-induced mean cross-shore currents are

of minor significance over the lower section of the spring-neap tidal phase at Morfa Dyffryn.

During the tides under consideration (Tides 26 to 29), only two pressure sensors were inundated (at 57 and 93 m along the Main Transect); consequently, most of the data were recorded within the surf zone. Therefore, the pressure sensor and current meter data from several subsequent tides were examined, to investigate further the relationship between tidal range and mean currents.

The data collected during Tides 31 to 33 are useful in assessing the relative importance of wave and tidal components on current flow, since the wind was generally calm and the waves were small ($H_s < 0.2$ m). The data obtained included both breaking and shoaling waves (Figure 5.8). These tides showed also an asymmetry in the mean cross-shore current and sea surface gradient (Figure 5.9). The mean cross-shore velocities during Tides 31 to 33 require some discussion, since the residual mean cross-shore current at High Water was ~ 0.06 ms^{-1} onshore (*i.e.* there was no undertow at this location); it was at its highest during the flood tide, reducing throughout the ebb (Figure 5.8 *a*). An explanation can be proposed which relates to the tendency towards higher, onshore velocities at HW -1.5 and HW +2; these may represent mean onshore currents relatively high up in the water column and, since these are in shallow water, the orbital velocities are at their maximum. The remaining flood phase measurements contained, therefore, an onshore wave-induced component enhanced (albeit weakly) by an onshore tidal component. After High Water, the tidal component opposed the onshore wave-induced mean velocity, increasingly so as the ebb progressed. Such opposition resulted in progressively smaller mean cross-shore currents outside the surf zone during the ebb tide, than occurred during the flood. The higher mean onshore flows in shallow water early in the flood (Tide 31) and late in the ebb (Tides 31 and 33) conformed to the pattern observed during Tides 26 to 28. Other possible reasons for the lack of undertow during these tides are summarised below:

(a) The small waves (< 0.2 m in height) did not induce a sufficient additional onshore flux of water, for a returning flow at the bed to influence the mean current, once Station C was located outside the surf zone. Masselink & Black (1995) observed reduced undertow outside the surf zone on the low tide terrace of a macro-tidal beach, although some small bed return flow was still present.

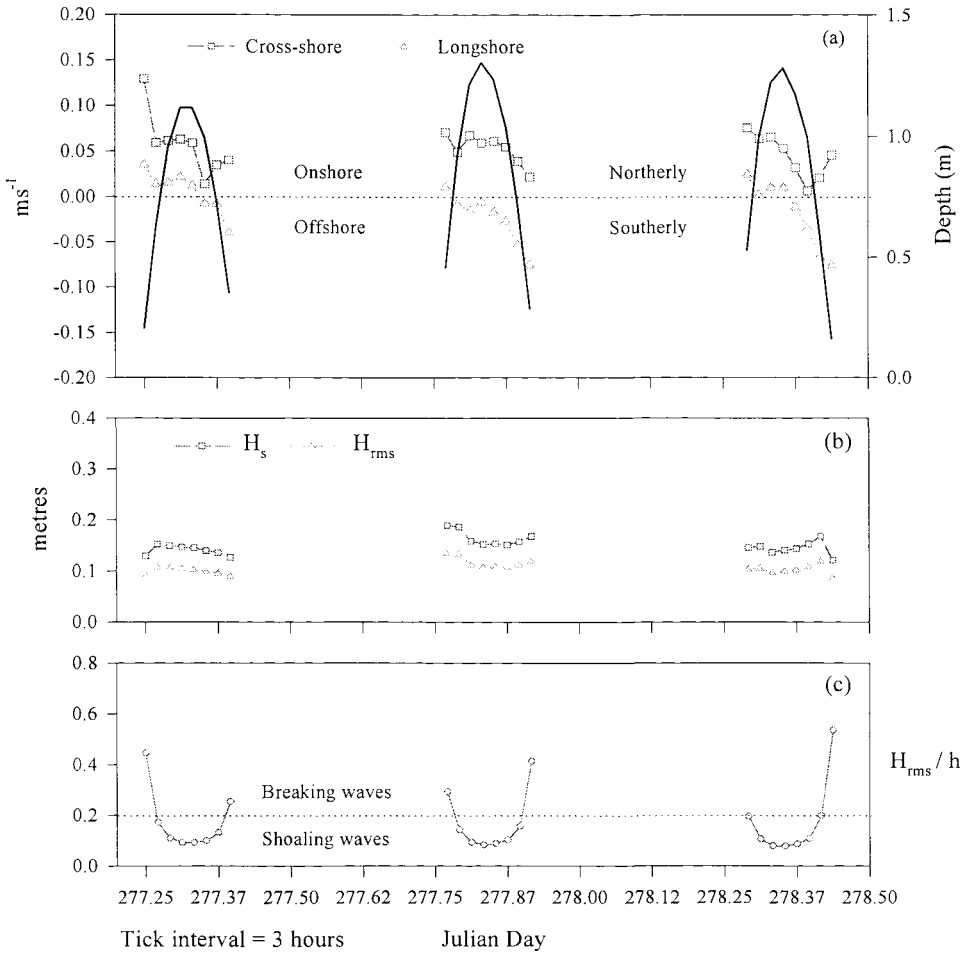

Figure 5.8 (a) Mean currents and water depth, (b) significant and RMS wave height and (c) ratio of H_{rms} to water depth for Tides 31 to 33

These investigators suggested that the velocity of the undertow is dependent upon the square root of the offshore wave height, rather than a linear relationship (Greenwood & Osborne, 1990; Hazen *et al.*, 1990). However, no data have been included for offshore wave heights less than 0.3 m, when the square root function is likely to exert most influence.

(b) The undertow was confined to a water depth which was less than 0.13 m

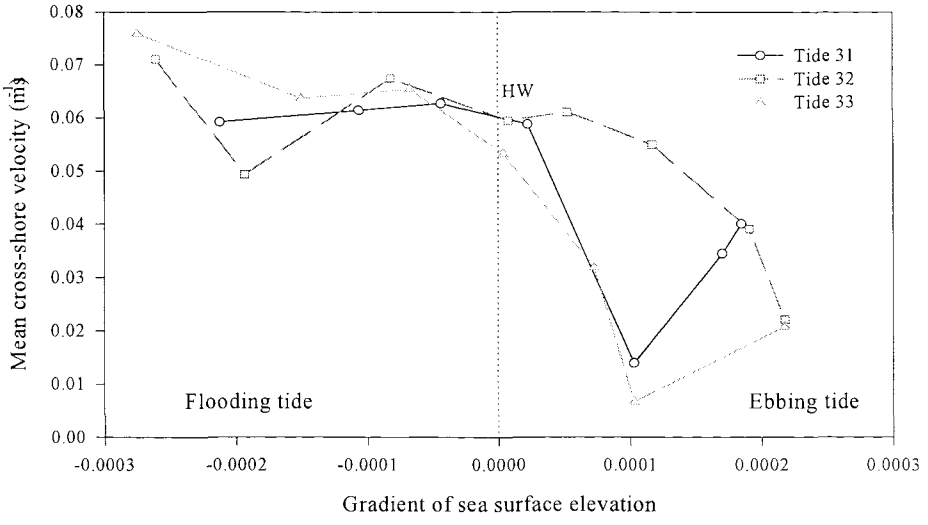

Figure 5.9 Tidal variation in sea surface elevation and mean cross-shore velocity during Tides 31 to 33

from the seabed. For comparison, Masselink & Black (1995) do not state the height at which their measurements of undertow were undertaken.

(c) The swash zone advanced over the shingle during the deeper water phase of these tides; therefore, excess onshore water mass may have been absorbed by infiltration into the bed. The permeability of the sediment has been found to affect the mean cross-shore flow in models for engineering structures; with net onshore flow across a steep, permeable slope, but with an undertow present in front of an impermeable structure of similar slope (Kobayashi & Wurjanto, 1992). Mean onshore currents should then show a net increase at this time, since the offshore component would be lower; this was not the case at Morfa Dyffryn. However, it is possible that after HW there was a contribution to offshore flow from exfiltrating groundwater, particularly when the shingle was inundated. It is difficult to apportion the net mean cross-shore current to wave- and tidally-induced components and exfiltration processes, each of which may be operating in a different direction.

5.3.4 Tidal asymmetry of longshore currents

The lag between the sea surface elevation and the longshore tidal currents was examined for Tides 31 to 33. The longshore currents during the flood were weakly northerly; they reduced during the flood tide, becoming slack around HW (the measured longshore currents are shown as triangles on Figure 5.10). Current direction reversed to southerly during the ebb and increased to reach maximum velocity at HW +2. This is the behaviour of a standing tidal wave, yet the Admiralty Tidal Stream Atlas records a progressive-type tidal wave offshore.

A least squares curve was fitted to the longshore current data of Tides 31 to 33 (Voulgaris, pers. comm.) since these tides were springs, approaching some of the highest of the year. At the same time, there were small, plunging waves and a narrow surf zone. Hence, the longshore currents can be expected to represent the tidal component. The best-fit tidal curve was achieved using the M_2 constituent only and is shown as the solid line in Figure 5.10. Visual inspection of the longshore current time series suggests that a minor harmonic is responsible for the "kink" around HW, but the measured data series was too short to be able to resolve additional constituents. The non-tidally induced component of the longshore current was obtained by subtracting the predicted longshore current from that measured (shown as diamonds in Figure 5.10 *b*).

Prevailing winds were calm throughout Tide 31, but increased to 8 knots (~ 4 m s^{-1}) for the following tide (Tide 32); this wind strength and direction can be decomposed into ~ 3.3 ms^{-1} alongshore, southerly and 2.3 ms^{-1} offshore. Atmospheric pressure was high and winds were calm for most of the period of inundation of Tide 33 (0700 to 1030 on 5 October), although an onshore sea breeze of 8 knots developed by 1200. There was some scatter in non-tidal component of the longshore current for Tide 31 whilst, in contrast, the non-tidal longshore current was entirely in a southerly direction, during Tides 32 and 33 (Figure 5.10 *b*); it is possible that some of the non-tidal component is an artefact of using the M_2 constituent only since, at its maximum, the non-tidal component did not exceed 0.04 ms^{-1}.

Practically all the longshore current during Tides 26 to 29 was non-tidally-induced, as might be expected since all recorded data were from within the surf zone (Figure 5.11). Surprisingly, the same applied to Tide 29; although previous analysis had

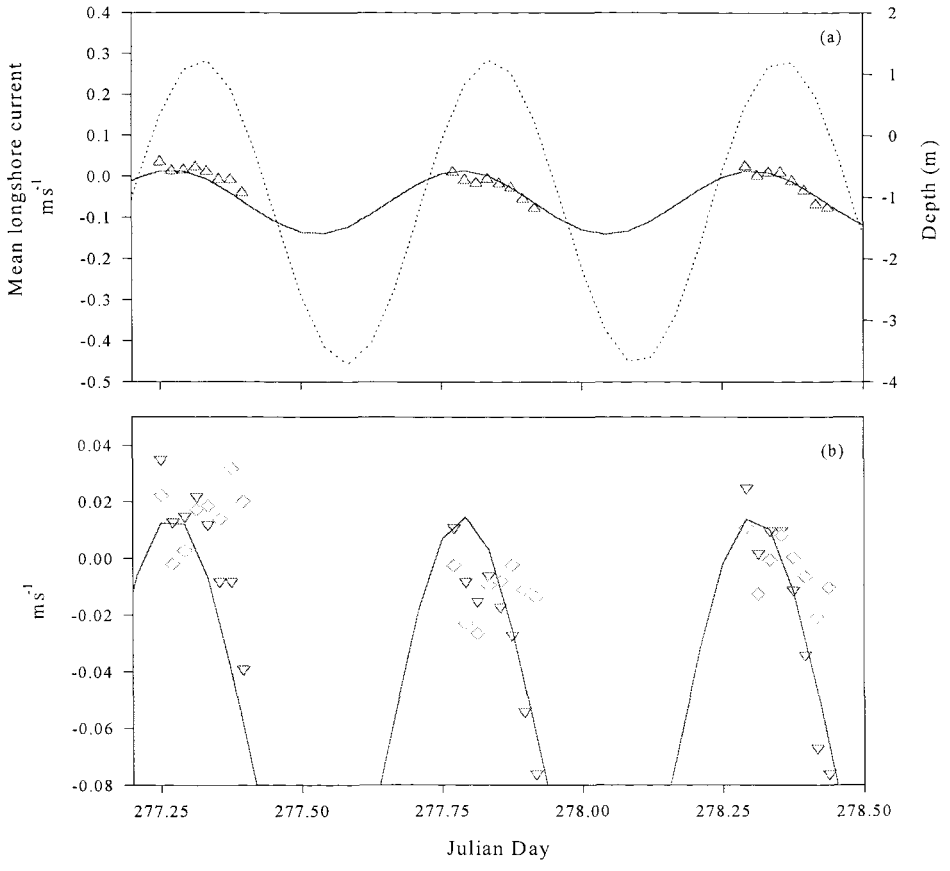

Figure 5.10 (a) Depth (dotted line), measured (triangles) and best-fit (solid line) mean longshore currents during Tides 31 to 33; (b) as (a) including non-tidal component of longshore current (diamonds).

suggested that the extremely high longshore currents which occurred during the ebb tide were unlikely to be purely wave generated (Section 5.3.2); the wide, dissipative surf zone meant that breaking waves were of near normal incidence to the beach. The harmonic analysis suggested that the maximum tidal component of longshore current is only 0.1 m s^{-1}, which is weak in comparison with Tide 29, given that the spring tidal currents offshore can reach1 knot (~ 0.5 ms^{-1}). Hence additional factors, such as wind/current interaction are needed to account for the high resultant currents during the ebb of Tide 29.

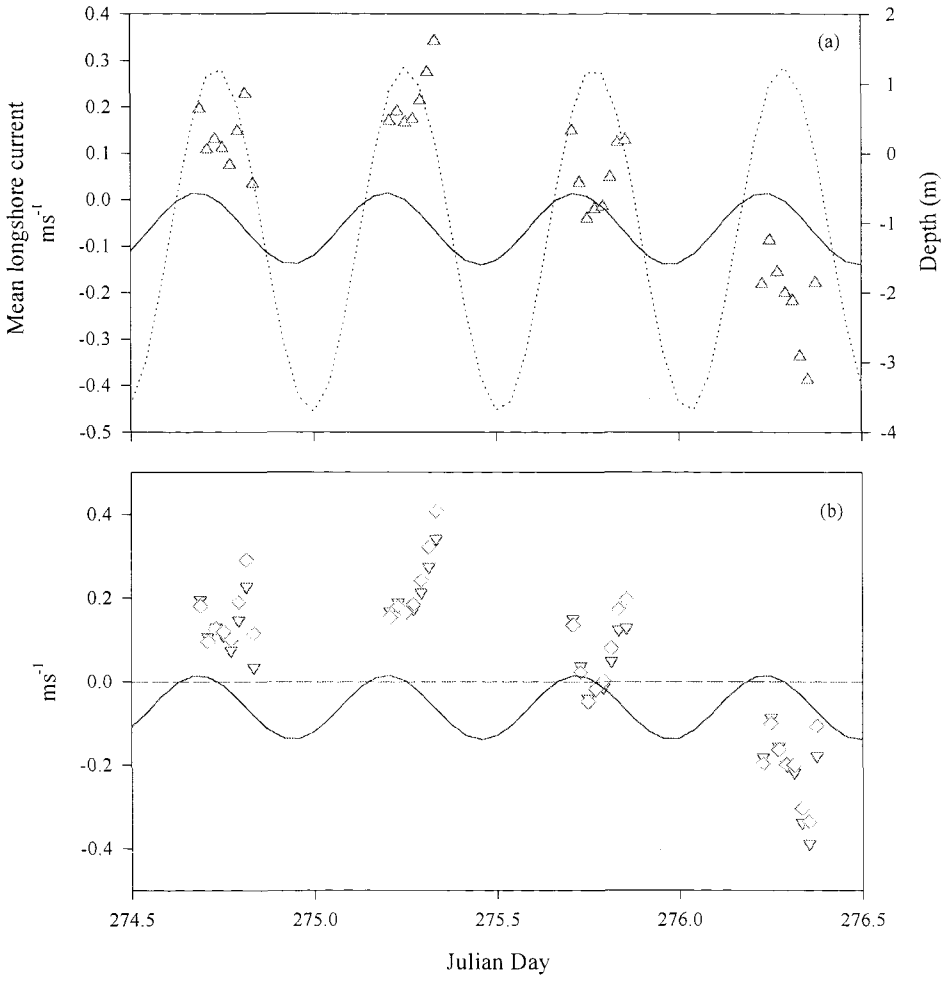

Figure 5.11 (a) Depth (dotted line), measured (triangles) and best-fit (solid line) mean longshore currents during Tides 26 to 29; (b) as (a) including non-tidal component of longshore current (diamonds)

5.3.5 Wind/current interaction and effect on wave height

Similar wave and current characteristics were recorded during Tides 26 and 27, but with some enhancement of the northerly longshore current during Tide 27, induced by the southwesterly Force 6-7 winds (at this time, the tidal current should have been towards the south). Nonetheless, even with following winds and currents, the stronger winds led to only a slight increase in H_s. Likewise, there was no noticeable tidal

influence on the waves or currents, during these tides. In contrast, the results obtained during Tide 28 illustrate a delicate balance between wind and current effects. The wind had backed to WNW and dropped to Force 2. The cross- and longshore mean currents were negligible or weakly northwards; however, they were in opposition to the surface winds, leading to a short, steep sea with breaker heights of nearly 0.5 m.

Meanwhile, during Tide 29, the surface winds of approximately 6 ms^{-1} (~ 12 knots) were almost parallel to the beach; these enhanced the southerly tidal currents, which increased in strength throughout the tide. During the ebb, the tidally-induced component of the cross-shore flow also progressively enhanced the offshore mean flow, so that the resultant mean current at HW +1.5 was almost 0.5 ms^{-1} in approximately 0.5 m of water (Figure 5.12). Once again, since both the surface winds and the cross- and longshore currents operated in the same quadrant throughout the tide, there was only minor modification in the significant wave height (other than through depth modulation).

5.3.6 Short/long wave energy

The total variance in the cross-shore velocities, together with the proportion of variance due to gravity ($0.05 < f < 0.75$ Hz) and infragravity ($f < 0.05$ Hz) waves are shown in Figure 5.13 . Cross-shore variance varied systematically throughout the tide, being highest around High Water; it was clearly dominated by the short waves, which contributed over 85% of the variance (Figure 5.13 *c*). Alongshore, the total variance was considerably less than the total across-shore variance; it was only of about the same magnitude as the *cross-shore longwave* variance (Figure 5.13 *b*). In contrast to the cross-shore, the longshore variance increased steadily throughout the tide, with the exception of Tide 28, for which the variance was tidally-symmetrical. This observation suggests the tide also made a significant contribution to the longshore variance, in addition to the mean longshore current.

The ratio of longshore to cross-shore variance may indicate the presence of long wave energy in the form of edge waves (Tatavarti *et al.*, 1988), with values of over 30% indicating a significant contribution of energy from low mode edge waves. However, the values of the ratio at Morfa Dyffryn (Figure 5.13 *d*) were lower than 30% ; this has been considered to represent predominance of cross-shore waves (Walton, 1992*a*).

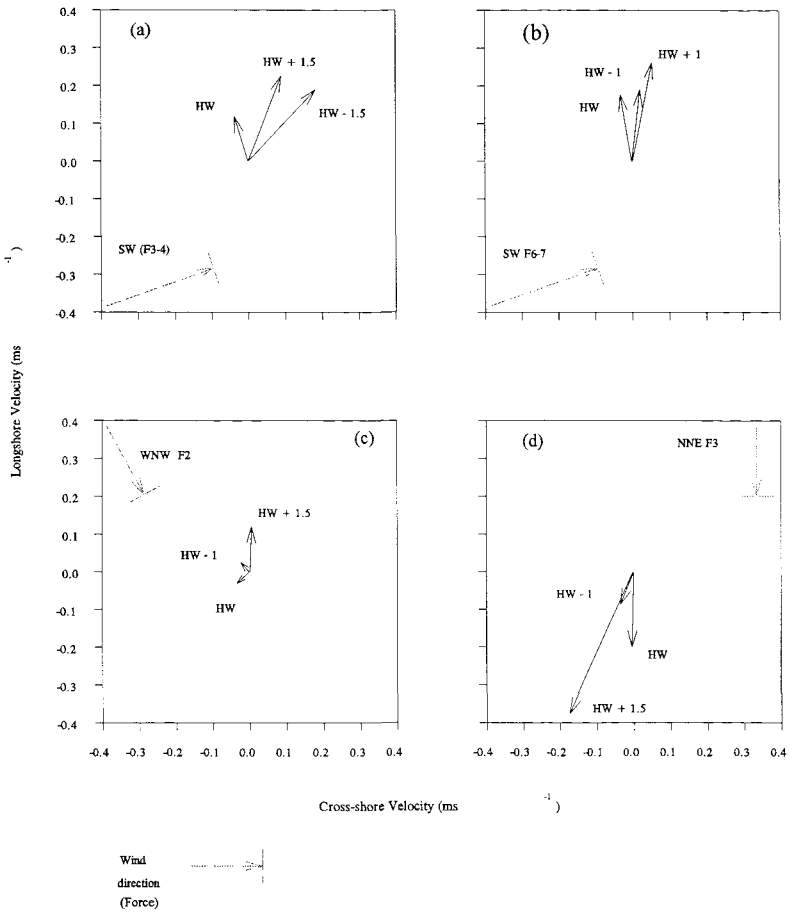

Figure 5.12 Resultant mean currents observed, in relation to prevailing wind direction during (a) Tide 26; (b) Tide 27; (c) Tide 28; and (d) Tide 29.

The long wave variance as a percentage of total variance against depth is shown in Figure 5.14. Cross-shore, the long wave contribution during all the tides was reasonably constant at 10%, in water depths up to 0.6 m; it was near zero in deeper water.

In proportion, the longshore long wave energy contributed more to longshore variance than did cross-shore long wave energy to the cross-shore variance. There was a steady increase in the proportion of longshore variance as the water became shallow, averaging about 25% of total variance in water less than 0.5 m deep.

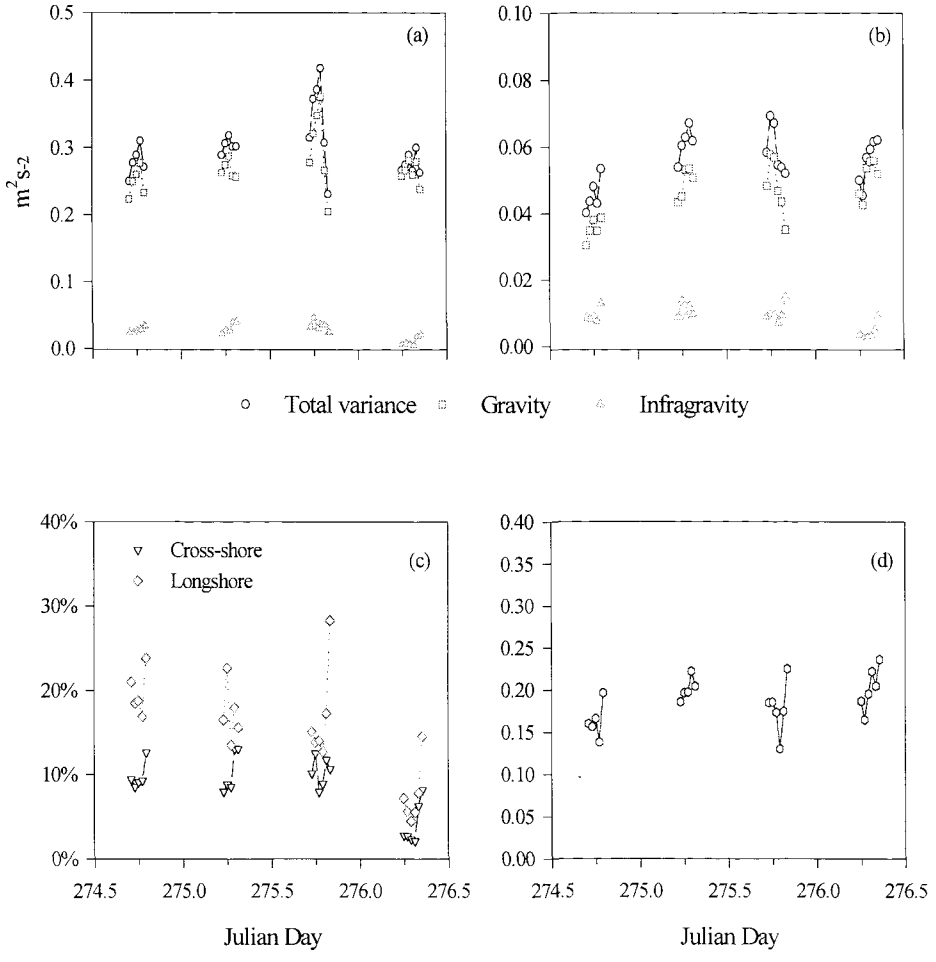

Figure 5.13 Tidal changes in variance for Tides 26 to 29: (a) Cross-shore and (b) longshore. (c) Long wave variance as percentage of total variance; and (d) ratio of longshore to cross-shore variance.

The total variance ratio ($<v^2>/<u^2>$) disguises the different nature of the variance, both tidally and between the various tides. For example, Tides 26 to 28 were associated with a generally high percentage of longshore long wave variance (~ 20%), which was higher in shallow water. In comparison, the long wave variance was less than 10% during Tide 29 both cross- and alongshore. However, the total variance was broadly similar for all of the tides monitored. Hence, the ratio values (for Tide 29 in particular)

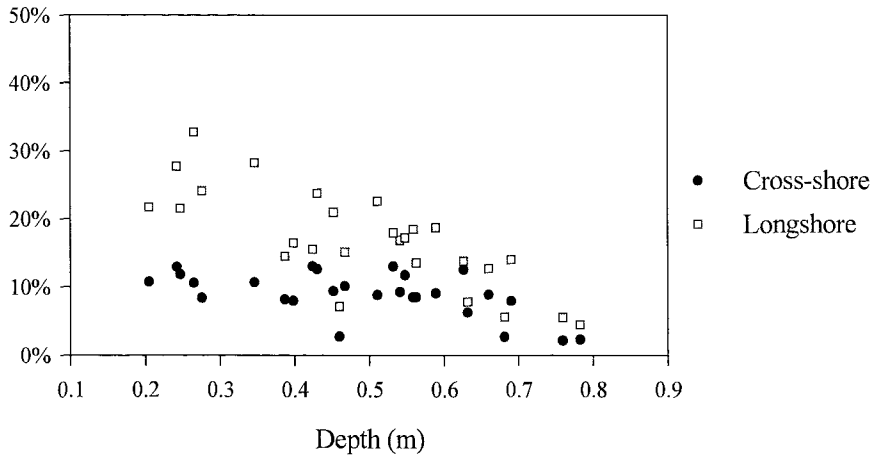

Figure 5.14 Long wave variance as a percentage of total variance in relation to water depth (Tides 26 to 29)

may not indicate significant long wave energy (either leaky waves or edge waves). Rather, they may include a component of tidal energy, in addition to the higher total variance was broadly similar for all tides, and hence the ratio values for Tide 29 in mean currents *i.e.* there was a tidal component to the oscillatory currents, as well as for mean currents.

In summary, analysis of the velocity variance at Morfa Dyffryn (during Tides 26 to 29) has indicated that gravity, rather than infragravity, waves dominated the cross-shore wave field. This observation is in common with the results obtained from other macro-tidal, intermediate beaches (Wright *et al.*, 1982; Davidson *et al.*, 1993). Longshore oscillatory velocities were also primarily gravity waves, except for shallow water conditions duringTide 28; overall, they were of minor significance compared to the cross-shore velocities. It follows, therefore, that eqn. (6.3) is valid for the range of conditions experienced at Morfa Dyffryn (Section 6.1.1) and that the subsequent reflection analysis (see Chapter 7) can be considered to be generally uncontaminated by edge wave motion.

CHAPTER 6: RESULTS - VELOCITY MOMENTS

6.1 Derivation of Moment Terms for Beaches with Significant Longshore Currents

The models described in Section 2.2 were derived under the specific assumption that mean longshore currents were negligible or weak *i.e.* less than 0.1 ms^{-1} (Guza & Thornton, 1985). At Morfa Dyffryn, the longshore currents were anything but negligible and, on most occasions, exceeded the mean cross-shore current (Section 5.3.2). Accordingly, the two velocity moments selected by Guza & Thornton (*op. cit.*) as contributing most to the sediment transport equations, were decomposed into a number of terms. This procedure was adopted in order to establish the individual influence of gravity waves, infragravity waves and mean currents, in both the cross- and longshore directions (Voulgaris & Collins, 1996). The terms make use of the resultant current, rather than the cross-shore or longshore currents in isolation. These approaches are an extension of the study undertaken by Foote (1994), who examined the contribution of cross-shore gravity and infragravity waves to the velocity moments.

6.1.1 Bedload moment terms

The most significant velocity moment for bedload transport by a random wave field, is (Guza & Thornton, 1985):

$$<|\vec{U}_t|^2 \vec{U}_t> \tag{6.1}$$

where $\vec{U}_t$ represents the total instantaneous vector. This moment is made up of an oscillatory vector and a mean flow component both cross-shore (represented by u) and longshore (v):

$$\vec{U}_t = (\tilde{u} + \bar{u}),(\tilde{v} + \bar{v}) \tag{6.2}$$

The overbar symbol represents mean flow and the tilde symbol the oscillatory component of the flow. Hence (6.1) can be divided into its constituent parts:

$$<|\vec{U}_t|^2 \vec{U}_t> = <(\bar{u}^2 + \tilde{u}^2 + 2\bar{u}\tilde{u} + \bar{v}^2)\ (\bar{u} + \tilde{u},\bar{v})> \tag{6.3}$$

The oscillatory component of the longshore vector is assumed to be negligible; this was verified for the Morfa Dyffryn data (Section 5.3.6). The cross-shore oscillatory vector $\tilde{u}$ consists of a short wave (subscript s) and long wave (subscript l) component:

$$\tilde{u} = u_s + u_l \tag{6.4}$$

Substitution of (6.4) into (6.3) and the subsequent expansion produces 20 individual terms, which are classified according to their mode of sediment transport and are defined in Table 6.1. The square component of each term is deemed responsible for mobilising the sediment; the remaining part for transporting the sediment, once it is set in motion.

6.1.2 Suspended load moment terms

The velocity moment identified by Guza & Thornton (1985) as important for suspended sediment transport is:

$$<|\vec{U}_t|^3 \vec{U}_t> \tag{6.5}$$

which can be expanded to:

$$<(\bar{u}^2 + \tilde{u}^2 + \bar{v}^2 + 2\bar{u}\tilde{u})^{3/2} \cdot (\bar{u} + \tilde{u}, \bar{v})> \tag{6.6}$$

However, (6.6) cannot be expanded further in a practical manner without further assumptions (Voulgaris & Collins, 1996). This analysis assumes that when moderate or storm conditions are encountered, the oscillatory velocities are likely to be more significant than the mean currents, such that the short waves will be responsible for mobilising the sediment for subsequent transport by short waves, long waves or mean flows, as appropriate. Under calmer weather conditions, the mean longshore flow will be responsible for mobilising the sediments, again for transport by any agent. Hence, a further 8 terms are defined in Table 6.2.

6.2 Analysis of Velocity Moment Terms

In order to isolate the most important terms within (6.1) and (6.5), the magnitude

Moment		Mobilising Component	Transporting Component
Cross-shore Bedload Moments			
CBM 1	$\overline{u}^3$	Mean cross-shore flow cubed	
CBM 2	$<u_s^3>$	Skewness of short wave component	
CBM 3	$<u_l^3>$	Skewness of long wave component	
CBM 4	$<3\,u_s^2\,\overline{u}>$	Short waves	Mean cross-shore flow
CBM 5	$<3\,u_l^2\,\overline{u}>$	Long waves	Mean cross-shore flow
CBM 6	$\overline{v}^2\,\overline{u}$	Mean longshore flow	Mean cross-shore flow
* CBM 7	$<3\,\overline{u}^2\,u_s>$	Mean cross-shore flow	Short waves
* CBM 8	$<3\,\overline{u}^2\,u_l>$	Mean cross-shore flow	Long waves
* CBM 9	$<\overline{v}^2\,u_s>$	Mean longshore flow	Short waves
* CBM 10	$<\overline{v}^2\,u_l>$	Mean longshore flow	Long waves
CBM 11	$<3\,u_l^2\,u_s>$	Long waves	Short waves
CBM 12	$<3\,u_s^2\,u_l>$	Short waves	Long waves
CBM 13	$6\,\overline{u}\,u_s\,u_l$	Correlation of mean cross-shore flow, short and long waves	
Longshore Bedload Moments			
LBM 1	$\overline{v}^3$	Mean longshore flow cubed	
LBM 2	$<u_s^2\,\overline{v}>$	Short waves	Mean longshore flow
LBM 3	$<u_l^2\,\overline{v}>$	Long waves	Mean longshore flow
LBM 4	$\overline{u}^2\,\overline{v}$	Mean cross-shore flow	Mean longshore flow
* LBM 5	$<2\,\overline{u}\,\overline{v}\,u_s>$	Correlation of mean cross- and longshore flows and short waves	
* LBM 6	$<2\,\overline{u}\,\overline{v}\,u_l>$	Correlation of mean cross- and longshore flows and long waves	
* LBM 7	$<2\,\overline{v}\,u_s\,u_l>$	Correlation of mean longshore flow, short and long waves	

Table 6.1 Composition of Bedload Moment terms. Note: terms marked * are considered to be insignificant.

of each non-normalised cross-shore bedload term can be compared with the remaining cross-shore bedload terms. The individual terms from each data file need not be normalised for this comparison, since each was obtained under the same flow conditions.

Moment		Mobilising Component	Transporting Component
Cross-shore Suspended Load Moments			
CSM 1a (storm)	$<(u_s^2)^{3/2}\,\bar{u}>$	Short waves	Mean cross-shore flow
CSM 1b (calm)	$<(\bar{v}^2)^{3/2}\,\bar{u}>$	Mean longshore flow	Mean cross-shore flow
CSM 2a (storm)	$<(u_s^2)^{3/2}\,u_s>$	Short waves	Short waves
CSM 2b (calm)	$<(\bar{v}^2)^{3/2}\,u_s>$	Mean longshore flow	Short waves
CSM 3a (storm)	$<(u_s^2)^{3/2}\,u_l>$	Short waves	Long waves
CSM 3b (calm)	$<(\bar{v}^2)^{3/2}\,u_l>$	Mean longshore flow	Long waves
Longshore Suspended Load Moments			
LSM 1a (storm)	$<(u_s^2)^{3/2}\,\bar{v}>$	Contribution of short waves (moderate or storm conditions)	
LSM 1b (calm)	$<(\bar{v}^2)^{3/2}\,\bar{v}>$	Contribution of mean longshore flow (calm conditions)	

Table 6.2 Composition of Suspended load Moment terms.

The values for each of the velocity moment terms listed in Tables 6.1 and 6.2, for the lowest EMCM (0.12 m from the seabed) at Station C are presented in Tables 6.3 (bedload, cross-shore), 6.4 (bedload, longshore) and 6.5 (suspended load, cross- and longshore). Each result represents a value averaged over 17.07 minutes which has been found to be a useful representative data file length; it is sufficiently long for the investigation of hydrodynamics which include long waves, yet short enough for the processes to be considered reasonably stationary on a macro-tidal beach (*e.g.* Davidson *et al.*, 1993; Foote, 1994 and Huntley, 1996). The most important terms will be identified now and their magnitudes and direction discussed briefly here. This will be followed by a more detailed examination of the rôle of the most significant moments for sediment transport over a tidal cycle.

6.2.1 Cross-shore bedload moment terms

CBM4 (Table 6.1, summarised in the adjacent box) was generally of the highest magnitude, but both its magnitude and direction varied considerably throughout the tidal cycle

	Stirrer	Carrier
CBM1	mean x flow	mean x flow
CBM2	short waves	short waves
CBM4	short waves	mean x flow
CBM5	long waves	mean x flow
CBM6	mean y flow	mean x flow
CBM12	short waves	long waves

Tide	Julian Day	Depth (m)	CBM1	CBM2	CBM3	CBM4	CBM5	CBM6	CBM7	CBM8	CBM9	CBM10	CBM11	CBM12	CBM13
26	274.69	0.28	0.006	0.012	0.000	0.064	0.006	0.007	0.000	0.000	0.000	0.000	0.000	0.003	0.001
	274.71	0.45	0.000	0.022	0.000	0.007	0.001	0.000	0.000	0.000	0.000	0.000	0.000	-0.001	0.000
	274.73	0.56	0.000	0.021	-0.001	0.004	0.001	0.000	0.000	0.000	0.000	0.000	0.000	0.000	0.000
	274.75	0.59	0.000	0.019	-0.001	-0.011	-0.002	0.000	0.000	0.000	0.000	0.000	0.000	0.000	0.000
	274.77	0.54	0.000	0.024	0.000	-0.003	0.000	0.000	0.000	0.000	0.000	0.000	0.000	-0.001	0.000
	274.79	0.43	0.000	0.014	0.001	-0.003	-0.001	0.000	0.000	0.000	0.000	0.000	0.001	0.004	0.000
	274.81	0.26	0.001	0.010	0.000	0.033	0.007	0.005	0.000	0.000	0.000	-0.001	0.000	-0.001	0.002
27	275.21	0.20	0.001	0.014	0.002	0.039	0.007	0.003	0.000	0.000	0.000	0.000	0.001	0.010	0.001
	275.23	0.40	0.000	0.021	0.000	0.010	0.001	0.001	0.000	0.000	0.000	0.000	0.000	-0.002	0.000
	275.25	0.51	0.000	0.024	0.000	-0.020	-0.004	-0.001	0.000	0.000	0.000	0.000	0.001	0.006	-0.001
	275.27	0.56	0.000	0.022	-0.001	-0.014	-0.002	-0.001	0.000	0.000	0.000	0.000	0.000	0.005	0.000
	275.29	0.53	-0.002	0.019	0.000	-0.046	-0.009	-0.005	0.000	0.000	0.000	0.000	0.000	0.000	-0.001
	275.31	0.42	0.000	0.019	-0.001	0.020	0.005	0.004	0.000	0.000	0.000	0.000	0.000	0.005	0.001
	275.33	0.25	0.001	0.009	-0.001	0.038	0.008	0.011	0.000	0.000	0.000	-0.001	0.000	-0.003	0.002
28	275.71	0.24	0.000	0.013	-0.001	0.017	0.004	0.001	0.000	0.000	0.000	0.000	-0.001	0.002	0.000
	275.73	0.47	0.000	0.030	0.000	-0.008	-0.001	0.000	0.000	0.000	0.000	0.000	0.000	0.003	0.000
	275.75	0.63	0.000	0.035	0.001	0.002	0.001	0.000	0.000	0.000	0.000	0.000	0.000	0.011	0.000
	275.77	0.69	0.000	0.046	0.000	-0.020	-0.003	0.000	0.000	0.000	0.000	0.000	0.000	0.002	-0.001
	275.79	0.66	0.000	0.062	-0.003	0.015	0.002	0.000	0.000	0.000	0.000	0.000	-0.001	-0.002	0.000
	275.81	0.55	-0.002	0.031	-0.002	-0.046	-0.012	0.000	0.000	0.000	0.000	0.000	-0.002	-0.001	-0.002
	275.83	0.35	0.000	0.022	-0.001	0.002	0.000	0.000	0.000	0.000	0.000	0.000	-0.001	0.002	0.000
29	276.25	0.46	0.000	0.035	0.000	-0.016	-0.001	0.000	0.000	0.000	0.000	0.000	0.000	-0.001	0.000
	276.27	0.68	0.000	0.033	0.000	-0.014	-0.001	-0.001	0.000	0.000	0.000	0.000	0.000	-0.004	0.000
	276.29	0.78	0.000	0.026	0.000	0.001	0.000	0.000	0.000	0.000	0.000	0.000	0.000	-0.005	0.000
	276.31	0.76	0.000	0.034	0.000	-0.015	0.000	-0.002	0.000	0.000	0.000	0.000	0.000	-0.003	0.000
	276.33	0.63	-0.001	0.034	0.001	-0.038	-0.004	-0.010	0.000	0.000	0.000	0.000	0.000	-0.002	-0.001
	276.35	0.39	-0.005	0.021	0.000	-0.063	-0.008	-0.027	0.000	0.000	0.000	0.000	0.000	0.003	-0.001

Table 6.3 Velocity moments at Station C for bed load, cross-shore

Tide	Julian Day	Depth (m)	LBM1	LBM2	LBM3	LBM4	LBM5	LBM6	LBM7
26	274.69	0.28	0.008	0.023	0.002	0.006	0.000	0.000	0.000
	274.71	0.45	0.001	0.013	0.001	0.000	0.000	0.000	0.000
	274.73	0.56	0.002	0.017	0.003	0.000	0.000	0.000	0.001
	274.75	0.59	0.001	0.015	0.002	0.000	0.000	0.000	0.000
	274.77	0.54	0.000	0.010	0.002	0.000	0.000	0.000	0.000
	274.79	0.43	0.003	0.018	0.004	0.000	0.000	0.000	0.001
	274.81	0.26	0.012	0.026	0.005	0.002	0.000	0.000	0.001
27	275.21	0.20	0.005	0.021	0.004	0.002	0.000	0.001	0.001
	275.23	0.40	0.007	0.026	0.003	0.000	0.000	0.000	0.000
	275.25	0.51	0.005	0.024	0.004	0.000	0.000	0.000	0.001
	275.27	0.56	0.005	0.026	0.003	0.000	0.000	0.000	0.001
	275.29	0.53	0.010	0.028	0.005	0.003	0.000	0.000	0.001
	275.31	0.42	0.021	0.035	0.008	0.001	0.000	0.000	0.001
	275.33	0.25	0.040	0.046	0.010	0.003	0.000	0.000	0.002
28	275.71	0.24	0.003	0.017	0.004	0.000	0.000	0.000	0.000
	275.73	0.47	0.000	0.005	0.001	0.000	0.000	0.000	0.000
	275.75	0.63	0.000	-0.006	-0.001	0.000	0.000	0.000	0.000
	275.77	0.69	0.000	-0.003	0.000	0.000	0.000	0.000	0.000
	275.79	0.66	0.000	-0.003	0.000	0.000	0.000	0.000	0.000
	275.81	0.55	0.000	0.007	0.002	0.001	0.000	0.000	0.000
	275.83	0.35	0.002	0.013	0.003	0.000	0.000	0.000	0.001
29	276.25	0.46	-0.001	-0.011	-0.001	0.000	0.000	0.000	0.000
	276.27	0.68	-0.004	-0.022	-0.001	0.000	0.000	0.000	0.000
	276.29	0.78	-0.008	-0.028	-0.002	0.000	0.000	0.000	0.000
	276.31	0.76	-0.010	-0.030	-0.001	0.000	0.000	0.000	0.000
	276.33	0.63	-0.039	-0.048	-0.005	-0.003	0.000	0.000	-0.001
	276.35	0.39	-0.059	-0.046	-0.006	-0.012	0.000	0.000	-0.001

Table 6.4 Velocity moments at Station C for bed load, longshore

Tide	Julian Day	Depth (m)	CSM1a	CSM1b	CSM2a	CSM2b	CSM3a	CSM3b	LSM1a	LSM1b
			Cross-shore						Longshore	
26	274.69	0.28	0.011	0.001	0.012	0.000	0.001	0.000	0.012	0.001
	274.71	0.45	0.001	0.000	0.021	0.000	0.000	0.000	0.007	0.000
	274.73	0.56	0.001	0.000	0.020	0.000	0.000	0.000	0.009	0.000
	274.75	0.59	-0.002	0.000	0.020	0.000	0.000	0.000	0.008	0.000
	274.77	0.54	-0.001	0.000	0.024	0.000	0.000	0.000	0.006	0.000
	274.79	0.43	-0.001	0.000	0.014	0.000	0.001	0.000	0.009	0.000
	274.81	0.26	0.006	0.001	0.010	0.000	0.000	0.000	0.013	0.003
27	275.21	0.20	0.007	0.000	0.014	0.000	0.002	0.000	0.012	0.001
	275.23	0.40	0.002	0.000	0.021	0.000	-0.001	0.000	0.015	0.001
	275.25	0.51	-0.004	0.000	0.026	0.000	0.002	0.000	0.014	0.001
	275.27	0.56	-0.003	0.000	0.024	0.000	0.001	0.000	0.016	0.001
	275.29	0.53	-0.009	-0.001	0.020	0.000	0.000	0.000	0.016	0.002
	275.31	0.42	0.004	0.001	0.019	0.000	0.001	0.000	0.020	0.006
	275.33	0.25	0.007	0.004	0.010	0.000	-0.001	0.000	0.026	0.014
28	275.71	0.24	0.003	0.000	0.012	0.000	0.001	0.000	0.009	0.001
	275.73	0.47	-0.002	0.000	0.032	0.000	0.001	0.000	0.003	0.000
	275.75	0.63	0.000	0.000	0.038	0.000	0.003	0.000	-0.004	0.000
	275.77	0.69	-0.004	0.000	0.052	0.000	0.001	0.000	-0.002	0.000
	275.79	0.66	0.004	0.000	0.075	0.000	0.000	0.000	-0.002	0.000
	275.81	0.55	-0.009	0.000	0.031	0.000	0.000	0.000	0.004	0.000
	275.83	0.35	0.000	0.000	0.021	0.000	0.001	0.000	0.007	0.000
29	276.25	0.46	-0.003	0.000	0.034	0.000	0.000	0.000	-0.007	0.000
	276.27	0.68	-0.003	0.000	0.034	0.000	-0.001	0.000	-0.013	-0.001
	276.29	0.78	0.000	0.000	0.027	0.000	-0.001	0.000	-0.016	-0.002
	276.31	0.76	-0.003	0.000	0.036	0.000	-0.001	0.000	-0.018	-0.002
	276.33	0.63	-0.008	-0.003	0.034	0.000	0.000	0.000	-0.029	-0.013
	276.35	0.39	-0.011	-0.010	0.021	0.000	0.001	0.000	-0.025	-0.023

Table 6.5 Velocity moments at Station C for suspended load, cross- and longshore

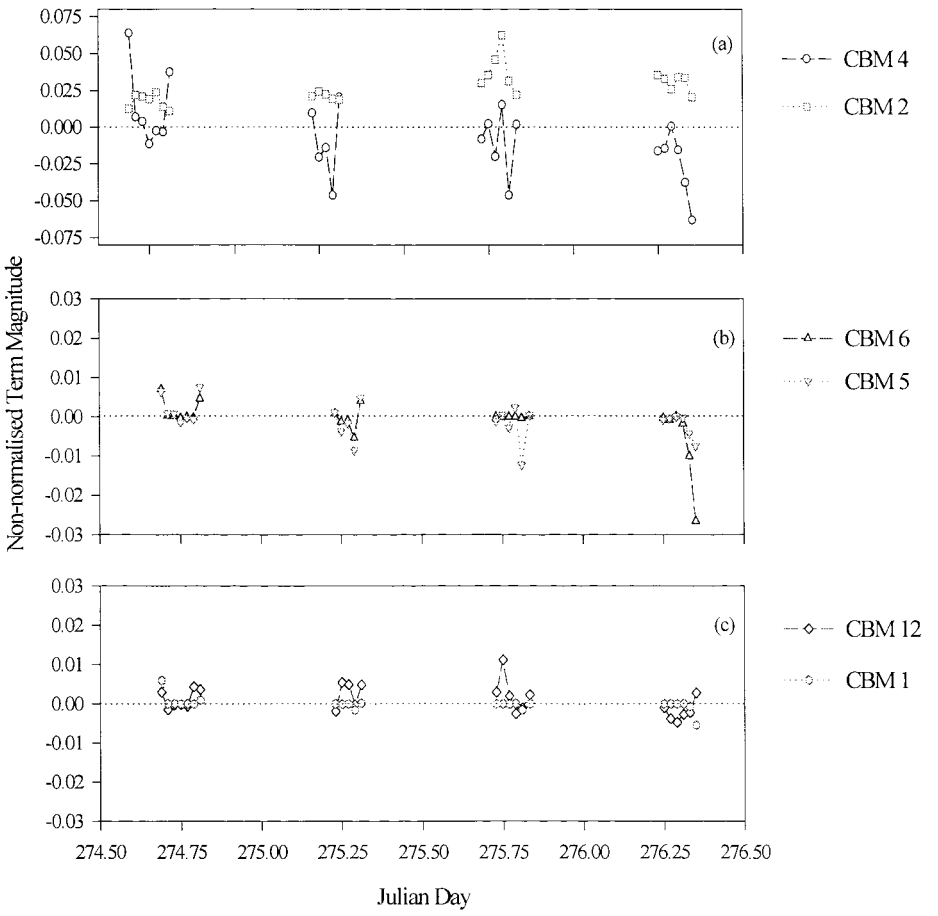

Figure 6.1 Cross-shore Bedload Moment terms, at 0.12 m above the seabed (Tides 26 to 29)

(Figure 6.1 *a*). The mean cross-shore flow determines the direction of CBM4; this was onshore early and late in the tide and offshore around high water for the first two tides (but primarily offshore for Tide 29). CBM2 was also an important term, although its magnitude tended to oppose that of CBM4, being at its maximum during high water. On occasions, the magnitude of CBM2 exceeded that of CBM4 although in no particularly systematic manner. CBM2 is always directed onshore, as identified in previous investigations undertaken elsewhere (*e.g.* Huntley, 1976).

CBM5 and CBM12 were of similar magnitude. CBM5 represents the characteristic trace of its carrier, the mean cross-shore flow, whilst CBM12 appeared to have little overall coherence (Figure 6.1 *b* and *c)*. An interesting feature revealed by this particular analysis is the influence of the mean *longshore* current on the *cross-shore* transport, as reflected in CBM6; this could be of a similar magnitude to CBM5 and CBM12, particularly for shallow water conditions. CBM1 was only of some minor importance in two shallow water files (Figure 6.1 *c*). CBM7, CBM8, CBM9 and CBM10 were insignificant, as expected.

6.2.2 Longshore bedload moment terms

LBM2 (Table 6.1 and adjacent box) was generally the largest of the longshore bedload terms; it mirrored the tidal pattern of the the transporter (Figure 6.2 *a*). In general, the response of LBM1 was more muted, although LBM1 achieved a similar magnitude to LBM2 late in the ebb phase of Tide 29, when the longshore current exceeded 0.35 ms^{-1}. The remaining Longshore Bedload Moment terms were of considerably smaller magnitude, although it is interesting to note that the cross-shore long waves at Morfa Dyffryn influenced also the longshore transport; LBM3 was of some significance during Tide 27, generally outweighing LBM4 (Figure 6.2 *b*). LBM5, LBM6 and LBM7 were insignificant, as expected.

	Stirrer	Carrier
LBM1	mean y flow	mean y flow
LBM2	short waves	mean y flow
LBM3	long waves	mean y flow
LBM4	mean x flow	mean y flow

6.2.3 Cross-shore suspended moment terms

CSM2a was by far the largest of the terms (Figure 6.3 *a*). As with the corresponding term for bedload transport (CBM2) it always represented onshore transport, with its highest magnitude during high water, whilst CSM1a operated both onshore and offshore in accordance with the mean cross-shore current. All the "storm" terms, (the CSMa terms) were of greater magnitude than any of those representing "calm" terms, with the exception of CSM1b during the ebb

	Stirrer	Carrier
CSM1a	short waves	mean x flow
CSM2a	short waves	short waves
CSM3a	short waves	long waves
CSM1b (calm)	mean y flow	mean x flow

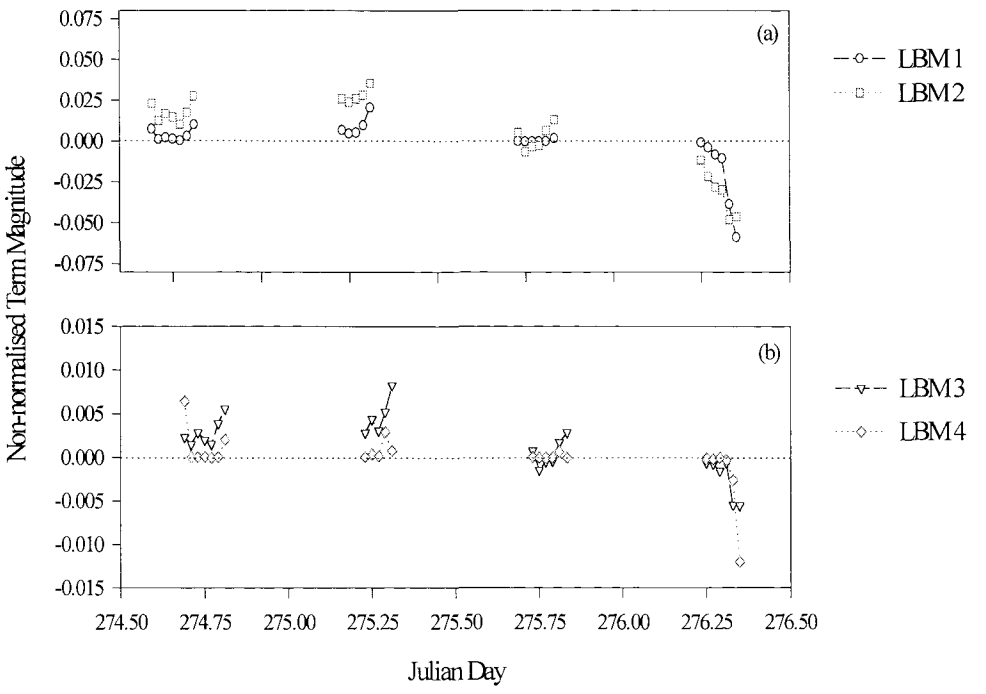

Figure 6.2 Longshore Bedload Moment terms (Tides 26 to 29)

phase of Tide 29; none of the remaining "calm" terms was of any importance. Moderate/storm conditions are defined as those when wave orbital velocities are more significant than the mean currents *i.e* $U_b >> \bar{u}, \bar{v}$ (Voulgaris & Collins, 1996). This relationship characterised the cross-shore waves at Morfa Dyffryn (Figure 6.4). However, "calm" conditions predominated over the final ebb phase of Tide 29, when the mean longshore current was approximately half the significant orbital velocity, U_b (Figure 6.4). Since the orbital velocities then were not dissimilar from the remainder of the tide (or, indeed, Tides 26 and 27), the strength of the longshore current was the crucial factor in determining "storm" or "calm" conditions, rather than the prevailing orbital velocities.

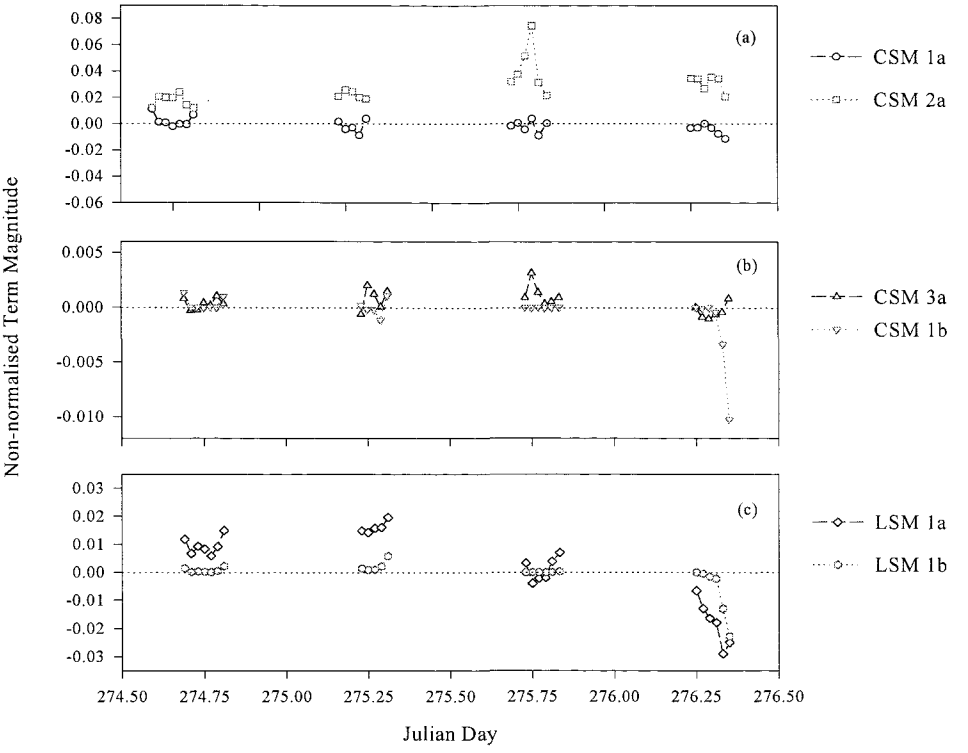

Figure 6.3 Cross-shore (a) and (b) and Longshore (c) Suspended load Moments (Tides 26 to 29)

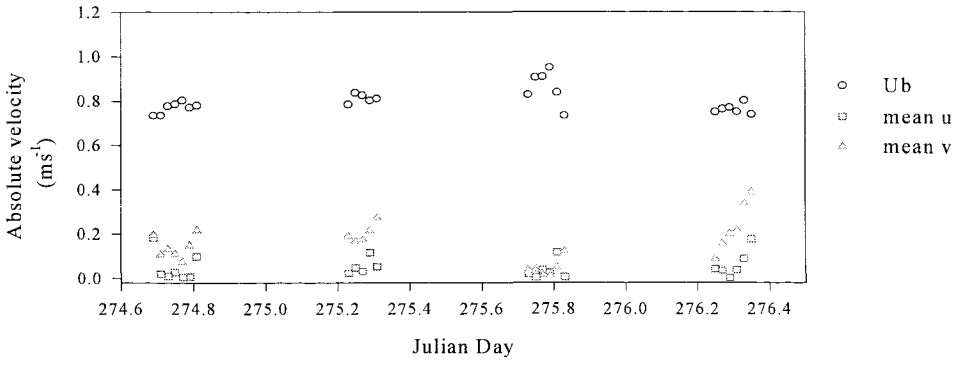

Figure 6.4 Comparison of absolute values of significant orbital velocity (U_b), mean cross-shore current (mean u) and mean longshore velocity (mean v), Tides 26 to 29.

6.2.4 Longshore suspended moment terms

The contribution of short waves to the longshore suspended sediment transport (LSM1a) always exceeded that of the mean longshore current (LSM1b), although LSM1b achieved parity during the late ebb phase of Tide 29 (Figure 6.3 *c*).

6.3 The Relative Rôle of the Moment Terms, Throughout the Tidal Cycle

In order to establish which of the moments (see above) contribute most to the overall sediment transport regime, each term was calculated as a percentage of the gross total moment for each transport mode *i.e.* the bedload and suspended load components, for cross-shore and alongshore.

6.3.1 Cross-shore bedload terms

The most important cross-shore bedload moments, in order of priority, for Tides 26 to 29, are shown in Figure 6.5. CBM2 and CBM4 were the dominant cross-shore bedload moments; together they comprised a minimum of 64% of the total. However, there was a clear tidal signature in the relative dominance of these two moments, which has important implications for net sediment transport over a tidal cycle (Section 6.5, below). CBM2 was generally the dominant moment around high water but, in the early stages of the flood tide and late in the ebb, CBM4 became the primary moment (with the exception of the late ebb phase of Tide 28). Since short waves mobilise the sediment in both (see box), the balance must lie with the transporting mechanism. Mean cross-shore currents were at their highest in shallow water (the lowest current meter was not covered during the early flood phase of Tide 29). During Tide 29, the mean cross-shore current was directed offshore throughout the tidal cycle, suggesting an element of undertow structure. Accordingly, CBM4 predicted offshore transport throughout the tide; only during the latter part of the ebb was the influence of the mean current sufficient to overcome the onshore nature of CBM2. The oscillatory waves should also become

	Stirrer	Carrier
CBM2	short waves	short waves
CBM3	long waves	long waves
CBM4	short waves	mean x flow
CBM5	long waves	mean x flow
CBM6	mean y flow	mean x flow
CBM12	short waves	long waves

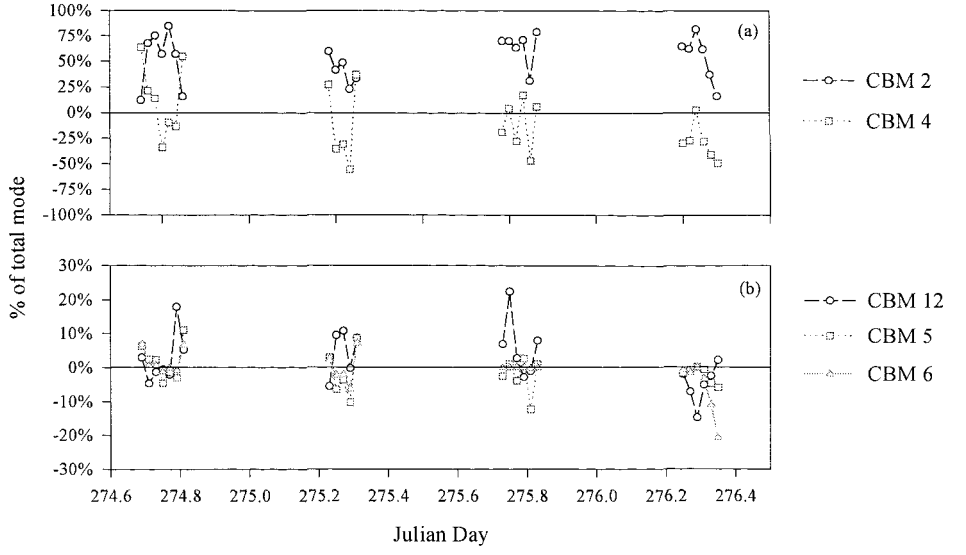

Figure 6.5 Cross-shore Bedload Moments, as a percentage of the total cross-shore bedload transport (Tides 26 to 29)

increasingly skewed as the waves shoal, leading to higher values of CBM2. However, in the shallow water depths and with the breaking waves measured at Morfa Dyffryn, the influence of increasing mean currents outweighed that of increasing skewness in the wave-induced currents. This situation arises because, once waves have broken, their skewness remains constant or decreases, whilst asymmetry increases as the waves are converted into highly asymmetric and high velocity bores. Wave asymmetry is not accounted for in (2.2).

Of the remaining moments, only CBM5, CBM6 and CBM12 accounted individually for more than 10% of the cross-shore bedload transport (Figure 6.5 *b*). During shallow water conditions (when both mean cross-shore currents and long wave variance tended to be at their highest), CBM5 could produce around 10% of the total cross-shore bedload transport; the direction is determined by the mean current. CBM5 and CBM12 were of approximately equal significance; if operating in a similar direction, they could be responsible together for around 10% of the transport, and up to 20% on occasions. However, without any directional signal, particularly in CBM12, these moments may merely cancel each other out in the overall balance. The mean longshore

current, when combined with the mean cross-shore flow (CBM6), accounted for between 10 and 20% of the cross-shore bedload transport in shallow water. CBM3 was of only minor significance during the conditions encountered during these tides; it accounted for a maximum of 5% of transport, in no systematic manner.

6.3.2 Longshore bedload terms

Velocity moment analysis suggests that LBM2 accounted for 72%, on average, of the total longshore bedload transport (Figure 6.6*a*). The results of Tide 28 showed the effect of even small variations in the longshore current,with transport reversing direction around high water, thus following the somewhat unusual longshore current curve (Figure 5.6 *b*). Given that the transporting mechanism is, by definition, the longshore current (Table 6.1 and adjacent box), the balance which determines the most important moment for longshore transport must be the stirring mechanism; this is in contrast to the cross-shore bedload transport (see

	Stirrer	Carrier
LBM1	mean y flow	mean y flow
LBM2	short waves	mean y flow
LBM3	long waves	mean y flow
LBM4	mean x flow	mean y flow

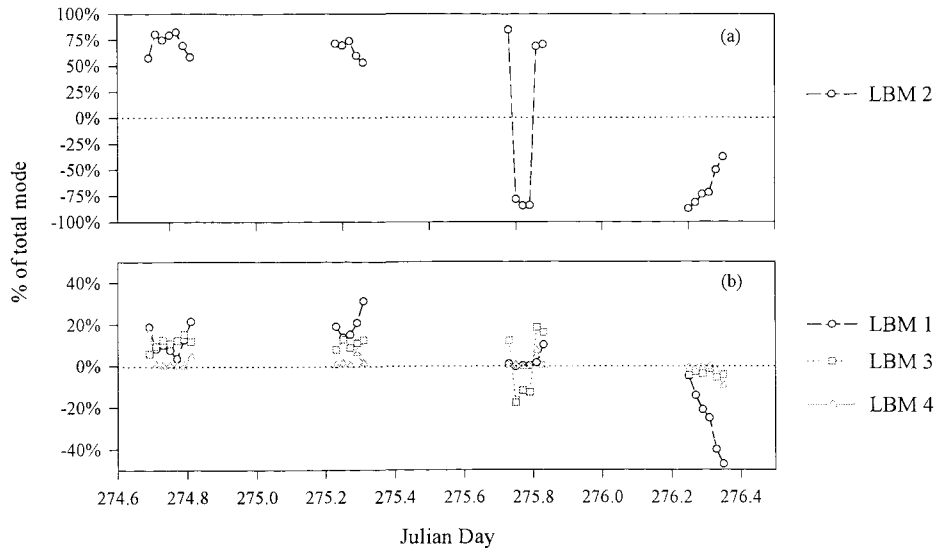

Figure 6.6 Longshore Bedload Moments, as a percentage of total longshore bedload transport (Tides 26 to 29)

above). Once again, there was a tidal signature in the data set; however, the changes were more subtle than for the cross-shore moments. During mid-tide and high water, the short wave mobilising term (LBM2) dominated. Towards the end of the ebb of Tide 29, the longshore current (LBM1) began to mobilise sediment at least as effectively as the short waves (Figure 6.6 *b*).

Long waves were most important during Tide 28, when LBM3 accounted for nearly 20% of the transport. However, since the long wave variance was not greatly dissimilar to that during other Tides (Figure 5.7 *b* and *c*), the difference must be accounted for by the reduction in strength of the longshore current; this was the weakest of all the (4) tides by almost an order of magnitude, reducing the relative role of LBM1 during Tide 28. The mean cross-shore flow term (LBM4) accounted for 10% or more of transport on only two occasions, when the cross-shore current exceeded approximately 0.17 m s^{-1}.

6.3.3 Cross-shore suspended sediment load

Cross-shore suspended moments were dominated overwhelmingly by the term CSM2a, which represents storm conditions (Figure 6.7*a* and *b*); at such times, short waves both mobilise and transport the sediments (Table 6.1 and adjacent box). Together with CSM1a, these two terms accounted for an average of 94% of the cross-shore suspended load transport (Table 6.6). On no occasion was any offshore tendency of CSM1a sufficiently strong to alter the net direction of transport, even with an offshore mean current of 0.18 ms^{-1}. Hence, if these two terms alone are deemed responsible for cross-shore suspended sediment transport, the *only* effect of the cross-shore undertow was to reduce the net magnitude of the onshore transport.

	Stirrer	Carrier
CSM1a	short waves	mean x flow
CSM2a	short waves	short waves
CSM3a	short waves	long waves
CSM1b (calm)	mean y flow	mean x flow

The long wave carrier term (CSM3a) had no strongly discernable tidal pattern; it was of similar magnitude to (although slightly lower than) the corresponding bedload term (CBM12). Even though CSM3a was the least dominant of the three "storm" terms, it was generally more important than the "calm" terms until the mean longshore current reached a velocity of approximately 0.3 ms^{-1}. Thus, for the range of conditions

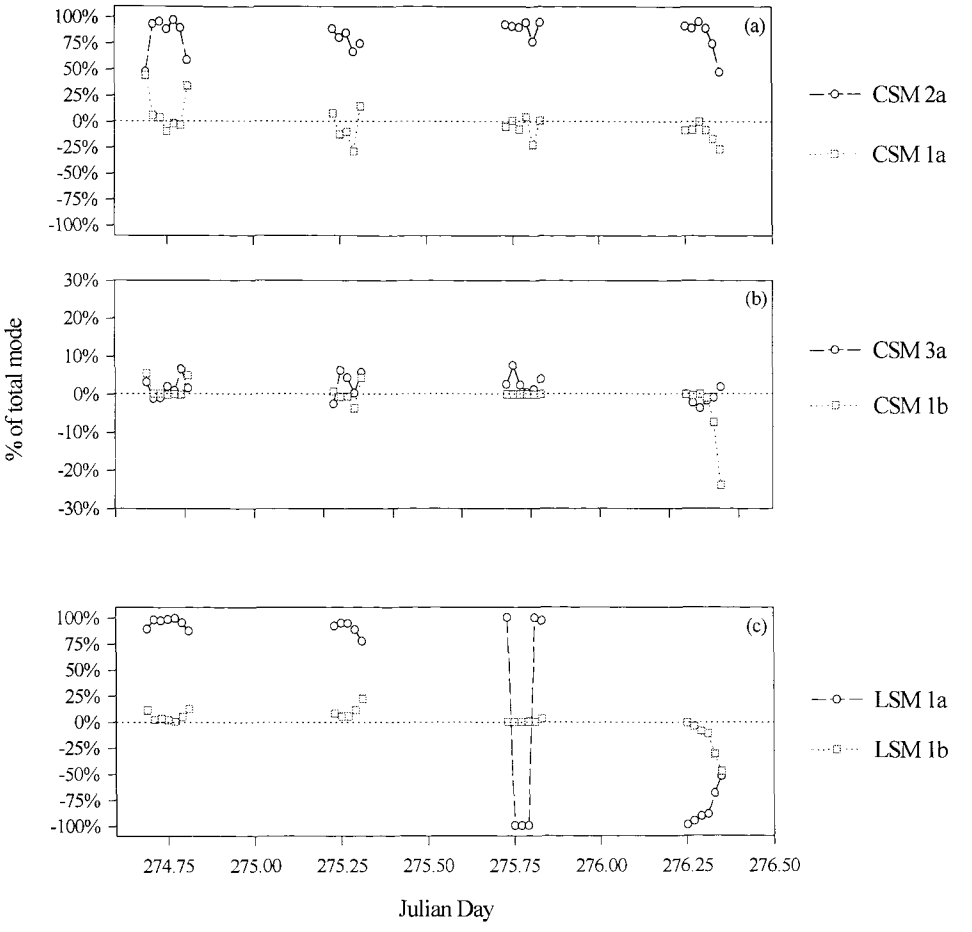

Figure 6.7 Suspended load Moments, as a percentage of the total cross-shore (a) and (b); and (c) longshore suspended load transport (Tides 26 to 29)

encountered during these tides,the short waves were the main mechanism for mobilising sediment; with few exceptions,they were responsible for mobilising more cross-shore suspended sediment than the longshore currents. Exceptions occurred during some of the shallow water conditions, notably the late ebb phase of Tide 29, when the mean longshore current contributed to mobilising the suspended sediment (CSM1b). When combined with strong cross-shore currents, up to 25% of transport was possible; however, this only outweighed CSM3a (the term involving long waves) and was never more important than the other two "storm" moment terms.

6.3.4 Longshore suspended sediment load

LSM1a was by far the most dominant moment (Figure 6.7 *c*). This term represents the contribution of the short waves during "storm" conditions (Table 6.1 and adjacent box). Nevertheless, the mean longshore flow was not ineffective in placing sediment in suspension, although only when the longshore current exceeded 0.35 m s^{-1}, was the contribution of LSM1b of equal magnitude to the short wave term (LSM1a); this occurred only once during the (4) tides analysed here. However, it may be that it is the ratio of significant orbital velocity, U_b, to mean longshore current, $\bar{v}$, which determines the contribution of LSM1b, rather than a threshold longshore current velocity. Since the significant orbital velocities did not vary greatly during these tides (Figure 6.4), it is not possible to assess whether a threshold current must be reached, or whether merely a threshold ratio of $U_b : \bar{v}$ is required before the longshore current suspends sediment as effectively as the short waves. Nonetheless, a longshore current of approximately 0.35 m s^{-1}, would appear to be a likely threshold for placing sediment into suspension, equally as importantly as the short waves.

	Stirrer	Carrier
LSM1a	short waves	mean y flow
LSM1b	mean y flow	mean y flow

6.4 Sediment Mobilising and Transporting Mechanisms

Analysis of the velocity moments can provide an insight into the relative importance of oscillatory and mean flows as agents for mobilising sediment, by comparing those moments which have a common transporting mechanism; similarly, for transporting mechanisms, when the mobilising agent is constant. Some indication has been provided already for suspended sediment transport (Sections 6.3.3 and 6.3.4) but, in order to draw some general conclusions for the cross-shore direction over the entire range of hydrodynamic conditions, the moments from all (4) tides are examined against water depth. For this comparison, the moments need to be normalised, since each was obtained under different flow conditions. The bedload moments were normalised (Guza & Thornton, 1985; Foote, 1994) using:

$$<u^2>^{3/2} \qquad (6.7)$$

and in order to compensate for the longshore currents, the suspended load moments were normalised by:

$$\sqrt{[2(\sigma_u + \sigma_v)]^2} \tag{6.8}$$

The moments used for the comparison of cross-shore bedload mobilising and transporting mechanisms, are described in Tables 6.6 and 6.7 and shown in Figures 6.8 to 6.10 (unimportant terms have been omitted, for the sake of clarity).

Overall, **short waves** are clearly the dominant agent for mobilising cross-shore bedload, whatever the transporting agent (Figure 6.8) and for both mobilising and transporting suspended load (Figure 6.3 and Section 6.3.3). Such waves are also the most important mechanism for mobilising sediment for transport alongshore, except when longshore currents exceed about 0.3 ms^{-1} (Figures 6.10 and 6.11 and Section 6.3.2). As transporters of cross-shore bedload, they are of similar importance to mean cross-shore currents, *only* in water depths greater than about 0.35 m (Figure 6.9 *a*).

Comparison of cross-shore mobilising mechanisms		
Moment Term	Mobilising agent	Transporting agent
CBM 4	short waves	mean cross-shore current
CBM 5	long waves	
CBM 1	mean cross-shore current	
CBM 6	mean longshore current	
CBM 2	short waves	short waves
CBM 11	long waves	
* CBM 7	mean cross-shore current	
* CBM 9	mean longshore current	
CBM 12	short waves	long waves
CBM 3	long waves	
* CBM 8	mean cross-shore current	
* CBM 10	mean longshore current	

Table 6.6 Moment terms for comparison of cross-shore bedload mobilising mechanisms (* unimportant terms omitted from Figure 6.8)

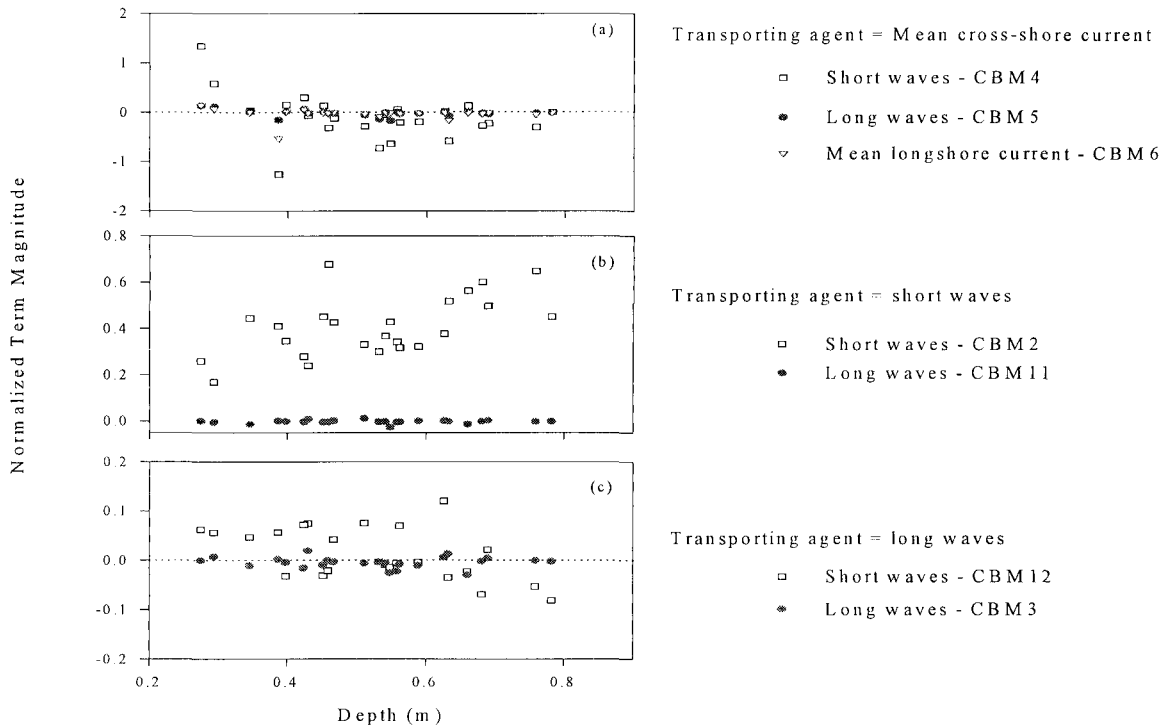

Figure 6.8 Comparison of mobilising mechanisms for cross-shore bedload (Tides 26 to 29)

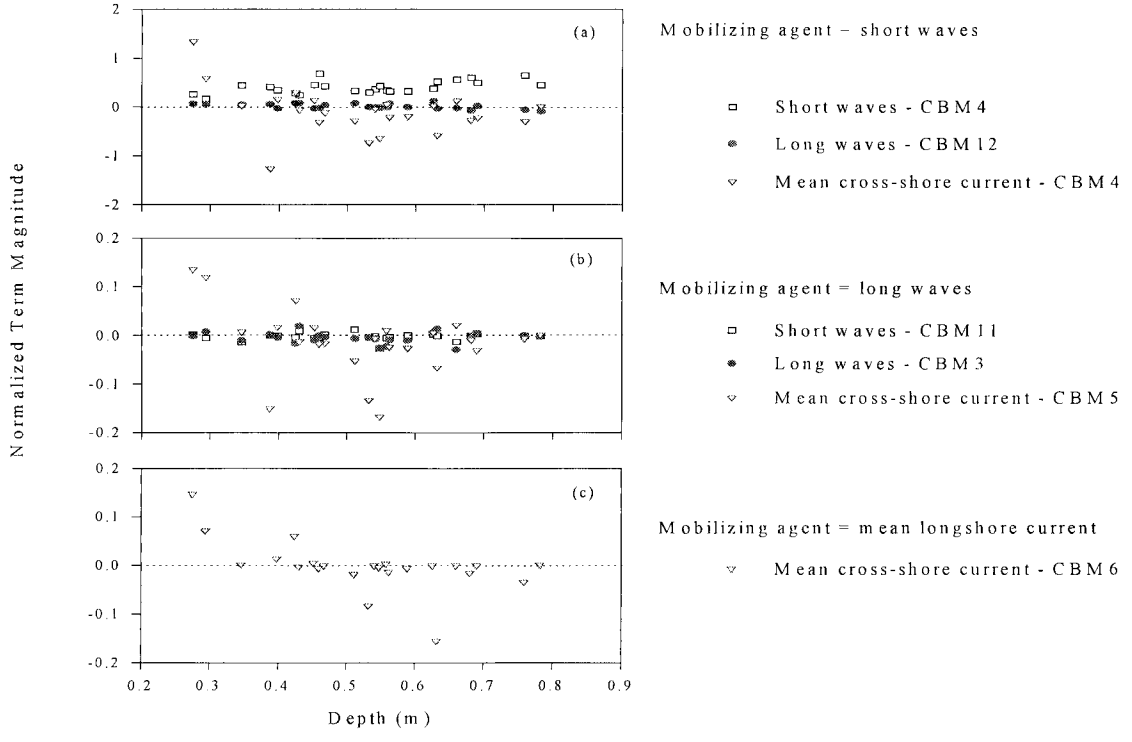

Figure 6.9 Comparison of transporting mechanisms for cross-shore bedload (Tides 26 to 29)

Comparison of cross-shore transporting mechanisms		
Moment term	Mobilising agent	Transporting agent
CBM 2	short waves	short waves
CBM 12		long waves
CBM 4		mean cross-shore current
CBM 11	long waves	short waves
CBM 3		long waves
CBM 5		mean cross-shore current
* CBM 7	mean cross-shore current	short waves
* CBM 8		long waves
CBM 1		mean cross-shore current
* CBM 9	mean longshore current	short waves
* CBM 10		long waves
CBM 6		mean cross-shore current

Table 6.7 Moment terms for comparison of cross-shore bedload transporting mechanisms (* unimportant terms, omitted from Figure 6.9)

Long waves are of only minor importance as a mobilising agent in the conditions encountered at Morfa Dyffryn (Figure 6.8); they were the least effective of the suspended sediment transporting agents (Figure 6.3). Indeed, the only rôle of the long waves was to transport any cross-shore bedload, mobilised by long waves, more effectively than transported by the short waves (Figure 6.9 *b*).

The above analysis confirms that the **mean cross-shore current** (even undertow, up to 0.19 m s^{-1}) is unimportant in mobilising bedload cross-shore (the remaining terms with mean cross-shore current as the mobilising agent are omitted from Figure 6.8 as unimportant) or alongshore (Figure 6.10). The main contribution of the cross-shore mean current is in transporting cross-shore bedload in shallow water; this is particularly in relation to water less than approximately 0.5 m deep, where it is the most important mechanism (Figure 6.9). The cross-shore mean current also has some significance in transporting suspended sediment cross-shore in shallow water, although it is a less effective transporting mechanism than the short waves (Figure 6.3). It is interesting to

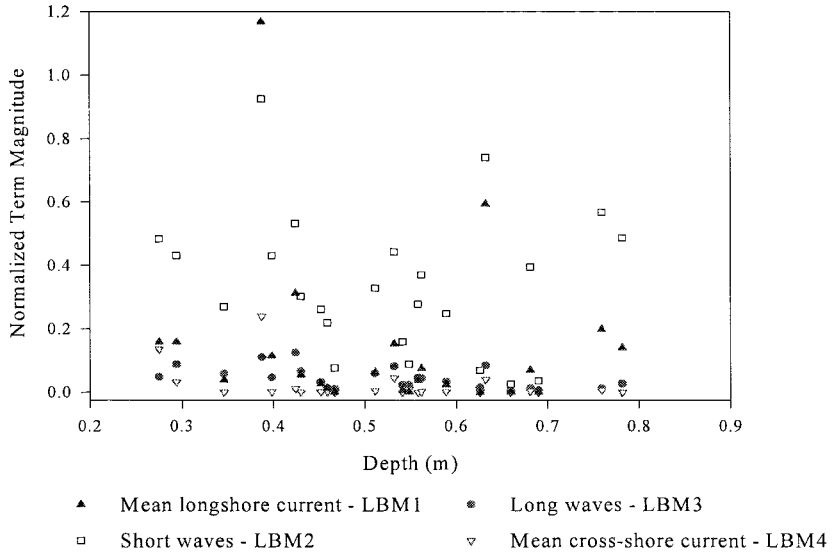

Figure 6.10 Comparison of mobilising mechanisms for longshore bedload (Tides 26 to 29). Note: transporting agent = mean longshore current.

note that the mean cross-shore current is also the main transporter of sediment mobilised by long waves (Figure 6.9 *b*); therefore, it may take on more significance, in conditions where more long wave energy is present.

In contrast, the **mean longshore current** has a significant effect on sediment transport, primarily as a transporting agent alongshore (by definition), but also in mobilising sediments. When the mean longshore current is below 0.2 m s^{-1}, the short waves mobilize about 75 % of the longshore bedload; longshore currents and long waves equally responsible for the mobilising the remainder of the sediment (Figure 6.11). When the longshore current exceeds 0.3 m s^{-1}, it mobilises nearly the same proportion of bedload as the short waves; if greater than 0.35 m s^{-1}, it mobilises more bedload than the short waves. Above 0.35 m s^{-1}, the longshore current also puts sediment into suspension as effectively as the short waves (Section 6.3.4).

The influence of the longshore current, on transport processes, is not confined to sediment transport alongshore, although it is of importance for cross-shore transport only when in combination with the mean cross-shore current (Figure 6.9 *c)*.

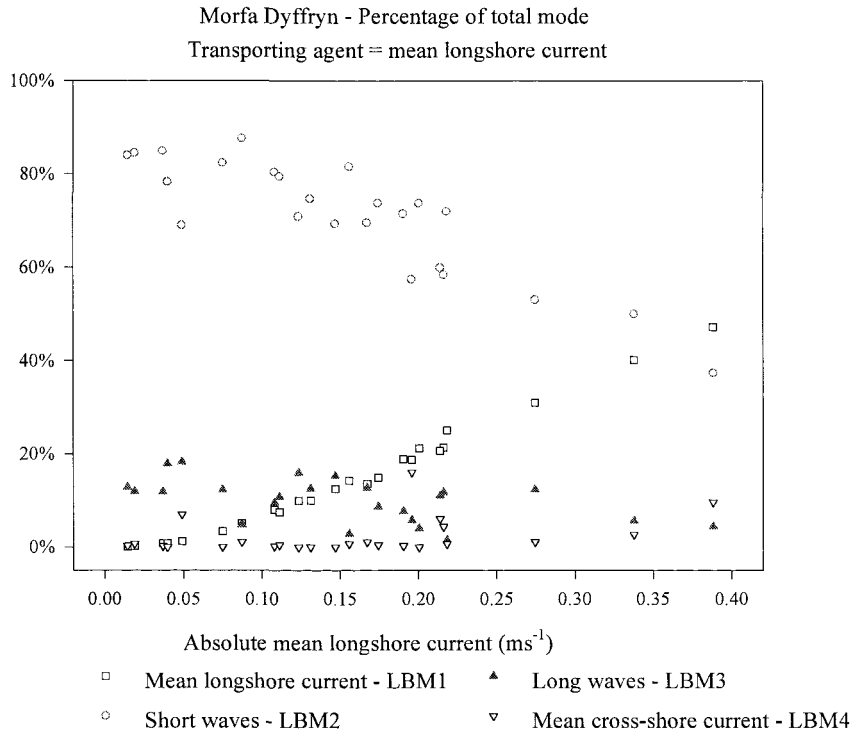

Figure 6.11 Influence of mean longshore current as a mechanism for mobilising sediment for longshore bedload transport (Tides 26 to 29)

6.5 Tidal Variations in Net Sediment Transport

Overall, the cross-shore bedload moment analysis undertaken for the first three tides (Tides 26 to 28) suggests potential strong net onshore transport during the early and late phases of the tide, with some small indication of offshore transport around high water (Figure 6.12 *a*). Hence, in the cross-shore direction, bedload and suspended load may be de-coupled from each other, since suspended sediment is directed onshore throughout (Figure 6.12*b*). This pattern is in contrast to the longshore direction, where the bedload and suspended load sediment transport are related, by definition, to a common transporting agent (Figure 6.12 *c* and *d*).

When the variation in the (normalised) net moments with depth is considered, an interesting relationship is revealed (Figure 6.13 *a* and *b*). Practically all the suspended sediment transport is onshore (as discussed above) but, overall, transport tends to be

reasonably constant with depth in shallow water but higher in water deeper than about 0.6 m, particularly during Tide 28. This is in direct contrast to cross-shore bedload (Figure 6.13 *a*) which shows an overall increase in transport with decreasing depth below 0.6 m and remains fairly constant in the remaining measured depths.

At this stage in the analysis, no inferences can be drawn concerning the relative levels of bedload and suspended load, since the suspended load terms are multiplied by additional constants (ϵ_s/W) before the transport rates are derived. Nevertheless, there may well be repercussions for the ongoing debate about relative importance of bedload and suspended load (*e.g.* Komar, 1978; Kraus, 1987; Hanes, 1988), since bedload is rarely measured in shallow water.

Net bedload transport alongshore is at its maximum in the early flood and late ebb phases of the tide, in water depths of less than 0.5 m deep. (Figures 6.12 *c* and 6.13 *c*). Net longshore suspended load moments are similar to those for net cross-shore bedload (Figures 6.12 *d* and 6.13 *d*).

6.6 Comparison with Velocity Moments from other Locations

In order to establish whether the dominant velocity moments at Morfa Dyffryn are site-specific, a similar analysis was undertaken using data from Nieuwpoort-aan-Zee, Belgium (obtained as part of the MAST II CSTAB programme).

The beach at Nieuwpoort is sandy, located within a macro-tidal setting and has an extensive ridge and runnel system. Details concerning the field site, methods of data collection and analysis and wave conditions can be found in the CSTAB Handbook (O'Connor, 1996). Three consecutive tides (from Julian Days 062 and 063, referred to henceforth as Tides 1, 2 and 3) were analysed using the same procedures presented previously (Sections 6.1.1 and 6.1.2). The average location of the trough between gravity and infragravity waves was at 0.06 Hz at Nieuwpoort and 0.05 Hz at Morfa Dyffryn. The wave period (T_z) was similar at Morfa Dyffryn and Nieuwpoort (about 3 to 5 s) but, whereas the spectral peak period (T_p) was similar to T_z at Nieuwpoort, suggesting a well developed sea, in Wales T_p was considerably higher.

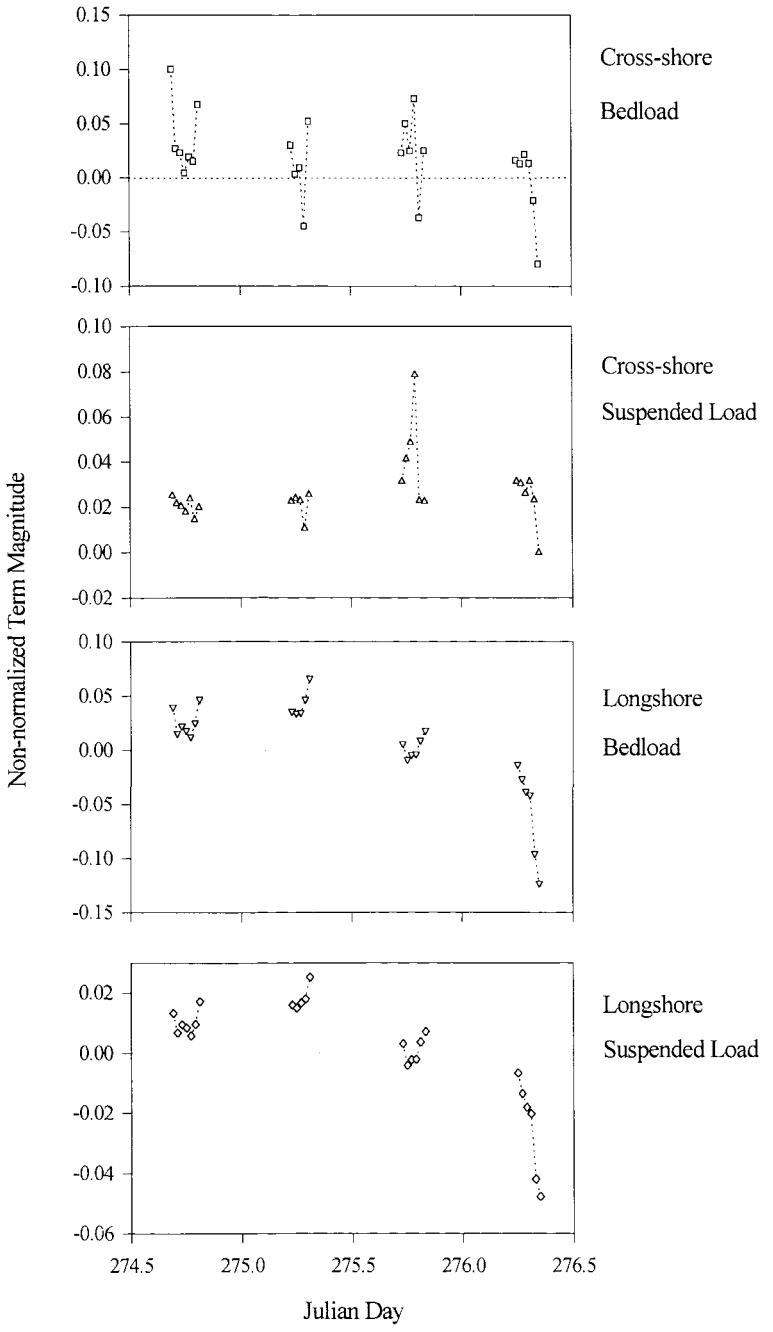

Figure 6.12 Tidal variation in the net velocity moments for (a) cross-shore bedload; (b) cross-shore suspended load; (c) longshore bedload and (d) longshore suspended load (Tides 26 to 29)

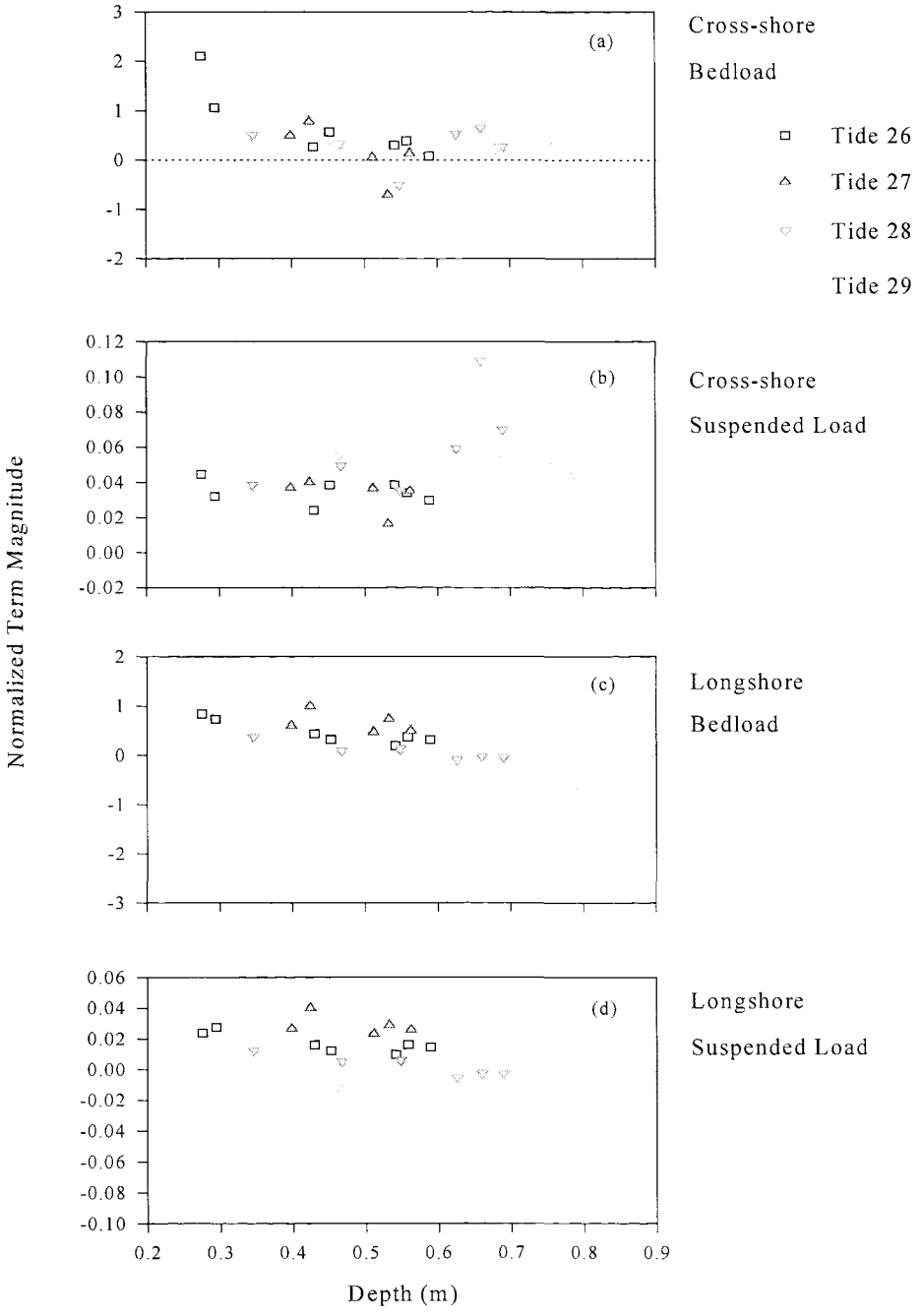

Figure 6.13 Variation in net velocity moments with depth: (a) cross-shore bedload; (b) cross-shore suspended load; (c) longshore bedload; and (d) longshore suspended load (Tides 26 to 29)

With the exception of the latter part of Tide 1, results from Nieuwpoort were from within the region of breaking waves *i.e.* within the surf zone, as occurred for the (4) tides under consideration at Morfa Dyffryn. The mean cross-shore currents were directed offshore throughout at Nieuwpoort, whilst the mean longshore currents were as strong as at Morfa Dyffryn.

The results obtained from Morfa Dyffryn and Nieuwpoort will be compared with those of Foote (1994), who analysed data from Spurn Head; this was collected as part of the B-BAND field experiment (Russell *et al.*, 1991; Davidson *et al.*, 1992). The environmental setting of Spurn Head is similar to that of Morfa Dyffryn, being a macro-tidal, intermediate beach with fringing sand and shingle bank. However, there is an absence of the ridge and runnel system found at Nieuwpoort and Morfa Dyffryn. Foote (1994) examined 3 tides, with varying hydrodynamic conditions, using velocities obtained from an EMCM at 0.1 m from the seabed. Tide 164PM was associated with a violent storm with an offshore H_s of 1.6 m and breaking wave heights of up to 3 m. Tide 184PM incorporated moderate swell conditions, with a choppy sea and a maximum offshore H_s of 1.1 m; there were similar, but calmer, conditions during Tide 234PM (H_s = 0.8 m). These data sets included results obtained from within and outside the surf zone; however, eqns. (6.1) and (6.5) were decomposed into short waves (> 0.05 Hz), long waves and mean flow in the cross-shore direction only. Hence, no account was taken of the strong longshore currents found to be present (*e.g.* Davidson *et al.*, 1993) All subsequent referrals to the Spurn Head results should be taken as a reference to Foote (1994) unless indicated otherwise.

The moments which averaged over 10% of total transport for each mode, during the entire data set under consideration are given an entry in Table 6.8 corresponding to their rank order (in descending order). Moment terms in brackets are those of Foote (1994). Terms with an *average* percentage transport of between 2 and 10% are identified by "✓", indicating that they may be of some importance at times; the remaining moments are not considered of significance. The results obtained from Spurn Head are ranked on the basis of information presented in Foote (*op. cit.*). The data from Morfa Dyffryn and Nieuwpoort have been averaged over the entire range for all the tides under consideration, since the change from shoaling to breaking conditions was not found to influence the significant moments (Voulgaris & Collins, 1996).

Moment Term	Morfa Dyffryn	Nieuwpoort	Spurn Head	
			Inside Surf Zone	Outside Surf Zone
CBM1 (CBT1)		✓	✓	
CBM2 (CBT2)	1	2	2	1
CBM3 (CBT3)				
CBM4 (CBT4)	2	1	1	2
CBM5 (CBT5)	✓		3	
CBM6	✓	✓	n/a	
CBM7 (CBT9)				
CBM8 (CBT10)				
CBM9			n/a	
CBM10			n/a	
CBM11 (CBT7)				
CBM12 (CBT8)	✓	✓	✓	3
CBM13 (CBT6)				
LBM 1	2	3	n/a	
LBM 2	1	1	n/a	
LBM 3	3		n/a	
LBM 4	✓	2	n/a	
LBM 5			n/a	
LBM 6		✓	n/a	
LBM 7			n/a	
CSM 1a (CST3)	2	2	2	2
CSM 1b	✓	✓	n/a	
CSM 2a (CST1)	1	1	1	1
CSM 2b			n/a	
CSM 3a (CST2)	✓	✓	✓	3
CSM 3b			n/a	
LSM 1a	1	1	n/a	
LSM 1b	✓	2	n/a	

Table 6.8 Comparison of moment terms obtained from the data collected at Morfa Dyffryn, Nieuwpoort-aan-Zee and Spurn Head

Some unimportant moments, common to all three data sets, are revealed in Table 6.8; these include most of those predicted by theory to be unimportant (namely CBM7, CBM8, CBM9, CBM10, LBM5 and LBM7). In addition, CBM3, CBM11, CBM13, CSM2b and CSM3b were found to be of no importance during the wide range of hydrodynamic conditions encountered. The remaining term predicted to be zero, LBM6, comprised an average of 3% of total longshore transport at Nieuwpoort where it remained less than one-sixth of the third-ranked Longshore Bedload Moment; it was found to be insignificant at Morfa Dyffryn and Spurn Head.

On the basis that the data from these three locations encompassed widely varying wave conditions, it may be concluded that for macro-tidal, intermediate beaches, only the following moment terms need be considered:

(a) Cross-shore Bedload Moments 1, 2, 4, 5 and 6;
(b) Longshore Bedload Moments 1, 2, 3 and 4;
(c) Cross-shore Suspended Moments 1a, 2a, 3a and 1b; and
(d) Longshore Suspended Moments 1a and 1b.

The inclusion of two cross-shore transport terms, CBM6 and CSM1b should be noted; these involve mobilisation of sediment by the mean longshore current. Such a relationship confirms that: (i) the importance of the mean longshore current is not confined to longshore sediment transport; and (ii) the Bailard-type equations for sediment transport prediction, which incorporate mean currents and which can be resolved between cross-and longshore, are applicable for macro-tidal beaches.

6.6.1 Variation with depth: cross-shore

The change in the relative importance of several of the moments, throughout the tidal cycle (at Morfa Dyffryn and Nieuwpoort and, by implication, at Spurn Head), appear to indicate an association between cross-shore velocity moments and water depth. The mean flows, in particular, follow a distinct tidal pattern; this is sometimes symmetrical, being stronger and onshore in shallow water and weaker and offshore around high water (for example, Tides 26 and 27 at Morfa Dyffryn). In other cases (*e.g.* Tide 29) the mean flow can be offshore throughout the tidal cycle.

Each of the important, normalised, velocity moment term are shown in Figure 6.14 as a function of water depth. The two dominant cross-shore bedload moments at Morfa Dyffryn show a distinctive, although opposing, trend with water depth (Figure 6.14 *a* and *b*). CBM2 shows a reasonably linear increase with depth. Both the values and the trend compare well with the surf zone data from Spurn Head, particularly with those observations obtained from Tide 234PM; this was the calmest of the 3 tides monitored. This relationship results from wave shoaling, leading to an increase in skewness only until just before breaking; after this, the short waves become less skewed and more Gaussian in character (Guza & Thornton, 1985).

	Stirrer	Carrier
CBM2	short waves	short waves
CBM4	short waves	mean x flow
CBM5	long waves	mean x flow
CBM6	mean y flow	mean x flow

In contrast, CBM4 at Morfa Dyffryn shows a steady decrease with water depth; onshore transport occurs in water depths of less than 0.3 m, reversing to generally (although not exclusively) offshore transport in deeper water. However, at Spurn Head the reverse holds; there is increasingly offshore transport in shallow water (with a maximum just shoreward of the breakpoint), reverting to zero transport near the breakpoint and generally increasing onshore transport to seawards of the breakpoint. The direction of this particular term is determined by the mean cross-shore current.

6.6.2 Variation with depth: longshore

The relationship between mean velocity and water depth is not so straightforward for longshore currents as for cross-shore currents. The longshore velocities reached during Tide 234PM at Spurn Head were comparable to those recorded at Morfa Dyffryn, but reached their maximum (of over 0.4 m s^{-1}) just inside the surf zone, both on the flood and the ebb. These currents were attributed to wave-driven currents, forced by high and groupy swell waves (Hb_s = 1.5 m) approaching with considerable obliquity (Davidson *et al.*, 1993). Outside the surf zone, the strong (up to 0.35 m s^{-1}), tidally-driven longshore current reversed in direction at high water. In contrast, all the longshore current data from Morfa Dyffryn were obtained from within the surf zone, although tidal influence was discernable, particularly during Tide 29 (Section 5.3.2). In addition, within the surf zone, the tidal *trend* of the longshore currents is the reverse of the surf zone currents reported by Davidson *et al.* (1993); they are at their stongest in very shallow water during

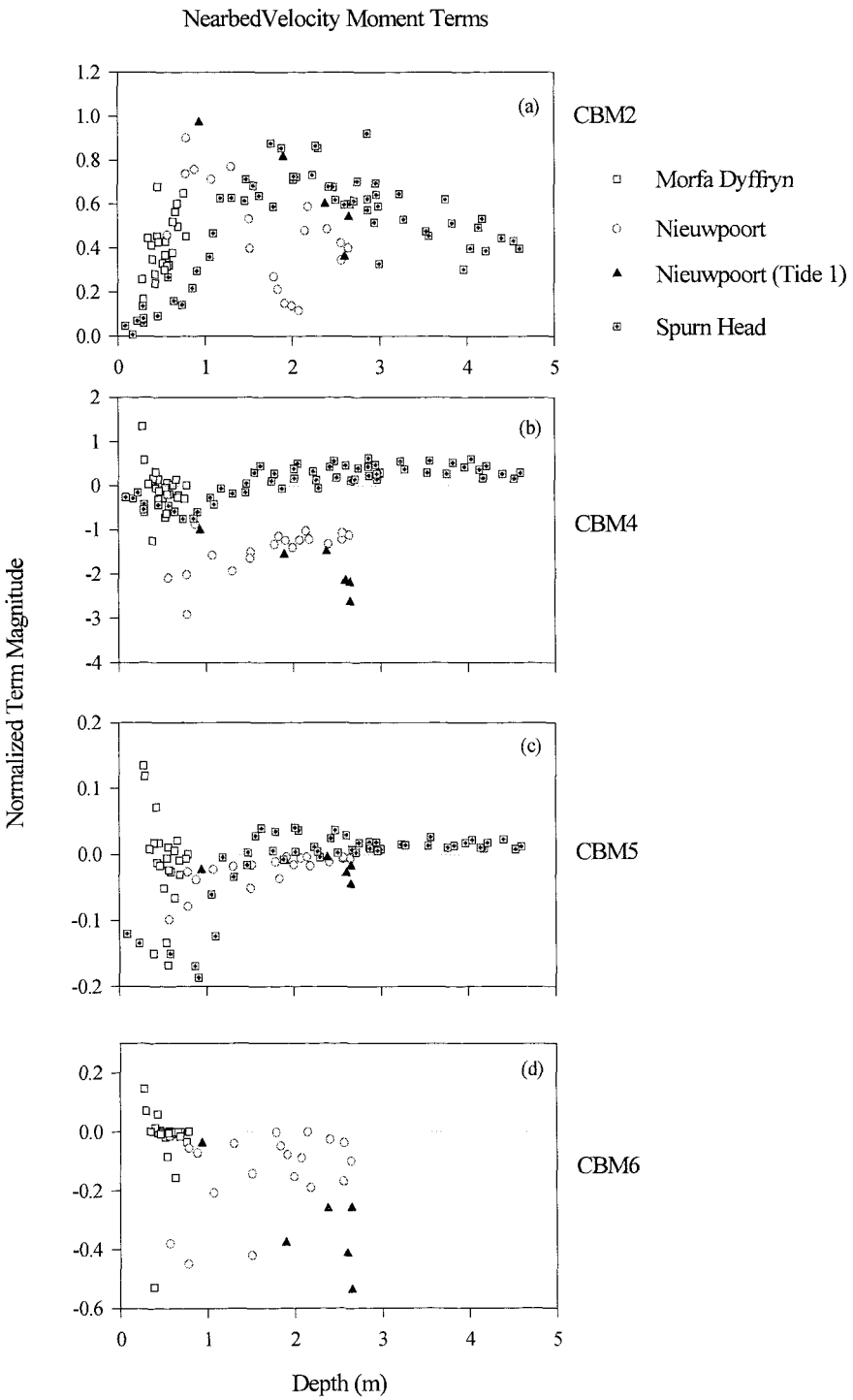

Figure 6.14 Significant Cross-shore Bedload Terms obtained from data collected at Morfa Dyffryn, Nieuwpoort and Spurn Head

both the flood and ebb (Tides 26 and 28) or during the ebb only (Tides 27 and 29).

6.6.3 Derivation of moment terms (according to Thornton *et al.*, 1996)

The longshore currents, which have been shown to be an important factor for controlling sediment transport on the macro-tidal beaches at Morfa Dyffryn and Nieuwpoort, were primarily tidally-generated. However, a similar analysis undertaken on velocity moments from a micro-tidal beach, under storm conditions, identified that strong wave-generated longshore currents can mobilise up to 50% of the total sediment transport (Thornton *et al.*, 1996).

In order to expand the suspended load velocity moment $<|\vec{U}_t|^3 U_t>$ (referred to subsequently as Ψ_3), a number of assumptions had to be made (Section 6.2.1). Thornton *et al.* (1996) conducted a similar exercise, to assess the ability of Bailard's equation (2.4) to predict cross-shore sediment transport rates in the presence of strong wave-generated longshore currents. The two dominant velocity moments (Ψ_1 and Ψ_3) were decomposed under different assumptions. The breakdown of the bedload moment (Ψ_1) was similar, but with only the four largest terms retained (Thornton *et al.*, 1996, equation 7); these will be referred to henceforth as T1, T2, T3 and T4 and are the same as CBM2, CBM6, CBM12 and CBM4, respectively.

For outside the surf zone, Thornton *et al.* (*op. cit.*) assumed that $\tilde{u}_s$ dominates, since longshore currents tend to zero. Therefore, $<|u|^3 u>$equates approximately to $<|\tilde{u}_s|^3 \tilde{u}_s>$; this provides onshore transport, due to short wave skewness. However, inside the surf zone and particularly during storm periods, the longshore current was the largest velocity component. Thus, $|u_t|^3$ was expanded under the assumption that $\bar{v} >> \tilde{u}_s \sim \bar{u} \sim \tilde{u}_l > \tilde{v}_l \sim \tilde{v}_s$, so that:

$$|u_t|^3 \approx |\bar{v}|^3 + \frac{3}{2}|\bar{v}||u|^2 + \cdots \qquad (6.9)$$

When substituted into the suspended velocity moment, Ψ_3 becomes:

$$\begin{aligned} <|u|^3 u> \approx\ & |\bar{v}|^3 \bar{u} + \frac{3}{2}|\bar{v}|\bar{u}\left(\bar{u}^2 + <\tilde{u}_s^2> + <\tilde{u}_l^2>\right) \\ & + \frac{3}{2}|\bar{v}|\left(<|\tilde{u}_s^2|\,\tilde{u}_s> + <|\tilde{u}_l|^2\tilde{u}_l>\right) \\ & + 3|\bar{v}\bar{u}|\,\bar{u}\left(<|\tilde{u}_s|> + <|\tilde{u}_l|>\right) \\ & + 3|\bar{v}\bar{u}|\left(<|\tilde{u}_s|\tilde{u}_s> + <|\tilde{u}_l|\tilde{u}_l>\right) + \cdots \end{aligned} \qquad (6.10)$$

The resultant moment terms are presented in Table 6.9.

Moment Term (Thornton *et al.*, 1996)		Transport mode	Equivalent Moment Term (Voulgaris & Collins, 1996)
T1	$<u_s^3>$	Bedload	CBM 2
T2	$<\bar{v}^2\bar{u}>$		CBM 6
T3	$3<\tilde{u}_s^2\,\tilde{u}_l>$		CBM 12
T4	$3<\tilde{u}_s^2\,\bar{u}>$		CBM 4
T5	$<\lvert\tilde{u}_s\rvert^3\,\tilde{u}_s>$	Suspended load (outside surf zone)	CSM 2a
T6	$<\lvert\tilde{u}_s\rvert^3\,\bar{u}>$		CSM 1a
T7	$<\lvert\tilde{u}_s\rvert^3\,\tilde{u}_l>$		CSM 3a
T8	$\lvert\bar{v}\rvert^3\,\bar{u}$	Suspended load (inside surf zone) storm conditions	CSM 1b
T9	$\frac{3}{2}\lvert\bar{v}\rvert\,\bar{u}(\bar{u}^2 + <\tilde{u}_s^2> + <\tilde{u}_l^2>)$		
T10	$\frac{3}{2}\lvert\bar{v}\rvert\,(<\lvert\tilde{u}_s\rvert^2\,\tilde{u}_s> + <\lvert\tilde{u}_l\rvert^2\,\tilde{u}_l>)$		
T11	$3\lvert\bar{v}\bar{u}\rvert\,\bar{u}(<\lvert\tilde{u}_s\rvert> + <\lvert\tilde{u}_l\rvert>)$		
T12	$3\lvert\bar{v}\bar{u}\rvert\,(<\lvert\tilde{u}_s\rvert\tilde{u}_s> + <\lvert\tilde{u}_l\rvert\tilde{u}_l>)$		

Table 6.9 Derivation of the moment terms after Thornton *et al.* (1996)

Each of the terms in Table 6.9 was examined using using the field data collected during the DELILAH experiment. The data spanned 3 weeks and included two storm periods. The first storm was associated with with waves (H_s of 2 m in 8 m water depth) approaching the beach at angles of about 40 deg; the second storm included narrow banded swell waves (H_s of 2.5 m), but at incident angles of about 20 deg. The first storm period generated strong longshore currents of around 1.5 m s^{-1} but, despite higher waves

during the second storm period, the narrow angle of incidence generated mean longshore currents of approximately 1 m s^{-1}.

Thornton *et al.* (1996)'s Current Meter No. 5 was located just to seaward of the crest of the nearshore bar; this was in a similar topographic location to that of Station C at Morfa Dyffryn. At Thornton *et al.* (*op. cit.*)'s field site, the mean longshore current was 180 deg out of phase with the tidal elevation, particularly during storms; it was also the location of the strongest undertow. Short wave velocities were relatively constant, due to wave height saturation over the bar. Interestingly, at low water on 12 October 1990, when the surf zone extended offshore from the bar, the mean longshore currents remained high across the whole of the profile; this occurred until inshore of the inner trough, where the weakest current on 12 October was around 0.5 m s^{-1}.

The mean longshore current term $|\bar{v}|^3\ \bar{u}$ was responsible for mobilising about half of the total transport during storm conditions; the majority of the remainder was mobilised by short wave activity. Under milder wave conditions, as predicted, the onshore skewness term pre-dominated. However, there was evidence of a tidal signature, with considerably higher transport at low water; this extended further offshore, as the waves broke farther from the shoreline.

Velocity moment terms T8 to T12 were calculated using the measured velocities at Morfa Dyffryn; the results are shown in Figure 6.15. The sum of these terms form Thornton *et al.* (*op. cit.*)'s eqn. 11, which is for suspended sediment inside the surf zone during storm conditions; the remaining moment terms have their equivalents in the Voulgaris & Collins (1996) de-composition (see Table 6.7).

The most dominant moment for Tides 26 to 29 was, not surprisingly, T5 (CSM2a), although Thornton *et al.* (*op. cit.*) would expect this dominance only outside the surf zone. Interestingly, T10, which represents the complex interaction between short waves, long waves and mean longshore current, is of some consequence during Tide 29, which is not represented, or revealed, in the breakdown of Voulgaris & Collins (*op. cit.*) velocity moments. This term indicates onshore transport and dominates the total suspended moment; it is, therefore, of more consequence than T8/CSM1b.

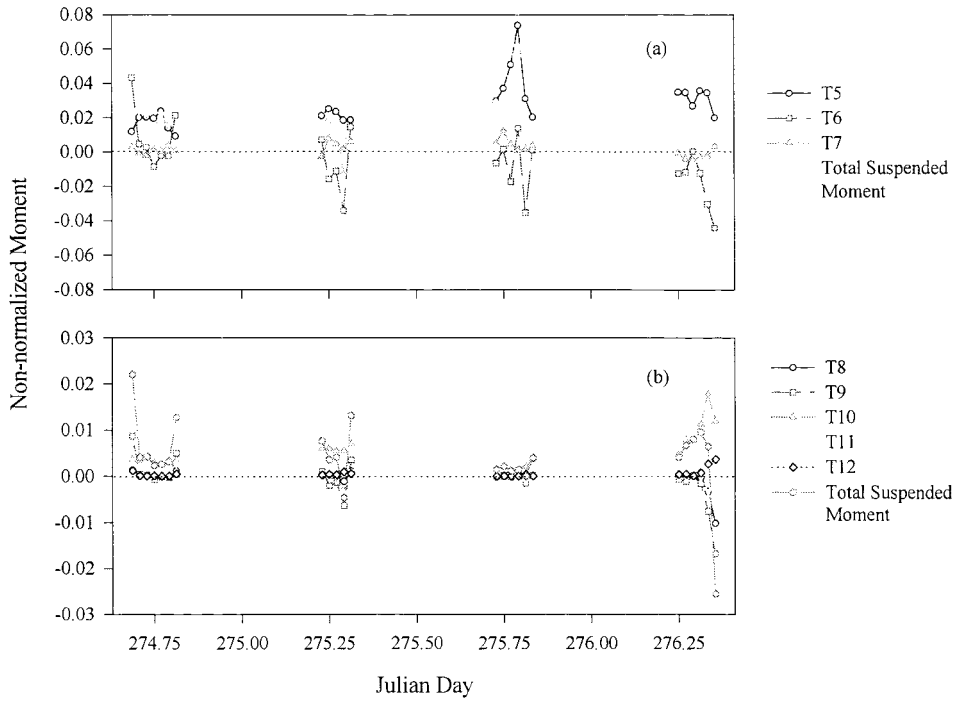

Figure 6.15 Suspended velocity moment terms as derived by Thornton *et al.* (1996) for: (a) outside surf zone; and (b) inside surf zone, for storm conditions (Tides 26 to 29)

Overall, the derivations of Thornton *et al.* (*op. cit.*) are less suited to the wave conditions on a macro-tidal beach, since they effectively confine the influence of the mean longshore current to within the surf zone; hence, to storm conditions. Furthermore, retention of only the first four bedload terms underestimates the contribution of the mean cross-shore current, both as a mobiliser (CBM1) and transporter (CBM1 and CBM5). Although the mean longshore current exceeded generally the mean cross-shore current at Morfa Dyffryn, the inclusion of mean cross-shore current in 4 of the 5 dominant bedload moments means illustrates its importance. Undertow and longshore currents (non-tidally induced), of the same order of magnitude as the wave orbital velocities, have also been observed where wave energy is dissipated across a series of offshore bars (Hazen *et al.*, 1990).

In contrast, the inclusion of mean longshore current in both the cross-shore bedload and suspended load terms (via CBM6 and CSM1a/T8), confirms that the derivation of moment terms by Foote (1994) are unsuitable where strong (either tidally-or wave-generated) longshore currents are present.

6.7 SUMMARY OF RESULTS

- The relative importance of each moment term varies according to tidal stage *e.g.* mean cross-shore current terms are more important early in the flood and late in the ebb tide. Accordingly, net sediment transport direction also has a tidal signature.

- Short waves are the dominant mobilizing mechanism and also the main transporter of suspended sediment.

- Mean cross-shore current was of most influence as a transporter of bedload in shallow water.

- Tidally-generated mean longshore currents can be important for cross-shore sediment transport in addition to transport alongshore, both inside and outside the surf zone. A mean longshore current greater than 0.3 m s^{-1} and 0.35 m s^{-1} mobilized bedload and suspended load respectively as effectively as the short waves.

- Long waves were of no importance in the conditions encountered at Morfa Dyffryn during Tides 26 to 29.

- The derivation of velocity moment terms in sections 6.1.1 and 6.1.2 (after Voulgaris & Collins, 1996) is better adapted to hydrodynamic conditions on macro-tidal beaches, than the solutions of Foote (1994) and Thornton *et al.* (1996), due to the different assumptions made about the relative importance of oscillatory currents and mean cross- and longshore currents.

In conclusion, providing the velocity field is decomposed according to the hydrodynamic conditions most appropriate to the field site, the energetics approach to

sediment transport modelling of Bailard (1981) and its derivatives, provides a simple yet powerful method of predicting the rate and direction of sediment transport. However, the true test of the model is how well its predictions fit against measured sediment transport data. A comparison of sediment transport rates predicted by Bailard (1981) as given by eqns (2.5) and (2.6) by Guza & Thornton (1985) with the measured suspended transport rates will be included in Chapter 8.

CHAPTER 7: RESULTS - WAVE REFLECTION

7.1 Introduction

The characterization of the velocity moments, on the ridge and runnel section of the composite beach at Morfa Dyffryn, has served to emphasise both the importance of mean currents in shallow water and the necessity of integrating hydrodynamic measurements throughout the entire (macro-) tidal cycle. An important element of this analysis is to include the influence of the relict sand/shingle ridge on wave reflection, since any marked change in the reflection characteristics of different parts of the profile will affect subsequently the sediment transport regime. On the macro-tidal beach at Morfa Dyffryn, the profile gradient and sediment composition of the reflecting surface varied throughout the tidal cycle. Both factors are first-order determinants of wave reflection. Hence, the shingle ridge is expected to be an important forcing factor for suspended sediment transport

In order to assess the nature of the wave reflection at Morfa Dyffryn, a comparison is made here with the reflection at Nieuwpoort-aan-Zee, Belgium (using data from the MAST II C-STAB project [O'Connor, 1996]).

7.2 Calculation of Reflection Coefficients

Detailed analysis of wave reflection undertaken at Nieuwpoort utilised a Modified Maximum Likelihood Estimator (MMLE) method, to calculate reflection coefficients (Huntley, 1996). For comparison with Morfa Dyffryn, the same (time domain) method of FDRF calculation had to be used. This approach provided a useful cross-check on the validity of the time-domain method (Section 4.3.5).

FDRF values were calculated for the data shown in Huntley (1996), Figure 8.4.4.8, which has been reproduced as Figure 7.1. The parameters used for the Nieuwpoort spectral analysis were the same as those used for Morfa Dyffryn (4096 data points sampled at 4 Hz; segments of 512 data points with 50% overlap; Hanning window). Figure 7.2 shows the results produced by the time-domain method for B0600340 (Figure 7.1), which spans high water.

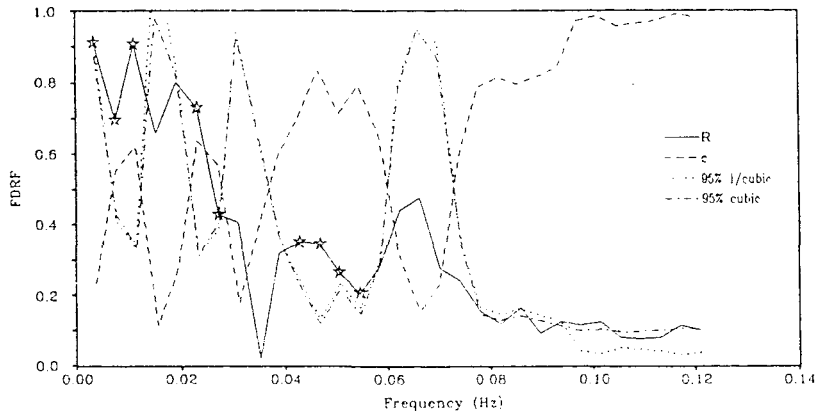

Figure 7.1 FDRF values and coherency for JD 0630340, calculated using MMLE method (reproduced from Huntley, 1996)

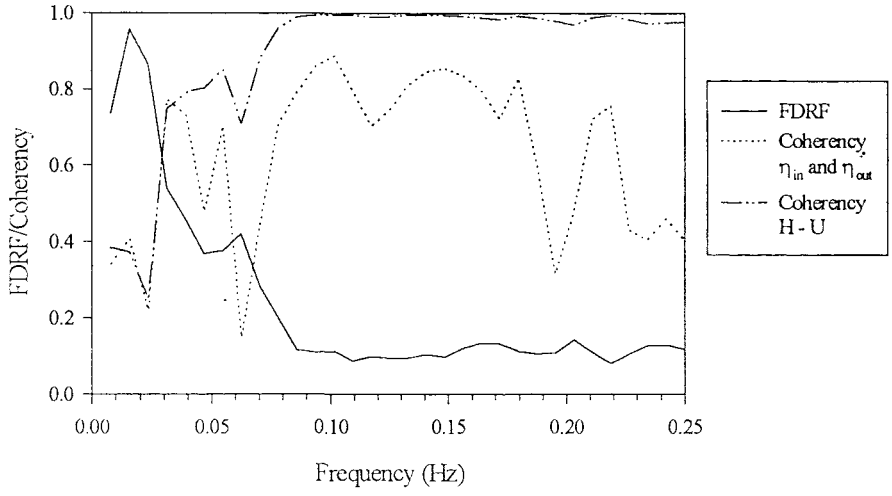

Figure 7.2 Results obtained from time-domain analysis of JD 0600340, Station B, Nieuwpoort-aan-Zee

Above 0.1 Hz, the H-U coherency and FDRF values are similar for both methods of analysis. From 0.1 to 0.04 Hz, the time-domain FDRF values follow the same trend as the MMLE method, but are about 0.1 higher. However, η_{in} and η_{out} coherency (which

Above 0.1 Hz, the H-U coherency and FDRF values are similar for both methods of analysis. From 0.1 to 0.04 Hz, the time-domain FDRF values follow the same trend as the MMLE method, but are about 0.1 higher. However, η_{in} and η_{out} coherency (which was used for the time-domain analysis) was below 0.6 for most of this frequency band (including the starred values shown in Figure 7.1); this would be reduced according to Figure 2 of Huntley *et al.* (1995). According to the criteria outlined previously (Section 4.3.5), only the FDRF value at 0.117 Hz would be accepted for the comparison with Morfa Dyffryn. At this frequency, the time-domain method produced a value of 0.1; this is very similar to the value suggested by Figure 7.1. The distinctive reduction in FDRF, at around 0.03 Hz, is not matched in the time-domain analysis. The FDRF at this frequency is well below the 95% confidence limits and, although the time-domain method gives an FDRF of 0.64 (reducing to 0.57) with a coherence of 0.56, the spectral peak at this frequency was not significant at 95% confidence limits. For frequencies lower than 0.02 Hz, the FDRF and coherence curves are similar, except that the lowest frequency (starred in Figure 7.1) was not coherent according to the time-domain method.

In summary, therefore, for incident wave frequencies above 0.1 Hz, the time-domain method is able to replicate the FDRF values given by the MMLE method. Between 0.04 and 0.1 Hz, the time-domain values are slightly higher, although lower coherence would result in their being adjusted downwards; this would bring them into line with the MMLE values. The very low frequency (below 0.02 Hz) FDRF values are similar for both methods, although the time-domain method would reject the starred peak as incoherent. Although much of the interesting detail of Figure 7.1 is lost in the analysis, it is nonetheless reassuring to note that using the time-domain method (with the criteria given in section 4.3.5) produces fewer, rather than more, significant FDRF values. The significant values are similar to those produced by the more rigorous MMLE method.

7.3 Wave reflection at Morfa Dyffryn

Data collected from 5 tides were selected to characterise wave reflection at Morfa Dyffryn. The composite nature of the beach profile at Morfa Dyffryn resulted in the inner surf and swash zones of a spring tide passing progressively across: a series of ridges and runnels, of varying gradient: a steeper mixed sand and shingle bed: and, finally, a steep shingle ridge (the profile can be seen in Figure 7.10 below). Only Tide 32 encompassed all three zones. Tides 31 and 33 inundated the sand/shingle ridge, whilst Tide 29 reached

the mixed section only during HW and HW +0.5. the latter tidal cycle is the highest tide for which suspended sediment concentration data are available. Tide 26 covered only the sand ridges and runnels. The analysis of results from Tide 32 are used as an example, since the tidal range of 4.7 m meant that the waves advanced over a variety of beach gradients and sediment types, as indicated in Table 7.1. Tidal stage in the table is given in hours relative to local High Water. The width of the surf/swash zone was derived visually whilst the beach gradient refers to the slope of the beachface which was covered by the surf/swash zone.

Tidal Stage	H_s (m)	Width of surf/ swash zone (m)	Gradient		Sediment type, at the shoreline
			tan β	degrees	
HW -1.5	0.19	10	0.022	1.24	Sand (inner ridge)
HW -1	0.19	8	0.079	4.49	Sand (beachface)
HW -0.5	0.16	7	0.087	4.95	Mixed sand/shingle
HW	0.15	5.8	0.101	5.74	Shingle and mixed
HW +0.5	0.15	7	0.087	4.95	Mixed sand/shingle
HW +1	0.15	8	0.078	4.45	Mixed sand/shingle
HW +1.5	0.16	10	0.018	1.01	Sand (inner ridge)

Table 7.1 Beach gradient, surf/swash zone width and significant wave height for Tide 32 (Morfa Dyffryn)

The spectral density plot of the sea surface elevation, during the tidal stages listed in Table 7.1, are shown in Figure 7.3. Three main spectral peaks can be seen at 0.07, 0.13 and 0.2 Hz (approximately 14, 8 and 5 s respectively). The peaks which are significant at the 95% confidence level and which were used in subsequent analysis are marked *. The peaks which are significant, but for which the coherence between η_{in} and η_{out} is less than 0.54, or have an FDRF above 1 are marked $*_1$ and $*_2$ respectively; these have been excluded from subsequent analyses (see Section 4.3.5). The energy at frequencies $0.05 < f < 0.1$ Hz is considered to represent swell waves (approximately 10 to 20 s period) and $f > 0.1$ Hz the wind waves (10 s periods and shorter).

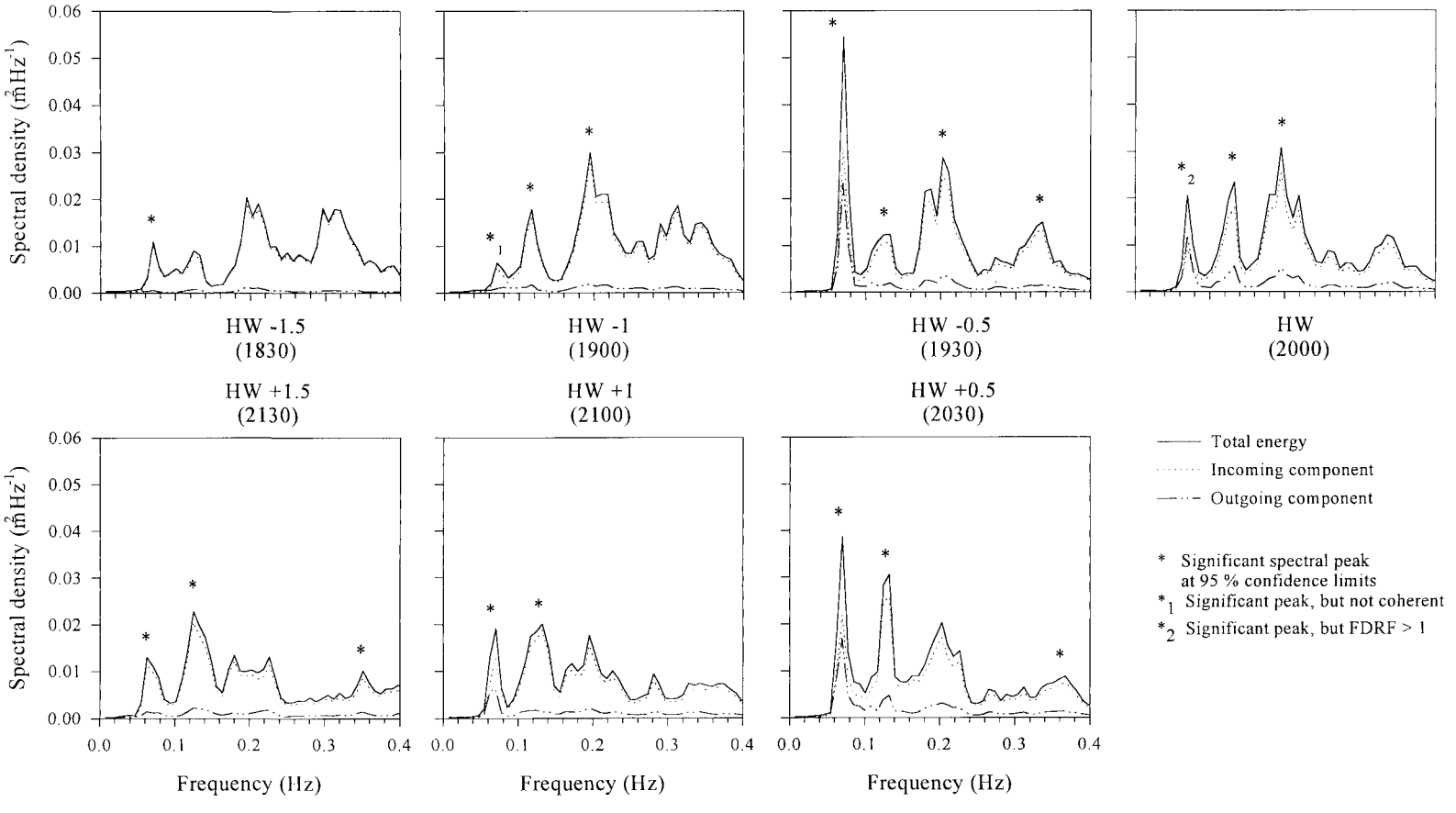

Figure 7.3 Spectral peaks of total energy and its incoming and outgoing components, for Tide 32 (Morfa Dyffryn)

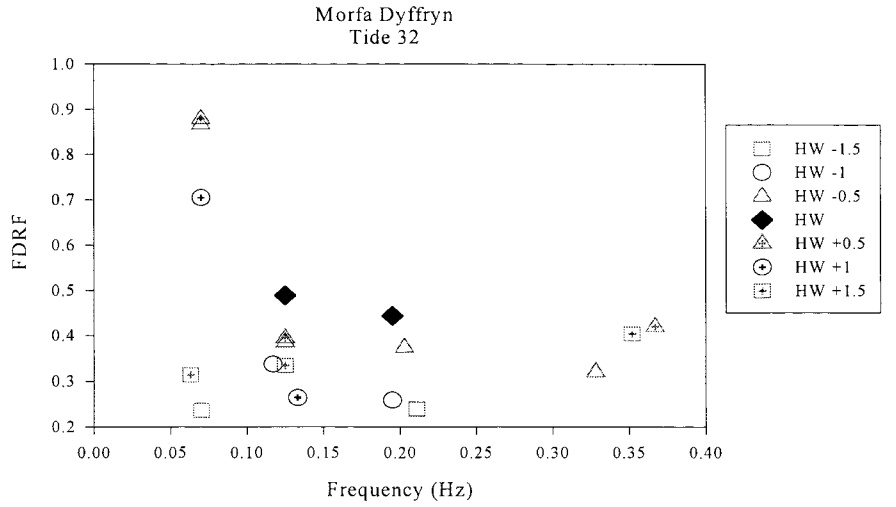

Figure 7.4 Tidal variation in FDRF values for Tide 32 (Morfa Dyffryn)

Examination of the change in FDRF, with frequency and throughout the tidal cycle (shown in Figure 7.4), reveals the following:

(a) At their maxima, there is a general decrease in FDRF with increasing frequency, up to approximately 0.2 Hz; after this, FDRF values become relatively constant. Hence, nearly 85 % of the swell wave amplitude is reflected within HW ± 0.5, whilst between about 30 and 40% of the shorter waves is reflected during this stage of the tidal cycle. Similar trends were observed for Tides 31 and 33.

(b) In contrast to the above, reflection around low water is reasonably constant (at 20% to 40% across all the significant frequencies).

(c) Within each frequency band the maximum FDRF values occur around High Water, at all significant frequencies up to 0.2 Hz. The increase is proportionally greater for swell waves, than for incident wind waves.

(d) Somewhat speculatively, where there are FDRF values for a given frequency at the same stage of the flood and ebb phase of the tide (*e.g.* HW ± 0.5), in three of the four cases, the reflection coefficient is higher on the ebb than on the flood.

The same characteristic related to all four of the cases during Tide 31, and for two of the four occasions during Tide 33.

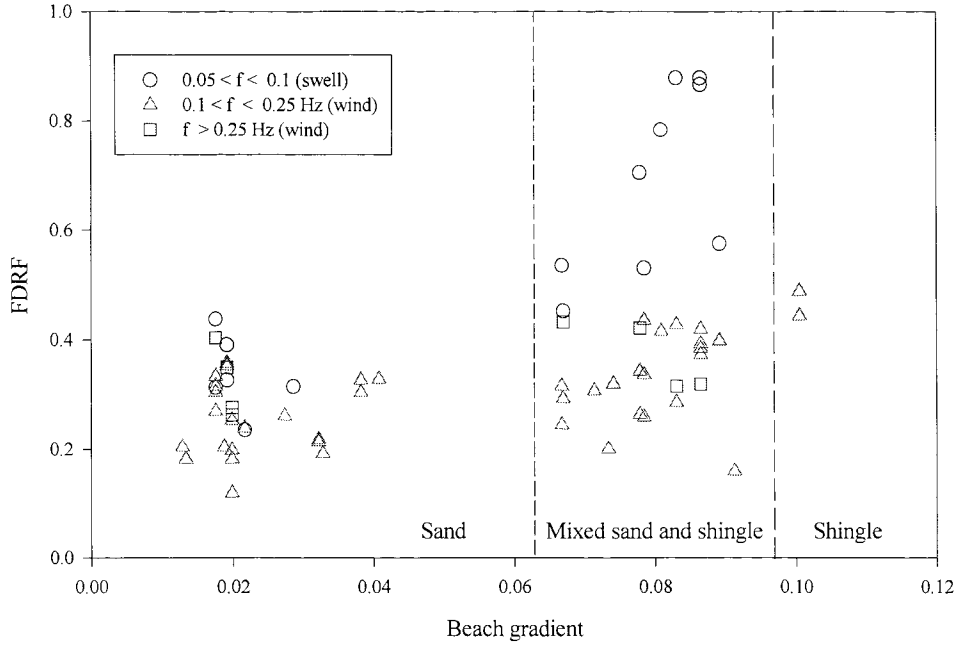

Figure 7.5 Variation in FDRF with beach gradient: Morfa Dyffryn, Tides 26, 29 and 31 to 33.

In view of the fact that the highest FDRF values occurred around High Water, FDRF data from Tides 26, 29 and 31 to 33 are plotted at Figure 7.5 against beach gradient, to examine any direct and simple relationship. The data were grouped into one of three frequency bands, which were selected to encompass the significant spectral peaks. These represent swell, wind waves and higher frequency wind waves, respectively.

The data presented in Figure 7.5 suggest that the relationship between beach gradient and FDRF accounts for much of the tidal variation in FDRF (Figure 7.4); hence, that the tidal signature in reflection may be of a general nature, where there is a marked increase in beach gradient landwards. Elsewhere, Elgar *et al.* (1994) found also that swell and sea wave reflection ($0.044 < f < 0.2$) was greatest at high tide, with reflection

occurring from the steepest section of the beachface. These investigators noted that the reflection coefficient for swell-sea waves was approximately proportional to β^5. However, on the gently sloping (tan $\beta < 0.05$) sandy section of the beach at Morfa Dyffryn, incident wave reflection remained at between 10% and 40% irrespective of frequency. On beach sections steeper than 0.06, reflection at wind wave frequencies remains constant. However, reflection of swell waves increases with beach gradient, to nearly 90%. Therefore, reflection of incident wind waves was not dependent upon beach gradient, whilst swell wave reflection increased proportionally with beach slope only above gradients of 0.06. The trend for higher reflection coefficients around high water together with greater variability at low water has been observed also for low frequency waves (Nelson & Gonsalves, 1990). These investigators attributed this trend to increased turbulence across a wider surf zone at low water, with accompanying interference and suppression of reflected waves.

The mixed sand/shingle section of the beach appears, therefore, to operate as a strong reflector of swell waves. Unfortunately, there are too few data points to establish whether this is due to the mixed nature of the sediment, or merely the increase in beach gradient. There are also too few data points from the shingle section of the beachface, to be able to assess the effect on wave reflection energy of dissipation through percolation. Although the highest reflection coefficients from two of the wind wave frequency bands were when the swash zone advanced across the shingle bank, they were not so noticeably higher as to be distinguishable from the mixed sediment section of the beach. The swell wave peak was not significant when the tide covered the purely shingle section of the beach during Tide 32. It may be conjectured that either percolation into the shingle and/or increased friction across the shingle reduced the energy at the peak of the swell wave frequency; this led to a broader and not significant peak.

Although the relationship with beach gradient and frequency has been noted above, wave frequency and wave amplitude or steepness are also known to influence the wave reflection from beaches. Each of these factors will be examined in greater detail below but, in practice, it is difficult to assign a relative importance to each of these factors given their inter-dependence. The most detailed study of wave reflection from natural beaches to date was carried out in Canada (Tatavarti, 1989); much of the present research will be compared with these findings. In the succeeding text, all further references to Tatavarti are to his 1989 thesis, unless stated otherwise.

7.4 FDRF and Frequency

Using data obtained from a concave beach profile with steep upper foreshore, Tatavarti identified three fairly distinctive bands of reflection: (i) low frequency waves ($f < 0.06$ Hz) which had a fairly high and reasonably constant reflection coefficient; (ii) a transitional frequency band between the long and short waves ($0.06 < f < 0.1$ Hz) where the reflection coefficients showed a steep downward gradient and (iii) a higher frequency region with small but constant reflection. The transitional region represented the change from non-breaking to breaking conditons.

Similar trends between frequency and FDRF were found for the (five) tides examined at Morfa Dyffryn (Figure 7.6). The highest reflection coefficients were for swell waves (~ 0.07 Hz), reaching FDRF values of nearly 0.9 *i.e.* the same as for Tatavarti's low frequency waves. However, there was considerable scatter in the data points, since some coefficients of below 0.4 were recorded at this frequency, rather than the clear transition between low frequency and swell waves (as observed by Tatavarti). There was also considerable scatter for the slightly shorter swell waves (~0.1 Hz) and the coefficients varied from 0.2 to 0.4. As anticipated, therefore, frequency is not a *unique* determinator of reflection from a natural beach.

7.5 FDRF and Wave Amplitude and Steepness

Although low amplitude waves are thought to be more reflective than those of high amplitude, the relationship between increasing wave amplitude and decreasing reflection coefficients is not linear. This is not surprising given the non-linear nature of wave transformation within the surf zone (Tatavarti, 1989). The generally mild reflection reduced with increasing wave amplitude. The FDRF values shown in Figure 7.7 are plotted against the non-dimensionalised Irribarren Number, which encompasses amplitude and steepness, frequency and beach gradient (further details of this expression are given in Section 7.6, below). However, for a given frequency and a constant beach gradient, any variation in FDRF is due to wave amplitude.

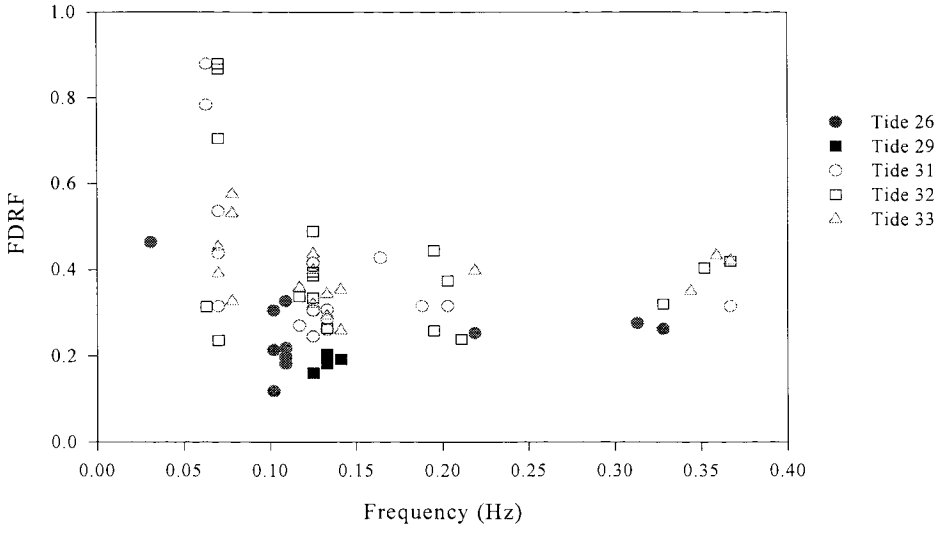

Figure 7.6 FDRF plotted against frequency for Tides 26, 29 and 31 to 33 (Morfa Dyffryn)

For the wind waves frequencies, the reduction in FDRF with wave amplitude was marked, particularly across the dissipative and intermediate domains of the beach. The higher amplitude waves (Tides 26 and 29, open diamonds and squares respectively on Figure 7.7 *b)*, had amplitudes of ~0.16 m and ~0.12 m, respectively; they reflected less than 30 % of their amplitude. The smaller waves of Tides 31 to 33 (crosses, open circles and crossed circles on the Figure, amplitude of ~0.08 m) reflected between 20% and 50% of amplitude. There are no data points available for the higher amplitude waves within the swell wave band, and only one data point in the low frequency band (the open diamond on Figure 7.7 *a*). However, it is tempting to speculate that the reduction in reflection with increasing wave amplitude is also dependent upon frequency; the lower the frequency, the more pronounced the reduction in reflection with increasing amplitude.

Even though qualitative, it is noteworthy that the influence of wave amplitude should be evident even for waves lower than 0.5 m; this is particularly relevant, since the comparatively recent recognition of the significant contribution of low-energy swell waves to longshore sediment transport (Whitcombe, 1995; Powell, 1996).

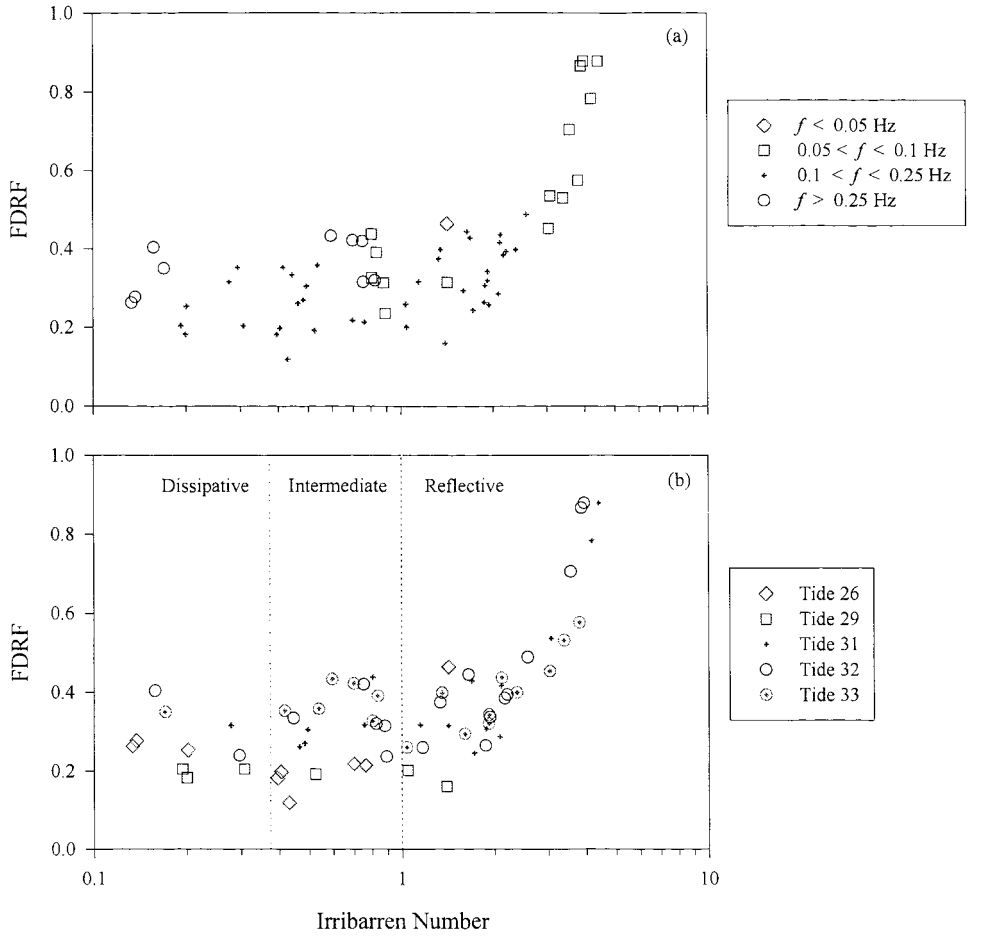

Figure 7.7 FDRF plotted against Irribarren Number for: (a) varying frequency bands; and (b) Tides 26, 29 and 31 to 33

A more rigorous assessment of the influence of the wave characteristics on reflection is through wave steepness, which includes both amplitude and frequency. Consequently, FDRF values for 5 tides are plotted against wave steepness at Figure 7.8; this illustrates once again that the steepest, high frequency waves ($f > 0.25$ Hz) reflected between 20% and 40% of their amplitude; the remaining proportion is likely to have been dissipated through wave breaking, friction and infiltration. The remaining wind wave frequencies ($0.1 < f < 0.25$ Hz) encompass an order of magnitude of wave steepness values, with an accompanying variety of reflection coefficients ranging from from 0.1 to 0.5. These coefficients represent probably a continuum of breaking and partially-breaking

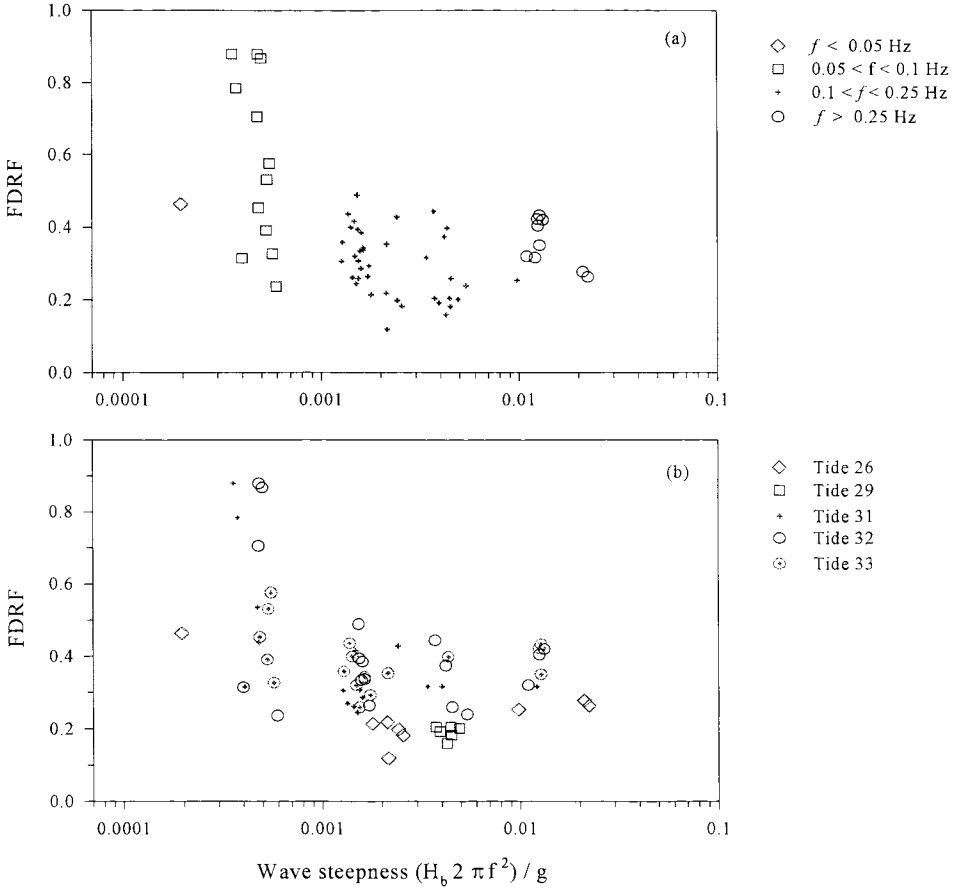

Figure 7.8 Wave steepness vs FDRF for (a) varying frequency bands and (b) Tides 26, 29 and 31 to 33

waves, depending upon tidal stage and thus on beach gradient and water depth. The data presented in Figure 7.8 demonstrate that the FDRF was uncorrelated with wave steepness, for all gravity waves from the (5) tides included in this analysis. Davidson *et al.* (1994) found a similar lack of correlation, but only in the presence of a surf zone.

Reflectivity of the swell waves increased sharply with decreasing wave steepness, over a narrow range of wave steepness from 0.003 to 0.006 (Figure 7.8 *a*, open squares). These were the low amplitude (~0.08 m) swell waves of Tides 31 to 33 (Figure 7.8 *b*); they encompassed both intermediate and reflective conditions and confirm, therefore,

that FDRF is not determined uniquely by wave conditions. Here, FDRF ranged from 0.2 to 0.9, even for these waves of low amplitude and low steepness.

7.6 Influence of Beach Gradient on FDRF

In order to assess the influence of beach gradient on wave reflection, the importance of which was noted in Section 7.3, FDRF values are compared with the non-dimensional Irribarren Number, Σ_b (also referred to variously as Σ and *Ir*). This expression embodies both wave conditions and beach gradient; it is the breaking wave version of the surf similarity parameter (Battjes, 1974) and includes wave steepness (which can be calculated as a function of frequency) and beach slope. The Irribarren Number may be expressed as follows:

$$\Sigma_b = \frac{\tan\beta}{\sqrt{H_b / L_o}} \tag{7.1}$$

where β is beach slope, H_b is breaking wave height and the deepwater wavelength, L_o, is calculated from:

$$L_o = \frac{g T^2}{2\pi} \tag{7.2}$$

For this comparison, T is represented as T_{peak} of each significant frequency, as defined in Section 4.3.1, so that Σ_b is calculated in the form of:

$$\Sigma_b = \frac{\tan\beta}{\sqrt{H_b \, 2\pi f^2 / g}} \tag{7.3}$$

Use of the Irribarren Number is widespread for engineering applications and indeed suggests that the relationship between this combination of frequency, gradient and wave amplitude, describes wave reflection quite well, particularly for FDRF values greater than 0.4, when $\Sigma_b > 1$ (Figure 7.7 *b*). This is discussed further in section 7.7.

In the published literature, wave reflection is also compared sometimes to the surf-scaling parameter, ϵ , which is interchangeable with the Irribarren Number through the expression:

$$\epsilon = \pi \Sigma_b^{-2} \tag{7.4}$$

During Tides 31 to 33 at Morfa Dyffryn, the wave amplitude was fortuitously similar (~ 0.08 m); there was a single line of small plunging breakers and narrow surf/swash zone, although the beach gradient varied throughout the tidal cycles. Therefore, for these tides and a constant frequency, variation in Σ_b is due primarily to beach gradient (Figure 7.9). For a gently sloping beach (gradient ~ 0.02, open symbols in Figure 7.9), FDRF is essentially constant between 0.25 and 0.45, for the entire gravity wave frequency range, despite Σ_b encompassing an order of magnitude (since the square of the frequency is involved). These FDRF values represent a substantial proportion of reflected wind wave energy.

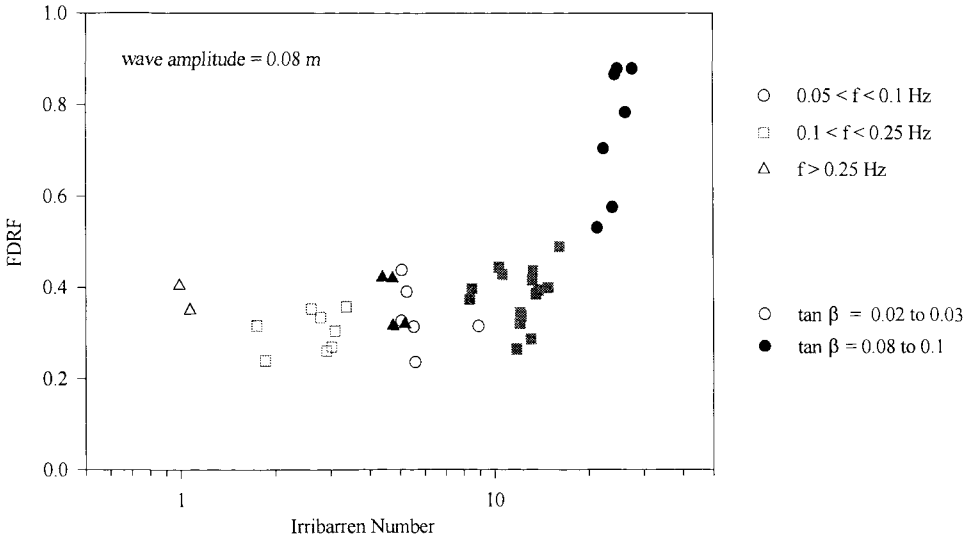

Figure 7.9 The relationship between Irribarren Number and FDRF for constant wave amplitude (0.08 m); beach gradient of 0.02 to 0.03 (open symbols) and 0.08 to 0.1 (filled symbols); Tides 31 to 33, Morfa Dyffryn

Across the steep section of the beach (filled symbols on the Figure) the somewhat surprising conclusion is that, once again, FDRF is relatively constant at between 0.25 and 0.5 for all frequencies above 0.1 Hz *i.e.* increasing beach slope (up to 0.1, 5.7°); it does not markedly increase the reflection of wind waves above 0.1 Hz. However, for swell wave frequencies (circles on Figure) FDRF increases with increasing gradient: between 50 and 90% of incident wave amplitude is reflected by gradients of 0.08 (4.5°).

A similar conclusion can be drawn from the data obtained from Tide 29, when the wave amplitude was double that observed during Tides 31 to 33. All the significant frequencies lay between 0.125 and 0.141 Hz (see Figure 7.7*b*, where Tide 29 is represented by open squares) *i.e.* there was a narrow band at wind wave frequencies together with a narrow range of wave steepness also (Figure 7.8 *b*, open squares). In this case, variation in Σ_b is due to changes in beach gradient (which included gradients up to 0.09). Once again, the constant FDRF value shows that this wind wave frequency band is not sensitive to beach gradient.

7.7 Irribarren Number as a Predictor of Wave Reflection

The Irribarren Number is used widely throughout the engineering literature as a predictor of wave reflection, although with variable success (e.g. Davidson *et al.*, 1995; Bird *et al.*, 1996). It has been found to over-compensate for slope when used with field data for reflection associated with engineering structures (Bird *et al.*, 1996); it also over-emphasises the influence of incident wave height in laboratory experiments (Postmar, 1989). Attempts have been made to include an element of mean water depth in the Irribarren Number, by using the local wavelength (rather than deep water wavelength), but the scatter in the plots of Σ against R was reduced only slightly; it did not produce a unique reflection coefficient (Bird *et al.*, 1996).

However, the parameter was derived originally for beaches, rather than for engineering structures and certainly the trends identified in Figure 7.7 show that beach slope, wave amplitude/steepness and frequency are important variables for predicting wave reflection. For a constant beach gradient, an increasing Irribarren Number indicates increasingly shallow and non-breaking waves; under constant wave conditions, increasing Σ represents an increase in beach gradient. Referring to Figure 7.7 *b*, the measurements obtained during Tide 29 (open squares) had a narrow range of frequencies

and wave steepness, with a generally constant wave amplitude. Hence, Σ_b represents changing beach gradient (from 0.013 to 0.09) very effectively.

Figure 7.7 also illustrates that when $\Sigma_b > 1$ (which generally marks the transition from intermediate to reflective conditions), the FDRF within each frequency band increases with increasing Σ_b; this is particularly characteristic of swell wave frequencies. Raubenheimer & Guza (1996*a*) found a similar increase in FDRF, with increasing Irribarren Number, for the swell and wind wave frequencies ($0.05 < f < 0.18$ Hz) once Σ exceeded about 0.7. Similarly, Bird *et al.* (1996) found that reflection increased with the Irribarren Number, until a maximum reflection coefficient of about 0.6. This constant value was a function of the transmission characteristics of the porous breakwater.

FDRF	1
Tan β	0.48
H_s	-0.49
Σ_b	**0.81**
H_s / L_o	-0.21
$(H_s / L_o)^{0.5}$	-0.32
modified Σ_b	**0.85**

Table 7.2 Correlation coefficients between FDRF and first and second order parameters for wave reflection

Results of multiple regression undertaken for a range of first and second order parameters, against FDRF, are presented in Table 7.2. The sample size was 62 data points obtained from Morfa Dyffryn. As expected, the beach gradient and wave height are first order parameters, with a direct and an inverse relationship between FDRF and beach gradient and wave height respectively. Davidson *et al.* (1996) found that wave steepness (in the form H_i / L_o) did not express properly the relative influence of H and L on wave reflection from a porous breakwater, suggesting that H_i / L_o^2 was more appropriate. A modified Irribarren Number expressed by::

$$\Sigma_{mod} = \frac{\tan\beta}{\sqrt{H_s / L_o^2}} \tag{7.5}$$

was found to increase the correlation coefficient with FDRF from 0.81 to 0.85. This result provides a respectable correlation, given that: (i) the sample data included some highly non-linear waves (*e.g.* Tide 32) which were excluded specifically from Davidson's earlier analyses; (ii) there was no linear relationship between FDRF and beach gradient, wave steepness or frequency under dissipative conditions; and (iii) FDRF and Σ were generally uncorrelated for wind waves, which formed the majority of the samples (Figure 7.7*a*). This conclusion lends weight to the importance of tan β and wave amplitude in accounting for wave reflection, in preference to either of the wave steepness terms.

Overall, for the conditions experienced at Morfa Dyffryn, the Irribarren Number provided a reasonable prediction of FDRF for swell waves across the intermediate and reflective sections of the beach profile. However, it is unrealistic to expect such a parameter to be more generally applicable to complex situations, including wave reflection from random waves across ridge and runnel topography; under such circumstances, a correlation between FDRF and Σ_b in excess of 80 % can be considered reasonable.

The results described above suggest that different frequency bands are sensitive to different parameters. The steep sand/shingle bank had relatively little influence on incident waves ($f > 0.1$ Hz), but reflection of the swell waves increased almost linearly with gradient across this section *i.e.* once the beach gradient exceeded 0.08 (4.5°). Meanwhile, all the frequency bands showed a reduction in reflection with increasing wave amplitude (except for the swell waves, for which there was no data for the higher amplitude waves), although the effect appears to be increasingly important as frequency decreases.

7.8 Influence of Sediment Composition on Wave Reflection

Unfortunately, co-located wave and current data were not available when the high spring tides inundated regularly the shingle section of the beach. Hence, any change in FDRF across the mixed sand/shingle sections of the beach cannot be dissociated from the accompanying increase in beach gradient. There was also too little low frequency energy at Morfa Dyffryn to assess the influence of sediment composition on long wave reflection.

However, two qualitative observations were noted which suggest that this particular process warrants further investigation. Firstly, Bird *et al.* (1996) examined an extensive field database of reflection characteristics of a porous rock island breakwater. Reflection was found to increase with Irribarren Number up to a value of 0.6; it remained constant thereafter, despite increasing Σ. These investigators considered that 60% reflection was the maximum level possible for the structure; similarly, the remaining wave energy was dissipated and transmitted through the porous rock island breakwater. It is interesting to note, therefore, that the steepest part of the mixed sand and shingle bed at Morfa Dyffryn reflected up to 90% of the swell wave energy. This observation suggests that where a significant proportion of energy can be dissipated through infiltration, reflection coefficients should be lower for a more permeable beach of similar gradient. Secondly, as noted previously, reflection was marginally higher during the ebb tide, when the sand and sand/shingle sediment can be considered as effectively saturated. The consequences of this particular process will be discussed further in Chapter 8.

7.9 Comparison of Wave Reflection at Morfa Dyffryn and Nieuwpoort

A comparison with the wave reflection measured at Nieuwpoort allows a more general assessment to be undertaken of the influence of sediment type and beach gradient. The beach at Nieuwpoort is also macro-tidal, with an extensive series of well-developed ridges and runnels. However, it is composed entirely of sand. The beach profiles from both sites are shown in Figure 7.10. Station C at Nieuwpoort was used for the comparison, since it was sited in a similar topographic location to TOSCA at Morfa Dyffryn *i.e.* on the seaward flank of the landward main ridge. Around High Water, the tide extended to landward of the inner runnel and, during the final phase of the tide, the run-up was located just to landward of the main runnel. Therefore, the profile presented a particularly complex reflecting surface and the variation in gradient was not systematic during the tide (as it was at Morfa Dyffryn).

There was evidence of some low frequency energy at Nieuwpoort, with partially-standing waves across-shore. A somewhat complex alongshore pattern of progressive edge wave motion was present at very low frequencies, but with standing edge waves at the higher range of the low frequency band (Huntley, 1996).

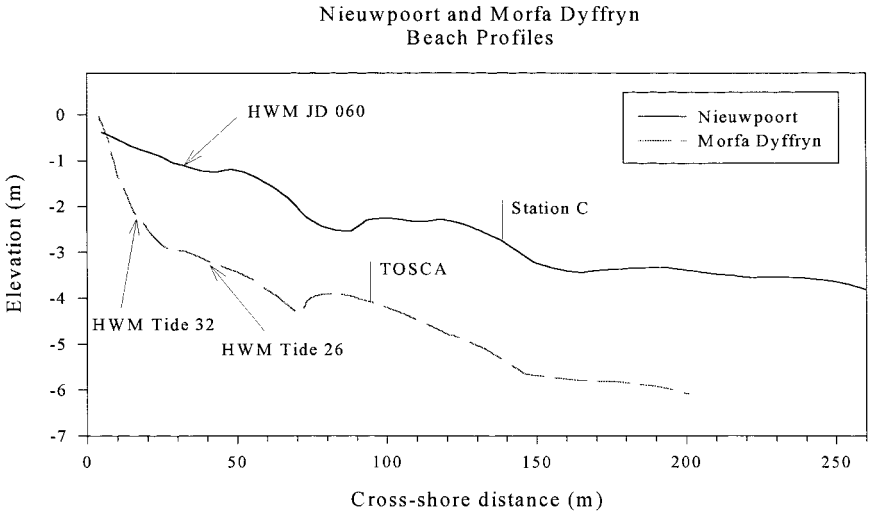

Figure 7.10 Representative beach profiles for Morfa Dyffryn and Nieuwpoort

Reflection coefficients were calculated for Nieuwpoort, using the same methods as for Morfa Dyffryn, for the afternoon tide of Julian Day 057. Wave conditions during these particular tides were most similar to Morfa Dyffryn, with a maximum H_s of 0.3 m. The T_z was around 4 s at both sites, although T_p at Nieuwpoort varied between 10 and 12 s; this compares to the 8 to 10 s peak period waves in Wales. At Nieuwpoort, there was a clear trend towards increasing reflection with decreasing frequency from 0.08 Hz and below, with 90% reflection at the lowest frequencies. Huntley (1996) has suggested that such low frequency energy could not be absorbed by percolation into the beach. On the other hand, there was considerable, unexpected, absorption at frequencies of between 0.03 and 0.06 Hz (since the FDRF was less than 0.5).

7.9.1 FDRF values

With the exception of the low frequency range (< 0.05 Hz), for which there were few data from Morfa Dyffryn, all significant FDRF values from Nieuwpoort were lower than from Morfa Dyffryn across each frequency band (Figure 7.11). However, some of this discrepancy may be accounted for by the effect of wave amplitude, as discussed previously (Section 7.5). Tide 26, (Morfa Dyffryn) resembled most closely the wave conditions at Nieuwpoort (Figure 7.12). FDRF values from Nieuwpoort were around 0.1

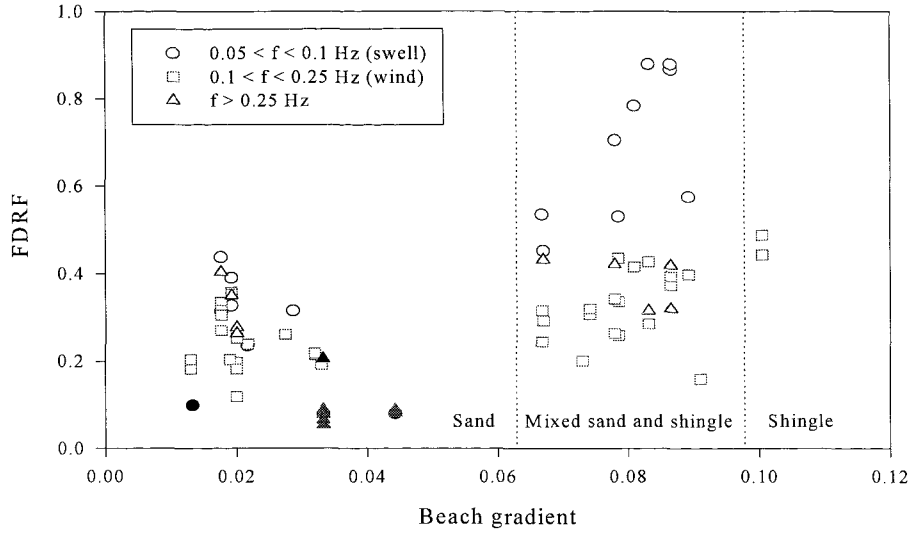

Figure 7.11 FDRF vs. beach gradient for Morfa Dyffryn Tides 26, 29 and 31 to 33 (open symbols) and Nieuwpoort JD 057 (filled symbols)

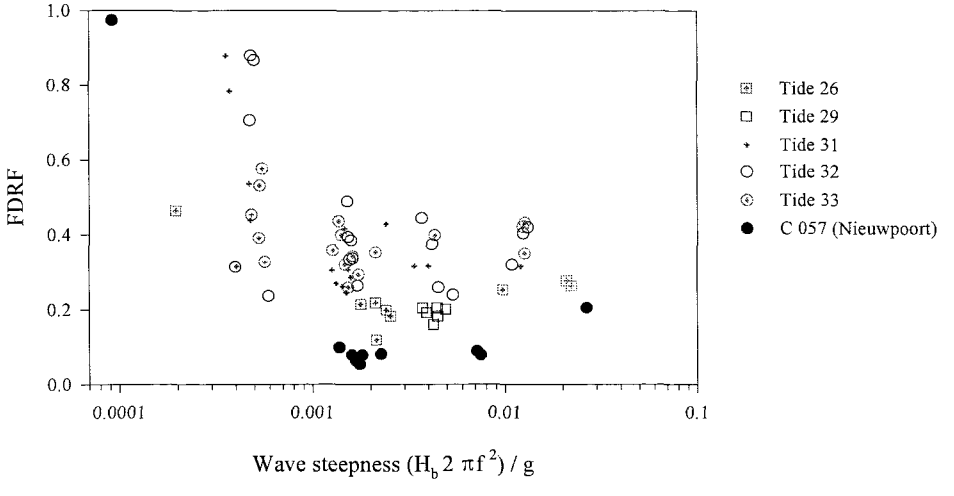

Figure 7.12 FDRF vs. wave steepness at Morfa Dyffryn and Nieuwpoort

or less below the equivalent frequency values for Morfa Dyffryn.

Although the reflection coefficients of wind waves at Morfa Dyffryn are considerably higher than those reported from other natural beaches, the discrepancy is not as large as it appears upon first consideration. Miles *et al.* (1996) have reported 10% reflection of incident waves from a beach slope of 0.06 (3.8°); this compares with 80% reflection of low frequency waves, although their incident waves referred to 0.25 Hz waves. The wave height was given as approximately 0.3 m, which is of a similar order of magnitude to Tide 26 at Morfa Dyffryn, for which incident wave FDRF values ranged from about 0.1 to 0.2. Tatavarti reported reflection coefficients of less than 0.1 for incident waves, *except* when low amplitude, groupy waves were surging and breaking close to the shoreline. In such conditions, reflection coefficients of ~ 0.6 to 0.8 and 0.4 were observed for swell (10 to 20 s) and incident (~ 6 s) waves, respectively.

7.9.2 Tidal variation in FDRF

Tidal variation in FDRF on the macro-tidal beach at Morfa Dyffryn was linked closely to the changing beach profile (Section 7.3). However, consideration needs to be given to whether the tidal symmetry in FDRF at Morfa Dyffryn is merely related to the measurement of a *local* reflection coefficient at a single point *i.e.* the tidal variation is caused by changing water depth. The complex topography at Nieuwpoort meant that variation in the gradient was not systematic during the tide, as at Morfa Dyffryn. The average gradient was 0.03 (~2°), but the steepest gradient was during the low water ebb (0.07, 4°) when the surf zone transgressed the steep seaward flank of the inner ridge. Therefore, a comparison between tidal variation in FDRF at Nieuwpoort and Morfa Dyffryn can be used to resolve this consideration since: (i) wave conditions were not dissimilar; (ii) the recording stations were in a similar position, topographically; and (iii) both sites are macro-tidal beaches. If a systematic tidal variation in FDRF occurs at both locations, then the change in water depth may influence the FDRF; the tidal variation, linked to slope thus being an artefact of the measuring regime

An estimate of tidally-varying beach gradient at the still water level at Nieuwpoort was made by simple trigonometry, extrapolating the mean water level at the beginning and end of each 17 minute data file and ignoring the effects of set-up. No variation in swell wave FDRF was found for gradients below 0.044 (2.5°) (see Figure 7.11); there

were no available data to compare at higher gradients. Unlike at Morfa Dyffryn, there was no tidal signature in wave reflection at any frequency, although the low frequency bands cannot be compared due to lack of sufficient data points. Possible reasons for the absence are that: (i) the beach gradient needs to be above a critical steepness (0.07, 4°) before frequency-selective wave reflection occurs - if this is the case, it emphasises the importance of the steep, sand/ shingle ridge at Morfa Dyffryn, and the rôle of the macro-tidal regime across a series of ridges and runnels, which effectively dissipate much of the higher frequency energy; and (ii) reflection from a number of surfaces masked any tidal signature in the FDRF.

7.10 Summary of Wave Reflection from a Composite-type Mixed Beach Profile

- Between 15% and 40% of wind wave incident energy was reflected, irrespective of beach gradient or sediment type.

- On steeper sections of the beach (gradient > 0.06), there was preferential reflection according to frequency. Once the swash zone advanced across the mixed and shingle regions, reflection of the swell wave component increased to 60% to 90%.

- Even during relatively calm conditions, a considerable proportion of incident wave energy was reflected, particularly when the breakpoint of the waves is very close to the shoreline. In such conditions, little energy is dissipated across a surf zone, which would be the case for higher and steeper waves which would break further from the shoreline.

- The time domain method of deriving reflection coefficients was verified by comparison with the MMLE method, through the utilisation of CSTAB data (Section 7.2). Hence, the observations of: (i) high and generally constant reflection coefficients at wind wave frequencies at Morfa Dyffryn; (ii) a marked increase in reflection with beach gradient for swell waves; and (iii) an increase in reflection at high tide at Morfa Dyffryn and reported elsewhere (Nelson & Gonsalves, 1990; Davidson et *al.*, 1994; Elgar *et al.*, 1994) are likely to be valid representations of the processes, rather than an artifical result of the measurements.

CHAPTER 8: RESULTS - SEDIMENT TRANSPORT

Analysis of the sediment transport at Morfa Dyffryn will concentrate upon suspended sediment transport rates, obtained from the OBS records at Station C; it includes also an estimate of total cross-shore sediment transport, derived from changes in the profile of one of the cross-shore transects. This Chapter examines also the interaction of the wave and current field, with the sand/shingle bank together with a comparison of measured suspended sediment transport rates, with those predicted by Bailard's (1981) model, as redefined by Guza & Thornton (1985), for random waves (Section 2.2.3).

8.1 Beach Profiles

Cross-shore changes in the beach profile along the Main Transect are shown in Figure 8.1. Profile 01 refers to the beach profile flooded by Tide 01. Profiles 01 to 15 encompassed the transition from spring to neap tides. The marked break-of-slope and incipient runnel, at the shingle/sand interface, became covered with a layer of sand by the time of measurement of Profile 09; this then became stranded by the rapidly-falling High Water levels. Tides 09 to 15 saw only minor profile changes, with slight accretion on the main ridge crest; erosion occurred on the seaward flanks of the main and landward ridges. The cross-shore position of the main runnel remained stationary, although the stoss side of the main ridge became steeper. There were no discernable profile changes during the neap tides (Profiles 16 to 22).

During the change from neap to spring tidal cycles (Profiles 23 to 39), there was little change between Profiles 22 and 26. However, by Profile 28, substantial accretion had occurred on the stoss side of the main ridge and on the seaward side of the runnel (Figure 8.1 *b* and Figure 8.2); this represented onshore movement of both the ridges during either Tide 26 or 27. Tide 29 washed out the inner runnel and lowered the seaward flank of the inner ridge. Detailed measurement of instrument heights, immediately following Tide 29 revealed an accumulation of sand across the inner ridge and approximately 0.03 m of erosion at Station C (at 93 m); this confirmed the considerable quantities of sand in transit during that particular tidal cycle. The data presented in Figure 8.2 suggest that the build up of sand on the inner ridge represented movement of material from seaward *i.e.* net onshore transport. Unfortunately, it is not

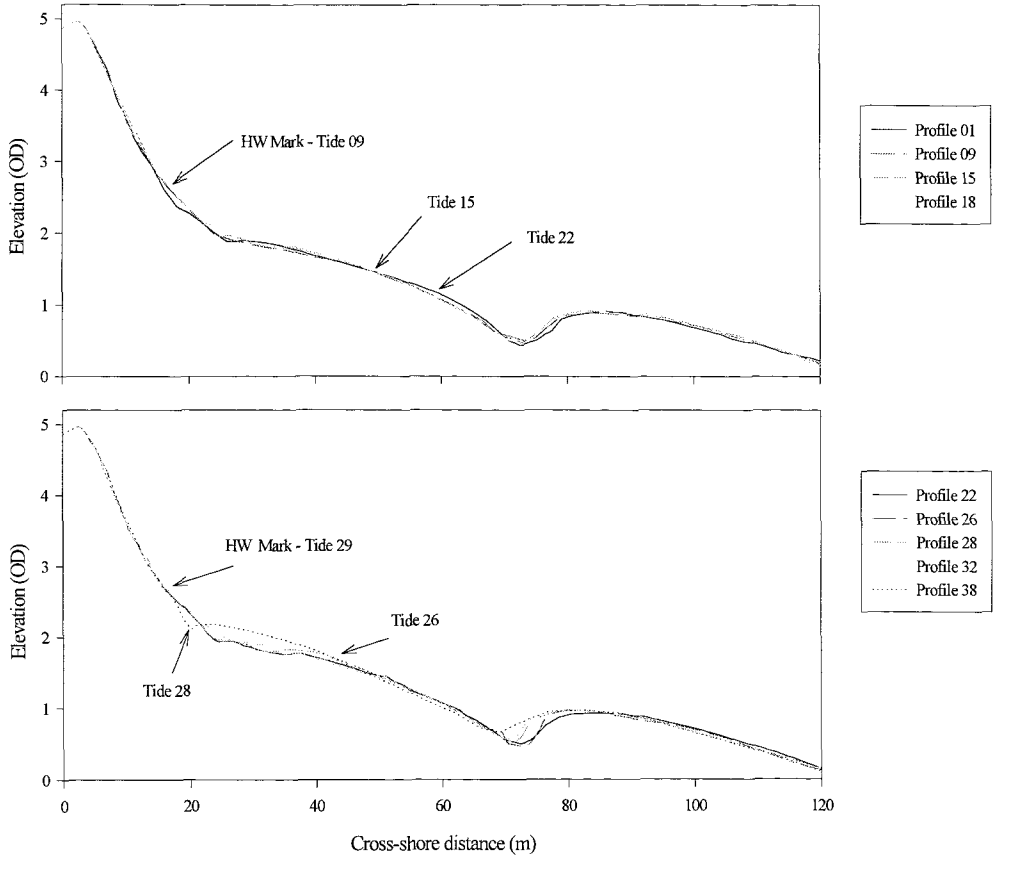

Figure 8.1 Change in profile of the Main Transect at Morfa Dyffryn

possible to confirm a net direction of transport across the whole profile during Tide 29, since the profile was not surveyed to closure depth during the night-time surveys.

Following Tide 29, the main ridge remained stable in profile. Profiles 30 to 31 showed slight accretion across the whole of the upper beach. However, Tide 31 eroded 5 cm from the layer of sand covering the shingle, leading to slight accretion at the base of the sand/mixed region of the beach; this included the landward 20 m or so of the sand beach. These changes are illustrated, in detail, by the measurements of sediment level at the graduated rods, which were spaced approximately 0.5 m apart, across the upper beach (Figure 8.3). Tide 32 eroded 10 cm across the sand/shingle Section (Rods 5 - 9) but this was restored by the following tide (Tide 33).

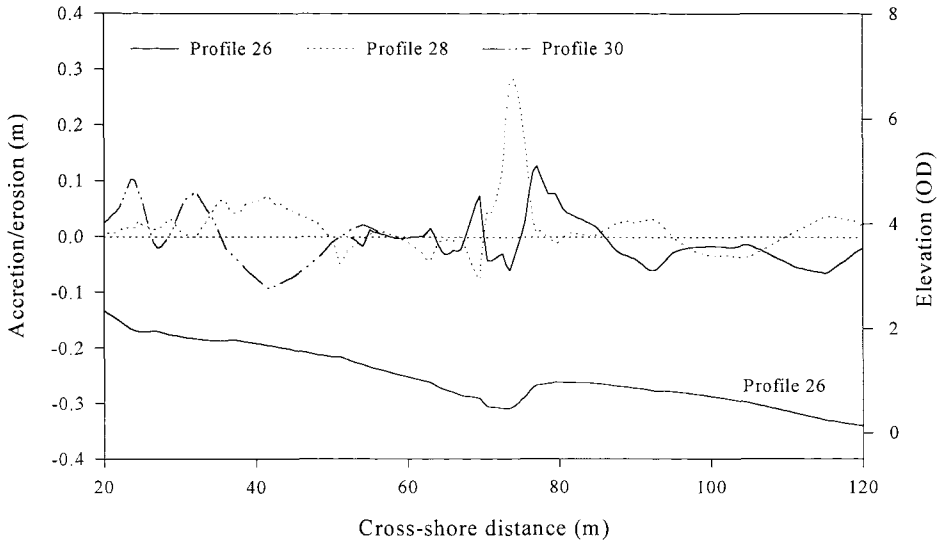

Figure 8.2 Accretion/erosion of Profiles 26 to 30 in comparison with previous profile along Main Transect

Tide 35 caused marked erosion across the whole of the upper beach, even near Rods 8 and 9 which were at about the limit of swash run-up, and the sand/shingle boundary was translocated some 2.5 m downslope *i.e.* cleared the 2.5 m horizontal width of the most shoreward sand layer. Erosion of the mixed sand/shingle region (with the boundary now at Rod 3) continued during the succeeding two tides.

The cross-sectional area located between 0.25 m contour levels of each of the profiles was calculated (using software written by Dr L. J. Whitcombe, Southampton University, Department of Oceanography). The results have revealed that the movement of the inner ridge accounts for the greatest areal change (Figure 8.4).

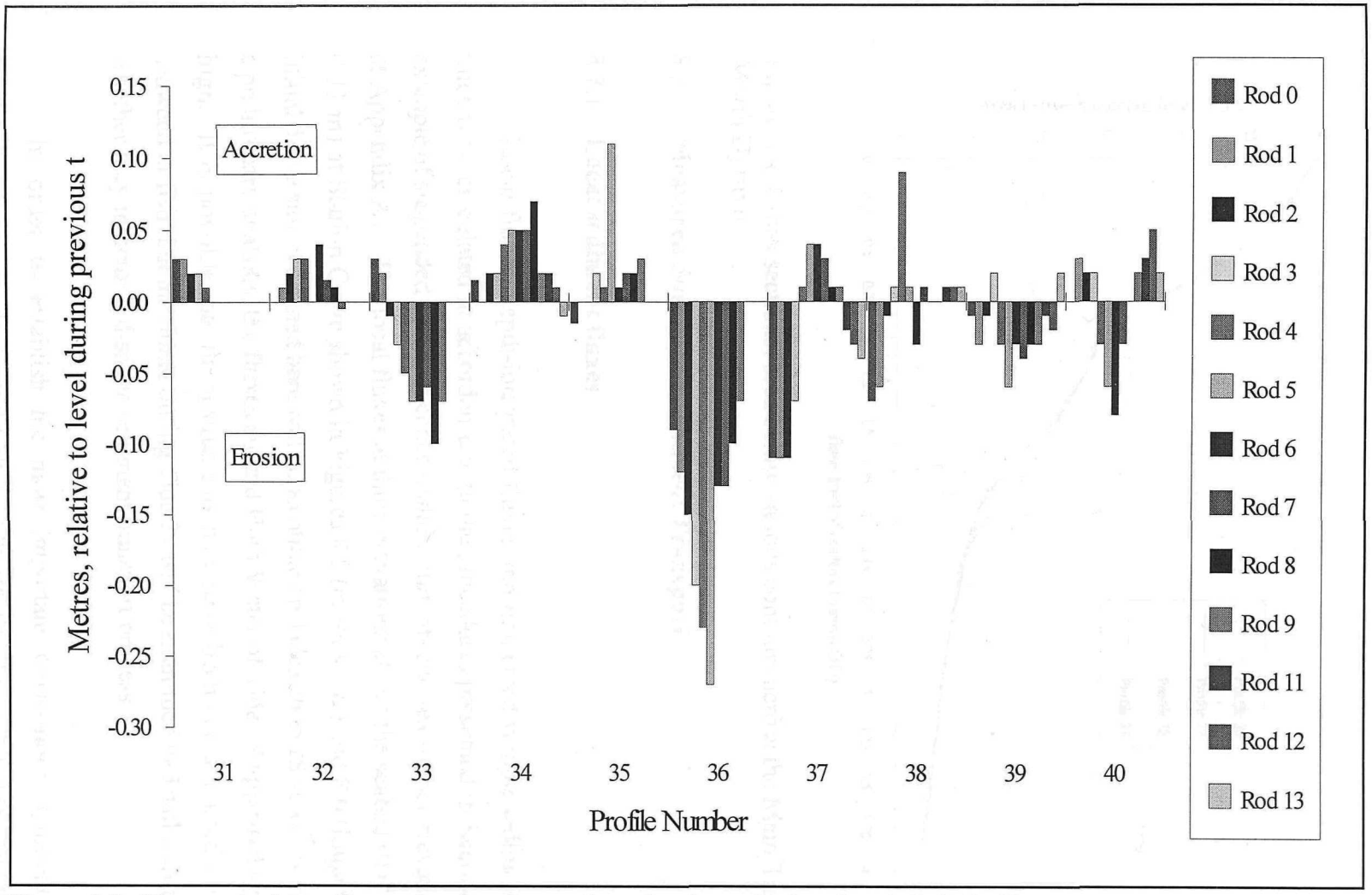

Figure 8.3 Changes in the sediment level at the graduated rods on the beach at Morfa Dyffryn

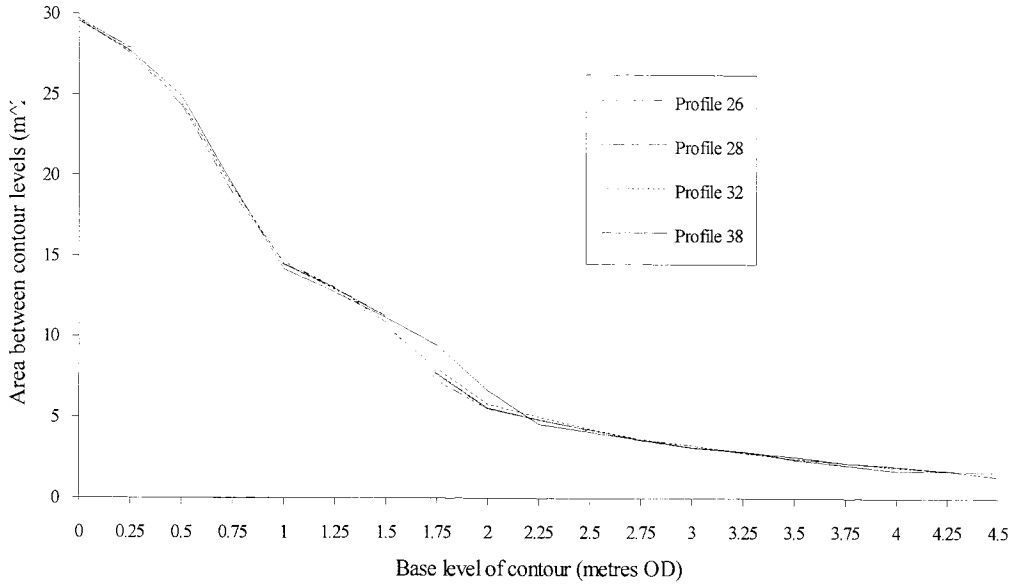

Figure 8.4 Cross-sectional area below various contours across the Main Transect at Morfa Dyffryn

8.2 Measured Suspended Sediment Transport

8.2.1 Local sediment fluxes

Local fluxes, depth-integrated fluxes and immersed weight sediment transport rates were calculated in accordance with the procedures presented in Section 4.3.3 (an example of suspended sediment concentration, currents and sea surface elevation is given at Appendix A). The local fluxes at three elevations above the seabed (0.09, 0.19 and 0.31 m) at Station C, are shown in Figures 8.5 (cross-shore) and 8.6 (longshore). The initial discussion presented here will concentrate on Tides 26 to 28 since, on the basis of a preliminary analysis, the fluxes around High Water of Tide 29 appeared anomalously high. It is possible that the instruments may have been contaminated (by, perhaps, seaweed or fish) but the fluxes during Tide 29 will be examined in detail later to establish whether they indicate a discrete sediment transport process.

In order to establish the most important cross-shore sediment transport mechanism, each mode (gravity flux, infragravity flux *etc.*) was calculated as a percentage of the total flux (*i.e.* the sum of the absolute values for gravity, infragravity and mean fluxes) for each data file and at each location above the bed. The results

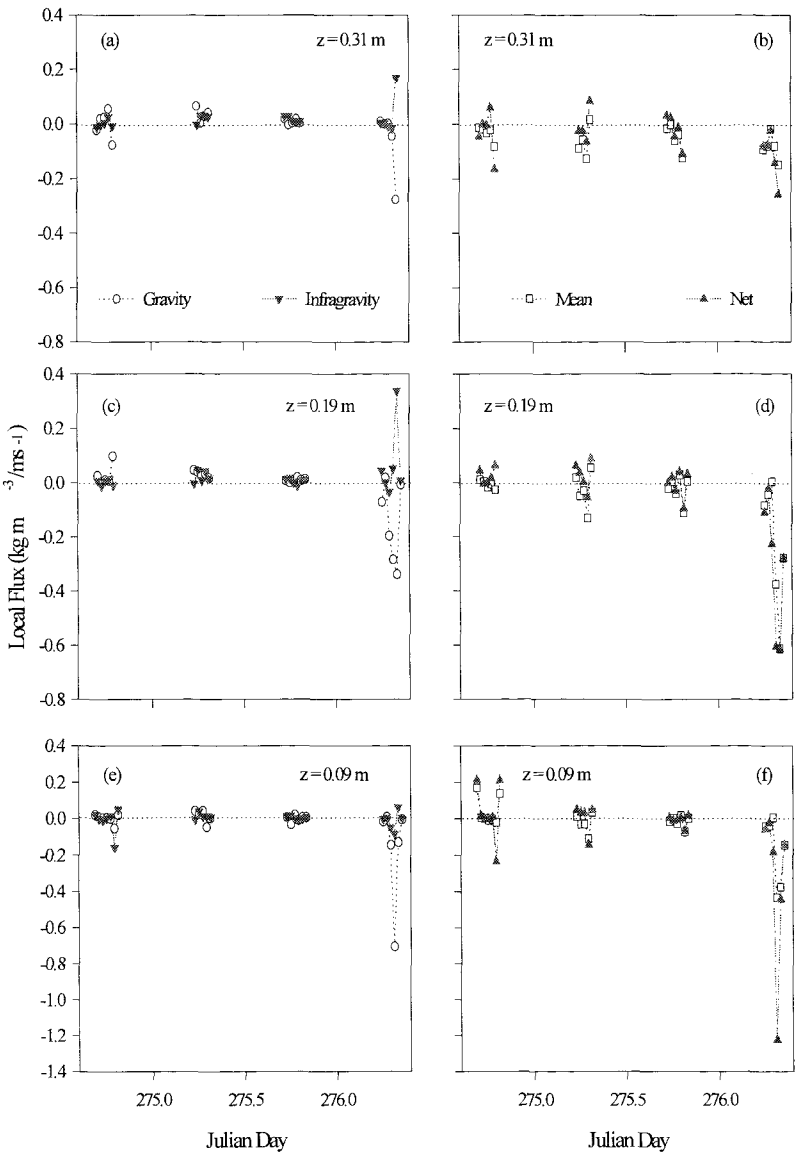

Figure 8.5 Local cross-shore suspended sediment fluxes (gravity, infragravity, mean and net) for Tides 26 to 29 at: (a) and (b) 0.31m above the seabed; (c) and (d) 0.19 m; (e) and (f) 0.09 m.

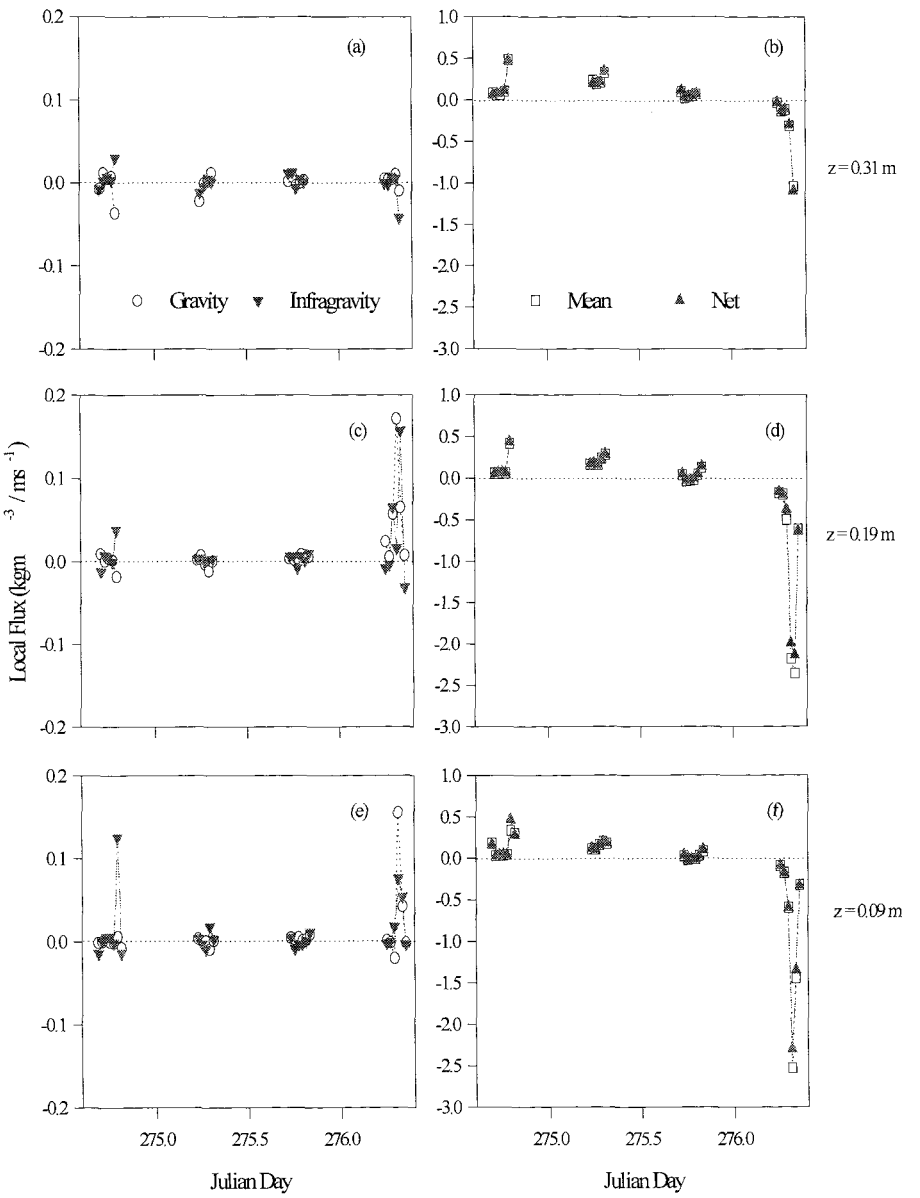

Figure 8.6 Longshore local suspended sediment fluxes for Tides 26 to 28 at: (a) and (b) 0.31 m above the seabed; (c) and (d) 0.19 and (e) and (f) 0.09 m.

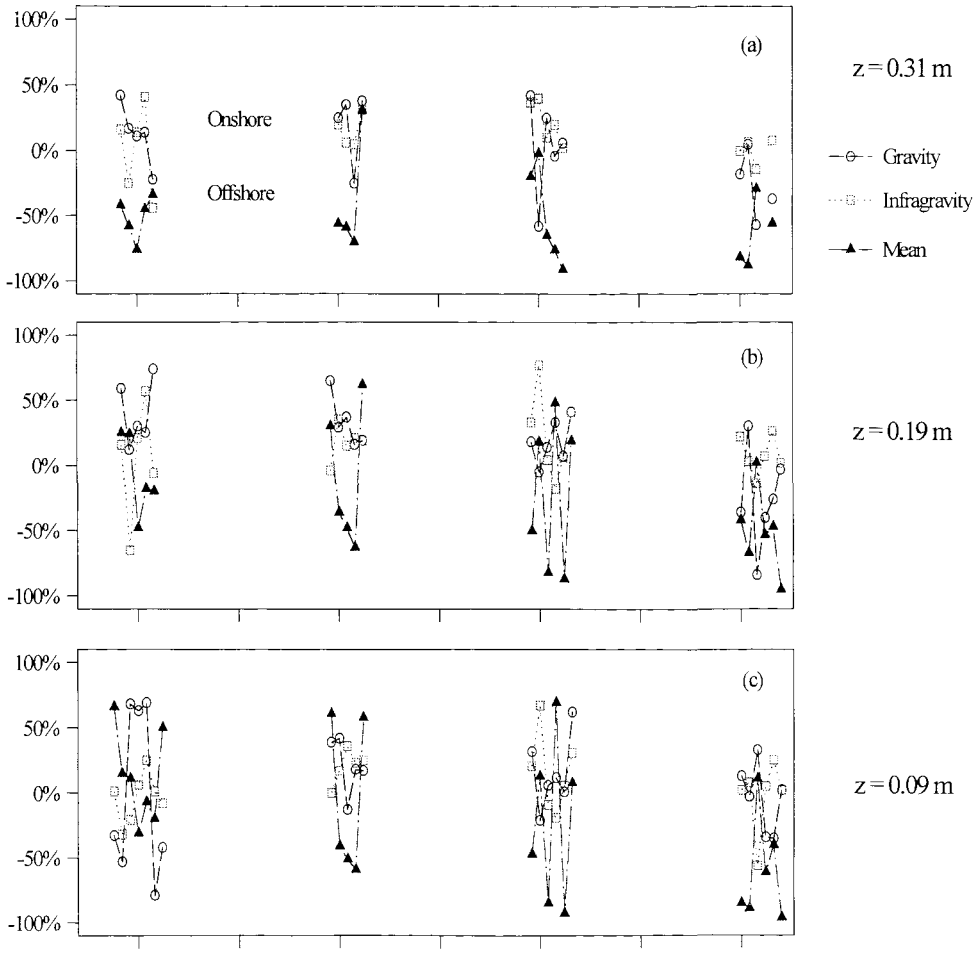

Figure 8.7 Local fluxes as a percentage of total cross-shore flux during Tides 26 to 29 at: (a) 0.31 above the seabed; (b) 0.19 and (c) 0.09 m.

obtained are shown in Figure 8.7. At 0.31 m above the bed, the mean flux was generally the dominant transport mechanism; it is directed mainly offshore. In contrast, the direction and importance of the mean flux nearer the seabed showed considerable variation. In shallow water, the mean flux dominated and was generally onshore for Tides 26 and 27; it was offshore for Tide 29. Around High Water, for all the tides, the

mean flux tended to be onshore. In contrast, the gravity flux was offshore during the early and late phases of the tide and onshore around High Water. However, even a large offshore gravity flux in shallow water (*e.g.* Tide 26) was offset by the influence of the onshore mean flux; similarly, the net nearbed flux was directed onshore.

The direction of the mean flux is determined by the mean current, by definition. Therefore, this flux represented both tidal variations in the mean current and the vertical structure of the cross-shore flow (see Figure 5.6, for the velocity structure of the cross- and longshore mean flows).

Alongshore, the net local fluxes were clearly the product of mean SSC and mean longshore current, although there was some small infragravity contribution during Tide 26.

8.2.2 Sediment transport rates

The measured depth-integrated, immersed weight sediment transport rates for Tides 26 to 28, calculated according to the methods presented in Sections 4.3.3 and 4.3.4, are shown in Figure 8.8. Net cross-shore transport rates were onshore during the early flood and late ebb phases of the tide *(i.e.* in shallow water) but were directed offshore once water depth exceeded about 0.5 m. The results obtained during Tide 29 differed. There was tidal aysmmetry in suspended sediment transport, with higher transport during the ebb tide when the offshore gravity flux was complemented by a large offshore mean flux; this led to offshore suspended sediment transport rates of 5 $Nm^{-2} s^{-1}$ (Figure 8.9). The record obtained at HW +0.5 deserves particular attention. Here, the main input to the large flux and subsequent sediment transport rate is the high concentration of sediment at 0.19 and 0.31 m above the seabed. This observation represents a reversal in the usual decrease in SSC, with height from the seabed; however, it is not unknown (*e.g.* Voulgaris, 1992) and may be attributed to horizontal advection.

The wave conditions during Tide 29 were only marginally different from the preceding three tides, which had led to only a gradual landward progression of the main ridge. Spectral peak periods for all four tides were ~ 8 to 10 s, with a T_z of about 4 seconds. The tidal maximum H_s was between 0.3 and 0.5 m (Figure 5.5 *c*). Clearly, therefore, the nature of the sediment transport may be too subtle to be characterised by

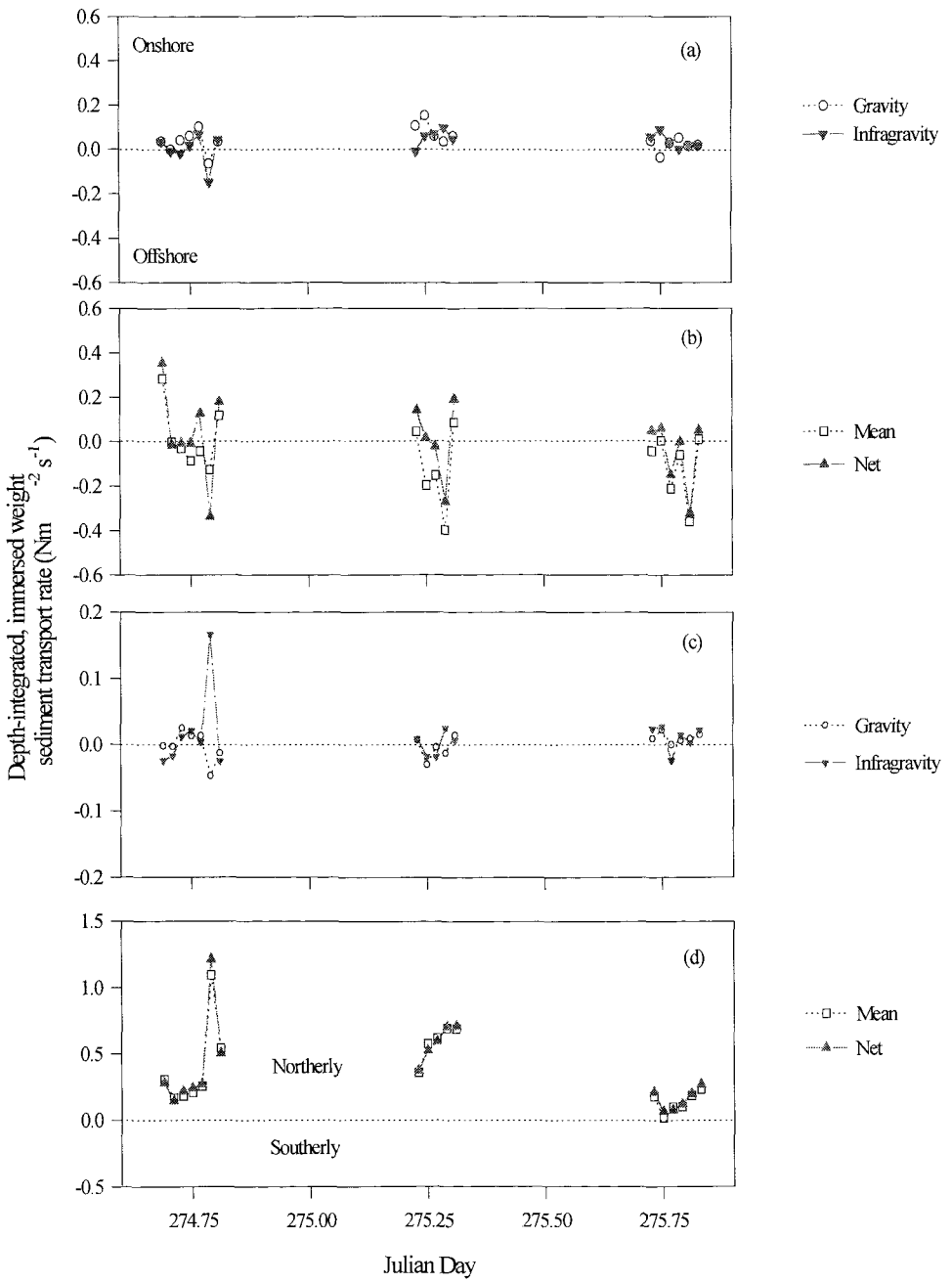

Figure 8.8 Measured cross-shore (a and b) and longshore (c and d) sediment transport rates, for Tides 26 to 28.

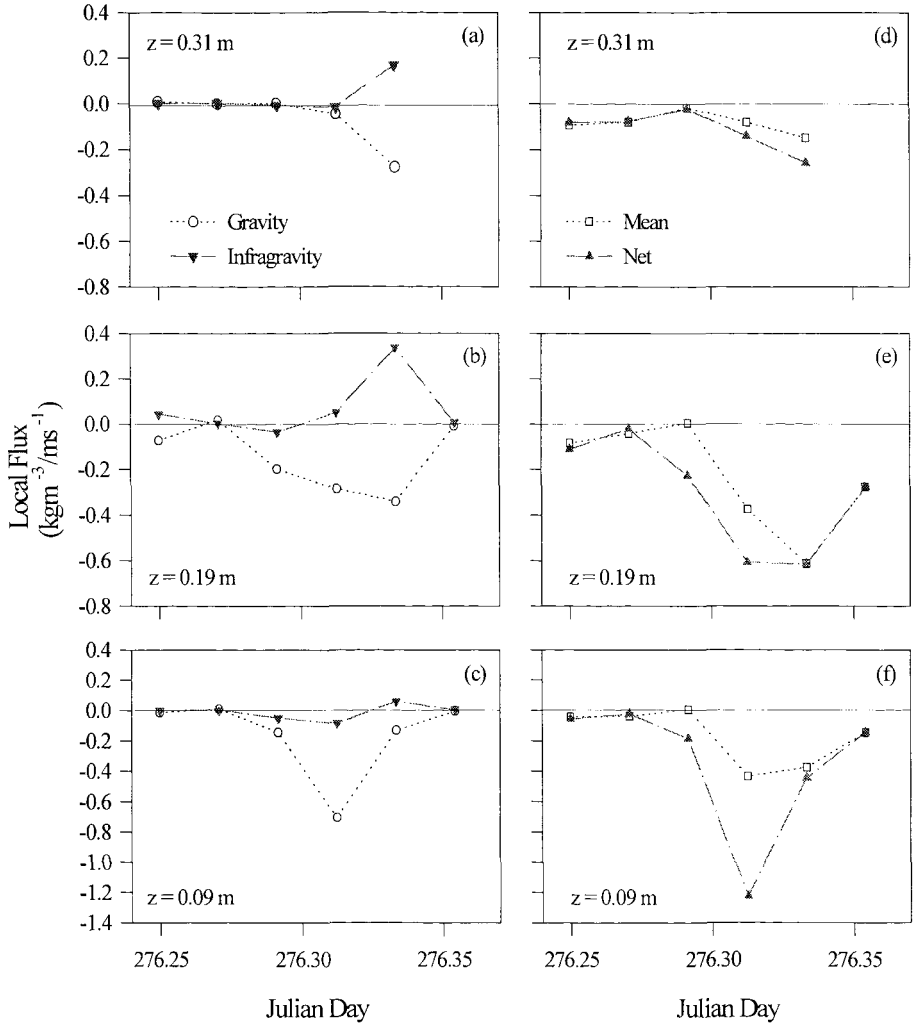

Figure 8.9 Cross-shore local suspended sediment fluxes, during Tide 29, at: (a) and (d) 0.31m from the seabed; (b) and (e) 0.19m and (c) and (f) 0.09m.

wave energy statistics alone. Indeed, it may not be coincidence that Tide 29 was the first tidal cycle to inundate the sand/shingle bank. Accordingly, there is a need to establish why there was so much sand in transit during Tide 29; similarly, if the sand/shingle bank influenced this transport pattern (see below).

8.2.3 Tide 29 - the influence of sand/shingle bank on sediment transport

An assessment of the influence of the sand/shingle bank is based only upon a restricted data set as suspended sediment data were available only until Tide 29; this was the first rising tide to actually reach the bank. However, wave and current data were available until Tide 33, when the wave conditions were generally calm throughout. The spring tides did not regularly cover the shingle section of the beach until Tide 34 but, by then, the current meters had to be removed from the beach due to impending gales.

In the subsequent discussion, the results from both methods of calculating sediment fluxes are used: (i) local fluxes, filtered into long, short and mean components, box-integrated to give depth-averaged sediment transport (Sections 4.3.3 and 4.3.4) and (ii) co-spectral analysis between SSC and the decomposed incoming and outgoing velocity time-series (Section 4.3.6), which indicates the net oscillatory transport direction and magnitude associated with each frequency binwidth.

Initially, increased wave reflection around high water was identified as a possible reason to account for the high sediment fluxes, since this was when the swash and inner surf inundated the sand/shingle bank and video recordings showed reflection from the step. However, upon closer inspection, there is some inconsistency with this argument; the main problem being that the FDRF values, for all the significant frequencies, remained at around 20% throughout the whole of the tide (Figure 7.7 *b*, where Tide 29 is represented by open squares). Nonetheless, it is possible that the selection criteria for significant FDRF (Section 4.3.5) may have screened out important details from this particular data set.

Figure 8.10 illustrates the spectral characteristics of the SSC from the lowest sensor and incoming and outgoing velocity spectra, together with the co-spectra and phase between them. In the mid surf zone at **HW -0.5** (0630), the phase relationship between incoming velocity time series and SSC shows that oscillatory transport was directed onshore at the velocity spectral peak frequency (this is marked with an arrow on Figure 8.10 *d*), although it is offshore at the next lower frequency bin. In both cases, there was low coherence between the two time-series and, therefore, net oscillatory transport was low. Mean cross-shore currents were also low (0.04 ms^{-1}) at this stage in the tidal cycle, but contributed to the total transport which was weakly offshore.

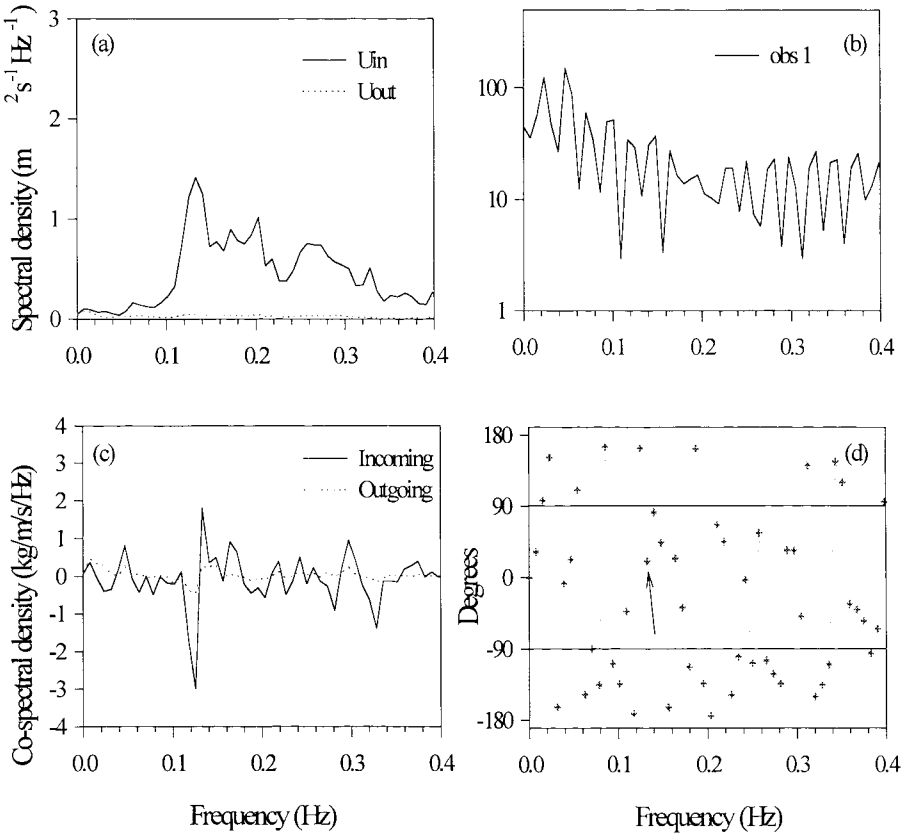

Figure 8.10 Morfa Dyffryn, Tide 29 at HW -0.5 (0630): (a) spectral density of incoming and outgoing velocities; (b) SSC at 0.09 m from the seabed; (c) co-spectrum; and (d) phase angle between the velocity and the SSC.

Around **HW** (0700), the oscillatory transport was higher than during the flood, but the difference was not particularly great. Oscillatory transport was offshore at the predominant gravity wave frequency and in the infragravity range, but once again the coherence between SSC and incoming velocities was low at these frequencies; hence, net oscillatory transport was only moderate (Figures 8.11 and 8.9). Similar gravity fluxes, at frequencies higher than the incident spectral peak, have been reported elsewhere (*e.g.* Voulgaris & Collins, 1996); these were attributed to non-linear interactions of breaking waves. Mean transport was almost negligible and, hence, at the seawards end of the surf

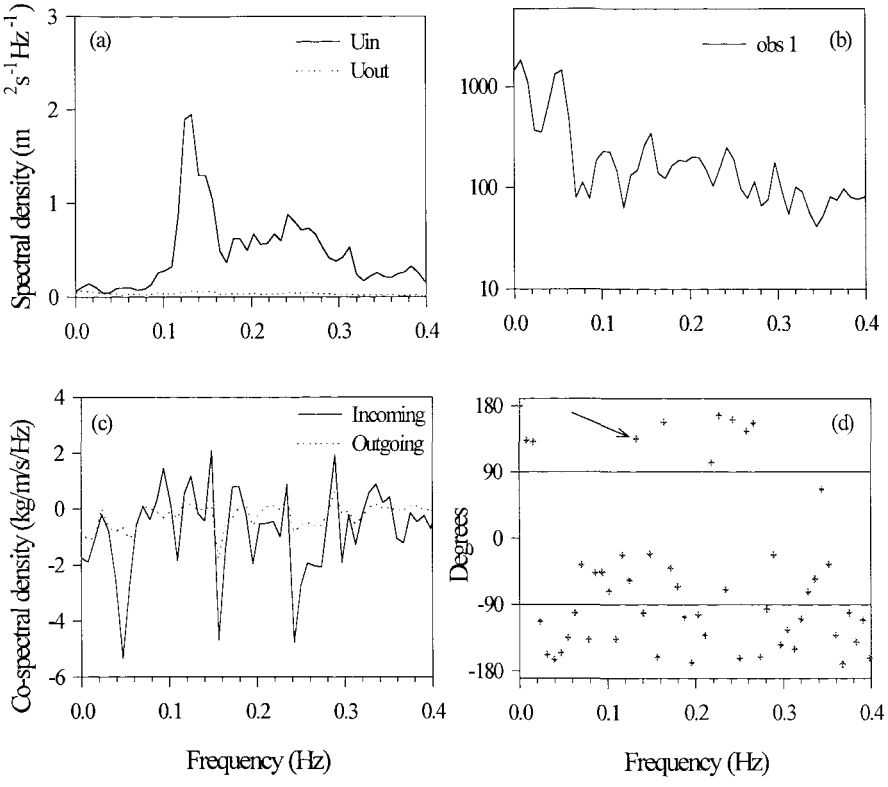

Figure 8.11 As Figure 8.10 but for Tide 29, High Water (0700)

zone, gravity fluxes dominated the total transport around high water.

Once the tide had turned, the sediment transport patterns became dramatically different. The filtered analyses of sediment flux showed that, at **HW +0.5** (0730) there was an extremely high gravity flux directed offshore, together with a high offshore mean flux. There was a small infragravity flux directed offshore (Figure 8.9). Consequently, *the total sediment transport was extremely high and directed offshore; it was dominated by the high gravity and mean fluxes.* The same conclusions are supported by the co-spectral analysis, between u_{in} and u_{out} and suspended sediment concentration (Figure 8.12 *c*). The infragravity peak at 0.016 Hz, for both the incoming and outgoing components, is directed offshore; the FDRF was 0.79. The η_{in} and η_{out} coherence was 0.64, although there was no clear peak in the sea surface elevation at this frequency, and hence it was

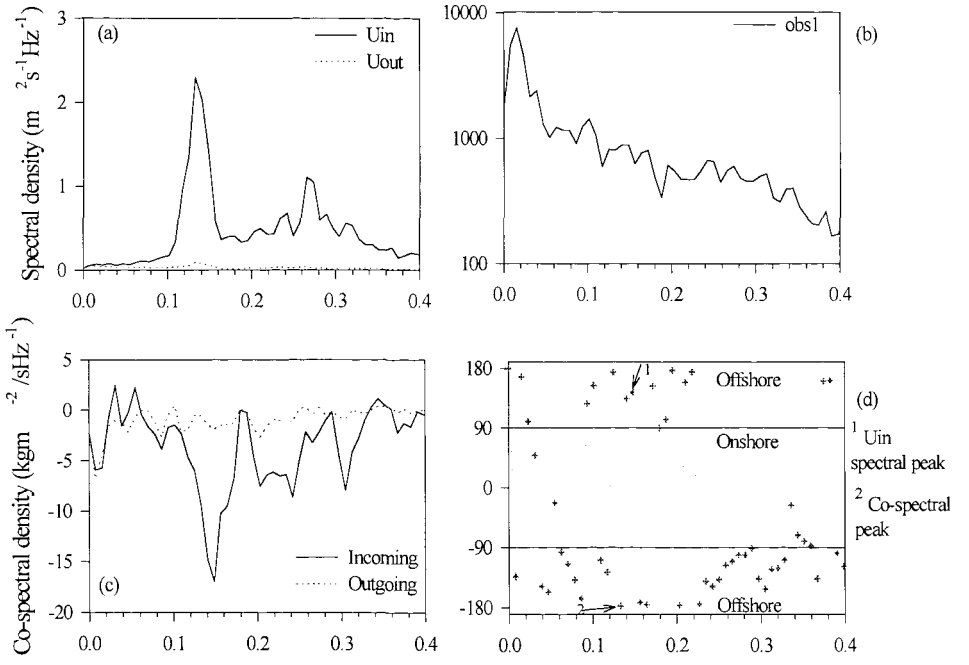

Figure 8.12 As Figure 8.11, but for Tide 29 (HW +0.5).

not included in the overall analysis of the FDRF values. In addition, the pressure-velocity (H-U) coherence was only 0.33.

Meanwhile, the fluxes of the incoming co-spectra at gravity wave frequencies were directed strongly offshore at a range of frequencies (Figure 8.12 *c* and *d*); there is a prominent offshore peak at 0.148 Hz, producing an offshore flux of over 1.2 kgm^{-3}/ms^{-1}. Both H-U and η_{in} and η_{out} coherences were high (over 0.9), although FDRF was only 0.21 and remained constant through the gravity band above 0.1 Hz. There was coherent swell wave reflection at 0.078 Hz whilst both the incoming and outgoing co-spectra were offshore at this frequency (FDRF = 0.53, H-U = 0.62 and η_{in} - η_{out} = 0.48). However, this FDRF value had been excluded from reflection analysis, since there was no distinct spectral peak at that frequency. On this basis, perhaps the criteria for the selection of valid FDRF values are overly specific *i.e.* there is not a requirement for a distinct spectral

peak, just reasonable energy levels *c. f.* Davidson *et al.* (1994) where the criterion was based upon a requirement of above 20% of spectral peak energy.

At HW +1 (0800), the two methods of calculating sediment fluxes revealed different information. Co-spectral analysis showed that, although the net flux at the main spectral peak of the incoming velocities was directed onshore, the incoming flux (averaged across the frequencies) was small and offshore; at the same time, the outgoing flux was small and directed weakly onshore (Figure 8.13). In the lower frequency range, however, both the incoming and outgoing co-spectra were directed onshore. The filtered method showed, meanwhile, an offshore gravity flux and an equivalent onshore infragravity flux which, together, produced only a small net offshore flux. However, the mean flux was large and offshore; hence, the net flux was fairly high and directed offshore. It should be noted that the tide did not cover the sand/shingle bank at this time. Therefore, in the middle surf zone during the ebb tide, *the total transport was dominated by the mean flux, since the gravity and infragravity fluxes were in opposing directions and effectively cancelled each other out.*

A similar pattern of transport occurred at 0.19 m from the seabed, except that the fluxes were generally lower; likewise at HW +1, the infragravity and gravity fluxes counterbalanced each other completely, leaving the mean flux as the total contributor to the total transport. The mean SSC at HW +1 was higher at 0.19 m above the seabed than at 0.09 and 0.31 m. This pattern is unusual, but not unknown and has been attributed to horizontal advection (Voulgaris, 1992). In the inner surf zone of the ebb tide at **HW +1.5** (0830), the total transport was dominated by the mean flux; this was, once again, offshore near the bed and more strongly offshore at 0.19 m from the seabed. This transport pattern is because oscillatory transport is weaker higher in the water column and, therefore, the mean component tends to dominate (Davidson *et al.*, 1993).

Overall, in the inner/middle surf zone, the mean currents were the most significant contributor to the total sediment transport, since there was low coherence between the SSC and the oscillatory velocities. The mean cross-shore currents were higher during the ebb, than the flood; consequently, so were the mean fluxes. Around High Water, in the outer surf zone, the mean current was weak, so that the gravity component contributed most to the total transport. In the outer surf zone of the ebbing tide, the total sediment transport was extremely high (a factor of 4 higher than at any other stage during the tidal

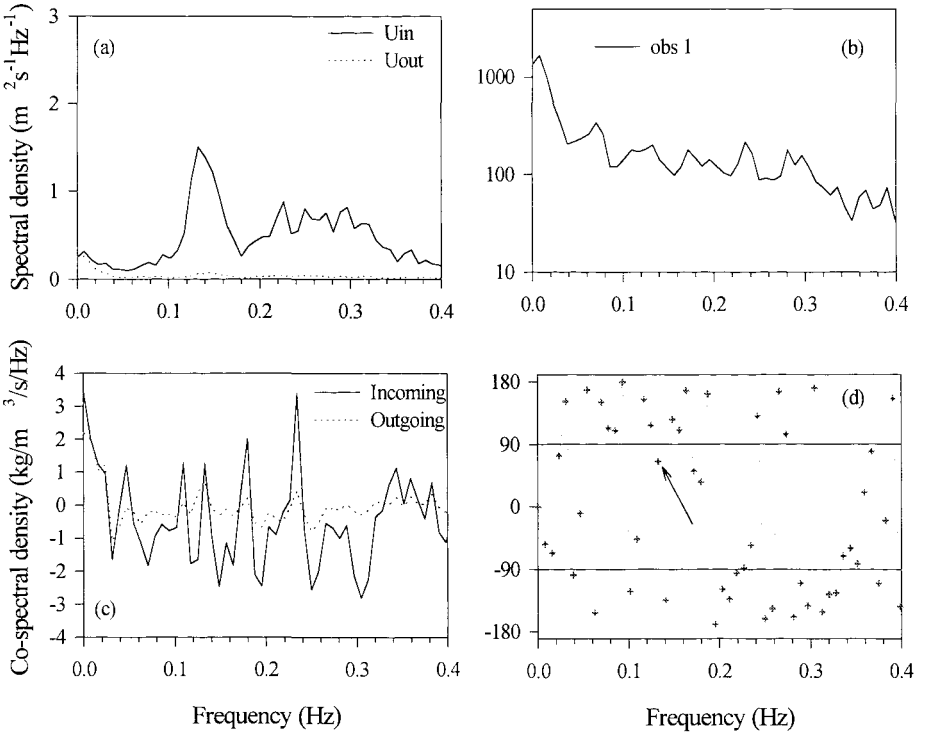

Figure 8.13 As Figure 8.10, but for Tide 29 (HW +1).

cycle), directed mainly offshore; it was dominated by the gravity wave components and was augmented by a high mean flux. The incoming velocity and SSC tended to be in quadrature during the flood tide and, progressively, in anti-phase during the ebb. Thus, where the SSC and oscillatory velocities were coherent, the sediment loads were high. However, where the gravity and infragravity fluxes opposed each other, the mean currents dominated the total transport. All the sediment fluxes were higher during the ebb tide, than during the flood.

Overall, the mean currents dominated the total suspended sediment transport during Tide 29 (with the exceptions of around High Water and the extremely high gravity component at HW +0.5). The total suspended sediment transport was greater during the ebb phase of the tide than at the equivalent tidal stage during the flood.

The large fluxes at HW +0.5 and HW +1 require further investigation. Enhanced outgoing fluxes due to enhanced wave reflection from the sand/shingle bank, is not considered to be a contributory mechanism (Section 8.2.3). The extremely high flux at HW +0.5 is the sum of two high fluxes (mean flux and gravity flux), operating in the same direction. A large mean flux can be caused either by a moderately high mean SSC combined with a moderately high mean current; alternatively, it may be the product of a very high SSC and a low mean current, or *vice versa*. The mean flux was of similar magnitude at HW +0.5 and HW +1; at HW +0.5, however, the controlling factor was the high SSC; at HW +1, it was the increasing undertow current which contributed more to the flux. Thus, the high SSC at HW +0.5 needs to be examined.

The offshore gravity flux was at the peak incident wave frequency (~0.14 Hz), despite the largest spectral peak in the SSC being at infragravity frequencies. The significant orbital velocities (which have been deemed responsible for most of the sediment resuspension) were high; these remained constant throughout the tidal cycle (Figure 8.14 *e*). This was also the case at Nieuwpoort, where the mean currents also dominated the suspended sediment transport and, similarly, the tidally-varying significant orbital velocities were strongly correlated with the mean cross-shore suspended sediment flux, throughout the whole of the tide (Voulgaris & Collins, 1996). These observations led to the conclusion that waves mobilised the sediment, which was transported then by the mean currents. Indeed, the mean sediment fluxes dominated the cross-shore suspended sediment transport throughout the tidal cycle at Nieuwpoort; they were an order of magnitude greater than the gravity or infragravity fluxes. It would seem, therefore, that the cross-shore oscillatory velocities *per se* were not the main cause of the quantity of sediment in suspension after High Water.

The pattern of suspended sediment transport over tidal cycle 29 at Morfa Dyffryn bears a strong resemblance to that reported by Davidson *et al.* (1993), from an intermediate, macrotidal beach (Spurn Head). However, there was less infragravity energy at Morfa Dyffryn. Davidson *et al.* (*op. cit.*) found that the mean component of the transport dominated during the flood tide, but also reported very strong offshore transport associated with incident waves during an ebbing tide. This observation was just to seaward of the surf zone when the peak oscillatory SSC was up to twenty times higher than that which occurred during the flood phase of the tide. Therefore, the offshore gravity transport was extremely high and was the dominant component of the total

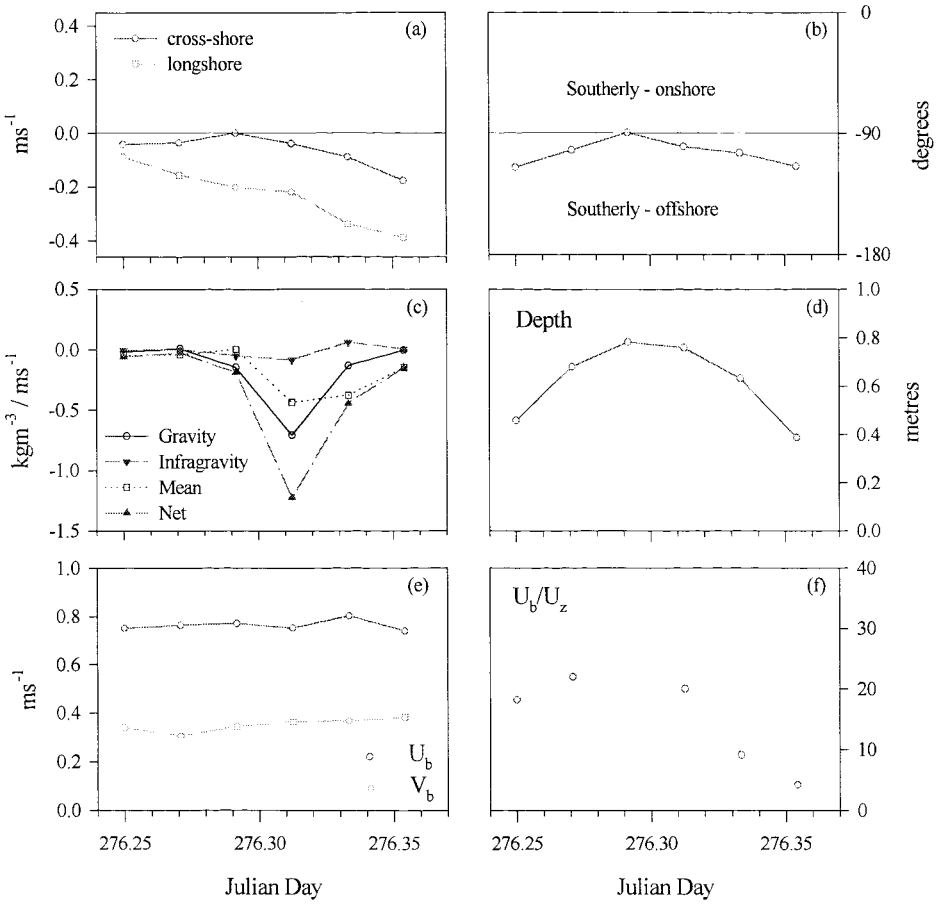

Figure 8.14 Tide 29 at Morfa Dyffryn: (a) mean current velocity; (b) resolved mean current direction; (c) suspended sediment flux; (d) mean water depth; (e) orbital velocities; and (f) wave strength.

transport. The very high SSC during the ebb tide was attributed by Davidson *et al.* (1993), to the destruction of a ripple field, which had formed around high water; their sampling location was outside the surf zone and the mean longshore and cross-shore currents and oscillatory velocities were at their minimum.

The main problem associated with the concept of bedform destruction to account for high SSC during the ebb at Morfa Dyffryn, is that there was a reduction in the observed orbital velocities and no period of relatively slack water for ripples to form.

Although the mean cross-shore current was at its weakest (0.002 ms^{-1}) at HW, the longshore current was fairly strong, producing a resolved current of |0.2| ms^{-1} at 90° to the shoreline (Figure 8.14 *b*). Maximum water depth was approximately 0.8 m and Station C (the sampling location) remained within the surf zone throughout the tidal cycle. Nonetheless, using these values of mean currents, the Wiberg & Harris (1994) model predicts the development of ripples of 0.04m in height; hence, the cause of the high SSC might lie in the nature of tidal enhancement of the mean currents during the ebb and wind/current interaction (referred to in Sections 5.3.4 and 5.3.5). It is possible that ripples developed during High Water, under the influence of the mean longshore current, when the cross-shore current was negligible. Once the tide began to ebb, the shore-parallel surface winds enhanced the increasing longshore current, whilst the tidally-enhanced undertow also increased throughout the ebb. Accordingly, the resolved current increased slightly in strength to 0.22 ms^{-1}, backing some 10 degrees offshore. Subsequent destruction of the ripple field, resulting from an increase in strength and change of direction, can lead to advection of the sediment into the water column. This pattern was observed during Tide 29 HW +0.5, when the SSC was higher at 0.19 and 0.31 than at 0.09 m above the seabed (Figure 8.5). The simplified model for offshore transport, over a rippled bed is described by Davidson *et al.* (1993).

A further possible cause of high SSC after High Water, speculated by Davidson *et al. (op. cit.)* is beach de-watering during the ebb phase of the tide. The position of the beach groundwater table has been considered previously to produce a propensity for deposition during the flood tide and erosion during the ebb (see Chapter 9), although the mechanisms by which beach groundwater interacts with waves remain largely undetermined. Indeed, rapid reversals in pore pressure gradients due to changes in hydrostatic overburden pressure of swash waves have been suggested recently as such a mechanism for fluidisation and enhanced sediment suspension in the swash zone (Baird *et al.*, 1996). However, beach de-watering seems unlikely to be the cause of the large SSC just after HW during Tide 29, due to several reasons: (i) the tide inundated the shingle bank for only an hour around HW, thus the resultant overheight of the water table is unlikely to be sufficiently large to create high hydraulic gradients at Station C; (ii) the gravity component of the flux, with which any wave-driven fluidisation should be correlated, was particularly high only at HW +0.5, although the effect of fluidisation would persist over much of the ebb tide; (iii) the higher suspended flux during HW +1 was more a result of increasing mean currents, than high SSC.

In summary:

- The mean fluxes dominated the measured suspended sediment transport at Morfa Dyffryn, in common with observations associated with other macro-tidal beaches *e.g.* Nieuwpoort and Spurn Head.

- The mean suspended sediment fluxes were generally at their highest at the beginning and end of the tidal cycle *i.e.* during the shallow water parts of the tide.

- The asymmetry in suspended sediment transport during Tide 29 was caused by the nature of the resultant mean currents and wind/current interaction, rather than due to enhanced offshore transport due to wave reflection from the sand/shingle bank or beach de-watering.

8.3 Predicted Sediment Transport Rates

The relative contributions of the long, short and mean components of the flow, in mobilising and transporting sediment, were assessed in Chapter 6. Sediment transport rates were predicted according to the model of Bailard (1981), which was re-derived for random waves by Guza & Thornton (1985), and is given by eqns. (2.5) and (2.6). A constant drag coefficient, C_f, of 0.005 was used, since the recording position was within the surf zone throughout the (four) Tides used for the analysis. In reality, C_f is likely to vary throughout the tidal cycle. Predicted sediment transport rates for Tides 26 to 29 are shown in Figure 8.15.

Subsequent discussion of the predicted transport rates is based upon the analysis undertaken for Nieuwpoort-aan-Zee (Voulgaris, 1996) with which the results from Morfa Dyffryn are compared. Figure 8.16, where the individual terms from eqns (2.5) and (2.6) have been multiplied by the appropriate factors *i.e.* $\rho\, C_f\, U_m^3$ or $U_m\, \epsilon_s / W$, illustrates which components contribute most significantly to predicted cross-shore and longshore sediment transport. In general, the same terms were found to dominate at Morfa Dyffryn and Nieuwpoort; these are presented in Table 8.1, together with their percentage contribution to the gross cross-shore or longshore predicted sediment transport rates.

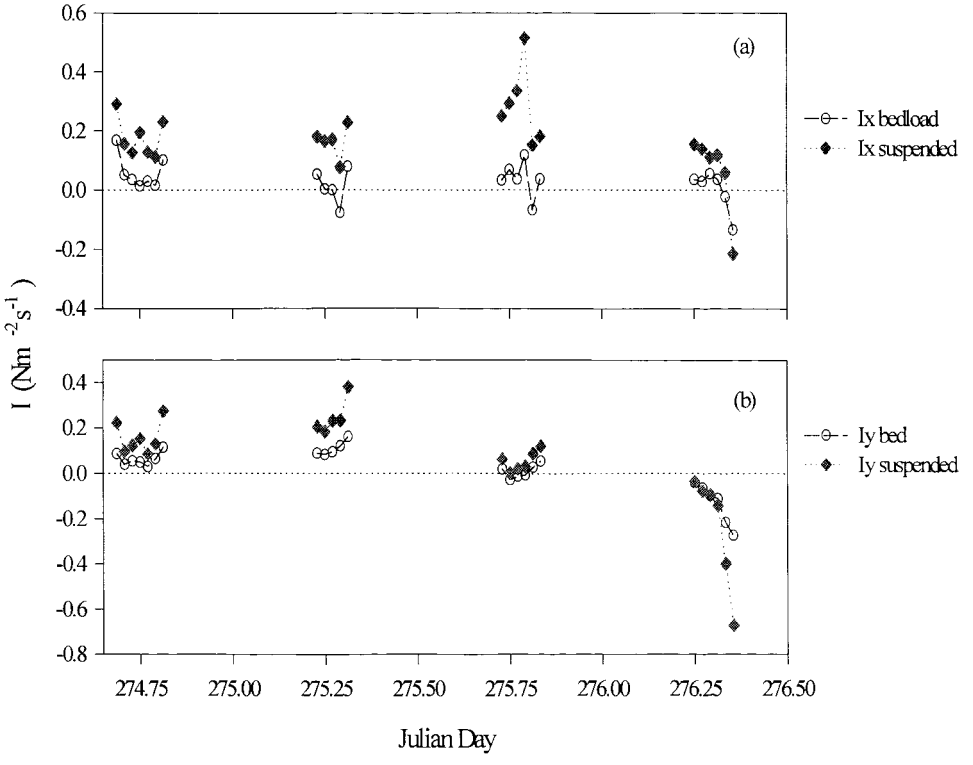

Figure 8.15 Predicted total immersed weight sediment transport rates (I) for Tides 26 to 29 for: (a) cross-shore and (b) longshore.

Thus, the suspended sediment transport is predicted to account for (on average) 70% of the total sediment transport, both cross- and longshore at Morfa Dyffryn; it accounts for in excess of 80% at Nieuwpoort.

The normalized current angles, α_1 and α_5 are combined with the non-linear (oscillatory) moments Ψ_1 and Ψ_2, so that α_1 and α_5 should be around 0 or 180°. Burst-averaged values of these parameters are shown in Figure 8.17*c*. At Morfa Dyffryn, α_1 was generally ± 10°, but reached 16° during the latter part of Tide 29 (Figure 8.17 *b*). Meanwhile, α_5 was seldom less than 20° during Tides 26 and 27, but was generally within ± 5° during Tide 29. High values of α_5 were observed also at Nieuwpoort, implying some contribution from the longshore oscillatory currents. However, since the angles are linked to sediment transport through their cosines, this translates into a

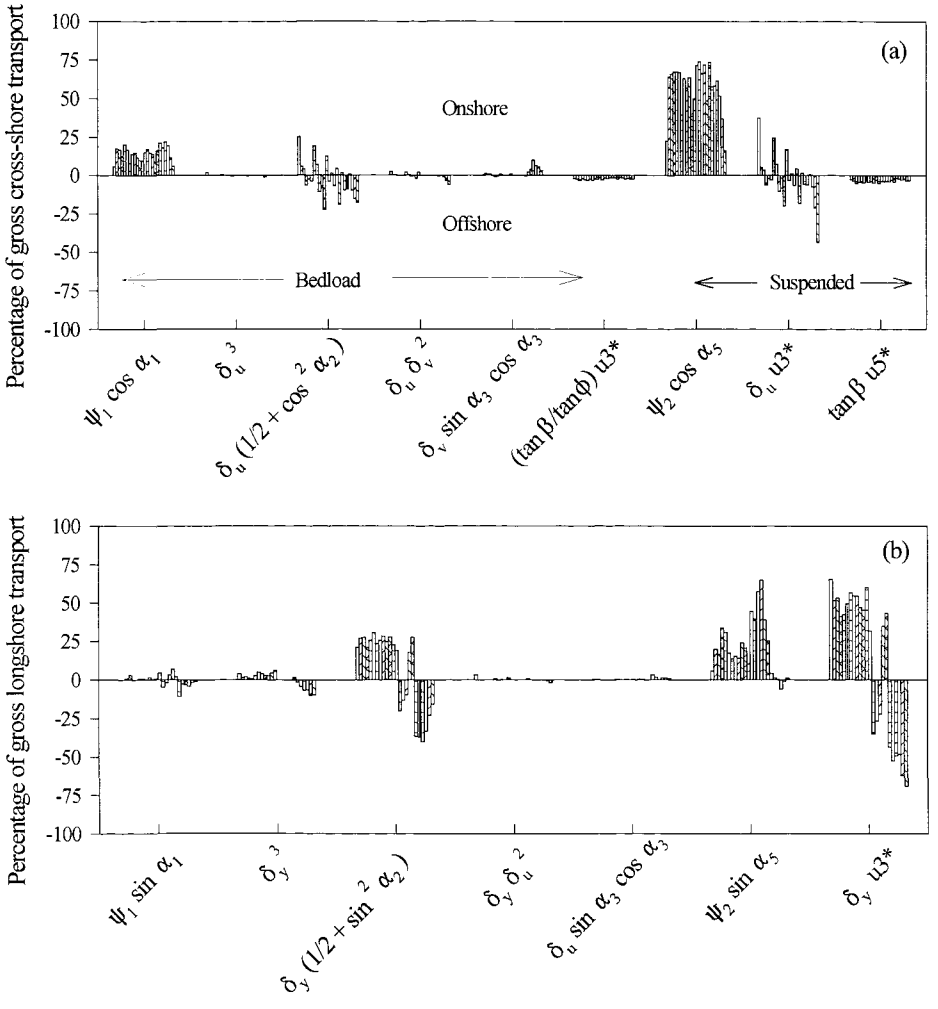

Figure 8.16 Tides 26 to 29, Morfa Dyffryn: contribution of the terms derived from eqns. (2.5) and (2.6) as percentage of gross sediment transport (a) cross-shore; and (b) longshore

potential error of 4% and 6% in predicted transport rates; it contains extreme values of α_1 and α_5 respectively. However, in the longshore direction, the sine of α_2 and α_5 is utilised and, since the sines of 20^0 and 24^0 are 0.34 and 0.41 respectively, the contribution of the oscillatory term Ψ_2 sine α_5 is of some importance (particularly for Tides 26 and 27 when α_5 was at its highest). Such influence may be attributed to waves approaching the shoreline at some angle of incidence since, if waves were close to shore-normal, sine

Transport direction	Transport mode	Term	Absolute percentage of gross transport, cross- or longshore	
			Morfa Dyffryn	Nieuwpoort
Cross-shore	Bedload	$\Psi_1 \cos \alpha_1$	14	4
		$\delta_u (½ + \cos^2 \alpha_2)$	10	15
		Others	~ 5	< 4
	Suspended load	$\Psi_2 \cos \alpha_5$	56	55
		δ_u u3*	11	37
		tan β u5*	4	n/a
Longshore	Bedload	$\delta_v (½ + \sin^2 \alpha_2)$	25	16
		δ_v^3	n/a	7
		Others	~ 6	<4
	Suspended load	$\Psi_2 \sin \alpha_5$	21	17
		δ_v u3*	48	70

Table 8.1 Contribution of the dominant terms in eqns (2.5) and (2.6), to the predicted gross sediment transport rates.

α_5 should be near to zero.

The dominant terms involving the normalized cross-shore and longshore mean currents, δ_u and δ_v, are linked with α_2 or u3*. However, it should be noted that u5* is not of importance for the predicted sediment transport rates, despite being both higher than u3* and having greater variability over the tidal cycle; this is because u5* is combined with the tangent of the beach gradient, to predict the downslope suspended sediment transport. The term u3* represents the contribution of the total currents, which are averaged over a wave period; it was quasi-constant, with a mean value from all four Tides of 0.67, and a standard deviation of 0.26. At Nieuwpoort, u3* was ~ 0.8, with a standard deviation of 0.22. These values are considerably higher than the theoretical values for u3* presented by Guza & Thornton (1985), for a sinusoidal wave (0.42) or for a Gaussian wave distribution (0.56). The high value of u3* at Nieuwpoort was attributed to an asymmetry in the instantaneous flow during a wave cycle, caused by the strong mean flows (Voulgaris & Collins, 1996). When high values of u3* were combined with

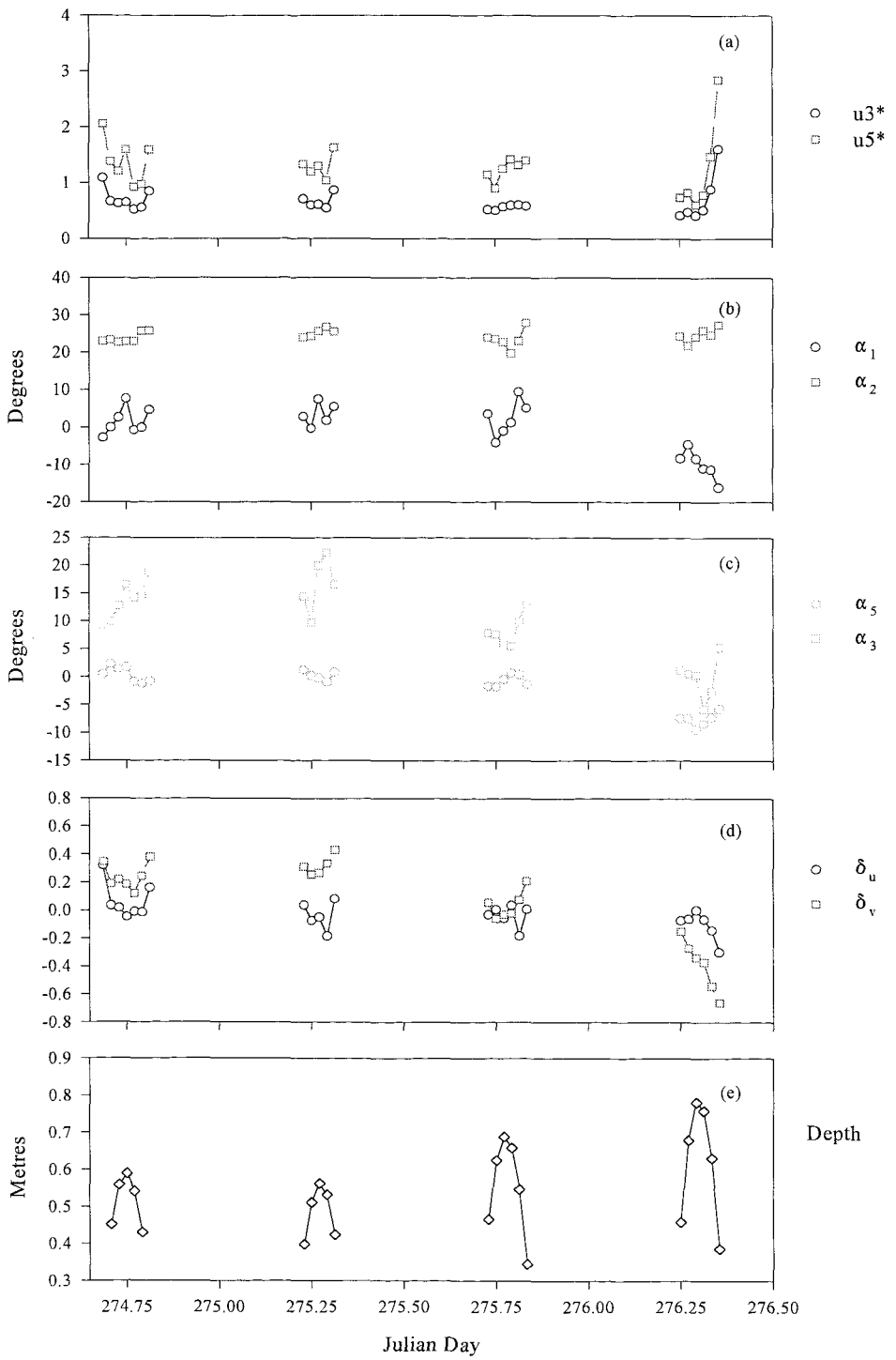

Figure 8.17 Tides 26 to 29, Morfa Dyffryn: burst averaged parameters of (a) u3* and u5*; (b) α_1 and α_2; (c) α_3 and α_5; (d) δ_u and δ_v; (e) depth

the maximum normalized mean currents, high suspended sediment transport could result *e.g.* during the later phases of the ebb of Tide 29, when u3*, δ_u and δ_v were 1.6, -0.3 and -0.7 respectively (Figure 8.17 *a* and *d*). During this particular burst, δ_u u3* contributed 44% of the cross-shore transport and δ_v u3* contributed 69% of the longshore transport. However, in general, the oscillatory suspended sediment term $\Psi_2 \cos \alpha_5$ was larger than the mean current term δ_u u3*.

Meanwhile, in the longshore direction, the mean current term δ_v u3* dominated the suspended sediment transport, as might be expected given the minor importance of longshore oscillatory currents. However, an exception was around the HW of Tide 28, when particularly small longshore currents reduced the contribution of δ_v u3* to around 25% of longshore transport, whilst $\Psi_2 \sin \alpha_5$ contributed about 60%.

In summary, suspended sediment transport is predicted to be the dominant mode at Morfa Dyffryn, as occurred at Nieuwpoort. The mean longshore current dominated longshore suspended sediment, in general. Cross-shore, the oscillatory term was the most important, except in shallow waters at the beginning of the flood and late in the ebb of Tides 26 and 29 respectively; at such times, both u3* and δ_u were at their highest.

8.4 Comparison of Measured and Predicted Sediment Transport Rates

The results of the predictions presented in Section 8.3 can now be compared with measured suspended sediment fluxes, to evaluate the accuracy with which eqns. (2.5) and (2.6) can predict both the magnitude and direction of the suspended sediment transport (Figure 8.18). The scale used for the vertical axes of the Figure is such to exclude the two extreme measured transport rates during Tide 29, in order to improve the resolution of the remainder.

Cross-shore, the predictions are seldom even in the correct direction; this is due to the dominance of the oscillatory term in the prediction, whilst the measured transport rates reflect clearly the importance of the mean component. The results obtained suggest that the mean cross-shore current term in (2.5) is insufficiently weighted since, on the two occasions that u3* is at its highest, the predicted results approach the measured; this relates to both direction and magnitude.

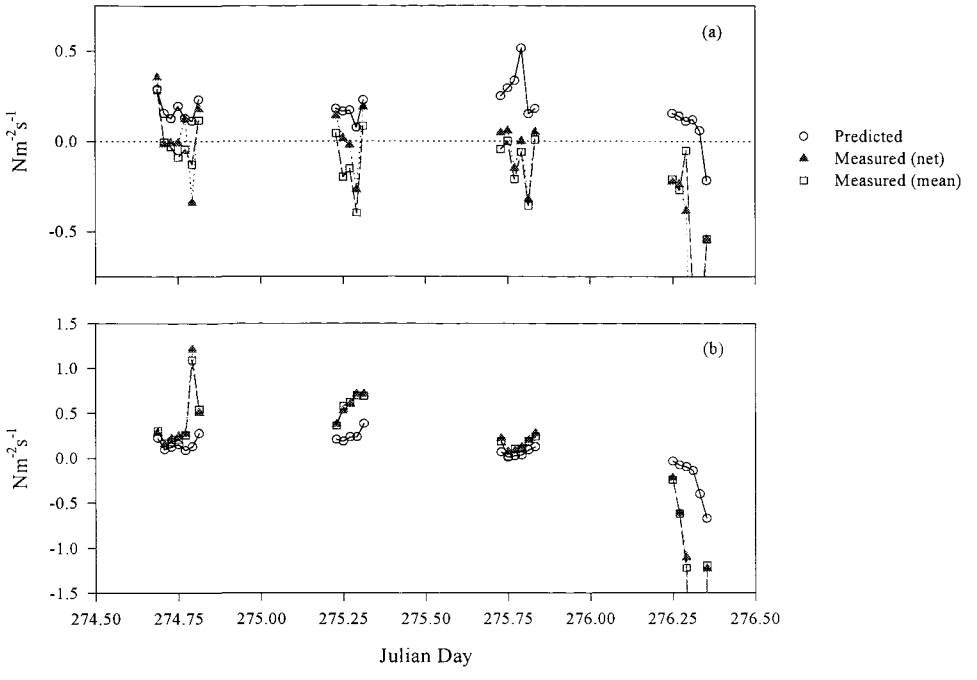

Figure 8.18 Tides 26 to 29, Morfa Dyffryn: predicted and measured suspended sediment transport rates (a) cross-shore; and (b) longshore

Alongshore, it is of interest to note that the near perfect fit between measurements and predictions for Tide 28 is when the mean longshore currents were at their weakest. On these occasions, the predictions are dominated by the longshore oscillatory term. Nonetheless, for the remaining tides, the longshore suspended sediment transport is generally well predicted. Differences between the measured and predicted values may include errors induced by both the constants of the drag coefficient, C_f and the efficiency factors, ϵ_b and ϵ_s.

Voulgaris & Collins (1996) argued that, since suspended sediment accounted for more than 80% of the gross sediment transport rate at Nieuwpoort, (2.6) could reasonably be reduced to:

$$I_{y\,susp} = \frac{\rho\, C_f\, U_m^4\, \epsilon_s}{W} \left(\psi_2 \sin \alpha_5 + \delta_v\, u3* \right) \tag{8.1}$$

Where sin α_5 approaches zero and substituting 0.7 for u3* and replacing δ_v by $\bar{v}/U_m$, (8.1) can be simplified to:

$$I_{y\,susp} = \frac{\rho\, C_f\, U_m^3\, \epsilon_s}{W} \cdot 0.7 \cdot \bar{v} \tag{8.2}$$

The results obtained from Tides 26 to 29 suggest that (8.2) is valid when the mean longshore currents exceed ~ 0.1 ms^{-1}. When the longshore currents are weak (and these are the conditions for which, it should be remembered, (2.5) and (2.6) were derived), eqn. (8.1) should be utilised.

In conclusion, the energetics-based model of Bailard (1981), as re-defined by Guza & Thornton (1985), predicted longshore sediment transport reasonably well, particularly so when mean longshore currents were weak in comparison to mean cross-shore and oscillatory currents. Cross-shore predictions are seldom in the direction of the observations, although are of a similar order of magnitude to those measured: similar conclusions were drawn by Foote (1994) and Voulgaris *et al.* (1996). The reason for the disparity appears to lie in the cross-shore vertical velocity structure. Figure 8.18 demonstrates that, whilst (2.5) does not account sufficiently for the mean current when it is directed offshore, the predictions are reasonable when the mean cross-shore current is onshore in the shallow waters early and late in the tidal cycle.

CHAPTER 9: RESULTS - BEACH GROUNDWATER

9.1 Introduction

The mean elevation and fluctuations in the water table are known to influence sediment transport on beaches, although the mechanisms by which groundwater interacts with surface waves have not yet been established (Section 2.4.1). A number of processes may be involved: (i) relative infiltration losses, as swash advances over an unsaturated beach (*e.g.* Grant, 1946); (ii) pressure/seepage forces at and below the sediment surface, which affect the threshold of entrainment (*e.g.* Nielsen, 1992*b*; Baird *et al.*, 1996); and (iii) alteration of flow in the boundary layer, with resultant changes in the horizontal shear stresses at the bed.

Fluctuations in the water table occur over a range of time scales from tidal to individual swashes, and are caused by: (i) vertical infiltration, percolation and seepage; (ii) horizontal mass transfer of water under hydrostatic conditions (seepage); and (iii) vertical propagation of pressure through the capillary zone *i.e.* the Wieringermeer effect (Section 2.4.7).

The relative importance of each of these forces and mechanisms is unknown and probably varies depending upon tidal stage and range, beach profile and sediment composition. However, the swash zone is where the influence of the water table is most critical (Section 2.4.11); this is consistent with the increasing appreciation of the importance of sediment transport within swash zone on tidally-integrated predictions of net sediment transport (Voulgaris *et al.*, 1997). An ambitious aim is to model numerically, over a tidal cycle, the progression of inner surf waves and swash/backwash, fluctuations of the water table due to infiltration through unsaturated and saturated sediment and pressure forces, together with prediction of shear stresses at the bed and the resultant swash zone sediment transport. Such objectives remain some way in the future (Turner *et al.*, 1997), but an important step towards an understanding is the accurate prediction of the asymmetric groundwater oscillations due to tides, given the importance of the seepage zone (Section 2.4.8). Models of seepage zone dynamics are now available (Section 2.4.9), but were derived for beaches where the hydraulic conductivity is taken as reasonably constant across the beach profile *i.e.* sandy beaches. This assumption may be invalid for mixed beaches, given their complex sedimentary structure.

The review undertaken of previous research into groundwater behaviour has not identified any measurements of groundwater fluctuations on mixed beaches, with only a single data set from a shingle barrier beach (Nicholls, 1985). Therefore, the first stage in assessing the importance of groundwater on sediment transport on a mixed beach is to model the groundwater response to tides; subsequently, to compare this to that of a sandy beach. This part of the study will be achieved through the use of the GRIST I model (Baird *et al.*, 1997) to predict groundwater fluctuations due to tidal inundation. The model has been found to produce accurate predictions of water table fluctuations during a tidal cycle, on a broadly homogeneous, sand beach, particularly in the absence of large swash excursions (Baird *et al.*, 1996). Use of the model at Morfa Dyffryn serves a number of useful purposes: (i) it provides a test of the global applicability of the model *i.e.* if successful, it ceases to be site-specific; (ii) it develops a rigorous assessment of the extent to which the physical processes are represented by the parameters, notably beach gradient and hydraulic conductivity, by extending the model outside the conditions for which it has already been validated; (iii) it indicates the relative importance of each of the particular properties of a mixed beach for groundwater behaviour; and (iv) if the model is found to represent adequately the tidal-fluctuations of groundwater on a mixed beach, it can be used in a predictive mode for beach replenishment schemes.

A description of the measured water table fluctuations of Tide 32 will be presented; this will be followed by details of the GRIST I model and a comparison of the model results with those measured.

9.2 Measured Groundwater Oscillation due to Tidal Inundation

The analysis presented here will concentrate upon the ebb phase of Tide 32, which inundated both the mixed and shingle sections of the profile. This analysis will permit also later consideration of any link with wave reflection from the mixed/shingle bank. In addition, the wave conditions were fairly calm during Tide 32 (Figure 5.13); therefore the change in elevation of the water table is attributable primarily to tidal progression across the profile. The measured water table elevation, during Tide 32, is given in Figure 9.1 (which includes the location of the dipwells).

The maximum water table elevation at D5 occurred at HW, and at D6 and D7 at HW+0.5 hrs. The elevation given is a 10 min average every 30 min, hence there was a

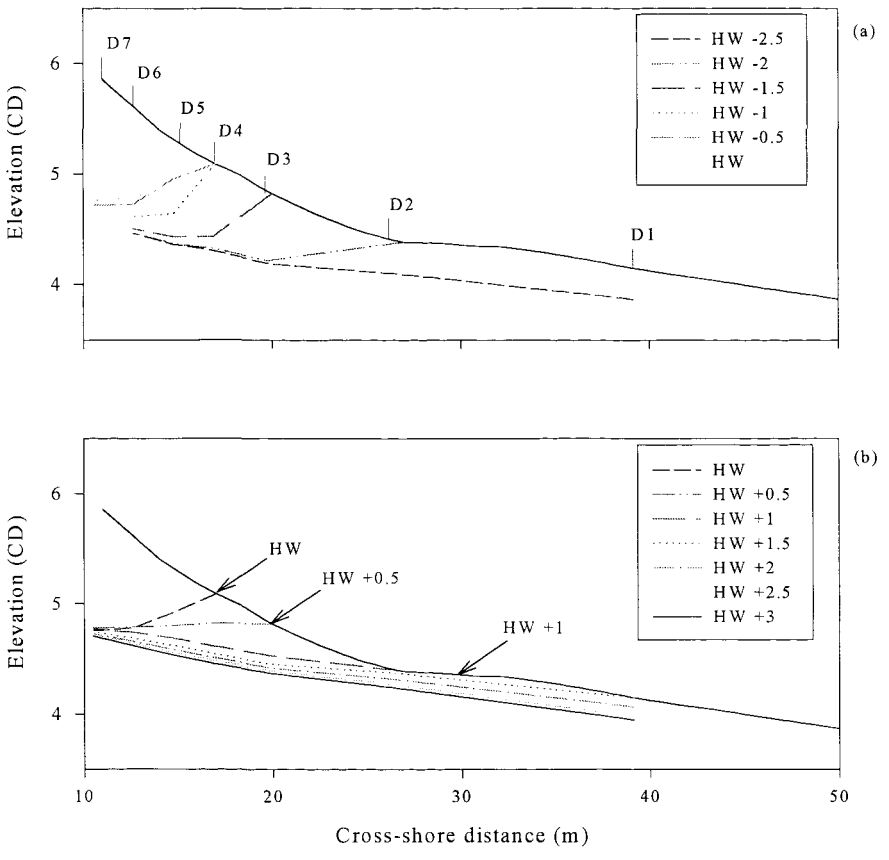

Figure 9.1 Measured water table elevation during Tide 32 during the flood (a) and ebb (b) phases of the tide

20 - 30 min lag in peak elevation over a horizontal distance of 2 m, although the resolution of the measurements was too coarse to identify accurately the tidal propagation phase lag across the profile. The water table was below the level of the dipwells farther inland. However, the observed fluctuation in water table at D7 was only 0.07 m from its maximum at HW +0.5 to HW +3; this suggests that the water table response to tidal inundation dies out not far landwards of D7, even on this 4.5 m spring tide. Figure 9.1*b* shows the development of a seepage face to seawards of D2, at HW +1.5. By HW +2, the measured elevation was 0.08 m and 0.09 m below the sediment surface at D2 and D1, respectively. Hence seepage face development was restricted to approximately 30 min after the retreat of the tide. The outcrop was located, however, at the sharp break of slope between the sand and mixed sections of the profile. Overall, water table fluctuations

between D1 and D4, where the rise and fall are at their greatest and which embrace the seepage zone, will prove to be the most serious test of the predictive ability of GRIST I.

9.3 Landward Attenuation of Groundwater Fluctuations, due to Waves

A 3 minute segment of the wave record at Station A (PT4) at HW-0.5 is shown at Figure 9.2 *a* , together with the concurrent groundwater at D4 and D5, situated 4 and 6 m to landward of PT4 respectively (refer to Figures 4.4 and 9.1). The mean and the trend of each trace in Figure 9.2 *a* was removed, whilst only the mean was removed in Figure 9.2 *b*, so that the trend of the record remained. Detailed visual observations have confirmed that D4 was covered periodically by swash waves, but that the surface water drained away completely between swashes.

The water levels in the wells exhibit a lag, due to the time taken for water to flow in and out of the tube, in response to changes in the water table elevation. This lag may be of the order of several seconds. It is unlikely such short-term water table fluctuations could be detected without using rapidly-responding piezometers; therefore, it is not possible to apportion the groundwater fluctuations into that due to horizontal translation of water and simple infiltration of swash, or to the Wieringermeer effect, or the pressure propagation suggested by Waddell (1973). Both the latter effects should produce an almost instantaneous rise in the water table, with no phase lag between the waves and the groundwater rise (Li *et al.*, 1996*a*). However, any water table fluctuations induced by swash waves have clearly died out within 2 m, to be replaced by a steady, head-induced, horizontal landwards flow. A similar landward attenuation was observed between D3 and D4, at HW +0.5.

9.4 The GRoundwater Interaction with Swash and Tides model (GRIST)[6]

The version of GRIST used for the analysis of beach groundwater at Morfa Dyffryn (GRIST I) is a finite difference model, where the beach cross-section is represented by a series of vertical cells (Figure 9.3).

6

The GRIST model for groundwater flow through beaches was written by Dr Andrew Baird of the University of Sheffield and further details can be found in Baird & Horn (1996) and Baird *et al.* (1996, 1997)

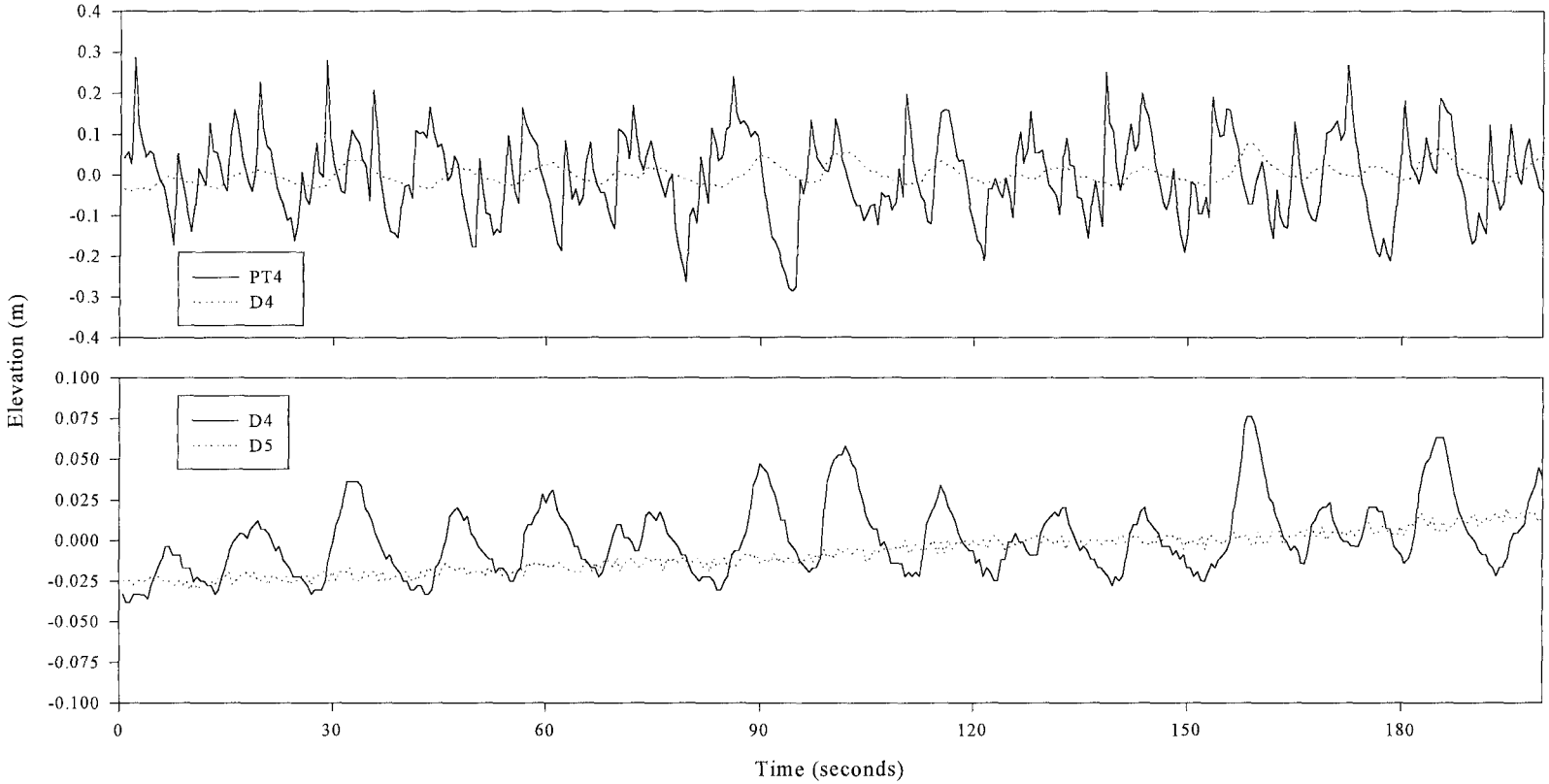

Figure 9.2 Tide 32 at Morfa Dyffryn: (a) sea surface elevation (PT4) and groundwater fluctuations (D4); (b) groundwater fluctuations at D4 and D5 at 1930 (HW -0.5)

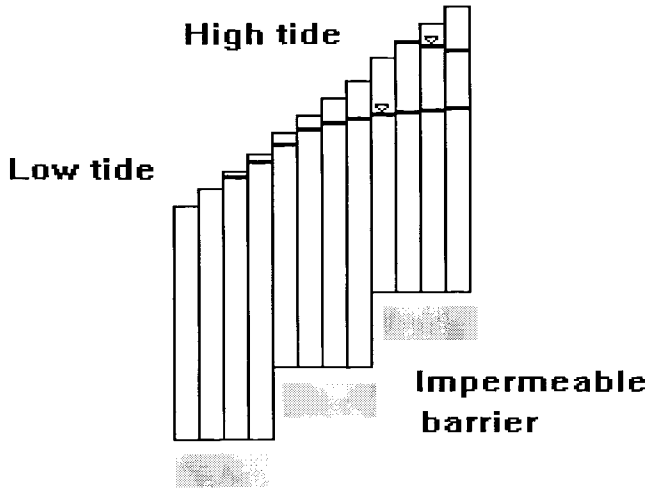

Figure 9.3 Schematic diagram of GRIST I model

9.4.1 Boundary conditions

The inland boundary condition can be either: (i) a fixed head, where the height of the water table is given (the Dirichlet condition); or (ii) a specified flux across the boundary (the von Neumann condition), which can include a zero flux boundary as would occur, for example, when the beach is backed by a sea wall. The lower boundary is the level of an impermeable layer below the beach sediment. The seaward boundary is represented by the most seaward cell which is permanently saturated; this is determined by the elevation of the tide and, hence, varies throughout the model run. The upper boundary is the interpolated beach profile. The sensitivity of the model results, to these boundary conditions, is assessed later (Section 9.8).

9.4.2 Model procedure

The model proceeds in four stages, presented schematically as:

Step 1 initialise variables.
Step 2 calculate stable time-step for iteration.
Step 3 at each timestep:
(a) derive tidal elevation
(b) calculate the net groundwater flux between cell i and cell i + 1

(c) derive new water table elevation for each cell using mass balance

Step 4 write results to file

Step 1 defines the length of time over which model is to be run and the interval, in seconds, when the results are written to file. Step 2 defines the minimum time-step which the model will utilise, to ensure that the finite difference solution remains stable (Remson *et al.*, 1971):

$$\frac{Kh\Delta t}{s(\Delta x)^2} \leq 0.5 \tag{9.1}$$

where h is the elevation of the water table (cm), t is the time (s), K is the hydraulic conductivity of the sediment (cm s^{-1}), s is the specific yield (dimensionless) and x is horizontal distance (cm). The maximum timestep is 600 seconds. During Step 3, the elevation of the tide is used to determine which cells are inundated. When covered by the tide, the height of the water table is deemed numerically equal to the height of the cell. The groundwater fluxes are calculated according to a one-dimensional version of the Boussinesq equation (Boussinesq, 1904; as referred to by Fetter, 1994):

$$\frac{\partial h}{\partial t} = \frac{K}{s}\frac{\partial}{\partial x}\left(h\frac{\partial h}{\partial x}\right) \tag{9.2}$$

where the variables are as for (9.1). Presently, the model utilises a constant value of K across the beach profile. Eqn (9.2) assumes that the Dupuit-Forchheimer approximation is valid (Section 2.4.5). The head gradient is obtained, therefore, from the slope of the water table (Kirkham, 1967). The assumption of horizontal groundwater flow was found to be reasonable for a micro-tidal sand beach at Canford Cliffs, Dorset, except near the exit point of the seepage face (Baird *et al.*,1997). However, the assumption has not been tested for mixed or shingle beaches.

With each iteration at the given time-step, the rate of discharge into and from each cell is calculated by:

$$q_i = \frac{h_{i-1} - h_i}{\Delta x} \quad \frac{K_{i-1} + K_i}{2} \quad \frac{h_{i-1} + h_i}{2} \tag{9.3}$$

where q_i is the rate of discharge of groundwater seaward from cell *i-1* during Δt, into cell *i*, q_{i-1} is the rate of discharge out of cell *i* during Δt and *z* is the elevation about the datum. The remaining parameters are as for (9.1). The new elevation of the water table is derived from a simple mass balance equation, where:

$$h_{i,t+\Delta t} = h_{i,t} - \left[\frac{Q_{i-1} + Q_i}{s} \right] \tag{9.4}$$

where $Q_i = q_i \Delta t$. In the case of a rising water table on a flood tide, the flux to the seaward cell is a negative value; hence, cell *i* receives water from cell *i+1*. The height of the water table within each cell is written to a results file every 1800 seconds. A seepage face is developed when:

$$h_{i,t} + \left(\frac{(Q_i - Q_{i-1})\Delta t}{\Delta x \, s_i} \right) > e_i \tag{9.5}$$

where *e* is the cell height and the remaining terms are as for (9.1) and (9.4). Development of a seepage face indicates that the tide and the groundwater table have become de-coupled.

9.4.3 Data requirements

Three sets of data are required as input for the model:

(a) *Initial water table position.* This is the water table as measured by the dipwells at the start of the selected tidal phase *e.g.* at low water or mid-tide. The model "profiler" interpolates this information to provide an initial height of the water table for each cell across the profile.

(b) *Beach profile.* Once again, the measured profile at Morfa Dyffryn was pre-processed by the "profiler", to interpolate a height for each cell. The profile is

regarded as immobile for the duration of the model run.

(c) *Tidal elevation.* For the Morfa Dyffryn data, a time-series of tidal elevation (at 10 min intervals) was used. The model interpolates this elevation, on a variable time-step basis. Alternatively, a sine function is used to generate tidal elevations if measured data are not available.

9.5 Model Predictions

The GRIST1 model was run using the Tide 32 mean water level from Station D (145 m offshore) to represent tidal elevation at 10 min intervals. The initial measured groundwater position was located midway between high and low water. Tests were run using hydraulic conductivities (K cm s^{-1}) of 1, 0.5, 0.1, 0.05, 0.025, 0.01, 0.005 and 0.001; these encompass also the values derived from laboratory hydraulic conductivity tests for 50:50 sand:fine shingle mixed sediments (Section 9.10). Specific yields, s, of 0.2, 0.25 and 0.3 were used, which represent average values for well-sorted sediments varying from very coarse sand to fine sand (Table 9.1).

The inland boundary condition was a specified head of 0.44 m (the Dirichlet condition). This value was selected as an extrapolation of the water table at its lowest position during the tide. The validity of this value cannot be verified, since the water table at the control dipwell (D10), sited in the sand dunes, was always below the length of the well *i.e.* below 2 m from the surface, except during times of heavy rainfall. No rain was recorded during the 3 days prior to Tide 32. However, the model sensitivity to this prescribed head value will be tested. The lower boundary was taken as Chart Datum (Section 2.4.7). The cell width adopted was 0.5 m. Each simulation was run from HW -0.5 to HW +3.5. The predicted elevation of the water table across the profile was compared to the measured water table, at half-hourly intervals from high water.

9.6 Comparison of Measured and Predicted Water Table Elevation

The goodness-of-fit of the model output was obtained simply by subtracting the measured water table elevation at each dipwell, from that predicted at the nearest cross-shore cell to the dipwell location; thus the procedure outlined below was adopted.

Sediment Type	Specific Yield (%)			Diameter (m)	K (ms^{-1})	K (cms^{-1})
	Max.	Min.	Ave.			
Fine sand	28	10	21	0.00125	0.0001	0.01
Medium sand	32	15	26	0.004	0.001	0.1
Coarse sand	35	20	27	0.01 0.0125	0.0065 0.01	0.65 1
Gravelly sand	35	20	25			
Fine gravel	35	21	25	0.025 0.04	0.04 0.16	4 16
Medium gravel	26	13	23			
Coarse gravel	26	12	22			

Table 9.1 Specific yield values for sediment in an unconfined aquifer (Fetter, 1994) and typical hydraulic conductivity values (Packwood & Peregrine, 1980)

(a) The deviation of modelled water table elevation from that measured was calculated, for each value of K used in the simulations; this was calculated at each dipwell location. A positive number indicates that the model over-predicted the height of the water table at that location. Conversely, a negative number means that the modelled elevation was lower than the measured.

(b) In order to assess the single value of hydraulic conductivity which predicted best the measured water table elevation across the profile, deviations across the profile were summed in two ways: (i) simple addition; (ii) on the basis of the sum of the absolute values of deviations.

The results are presented in Table 9.2, where the bold typeface indicates the smallest deviation. It should be noted that specific yield was held constant for these comparative tests of measured vs. predicted water table elevation. This approach was adopted because K is expected to be a more important factor in (9.2) than s. The sensitivity of the modelled water table to variation in s is assessed in Section 9.8.2.

K (cm s^{-1})	HW	HW +0.5	HW +1	HW +1.5	HW +2	HW +2.5	HW +3
Total deviation (m)							
1	-1.317	-1.562	-1.452	-1.509	-1.455	-1.453	-1.624
0.5	-1.315	-1.536	-1.385	-1.385	-1.293	-1.229	-1.285
0.1	-1.262	-1.362	-1.095	-0.997	-0.839	-0.703	-0.625
0.05	-1.120	-1.202	-0.881	-0.779	-0.621	-0.479	-0.391
0.025	-0.871	-0.929	-0.568	-0.465	-0.324	-0.197	**-0.118**
0.010	-1.448	-1.178	-0.596	**-0.355**	**-0.132**	**0.039**	0.141
0.005	-0.395	-0.204	**0.297**	0.485	0.660	0.802	0.868
0.001	**-0.185**	**0.101**	0.715	0.988	1.245	1.448	1.578
Total absolute deviation (m)							
1	1.317	1.562	1.452	1.509	1.455	1.453	1.624
0.5	1.315	1.536	1.385	1.385	1.293	1.229	1.285
0.1	1.262	1.362	1.095	0.997	1.007	1.047	**0.999**
0.05	1.120	1.202	0.895	0.855	0.939	1.019	1.007
0.025	0.871	0.929	**0.788**	**0.773**	**0.868**	**0.975**	1.006
0.010	1.448	1.178	0.860	0.833	0.928	1.037	1.073
0.005	0.463	**0.638**	1.091	1.183	1.318	1.452	1.492
0.001	**0.355**	0.737	1.283	1.498	1.729	1.926	2.030

Table 9.2. Deviation of the modelled water table elevation from the measured levels (prescribed head of 4.4 m, impermeable barrier at CD and specific yield of 0.25).

The simple addition of the deviations provides the net error, but does not necessarily reflect the spread of errors across the profile. For example, it would be possible for large gross errors to cancel each other out. Summation of the absolute deviations accounts for this possibility, but produces an artificially high estimation of the errors. Also, a large error at a single location could distort considerably the results. Ultimately, the estimate of best-fit K will be established in conjunction with graphical representation (see below).

However, some preliminary conclusions can be drawn from the results presented in Table 9.2. The model output for a K of 0.025 cm s^{-1} appears to predict most accurately

the measured water table across the profile during the ebbing tide (HW +1 and later), whilst the lowest net error was for a K of 0.01 cm s^{-1}. For values of K of 1 and 0.5 cm s^{-1}, the total (negative) error was the same as the absolute error. Hence, these values of K consistently under-predicted the elevation of the water table across the whole profile at high water and throughout the ebbing tide. The sum of the deviations at HW and HW +0.5 involved only those wells not covered by the tide (D5 to D7), when the swash was infiltrating into mixed sand and shingle. HW + 1 included the deviations from D2 to D7 only. By HW +1.5 all wells were uncovered by the tide.

A graphical comparison of the measured water table and the results of the model simulations, for varying K, is shown at Figure 9.4. K values of 1 and 0.5 cm s^{-1} (representative of a coarse sand, see Table 8.1) are too high; they predicted consistently more drainage than was measured. The results for a K of 0.001 cm s^{-1} were omitted from Figure 9.4, since they were grossly inaccurate and predicted practically no drainage at all (as might be expected from the values presented in Table 9.1). It should be noted also that the measured water table elevations shown in Figure 9.4 are linear interpolations between the various wells. This procedure leads to the appearance of drainage across the inner ridge between D1 and D2 when, in fact, the ridge may remain saturated at the surface. When viewed graphically, the K of 0.1 cm s^{-1} predicts best the water table fluctuation during the ebb, from D3 and farther to seawards. This value of K represents the hydraulic conductivity of a medium sand (Table 9.1). It is particularly accurate during HW +1.5 and HW +2, when the model is at its most critical for seepage zone development (Section 9.6). For the section of the profile from D1 to D4, the total deviation of the water table predicted by K of 0.1 at HW +1.5 is -0.179m (with an absolute total of 0.179m). By HW+2, the total deviation is 0.075m (absolute total is 0.243 m), reducing to +0.061 by HW +3 (absolute deviation 0.313 m).

To landward, the pattern is more complicated; it is hampered by the interaction of one model cell upon its adjacent cells. Landward of D4, all the modelled water table elevations slope inland and converge at the height of the prescribed (constant) head. In contrast, the measured water table slopes to seaward, in common with that observed from other sandy beaches (*e.g.* Emery & Foster 1948, Erickson, 1970). It would appear, from Figure 9.4, that the inland boundary condition is set too low; the impact of this will be

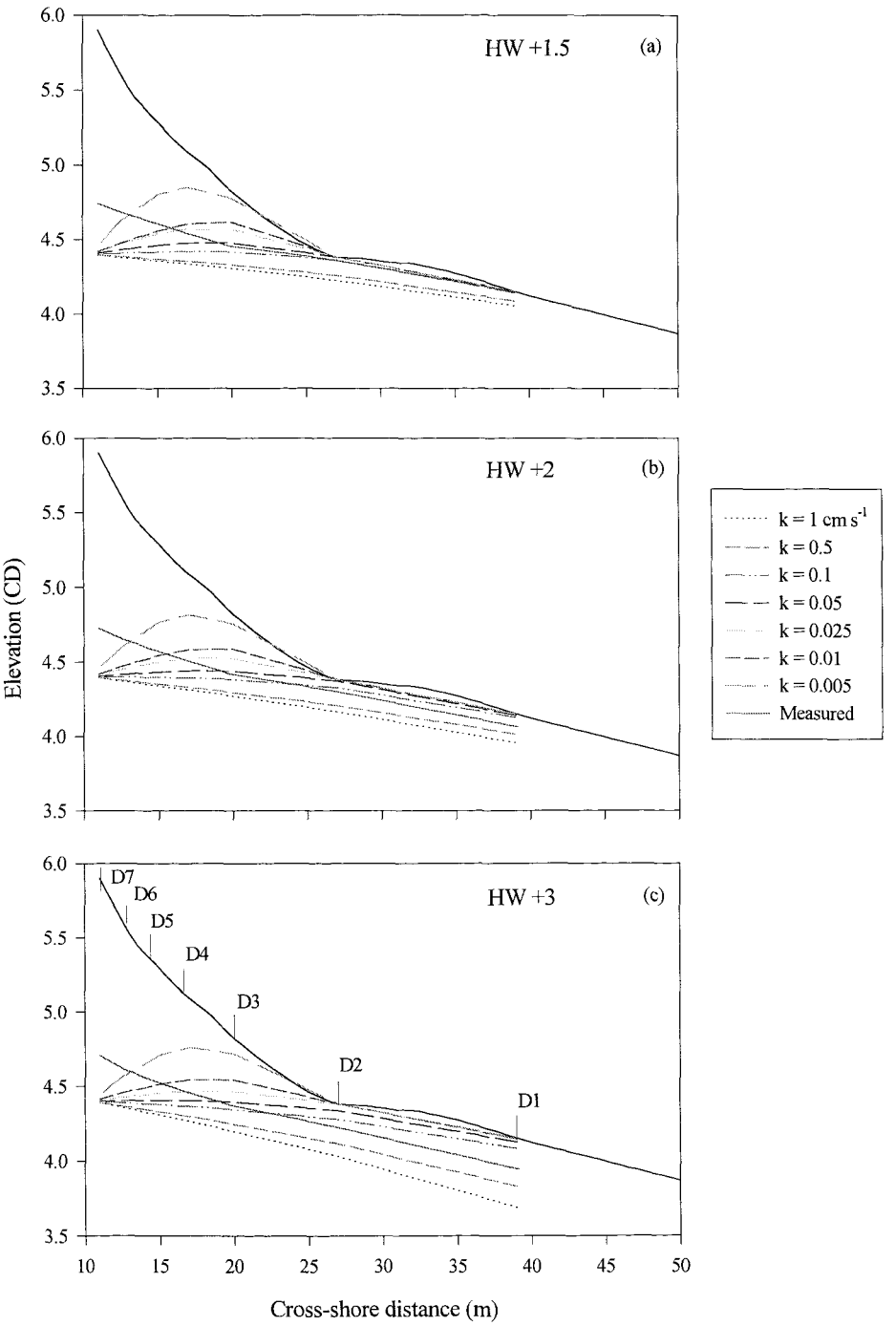

Figure 9.4. Tide 32 at Morfa Dyffryn: measured and predicted water table elevations at (a) HW +1.5; (b) HW +2; and (c) HW +3. Specific yield = 0.25

discussed further, during the sensitivity analysis (Section 9.8).

9.7 Prediction of the Seepage Zone

The best-fit value of K (0.1 cm s^{-1}) predicted a seepage zone from the base of the sand/shingle slope at HW +1.5 (Figure 9.4 *a*), but with no outcropping at the surface by HW +2. This prediction is reasonably representative of the measured water table. The result illustrates also that the location and timing of the seepage face development is acutely sensitive to hydraulic conductivity and beach slope; a value of K of 0.05 cm s^{-1} maintained the presence of a seepage zone up to 30 min longer than was observed, although the location of the outcrop was at the break of slope. In contrast, a K of 0.005 cm s^{-1} predicted a continuous seepage zone on the sloping mixed beach profile.

Considering the complexity of the sediment composition at Morfa Dyffryn, the accuracy with which GRIST I predicts: (i) the water table oscillation across the majority of the profile during the ebb tide; and (ii) the position and timing of the seepage face, is surprising. This compatibility may be due, in part, to the fact that the sediment in the vicinity of the break of slope was a broadly homogeneous, medium sand (although with isolated large cobbles); hence, the seepage zone location is profile-controlled. A further and surprising conclusion is that the influence of the mixed sediments does not affect markedly the behaviour of the water table farther to seaward. It might have been expected that the timing of the fluxes through the sediment would have been affected. Such conditions would be represented in a larger or smaller modelled value of K, than suggested for a medium sand; however, this was not found to be the case.

9.8 Sensitivity Analysis

Despite the reasonable prediction by GRIST I of seepage face location and timing on an ebbing tide, a sensitivity analysis was carried out to assess the impact of the given parameters (K and s) and the boundary conditions. Average values of specific yield vary from 0.2 to 0.3, as presented in Table 9.1. The remaining variables are: depth to the impermeable barrier (the lower boundary); and the prescribed head inland boundary. The model was re-run using three representative K values (1, 0.1 and 0.01 cm s^{-1}) for the simulations given in Table 9.3. The elevation of the lower boundary is provided relative to Chart Datum *i.e.* CD -3 reduces the depth to the impermeable layer by 3 m, which

Simulation	K (cm s^{-1})	s	Elevation of lower boundary (CD) (m)	Inland boundary head (m)
1	0.1	0.2	CD	4.4
2	0.01	0.2	CD	4.4
3	0.1	0.25	CD	4.4
4	0.01	0.25	CD	4.4
5	0.1	0.3	CD	4.4
6	0.01	0.3	CD	4.4
7	0.1	0.25	CD - 2	4.4*
8	0.01	0.25	CD - 2	4.4*
9	0.1	0.25	CD - 3	4.4*
10	0.01	0.25	CD - 3	4.4*
11	0.1	0.25	CD	5
12	0.01	0.25	CD	5
13	0.1	0.25	CD	3.4
14	0.01	0.25	CD	3.4
15	0.1	0.25	CD	0
16	0.01	0.25	CD	0
17	0.1	0.25	CD -2	0
18	0.01	0.25	CD -2	0
19	0.1	0.25	CD - 3	0
20	0.01	0.25	CD - 3	0
21	0.1	0.2	CD	0
22	0.01	0.2	CD	0
23	0.1	0.3	CD	0
24	0.01	0.3	CD	0
25	1	0.2	CD	0
26	1	0.25	CD	0
27	1	0.3	CD	0

Table 9.3 Parameters used in the GRIST I sensitivity analysis (* refers to prescribed head, relative to CD).

represents a permeable layer of 1.15 m at Dipwell 1 and 0.25 m at the seaward end of the profile (65 m cross-shore). The inland boundary head of zero represents a zero flux (the von Neumann condition).

9.8.1 Sources of error

The results of the sensitivity analysis of the predicted water table elevation, to the boundary conditions and input parameters, can be put into context by assessing the likely measurement error. Instrumental noise levels were obtained from the standard deviation over 17 min, when the wells were not covered by the tide. Table 9.4 presents the noise levels at Tide 32, HW +3. Hence, the maximum total instrumental error is 0.012 m.

Instrument	Standard deviation (m)
D1	0.004
D2	0.004
D3	0.006
D4	0.006
D5	0.004
D6	0.005
D7	0.005

Table 9.4 Instrument noise levels (for details, see text)

9.8.2 Model sensitivity to specific yield

A preliminary assessment of the model sensitivity, to specific yield, is shown graphically at Figure 9.5 for HW +1.5; this was a critical period for seepage face development. For a K of 0.1 cm s^{-1} the selected value of specific yield had a negligible effect on the predicted elevation of the water table (Figure 9.5 *a*). The influence was greater for the lower K value (Figure 9.5 *b*), but the maximum difference in the predicted elevation was 0.075 m.

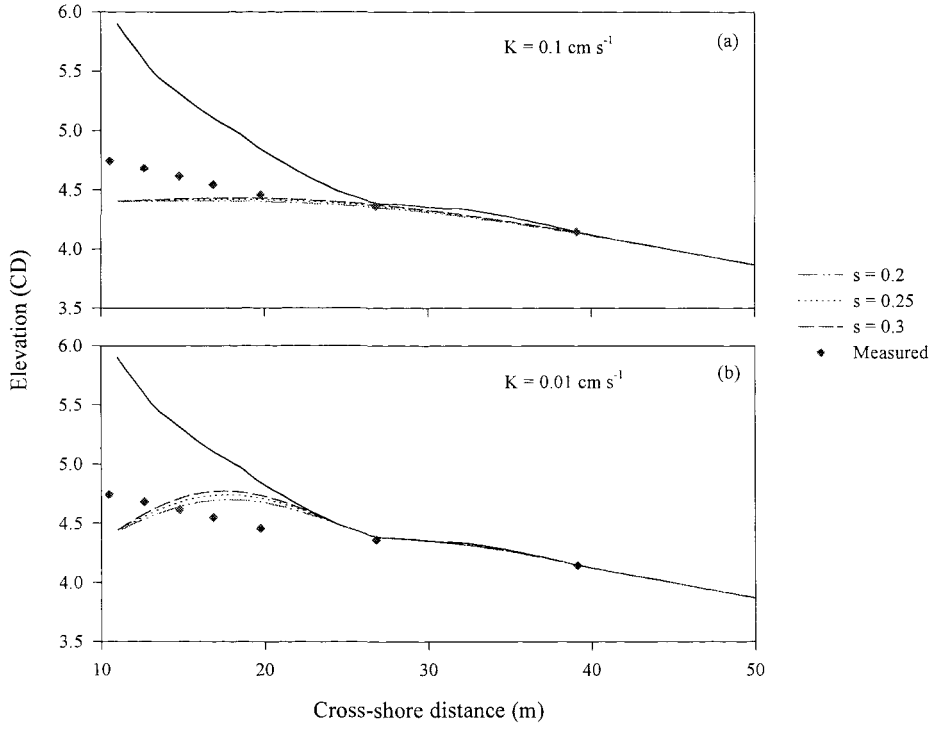

Figure 9.5 Tide 32, HW +1.5: sensitivity of model to specific yield for (a) K = 0.1cm s^{-1} and (b) K = 0.01 cm s^{-1}. Impermeable barrier at CD, prescribed head = 4.4 m

9.8.3 Model sensitivity to *K/s*

Although the specific yield is a constant in (9.2), it is used as a ratio with hydraulic conductivity, in the form of *K/s*. Consequently, a series of tests was run to examine the combined effect of hydraulic conductivity and specific yield, through *K/s*. A zero flux condition was used for these tests to avoid the influence of a prescribed flux through the landward boundary (it will be shown later that this zero flux condition modelled the measured water table reasonably well). The impermeable barrier was located at CD. Figure 9.6 shows the predicted elevation of the water table at HW +1.5 for K values of 1, 0.1 and 0.01 cm s^{-1} with s of 0.2, 0.25 and 0.3. The K value for a coarse sand (1 cm s^{-1}) was also included in these simulations, although it was found to produce grossly

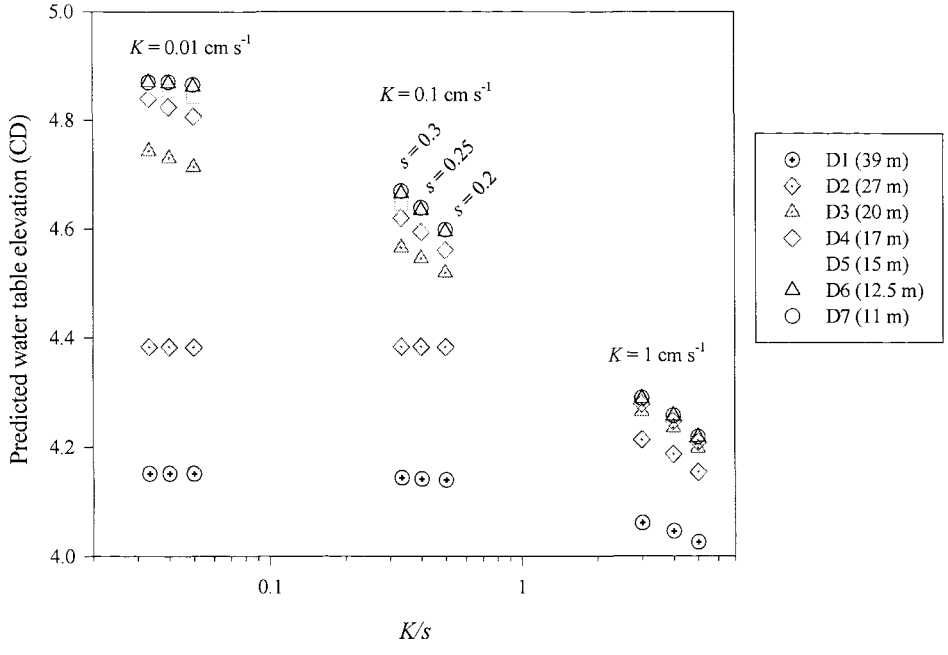

Figure 9.6 Tide 32, HW +1.5: variation in predicted water table elevation with K/s

inaccurate estimations of the measured water table (Section 9.6).

The results obtained for parameters for medium and fine sand will be discussed initially *i.e.* $K/s < 1$, which show a marked dependence on cross-shore position. On the ridge (D1), all the combinations of K/s predicted practically the same elevation. Such a consistency is probably because this location always receives water and, therefore, the water table is at or near the surface; any excess water volume is "lost", as overland flow. All the values of $K/s < 1$ predicted a seepage zone at D2 (hence, no variation in water table elevation which is, by definition, at the sediment surface).

At all the remaining cross-shore locations, the difference in the predicted water table elevation due to variation in specific yield is considerably lower than the difference in elevation caused by variation in hydraulic conductivity. This relationship is shown clearly in Figure 9.6, where the variation within the three K groupings is considerably less than the difference between the groupings. For example, for a K of 0.1 cm s^{-1} (medium

sand), the predicted water table elevation at D3 was 4.543 m; of this, 0.046 m accounts for the variation due to changing specific yield from 0.2 to 0.3 (*i.e.* ± 0.023), as shown in Table 9.5. For fine sand, the difference due to specific yield is ± 0.015 m; it is only ± 0.33 m for coarse sand.

Meanwhile, the variation in the predicted water table elevation at D3 due to hydraulic conductivity is 0.301 m (varying from coarse to medium sand) and 0.179 m (medium to fine sand). Hence, at this most sensitive location, the *most extreme* influence of specific yield was approximately one quarter that of hydraulic conductivity. This balance remained the case at all other locations but, whilst the influence of *s* was constant from D4 to D7 for coarse and medium sand, its influence became progressively negligible landwards for fine sand (Table 9.5).

	D1	D2	D3	D4	D5	D6	D7	
s	Variation in predicted water table elevation due to varying *K*							
0.2	0.114	0.228	0.321	0.352	0.367	0.377	0.380	Coarse to medium sand
0.25	0.096	0.196	0.310	0.347	0.364	0.377	0.381	
0.3	0.083	0.170	0.301	0.342	0.362	0.377	0.380	
0.2	0.012	0	0.196	0.247	0.262	0.268	0.268	Medium to fine sand
0.25	0.010	0	0.186	0.231	0.238	0.235	0.233	
0.3	0.008	0	0.179	0.220	0.220	0.206	0.202	
K (cm s^{-1})	Variation in predicted water table elevation due to varying specific yield							
1	0.035	0.058	0.066	0.069	0.070	0.070	0.071	Coarse sand
0.1	0.004	0	**0.046**	0.059	0.065	0.070	0.071	Medium sand
0.01	0	0	0.029	0.032	0.023	0.008	0.005	Fine sand

Table 9.5 Sensitivity of GRIST I to *K/s* at HW +1.5. Impermeable barrier at CD, zero flux inland boundary.

In conclusion, the selection of a value for specific yield is of minor importance, in comparison with hydraulic conductivity, for both medium and fine sand; although its influence is progressively of more consequence for coarse-grained sediments, it remains a less important parameter than *K*. It is also important to note that, in nature, *K* is a notoriously variable parameter; 100% difference in estimates of *K* for closely-spaced samples is not uncommon (Landon, 1991) whilst specific yield has less variability (Table

9.1). It is appropriate, therefore, that the model is considerably more sensitive to K than to s.

9.8.4 Model sensitivity to inland boundary condition

The inland boundary condition was tested using a K of 0.1 cm s^{-1} , an s of 0.25, an impermeable barrier at CD, and the range of prescribed heads given in Table 9.3, in addition to the 4.4 m prescribed head results described in Section 8.5. These values were selected to include the extremes of likely conditions. The results are shown in Figure 9.7, again for HW +1.5 given its importance for seepage zone development.

Clearly, the selection of an appropriate inland flow condition is crucial for the adequate prediction of the water table. If the prescribed head is over-estimated, the model results become increasingly inaccurate as the tide ebbs; for example, the prescribed head of 5 m continued to predict outcropping of the water table at the break of slope at HW +3. Conversely, an under-estimation of prescribed head, as for example, the 3.4 m head in Figure 9.7, had a significant influence on the water table prediction, since it resulted in continued landward drainage even 3 hr after high water. Interestingly, the boundary condition which predicted most closely that measured was zero flux. Whether this is an artefact of the construction of the model, or represented the actual aquifer conditions at the field site, remains to be established. It suggests though, that the inland boundary condition may be tied closely to the depth to the impermeable barrier *i.e.* the lower boundary condition. Such conditions are only to be expected because the depth of flow defines the length of the vertical boundary (of each cell) across which water can flow.

9.8.5 Model sensitivity to lower boundary condition (depth to impermeable barrier)

The sensitivity of the GRIST I model to the depth to the impermeable barrier was assessed using the two inland boundary conditions, which represented most closely the measured water table elevation *i.e.* a prescribed head of 4.4 m relative to CD and zero flux. The results for HW +1.5 are shown in Figure 9.8.

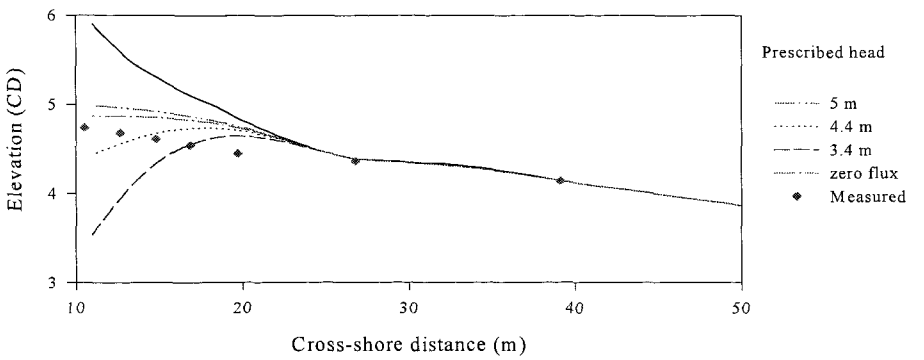

Figure 9.7 Tide 32, HW +1.5: sensitivity of the GRIST I model predictions to inland boundary condition. Impermeable barrier at CD, K = 0.1 cm s^{-1} s = 0.25

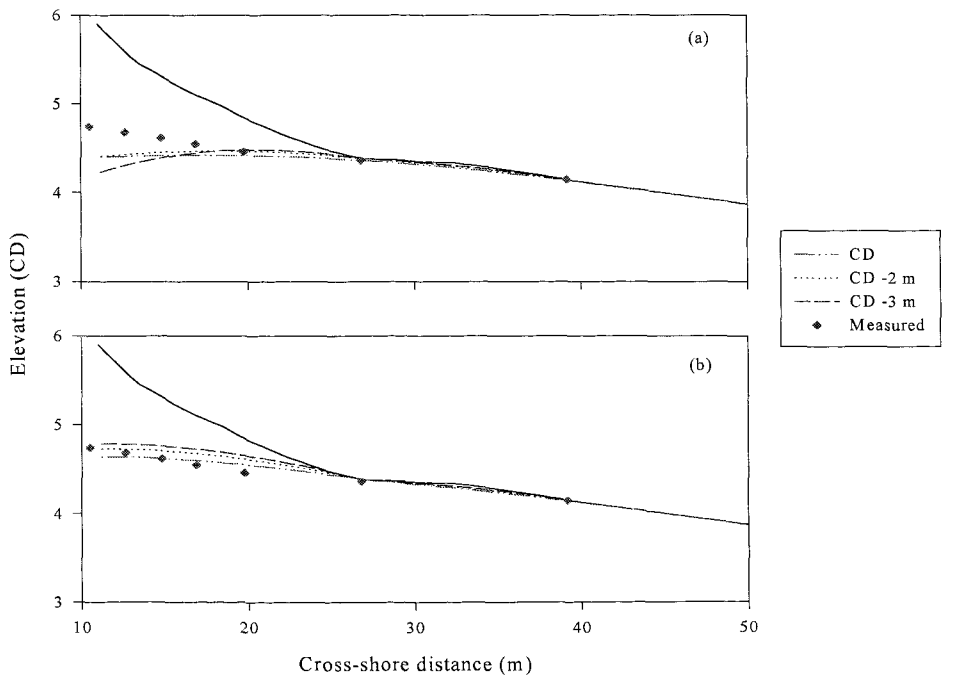

Figure 9.8 Tide 32, HW +1.5: sensitivity of GRIST 1 to lower boundary condition (depth to impermeable barrier) for inland boundary condition of (a) prescribed head (4.4 m relative to CD) and; (b) zero flux. K = 0.1 cm s^{-1}, s = 0.25.

For the prescribed head inland boundary, varying the depth to the impermeable layer makes negligible difference to the predicted water table elevation, except for the two most landward wells. CD -3 m represents a reduction in depth to the impermeable barrier of 3 m, hence, the lower boundary is at 3 m relative to CD. Assuming that the lower boundary is horizontal, this meant that the impermeable barrier was ~ 0.25 m below the surface at the seaward edge of the model (65 m cross-shore). Therefore, CD -3 is an extreme estimate of the minimum depth to the impermeable barrier, particularly across the ridge and runnel section of the beach.

In contrast, for the zero flux inland boundary, the shallower the aquifer, the higher the predicted water table at all the locations. Such a relationship is to be expected, since the thickness of the aquifer determines the vertical length of the boundary across which seaward flow can occur. At high water, a reduced aquifer thickness leads to a more pronounced super-elevation.

It is interesting to note that, regardless of the inland boundary condition: (i) the aquifer depth makes no difference at all to the prediction of the seepage face location and; (ii) drainage across the landward runnel (between D1 and D2) is also predicted, regardless of aquifer depth. Within this region, the topography appears to be the dominant control.

9.8.6 Conclusions of the sensitivity analysis

It should be noted that the analysis of the sensitivity of GRIST I was carried out using extreme values of one parameter, but maintaining the remainder as reasonable estimators of the natural field conditions. A more detailed sensitivity analysis of GRIST I involving multiple combinations of extreme values, is ongoing (Baird, pers. comm.).

Overall, the results of the sensitivity analysis for Tide 32, HW +1.5 may be summarised as follows:

(a) Hydraulic conductivity is generally the most important parameter and its correct parameterisation is extremely crucial for the prediction of the location and timing of seepage zone, even across a steep profile (Section 9.7).

(b) The specific yield is of less importance than hydraulic conductivity. For a medium sand, its influence is approximately 10% that of hydraulic conductivity, increasing to 25% for coarse sand (Section 9.8.3).

(c) The inland boundary condition is important, but less so than hydraulic conductivity. The depth to impermeable barrier is of less importance than the inland boundary condition.

Overall, for this aquifer (beach deposit), which is approximately the same height as the tidal range, the two most important parameters are hydraulic conductivity and the inland boundary condition. Specific yield and depth to impermeable layer had, generally, only a small influence on the predicted height of the water table.

9.9 Accuracy of the GRIST I Predictions

The most accurate prediction of the measured water table, at HW +1.5, was achieved by the following parameters:

Hydraulic conductivity:	0.1 cm s^{-1} (medium sand)
Specific yield:	0.25
Impermeable barrier:	Chart Datum
Inland flow condition:	Zero flux

The accuracy of this prediction can be seen in Figures 9.7 and 9.8 *b* for CD and the deviation from the water level measured at each well (in metres) is given in Table 9.6. The total error for all 7 wells was -0.007 m (the absolute error was 0.313 m). Using these same parameters, but a prescribed head of 4.4 m, the total error was -0.997 m and the absolute error was 0.997 (Section 9.6).

D1	D2	D3	D4	D5	D6	D7
0.005	0.020	0.087	0.046	0	-0.049	-0.106

Table 9.6 Deviation (m) of predicted water table elevation from measured at HW +1.5 (Tide 32)

It is important to establish how realistic these model parameters are for the conditions at Morfa Dyffryn. The hydraulic conductivity is representative of the medium sand which was found across the flat, intertidal profile, and within the mixed sand/shingle ridge. An average value of specific yield was used, but had little impact on the predicted results (Sections 9.8.2 and 9.8.3).

The depth to the impermeable barrier is difficult to establish without access to borings across the profile. However, the data obtained from the nearby Mochras Point Borehole showed a surface layer of 6.5 m of sand, shingle, silt and shells (Section 4.1.1). In addition, the extensive Quaternary deposits present across Cardigan Bay are thought to be unlithified (Tappin *et al.*, 1994) and, hence, CD appears to be a reasonable minimum estimate of the aquifer depth.

Unfortunately, the validity of the inland boundary cannot be established without extensive knowledge of the regional pattern of groundwater flow. However, the zero flux condition might not be unrealistic. The beach at Morfa Dyffryn was backed by an extensive range of sand dunes, which appeared to be underlain by sand and shingle *i.e.* the dunes developed subsequent to the formation of the shingle barrier. Behind the dunes was low-lying farmland. It may be that there is a groundwater divide below the dunes; therefore, any recharge by rainfall would drain both landwards and seawards from the divide (but not across it). No rain was recorded for three days prior to Tide 32; hence, a zero flux condition might have existed at that time.

It is probable that fine tuning of the parameters, particularly K and the inland boundary condition, could produce an even more accurate prediction of the measured water table. Further model development, to include variable K both horizontally and vertically, may also improve predictions. However, the natural inhomogeneity of sediments and the variation in measurements of hydraulic conductivity, both in the field (*e.g.* Baird *et al.*, 1997) and laboratory, suggest that order of magnitude estimates may be the most workable solution.

The primary aim of this analysis was not to produce the most accurate predictions but, instead, to examine how well the water table fluctuation across a mixed beach profile could be modelled using reasonable estimates of the parameters. It is important to note that GRIST I contains no additional coefficients *i.e.* it has been validated, not

calibrated, for field conditions (Baird *et al.*, 1997). In common with all other beach groundwater models, GRIST I was designed for use on sandy beaches; by extending its application to a wider range of sediment types and beach slope, it provides useful confirmation that the physical representation of the processes involved is well defined.

9.10 Hydraulic Conductivity of Mixed Sand and Shingle Sediments

Results from the sensitivity analysis of the GRIST model have demonstrated the importance of correct parameterisation of K. Accordingly, a series of laboratory permeameter tests was carried out to establish the hydraulic conductivity of sand/shingle mixtures, according to the procedures presented in Section 4.3.7. The tests used fine beach shingle (D_{50} = 4 mm), with 10% incremental proportions of fine, medium and coarse sand. The results are shown at Figure 9.9, where each data point represents the mean of between 20 and 30 measurements. Unfortunately, only 7 of the 10 tests for coarse sand could be completed, due to subsequent equipment failure.

The trends in the variation in hydraulic conductivity were common to the three types of sand used in the tests. There was a substantial decrease in the permeability of 4 mm shingle, with the addition of small quantities of sand; an admixture of only 20% (by weight) medium sand reduced the hydraulic conductivity of the shingle, to around one third of the value of shingle alone. The influence of fine sand was particularly marked, with a nearly 90% reduction. Hydraulic conductivity was generally at its lowest at 40% medium and coarse sand content. The values for 40% to 80% fine sand content are more variable, but represent extremely low permeability; this is an order of magnitude lower than for medium sand. This reduction in hydraulic conductivity, with increasing sand content, is due to the packing arrangement of the sediment particles; at such times the pore spaces between the shingle grains (which conduct water in the 100 % shingle samples) become filled with sand grains. However, an interesting finding was the noticeable increase in hydraulic conductivity of 100% coarse and medium sand, in comparison with mixtures containing up to 60% fine shingle *i.e.* the addition of between 10% and 60% of shingle to coarse and medium sand actually served to *reduce* the permeability of the mixture, rather than improve its drainage. This modification is attributed to the tortuosity of the fluid path through the mixture, in comparison with the 100% version; through the latter, the fluid path is relatively regular, depending upon grain

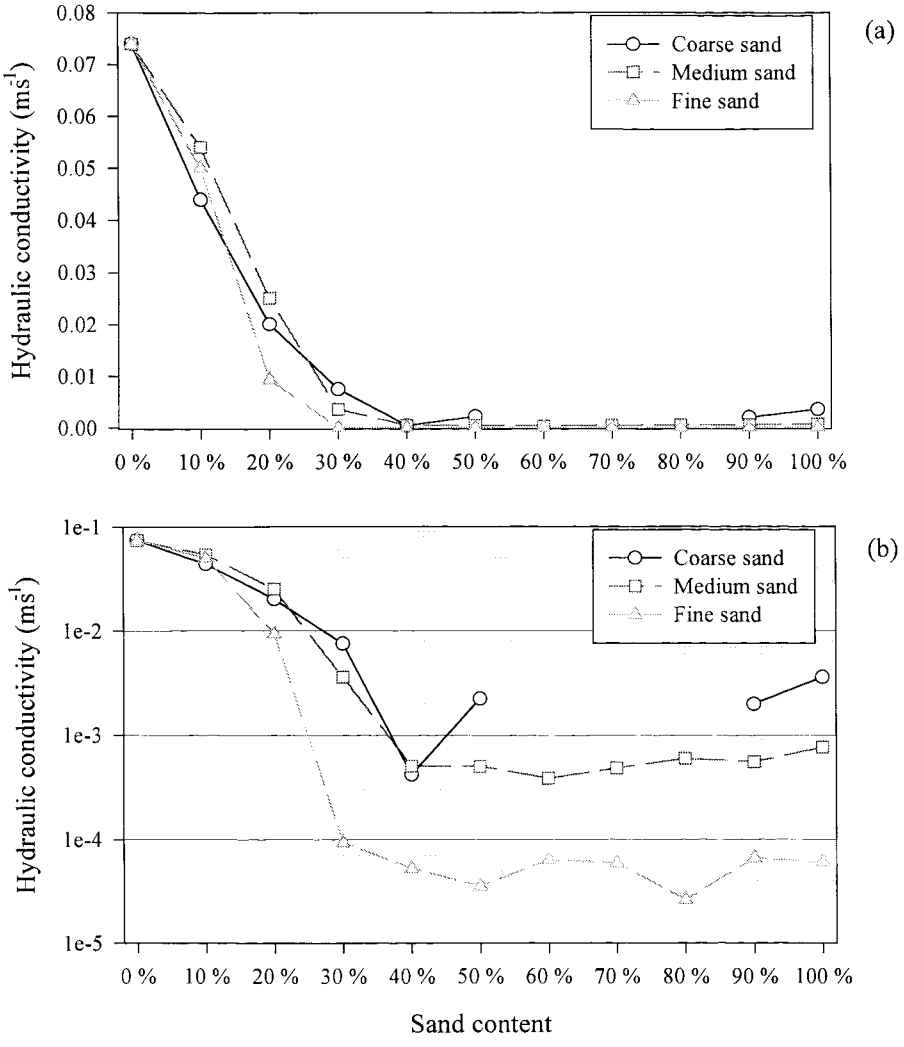

Figure 9.9 (a) Variation in the hydraulic conductivity of 4 mm shingle, with sand admixture; (b) the same data, but with a semi-log abscissa

size, shape and packing. The addition of even a small number of significantly larger grains means that the fluid must take a longer and more tortuous path around the obstacles.

9.11 Conclusions from Measured and Modelled Water Table Fluctuations

- The GRIST I model predicted adequately the location and timing of a seepage face development, during a spring tide of 4.5 m across the mixed sand/shingle barred profile at Morfa Dyffryn. No calibration was required; hence, the model is *not* site specific.

- The occurrence of a water table outcrop near the break of slope is more a function of the hydraulic conductivity, than the mixed beach profile; lower hydraulic conductivity values predicted a seepage zone higher up the profile. This result contrasts with Turner's (1993*b*, *c*; 1995*a*, *b*) suggestion that the position of the outcrop determines the location of the intertidal break of slope, common on macro-tidal beaches, by denominating two differing swash regimes on either side of the break of slope (Section 2.4.11). This particular explanation does not hold for a mixed beach; similarly, it is probably not valid for a ridge and runnel beach. The beaches investigated by Turner (*op. cit.*) were generally plane and sandy with the seepage zone remaining at the break of the slope throughout most of the tidal cycle. On a mixed, macro-tidal beach (such as Morfa Dyffryn), the break of slope occurs much higher up the intertidal profile and, therefore, does not mark the boundary between different surface saturation regimes. Instead, the break of slope at the toe of a mixed beach divides two contrasting hydrodynamic regimes, one dissipative and one reflective.

- The series of ridges and runnels distorts the cross-shore drainage pattern. In this region, where all parameters can be considered constant *(i.e. K, s* and boundary conditions) the micro-topography is the controlling factor for the seepage face location, but it does not involve a break of slope.

- The sand fraction continued to determine the response of the water table from D5 seaward, as indicated by the use of K for a medium sand deposit.

CHAPTER 10: DISCUSSION AND CONCLUSIONS

10.1 Mean Currents and Sediment Transport on a Macro-tidal Beach

The results of this research demonstrate that the effect of a high tidal range is not confined merely to "smoothing" out the beach profile, by progressively changing the location and period for which each section of the beach profile is subject to shoaling waves, surf and swash zone processes, but implies that the whole rationale of storm-dominated sediment transport does not necessarily apply to macro-tidal beaches. Mean currents dominated suspended sediment transport at Morfa Dyffryn, in common with other macro-tidal beaches at Nieuwpoort-aan-Zee (Voulgaris & Collins, 1996) and, in general, at Spurn Head (Davidson *et al.*, 1993). Hence, mean currents (whether tidally- or wave-induced) have an important rôle in the sediment transport regime in both the cross- and longshore directions, over the whole of the intertidal profile. Such currents can be responsible for significant quantities of sediment transport even on a dissipative beach, under relatively mild conditions.

Moreover, although almost totally responsible for net longshore sediment transport, the effect of the mean longshore current is not confined *only* to longshore transport; velocity moment analysis identified that once the current exceeds about 0.3 ms^{-1} it can make as significant a contribution to mobilising sediment for cross-shore transport as do the short waves. This conclusion applied similarly to bedload, which is seldom measured in the field. It must be emphasized that such high currents are not atypical of macro-tidal beaches and that tidally-generated longshore currents can be considerable both inside and outside the surf zone. Therefore, the importance of longshore currents is not restricted to surf zone longshore currents generated by oblique waves or by moderate or storm conditions.

The results obtained from the velocity moment analysis also indicate the possibility that the vertical velocity structure can lead to bedload and suspended load becoming decoupled at some stages of the tidal cycle, when short wave-induced suspended transport is onshore, whilst the mean currents transport bedload offshore. More importantly, perhaps, analysis of the velocity moments showed that cross-shore bedload transport increases with decreasing water depth, particularly in water shallower than 0.4 m. This prediction was validated by the measurement of suspended sediment transport which, with the exception of the high rates of transport at the start of the ebb

during Tide 29, was highest in shallow water. Consequently, the tidal signature in the sediment transport patterns is evident: enhanced transport is associated with the early flood phase and late in the ebb tide. It is of importance also that the direction of the high cross-shore mean currents tended to be onshore in shallow water. Thus, the inability of existing instrumentation to measure in shallow water remains a serious obstacle to integrating sediment transport over a tidal cycle. This limitation was illustrated at Nieuwpoort, where tracer experiments and a comparison of changes in beach profile indicated general net onshore transport over the tide, whilst the hydrodynamic and suspended sediment data revealed net offshore transport due primarily to undertow (Voulgaris *et al.*, 1997).

10.2 Tidal Asymmetry in Sediment Transport

The flood/ebb asymmetry in the mean currents and, in particular, subsequent wind/current interaction has important implications for morphodynamic and sediment transport modelling on beaches with a large tidal range. An asymmetry in suspended sediment transport appears to be a feature of macro-tidal beaches (although it was not observed in the same manner at Nieuwpoort). The cause of the asymmetry at Morfa Dyffryn was attributed to a change in the direction of resolved mean currents, rather than an increase in oscillatory and mean velocities after the turn of the tide, as occurred at Spurn Head (Davidson *et al.*, 1993). However, the extremely high suspended sediment concentrations resulting from the bedform destruction was the same at both locations. Thus, overall sediment transport patterns may be influenced strongly by the result of relatively high quantities of sediment in suspension, for a relatively limited part of the tidal cycle; this would then be available for transport by the mean currents, which may or may *not* be symmetrical about High Water.

Tidal asymmetry in the mean longshore current velocity will also differentially affect tidally-integrated sediment transport, depending upon the offshore tidal regime. At Nieuwpoort, the highest longshore currents were at the beginning of the flood and diminished through tide; the pattern was reversed at Morfa Dyffryn. Hence, different sections of the beach profile will be subjected to the possibility of suspended sediment transport being enhanced by strong longshore currents, depending upon the nature of the offshore tidal currents.

A third factor is the observed translation of an offshore progressive tidal wave into a nearshore standing tidal wave, during spring tides. Given the importance of tidally-generated longshore currents nearshore (discussed above), this implies that longshore sediment transport can be in different directions at different locations across the beach profile. For example, when the tidal wave is standing in character, the net transport due to tidally-induced longshore currents will be zero, since the current direction and strength is symmetrical about High Water. If the tidal wave is progressive, the upper part of the beach can incur net (essentially unidirectional) tidally-induced longshore transport in the direction of propagation of the tidal wave. This mechanism for longshore transport was identified elsewhere by Wilkinson (1980), but has received little attention before or since. A consequence is that, on macro-tidal beaches, the direction of longshore sediment transport may be different over the upper and lower parts of the intertidal zone.

Furthermore, since the tidal influence on current conditions is distinctive, the spring-neap tidal cycle is also crucial to the sediment transport regime. At Morfa Dyffryn, the intertidal zone to landward of the main ridge was subject to these tidally-induced currents during the (7) tides prior to the highest spring tide of the cycle, and presumably the following (7) tides. Hence, the enhancement/opposition of wave-induced currents by a tidal component should be considered for sediment transport during these tides; for the remaining neap tides, the tidal component is of less importance in this zone and wind-wave processes will dominate.

10.3 Sediment Transport Predictions

An important conclusion from the research undertaken here is that, for macro-tidal beaches, where mean currents dominate sediment transport processes, sediment transport rates are unlikely to be well characterised by use of significant wave height to represent the energy available for sediment transport in the CERC-type longshore transport formulæ (of which eqn. 10.2 is an example). In fact, oscillatory current energy is often higher than is represented by the sea surface elevation and an average of these two types of energy would provide a more accurate measure of the nearshore energy available for the transport of sediment, than the use of significant wave height alone.

The k coefficient produced from most field studies empirically relates the wave energy flux to measured bulk sediment transport rates and thus, inherently (if

inadvertently) includes the influence of currents at the field site. However, the outcome is that the k value could be significantly altered by variations in current conditions, which are not represented by the wave energy flux. In particular, sediment transported by tidally-generated mean currents is not accounted for in the analysis. Effectively, this restricts each k value to the site for which it was developed, unless the current conditions can be shown to be similar, or unless variations in tidally-generated currents can be incorporated into the CERC-type equations. Indeed, this was the case for the original derivation of Komar & Inman (1970):

$$I_l = k\,(EC_n)_b \cos\theta_b \frac{<v_l>}{U_m} \tag{10.1}$$

where I_l is the immersed weight sediment transport rate, $(EC_n)_b$ is the wave energy flux at the breakers, θ_b is the angle of incidence of the waves at the breakers, U_m is wave orbital velocity and $< v_l >$ is a longshore current of unspecified origin (Wilkinson, 1980). Only by the assumption that the longshore currents are wave-induced, does (10.1) revert to the more familiar:

$$I_l = k\,(EC_n)_b \sin\theta_b \cos\theta_b \tag{10.2}$$

However, the value of k produced by (10.1) and (10.2) will not be the same, even for the same field site, if tidally-generated longshore currents persist into the surf zone.

The prediction of gross sediment transport, using the Bailard formula, has been found to be reasonably successful for macro-tidal beaches; this is due mainly to the predominance of the mean flows, both cross- and longshore, over oscillatory flow (Foote, 1994; Voulgaris *et al.*, 1996). For shingle beaches, the influence of the mean currents may be of less importance, given the high threshold of motion for larger sediment. However, on macro-tidal sandy beaches, velocity moment analysis suggests that strong tidal longshore currents can both suspend and mobilise sediment. Accordingly, the Bailard-type equations (which predict sediment transport rates from the total velocity field) are likely to be better predictors of sediment transport for macro-tidal beaches with short-fetched seas, than the CERC-type (wave energy flux) equations. The Bailard equations have other advantages: (i) they also include some measure for grain size (through fall velocity) and beach slope. These two parameters are likely to be of

significance on shingle beaches although, to the author's knowledge, the Bailard equations have never been applied to, or "calibrated" for sediment transport predictions on shingle or mixed beaches; (ii) the results are usually a time average of anything from a few wave periods to 18 or 30 min. Hence, the resultant sediment transport can be integrated over the tidal cycle to account for asymmetries in the mean currents and variations in net longshore transport induced by any deviation from a standing tidal wave.

10.4 What is Different about a Mixed Beach?

The implications of tidally-induced currents for sediment dynamics (given above), will apply to many macro-tidal beaches around the UK, particularly those with wide, dissipative intertidal and sub-tidal sections; these permit the relative dominance of currents over waves, regardless of sediment composition. However, an examination of two of the ways in which the distinctive sedimentary characteristics of a composite mixed beach interact with the hydrodynamic regime (tidally-induced groundwater fluctuations and wave reflection) have demonstrated that there is no clear sand <==> mixed <==> shingle beach continuum.

The measured groundwater response of the mixed sand/shingle beach was not significantly different to that of a sand beach. This conclusion suggests that if a mixed sand/shingle layer exists at a depth below the surface which is higher than the tidally-induced fluctuation of the water table, then the shingle will not fulfill its "rôle" in dissipating its energy through percolation (although energy will still be lost through friction at the sediment/water interface).

Although steep berms can form on shingle beaches, the higher hydraulic conductivity permits greater energy dissipation (through infiltration and non-Darcian flow) than occurs on similarly steep mixed beaches, where even a 20% sand content reduces the hydraulic conductivity by an order of magnitude. Nonetheless, the tidally-induced fluctuations in the groundwater table, over such a complex sedimentary structure, can be modelled successfully using the single value of hydraulic conductivity for medium sand. This observation suggests that the main impact of the shingle fraction is not on the groundwater behaviour, but through the beach gradient and its subsequent influence on wave reflection. Ultimately then, the major significance of the sand/shingle mixture for the morphodynamic response of the ridge is through its ability to maintain a steeper

slope, than would be achieved by a beach consisting of sand alone. Hence, the abrupt change in beach gradient has more impact on the hydrodynamics, than does the sediment composition.

The steep gradient which the shingle fraction is able to support increases reflection of swell waves, greatly in excess of that from unrestrained sand beaches. The differential response of the sections of different sediment composition, together with the likely consequences for suspended sediment transport are listed in Table 10.1.

Beach type	Reflection		Hydraulic conductivity (dissipation through percolation)	Effect on suspended sediment transport
Shingle	Moderate (maximum 60% ?)		High	Moderate
Mixed sediment	Swell wave	High	Low	Enhanced
	Wind wave	Moderate		
Sand	Swell wave	Low	Low	Low
	Wind wave	Low		

Table 10.1 Possible consequences of sediment composition on suspended sediment transport from beaches of various sediment types

In summary, the mixed sand/shingle beach reflects more energy than a sandy beach and dissipates less energy through infiltration than a shingle beach. Both factors have been examined here in the cross-shore direction only, but the likely implication is that sediment mobility may be enhanced in comparison to either a purely sand or shingle beach. The subsequent net transport is determined by the wave- and tidally-induced mean currents, cross- and alongshore on this macro-tidal beach.

Swell waves are generally thought of as "constructive", but the consequences for sediment transport by swell waves may be different for mixed beaches. On such beaches, the breaker zone can advance closer to the shoreline, with less energy dissipation across

the surf zone than would be the case on a flatter sandy beach. Low energy swell waves have been recognised as a significant contributor to longshore sediment transport (Whitcombe, 1995; Powell, 1996) and, since their reflection was proportional to beach gradient, the influence of the steep sand/shingle bank for wave reflection at Morfa Dyffryn is crucial (particularly during mild conditions). The waves and currents encountered during the experimental period are not atypical of the average seasonal conditions for the whole of Cardigan Bay and, since composite beaches form a considerable proportion of the coastline of the Bay, the influence of the shingle ridge may contribute significantly to the overall sediment dynamics of the nearshore region.

10.5 Implications for Beach Replenishment Schemes

There are important implications from the results of the research described herein, for beaches replenished artificially with shingle *e.g.* Hayling Island (Hampshire) and Seaford (East Sussex). Such schemes are designed generally as replenished shingle beaches, although the borrow material consists rarely of pure shingle, but is dredged from offshore and contains a proportion of sands and fines. The rapid and unforeseen "cliffing" (formation of near-vertical walls), observed on replenished beaches (McFarland *et al.*, 1996), has been attributed to the combined effects of compaction and cementation. However, the response of a natural mixed beach suggests that the additional sands and fines content may be the controlling factor in the profile response of the replenished beach, by severely reducing energy losses through infiltration. The laboratory hydraulic conductivity tests on sand/shingle mixtures suggest that the shingle content should be in excess of 80 to 90%, to increase energy losses through percolation.

10.6 Conclusions

- The nearshore wave field itself is insufficient either to characterise or to predict sediment transport on a macro-tidal beach; current information is needed in addition.

- Mean currents dominate the suspended sediment transport, in common with other macro-tidal beaches. High sediment transport rates can occur in the absence of storm conditions.

- Tidally-induced longshore currents can persist into the surf zone.

- A tidal signature was present in the mean currents and suspended sediment transport (both cross- and alongshore). Therefore, observations from shallow water are needed for tidally-integrated sediment transport.

- Sediment transport due to swell waves need not be essentially "constructive" *i.e.* onshore, on mixed/ shingle beaches since swell wave reflection increases with beach gradient.

10.7 Future Work

The conclusions concerning swell wave reflection should be extended to include a wider variety of hydrodynamic conditions than occurred at Morfa Dyffryn (during the experimental period). Reflection should be verified also against similar field data from shingle beaches; none exists at present, to the author's knowledge. Although the field and laboratory data concerning reflection from porous structures is informative, there remains one major difference - porous breakwaters are not potentially mobile and, hence, energy dissipated in transporting sediment is not considered.

Similarly, the consequences of beach groundwater fluctuations for sediment transport are increasingly being recognised and high frequency measurements of pore pressure gradients are required, to establish whether the high, reversing, vertical gradients recently observed on sand beaches, can occur on either mixed or shingle beaches.

The effects of tidal currents on sediment transport in the nearshore zone of macro-tidal beaches should be investigated further; in particular, the tidal translation landwards from a progressive to a standing wave may have important consequences for net sediment transport across different sections of the intertidal zone. It is necessary, therefore, for medium term morphodynamic sediment transport models to integrate the transport both over a single tide and over a spring/neap cycle. Such research will involve an extensive cross-shore array of current meters and deployment periods which incorporate spring and neap tides.

REFERENCES

Allen P M & Jackson A A (1985). Geology of the country around Harlech, British Geological Survey, HMSO.

Aseervatham A M, Kang H Y & Nielsen P (1993). Groundwater movement in beach watertables. *Proceedings of the 11th Australasian Conference on Coastal and Ocean Engineering*; 589-594.

Bagnold R A (1963). Mechanics of marine sedimentation. In: The Sea Vol III, Interscience, New York.

Bagnold R A (1966). An approach to the sediment transport problem from general physics. *US Geological Survey, Professional Paper*, 422-I.

Bailard J A (1981). An energetics total load sediment transport model for a plane sloping beach. *Journal of Geophysical Research,* 86; 10938-10954.

Baird A J & Horn D P (1996). Monitoring and modelling groundwater behaviour in sandy beaches. *Journal of Coastal Research,* 12; 630-640.

Baird A J, Mason T & Horn D P (1996). Mechanisms of beach ground water and swash interaction. *Proceedings of the 25th International Conference on Coastal Engineering,* American Society of Civil Engineers; 4120-4133.

Baird A J, Mason T & Horn D P (1997). Validation of a beach ground water model. *Marine Geology* (submitted).

Barry D A, Barry S J & Parlange J-Y (1996). Capillarity correction to periodic solutions of the shalow flow approximation. Mixing in Estuaries and Coastal Seas, Coastal and Estuarine Studies, Volume 50; 496-510.

Battjes J A (1974). Surf similarity. *Proceedings of the 14th International Conference on Coastal Engineering*, American Society of Civil Engineers; 466-479.

Beach R A (1989).

Beach R A & Sternberg R W (1991). Infragravity driven suspended sediment transport in the swash, inner and outer-surf zone. *Proceedings of Coastal Sediments '91*, American Society of Civil Engineers; 114-128.

Benoit M & Teisson C (1994). Laboratory study of breakwater reflection - effect of wave obliquity, wave steepness and mound slope. *International Symposium: Waves - physical and numerical modelling.* Canadian Society of Civil Engineers; 1021-1030.

Bird P A D, Davidson M A, Bullock G N & Huntley D A (1994). Wave measurement near reflective structures. *Proceedings of Coastal Dynamics '94*, American Society of Civil Engineers; 701-711.

Bird P A D, Davidson M A, Ilic S, Bullock G N, Chadwick A J, Axe P and Huntley D A (1996). Wave reflection, transformation and attenuation characteristics of rock island breakwaters. Advances in Coastal Structures and Breakwaters ed. J E Clifford, Thomas Telford; 93-109.

Bishop C T & Donelan M A (1987). Measuring waves with pressure transducers. *Coastal Engineering*, 11; 309-328.

Bluck B J (1967). Sedimentation in beach gravels: examples from South Wales. *Journal of Sedimentary Petrology*, 37; 128-156.

Boussinesq J (1904). Recherches théoriques sur l'ecoulement des nappes d'eau infiltrées dan le sol et sur le débit des sources. *Journal de Mathématiques Pures et Appliquées*, 10; 5-78.

Bowen D Q (1977). The Quaternary History of the Irish Sea Editors: C Kidson & M J Tooley, Seel House Press, Liverpool;223-256.

Bradbury A P (1995). The hydrodynamic response of shingle beaches to wave attack with particular reference to eastern Christchurch Bay. Unpubl. Mphil/PhD upgrading report. Department of Oceanography, University of Southampton.

Bradbury A P & Powell K A (1992). The short term profile response of shingle spits to storm wave action. *Proceedings of the 23rd International Conference on Coastal Engineering*, American Society of Civil Engineers; 2694-2707.

British Standards Institution (1990). Methods of test for soils for civil engineering purposes. BS1377. British Standards Institution, London.

Bujalesky G G & González-Bonorino G (1991). Gravel spit stabilized by unusual (?) high-energy wave climate in Bay Side, Tierra del Fuego. *Proceedings of Coastal Sediments '91*, American Society of Civil Engineers; 960-974.

Caldwell N E & Williams A T (1985). The use of beach profile configuration in discrimination between differing depositional environments affecting coarse clastic beaches. *Journal of Coastal Research*, 1; 129-139.

Carter R W G (1988). Coastal Environments. Academic Press.

Carter R W G & Orford J D (1984). Coarse clastic beaches: a discussion of the distinctive dynamic and morphosedimentary features. *Marine Geology*, 60; 377-389.

Carter R W G & Orford J D (1991). The sedimentary organisation and behaviour of drift-aligned gravel barriers. *Proceedings of Coastal Sediments '91*, American Society of Civil Engineers; 934-948.

Carter R W G & Orford J D (1993). The morphodynamics of coarse clastic beaches and barriers: a short- and long-term perspective. *Journal of Coastal Research*, 15; 158-179.

Carter R W G, Jennings S C & Orford J D (1990). Headland erosion by waves. *Journal of Coastal Research*, 6; 517-529.

Carter R W G, Johnson T W & Orford J D (1984). Stream outlets through mixed sand and gravel coastal barriers; examples from southeast Ireland. *Zeitschrift für Geomorphologie*, Neue Folge 28; 427-442.

Carter R W G, Forbes D L, Jennings S C, Orford J D, Shaw J & Taylor R B (1989). Barrier and lagoon coast evolution under differing relative sea-level regimes: examples from Ireland and Nova Scotia. *Marine Geology*, 88; 221-242.

Carter R W G, Orford J D, Forbes D L & Taylor R B (1990). Morphosedimentary development of drumlin-flank barriers with rapidly rising sea level, Stony Head, Nova Scotia. *Sedimentary Geology*, 69; 117-138.

Chadwick A J, Pope D J, Borges J & Ilic S (1995). Shoreline directional wave spectra Part 2. Instrumentation and field measurements. *Proceedings of the Institution of Civil Engineers, Water, Maritime & Energy*, 112; 209-214.

Chappell J, Eliot I G, Bradshaw M P & Lonsdale E (1979). Experimental control of beach face dynamics by water-table pumping. *Engineering Geology*, 14; 29-41.

Clarke D J & Eliot I G (1987). Groundwater-level changes in a coastal dune, sea level fluctuations and shoreline movement on a sandy beach. *Marine Geology*, 77;

319-326.

Cornish V (1898). On sea beaches and sand banks. *Geology*, 2; 628-674.

D & A Instruments (1988). Optical Backscatterance Sensor Manual, Rev. 8/88.

Davidson M A (1992). Implementation of linear wave theory in the frequency domain for the conversion of sea bed pressure to surface elevation. School of Civil and Structural Engineering Internal Report 92/008, University of Plymouth.

Davidson M A, Bird P A D, Bullock G N & Huntley D A (1994). Wave reflection: field measurements, analysis and theoretical developments. *Coastal Dynamics '94,* American Society of Civil Engineers; 642-655.

Davidson M A, Bird P A D, Bullock G N & Huntley D A (1996). A new non-dimensional number for the analysis of wave reflection from rubble mound breakwaters. *Coastal Engineering*, 28; 93-120.

Davidson M A, Russell P E, Huntley D A & Hardisty J (1993). Tidal asymmetry in suspended sand transport on a macrotidal intermediate beach. *Marine Geology*, 110; 333-353.

Davidson M A, Russell P E, Huntley D A, Hardisty J & Cramp A (1992). An overview of the British Beach and Nearshore Dynamics (B-BAND) programme. *Proceedings of the 23rd International Conference on Coastal Engineering*, American Society of Civil Engineers; 1987-2000.

Davies J L (1964). A morphogenic approach to world shorelines. *Zeitschrift f□r Geomorfologie*, Neue Folge, 8; 127-142.

Diggle P J (1990). Time Series: a biostatistical introduction Oxford University Press.

Diserens A P & Coates T T (1993). UK South Coast shingle beach study: storm response of shingle beaches. HR Wallingford Report SR 323.

Doering J C & Bowen A J (1987). Skewness in the nearshore zone: a comparison of estimates from Marsh-McBirney current meters and colocated pressure sensors. *Journal of Geophysical Research*, 92 (C12); 13173-13183.

Dominick T F, Wilkins B & Roberts H (1971). Mathematical model for beach groundwater fluctuations. *Water Resources Research*, 7; 1626-1635.

Downing J P & Beach R A (1989). Laboratory apparatus for calibrating optical suspended solid sensors. *Marine Geology*, 86; 243-249.

Downing J P, Sternberg R W & Lister C R B (1981). New instrumentation for the investigation of sediment suspension processes in the shallow marine environment. *Marine Geology*, 42; 19-34.

Draper L (1991). Wave climate altas of the British Isles. Department of the Environment, Offshore Technology Report. HMSO.

Duncan J R (1964). The effects of water table and tide cycle on swash backwash sediment distribution and beach profile development. *Marine Geology*, 2; 186-197.

Elgar S, Guza R T & Freilich M H (1988). Eulerian measurements of horizontal accelerations in shoaling gravity waves. *Journal of Geophysical Research*, 93 (C8); 9261-9269.

Elgar S, Herbers T H C & Guza R T (1994). Reflection of ocean surface gravity waves from a natural beach. *Journal of Physical Oceanography*, 24; 1503-1511.

Eliot I G & Clarke D J (1986). Minor storm impact on the beachface of a sheltered sandy

beach. *Marine Geology*, 73; 61-83.

Eliot I G & Clarke D J (1988). Semi-diurnal variation in beachface aggradation and degradation. *Marine Geology*, 79; 1-22.

Emery K O & Foster J F (1948). Water tables in marine beaches. *Journal of Marine Research*, 7; 644-654.

Erickson N J (1970). Measurement of tide induced changes to water table profiles in coarse and fine sand beaches along Pegasus Bay, Canterbury. *Earth Sciences Journal*, 4; 24-31.

Evans C D R (1995). Geology and Physical Environment. In: Coasts and Seas of the UK Region 12. Wales: Margam to Little Orme. Editors J H Barne, C F Robson, S S Kaznowska & J P Doody, Joiint Nature Conservancy Council, Peterborough; 19-47.

Fang C S, Wang S N & Harrison W (1972). Groundwater flow in a sandy tidal beach. Two-dimensional finite element analysis. *Water Resources Research*, 8; 121-128.

Ferguson R I, Prestegård K L & Ashworth P J (1989). Influence of sand on hydraulics and gravel transport in a braided gravel bed river. *Water Resources Research*, 25; 635-643.

Fetter C W (1994). Applied Hydrogeology. Prentice-Hall.

Finkelstein K (1982). Morphological variations and sediment transport in crenulate-bay beaches, Kodiak Island, Alaska. *Marine Geology*, 47; 261-281.

Folk R L & Ward W C (1957). The Brazos River Bar: a study in the significance of grain size parameters. *Journal of Sedimentary Petrology*, 27; 3-26.

Foote Y L M (1994). Waves, currents and sand transport predictors on a macro-tidal beach. Unpubl. PhD thesis, Institute of Marine Studies, University of Plymouth.

Frigård P & Brorsen M (1995). A time-domain method for separating incident and reflected irregular waves. *Coastal Engineering*, 24; 205-215.

Garrard R A (1977). The Quaternary History of the Irish Sea Editors: C Kidson & M J Tooley, Seel House Press, Liverpool; 69-72.

Gillham R W (1984). The capillary fringe and its effect on water-table response. *Journal of Hydrology*, 67; 307-324.

Gillott P W K & Southgate H N (1996). A one component spectral model for low frequency waves. HR Wallignford Report TR1, April 1996.

Goda Y & Suzuki Y (1976). Estimation of incident and reflected waves in random wave experiments. *Proceedings of the 15th International Conference on Coastal Engineering*, American Society of Civil Engineers; 828-865.

Gourlay M R (1992). Wave set-up, wave run-up and beach water table: interaction between surf zone hydraulics and groundwater hydraulics. *Coastal Engineering*, 17; 93-144.

Grant U S (1946). Effect of ground-water table on beach erosion. *Bulletin of the Geological Society of America*, 57; 1252.

Grant U S (1948). Influence of the water table on beach aggradation and degradation. *Journal of Marine Research*, 7; 655-660.

Greenwood B & Osborne P D (1990). Vertical and horizontal structure in cross-shore flows: an example of undertow and wave set-up on a barred beach. *Coastal*

Engineering, 14; 543-580.

Greenwood B, Osborne P D & Bowen A J (1991). Measurements of suspended sediment transport: prototype shorefaces. *Proceedings of Coastal Sediments '91*, American Society of Civil Engineers; 284-299.

Grochowski N T L (1995). (Re)suspension of fine grained sediments by currents and waves. Unpubl. Mphil/PhD Upgrading Report, Department of Oceanography, University of Southampton.

Guza R T & Bowen A J (1976). Resonant interacions for waves breaking on a beach. *Proceedings of the 15th International Conference on Coastal Engineering*, American Society of Civil Engineers; 560-577.

Guza R T & Thornton E B (1985). Velocity moments in nearshore. *Journal of Waterway, Port, Coastal & Ocean Engineering*, 111; 235-256.

Guza R T, Thornton E B & Holman R A (1984). Swash on steep and shallow beaches. *Proceedings of the 19th International Conference on Coastal Engineering*, American Society of Civil Engineers; 708-723.

Hanes D M (1988). Intermittent sediment suspension and its implications to sand tracer dispersal in wave-dominated environments. *Marine Geology*, 81; 175-183.

Hanes D M (1990). The structure of events of intermittent suspension of sand due to shoaling waves. In: B Le Méhauté and D M Hanes (Editors) The Sea, Volume 9, Part B; 941-952.

Hanes D M & Huntley D A (1986). Continuous measurements of suspended sand concentration in a wave dominated nearshore environment. *Continental Shelf Research*, 6; 585-596.

Harrison W (1969). Empirical equations for foreshore changes over a tidal cycle. *Marine Geology*, 7; 529-551.

Harrison W & Boon J D (1972). Beach water table and beach-profile measuring equipment. *Shore & Beach,* 40; 26-33.

Harrison W, Fang C S & Wang S N (1971). Groundwater flow in a sandy tidal beach 1. One-dimensional finite element analysis. *Water Resources Research*, 7; 1313-1322.

Hazen D G, Greenwood B & Bowen A J (1990). Nearshore current patterns on barred beaches. *Proceedings of the 22nd International Conference on Coastal Engineering*, American Society of Civil Engineers; 2061-2072.

Heathershaw A D, Carr A P, Blackley M W L & Wooldridge C E (1981). Tidal variations on the compaction of beach sediments. *Marine Geology*, 41; 223-228.

Hegge B J & Masselink (1991). Groundwater-table responses to wave run-up: an experimental study form Western Australia. *Journal of Coastal Research*, 7; 623-634.

Herruel B (1994). Création et mise au point d'un système de mesure du niveau de l'eau dans le sol des plages. Rapport de stage de fins d'études pour l'obteration du diplôme de Technicien Supérieur de la mer. Institut National des Sciences et Techniques de la Mer.

Hill P R (1990). Coastal geology of the King Point Area, Yukon Territory, Canada. *Marine Geology*, 91; 93-111.

Hillel D (1982). Introduction to Soil Physics. Academic Press.

Holmes P, Baldock T E, Chan R T C & Neshaei M A L (1996). Beach evolution under random waves. *Proceedings of the 25th International Conference on Coastal Engineering*, American Society of Civil Engineers; (in press).

Hughes S A (1993). Laboratory wave reflection analysis using co-located gages. *Coastal Engineering*, 20; 223-247.

Hunt J N (1979). Direct solution of wave dispersion equation. *Journal of Waterway, Port, Coastal and Ocean Division*, 105; 457-459.

Huntley D A (1976). Long-period waves on a natural beach. *Journal of Geophysical Research*, 81; 6441-6449.

Huntley D A (1991). Beach response to waves and currents - detailed field measurements. Proceedings, Developments in Coastal Engineering, University of Bristol Press; 101-110.

Huntley D A (1996). Long period motion and wave reflection. *In*: BA O'Connor (Editor), Circulation and Sediment Transport Around Banks (CSTAB) Handbook, Department of Civil Engineering, University of Liverpool; 485-495.

Huntley D A & Hanes D M (1987). Direct measurement of suspended sediment transport. *Proceedings of Coastal Sediments '87*, American Society of Civil Engineers; 723-737.

Huntley, D A, Simmonds D J & Davidson M A (1995). Estimation of frequency-dependent reflection coeffficients using current and elevation sensors. *Coastal Dynamics ,95,* American Society of Civil Engineers; 57-68.

Huntley D A, Davidson M, Russell P, Foote Y & Hardisty J (1993). Long waves and sediment movement on beaches: recent observations and implications for modelling. *Journal of Coastal Research*, Special Issue 15; 215-229.

Hydrographer of the Navy (1992). Admiralty Tidal Stream Atlas Irish Sea and Bristol Channel. NP 256.

Hydrographer of the Navy (1996*a*). Admiralty Tide Tables Vol 1 European Waters including the Mediterranean Sea. NP 210-96.

Hydrographer of the Navy (1996*b*). West Coasts of England and Wales Pilot. NP37.

Inman D L (1949). Sorting of sediments in the light of fluid mechanics. *Journal of Sedimentary Petrology*, 19; 51-70.

Inman D L & Bagnold R A (1963). Littoral processes. In: M N Hill (Editor), The Sea. Interscience, New York.

Isaacs P D & Bascom W N (1949). Water table elevations in some Pacific coast beaches. *Transactions of the American Geophysical Union*, 30; 293-294.

Isaacson M (1991). Measurement of regular wave reflection. *Journal of Waterway, Port, Coastal and Ocean Engineering*, 117; 533-569.

Isla F I (1993). Overpassing and armouring phenomena on gravel beaches. *Marine Geology*, 110; 369-376.

Jacob C E (1940). On the flow of water in an elastic artesian aquifer. *Transactions of the American Geophysical Union*, 21; 574-586.

Jaffe B, Sternberg R W & Sallenger A (1984). The role of suspended sediment in shore-normal beach profile changes. *Proceedings of the 19th International Conference on Coastal Engineering*, American Society of Civil Engineers; 1983-1996.

Joint Nature Conservancy Council (1995).

Kajima R (1969). Estimation of incident wave spectrum in the sea area influenced by reflection. *Coastal Engineering in Japan,* 12; 9-16.

Kang H-Y & Nielsen P (1994). Wave runup and the coastal watertable. *Proceedings of the International Conference on Hydraulics in Civil Engineering*; 283-286.

Kang H-Y, Nielsen P & Hanslow DJ (1994*a*). Watertable overheight due to wave runup on a sandy beach. *Proceedings of the 24th International Conference on Coastal Engineering*, American Society of Civil Engineers; 2115-2124.

Kang H-Y, Aseervatham A M & Nielsen P (1994*b*). Field measurements of wave runup and the beach watertable. Research Report No CE148, Department of Civil Engineering, University of Queensland.

Kirk R M (1969). Beach erosion and coastal development in the Canterbury Bight. *New Zealand Geographer*, 25; 23-35.

Kirk R M (1970). Swash zone processes: an examination of water motion and the relations between water motion and foreshore response on some mixed sand and shingle beaches, Kaikoura, New Zealand. PhD thesis, Department of Geography, University of Christchurch, New Zealand.

Kirk R M (1975*a*). Coastal changes at Kaikoura 1942-74, determined from air photographs. *New Zealand Journal of Geology and Geophysics*, 18; 787-801.

Kirk R M (1975*b*). Aspects of surf and runup processes on mixed sand and gravel beaches. *Geografiska Annaler*, 57A; 117-133.

Kirk R M (1980). Mixed sand and gravel beaches: morphology, processes and sediments. *Progress in Physical Geography*, 4; 189-210.

Kirk R M (1992). Experimental beach reconstruction - renourishment on mixed sand and gravel beaches, Washdyke Lagoon, South Canterbury, New Zealand. *Coastal Engineering*, 17; 253-277.

Kirk R M, Owens I F & Kelk J G (1977). Coastal dynamics, east coast of New Zealand, South Island. *Third Australian Conference on Coastal and Ocean Engineering*, Melbourne; 240-244.

Kirkham D (1967). Explanation of paradoxes in Dupuit-Forchheimer seepage theory. *Water Resosurces Research*, 3; 609-622.

Kobayashi N & Wurjanto A (1992). Irregular wave interaction with permeable slopes. *Proceedings of the 23nd International Conference on Coastal Engineering*, American Society of Civil Engineers; 1299-1312.

Kobayashi N, Cox D T & Wurjanto A (1991). Permeability effects on irregular wave runup and reflection. *Journal of Coastal Research*, 7; 127-136.

Kobayashi N, Tega Y & Hancock M W (1996). Wave reflection and overwash of dunes. *Journal of Waterway, Port, Coastal and Ocean Engineering,* 122; 733-950.

Komar P D (1976). Beach Processes and Sedimentation Prentice Hall, Englewood Cliffs, New Jersey.

Komar P D (1978). Relative quantities of suspension versus bed-load transport on beaches. *Journal of Sedimentary Petrology*, 48; 921-932.

Komar P D & Inman D L (1970). Longshore sand transport on beaches. *Journal of Geophysical Research*, 75 (C30); 5914-5927.

Kraus N C (1987). Application of portable traps for obtaining point measurements of sediment transport rates in the surf zone. *Journal of Coastal Research*, 3; 139-

152.

Kubota S, Mizuguchi M & Takezawa M (1990*a*). Reflection from swash zone on natural beaches. *Proceedings of the 22nd International Conference on Coastal Engineering*, American Society of Civil Engineers; 570-583.

Kubota S, Mizuguchi M & Takezawa M (1990*b*). A field study of swash oscillation on a gentle beach face. *4th Pacific Congress on Marine Science and Technology*; 282-289.

Kubota S, Mizuguchi M & Takezawa M (1993). Prediction of field swash and reflected wave distributions. *Coastal Engineering in Japan*, 36; 111-131.

Landon J R (1991). Booker Tropical soil Manual (editor). Longman Scientific & Technical.

Lanyon J A, Eliot I G & Clarke D J (1982*a*). Groundwater-level variation during semidiurnal spring tidal cycles on a sandy beach. *Australian Journal of Marine and Freshwater Research*, 33; 377-400.

Lanyon J A, Eliot I G & Clarke D J (1982*b*). Observations of shelf waves and bay seiches from tidal and beach groundwater level records. *Marine Geology*, 49; 23-42.

Lewandowski A & Zeidler R B (1978). Beach ground-water oscillations. *Proceedings of the 16th International Conference on Coastal Engineering*, American Society of Civil Engineers; 2051-2065.

Li L, Barry D A, Parlange J-Y & Pattiarachi C B (1996*a*). Beach water table fluctuations due to wave run-up: capillarity effects. *Water Resources Research*

Li L, Barry D A & Pattiarachi C B (1996*b*). Modeling coastal ground-water response to beach dewatering. *Journal of Waterway, Port, Coastal and Ocean Engineering,* 122; 273-280.

Li L, Barry D A & Pattiarachi C B (1996*c*). Numerical modelling of tide-induced water table fluctuations. *Coastal Engineering*,

Longuet-Higgins M S & Parkin D W (1962). Sea waves and beach cusps. *Geographical Journal*, 128; 194-220.

Madsen O S & Grant W D (1976). Sediment transport in the coastal environment. Ralph M Parsons Laboratory, Massechusetts Institute of Technology Report No. 209.

Mansard E P D & Funke E R (1980). Estimation of incident and reflected spectra using a least squares method. *Proceedings of the 17th International Conference on Coastal Engineering*, American Society of Civil Engineers; 154-172.

Masselink G & Black K P (1995). Magnitude and cross-shore distribution of bed return flow measured on natural beaches. *Coastal Engineering*, 25; 165-190.

Masselink G & Short A D (1993). The effect of tide range on beach morphodynamics and morphology: a conceptual beach model. *Journal of Coastal Research,* 9; 785-800.

McArdle S B & McLachlan A (1991). Dynamics of the swash zone and effluent line on sandy beaches. *Marine Ecology Progress Series*, 76; 91-99.

McFarland S, Whitcombe L J & Collins M B (1996). Recent shingle beach renourishment schemes in the UK: some preliminary observations. *Ocean and Coastal Management*, 25; 143-149.

McKay P J & Terich T A (1992). Gravel barrier morphology: Olympic National Park, Washington State, USA. *Journal of Coastal Research,* 8; 813-829.

McLachlan A (1982). A model for the estimation of water filtration and nutrient regeneration by exposed sandy beaches. *Marine Environmental Research*, 6; 37-47.

McLachlan A (1989). Water filtration by dissipative beaches. *Limnology and Oceanography*, 34; 774-780.

McLachlan A, Eliot I A & Clarke D J (1985). Water filtration through reflective microtidal beaches and shallow sublittoral sands and its implications for an inshore ecosystem in Western Australia. *Estuarine, Coastal and Shelf Science*, 21; 91-104.

McLean R F (1967). Plan shape and oreintation of beaches along the east coast, South Island. *New Zealand Geographer*, 23; 16-22.

McLean R F (1970). Variations in grain-size and sorting on two Kaikoura beaches. *New Zealand Journal of Marine and Freshwater Research,* 4; 141-164.

McLean R F & Kirk R M (1969). Relationships between grain-size, size-sorting and foreshore slope on mixed sand-shingle beaches. *New Zealand Journal of Geology and Geophysics*, 12; 138-155.

McLean S R (1992). On the calculation of suspended load for noncohesive sediments. *Journal of Geophysical Research*, 97 (C4); 5759-5770.

Miles J R, Russell P E & Huntley D A (1996). Sediment transport and wave reflection near a seawall. *Proceedings of the 25th International Conference on Coastal Engineering*, American Society of Civil Engineers; (in press).

Miller K A (1997). Sediment dynamics on Wemyss Beach, South Fife. Unpubl. MPhil thesis, Department of Geology, University of St Andrews.

Motorola (1994). Semiconductor Technical Data. Rev 1/94; 3-48.

Motyka J M & Brampton A H (1993). Coastal management: mapping of littoral cells. Hydraulics Research Report SR 328, Wallingford.

Nagata Y (1964). The statistical properties of orbital wave motions and their application for the measurement of directional wave spectra. *Journal of the Oceanographical Society of Japan*, 19; 1-13.

Nairn R B (1990). Prediction of cross-shore sediment transport and profile evolution. Unpubl. PhD thesis, Imperial College, University of London.

Nairn R B & Southgate H N (1993). Deterministic profile modelling of nearshore processes. Part 2. *Coastal Engineering,* 19; 57-96.

Nelson R C & Gonsalves J (1990). A field study of wave reflections from an exposed dissipative beach. *Coastal Engineering*, 14; 457-477.

Nelson C L & Miller R L (1974). The interaction of fluid and sediment on the foreshore. University of Chicago, Department of Geophysical Sciences, Fluid Dynamics and Sediment Transport Laboratory, Technical Report 15.

Nicholls R J (1985). The stability of the shingle beaches in the eastern half of Christchurch Bay. Unpublished PhD thesis, Department of Civil Engineering, University of Southampton.

Nielsen N (1991). A boulder beach formed by waves from a calving glacier; Eqip Sermia, West Greenland. *Boreas*, 21; 159-168.

Nielsen P (1988*a*). Wave setup: a field study. *Journal of Geophysical Research*, 93 (C12); 15643-15652.

Nielsen P (1989). Wave setup and runup: an integrated approach. *Coastal Engineering*, 13; 1-9.

Nielsen P (1990*a*). Tidal dynamics of the water table in beaches. *Water Resources Research*, 26; 2127-2134.

Nielsen P (1990*b*). Runup, setup and the coastal watertable. *Proceedings of the 22nd International Conference on Coastal Engineering,* American Society of Civil Engineers; 867-881.

Nielsen P (1991*a*). Wave runup distributions on natural beaches. *Journal of Coastal Research*, 7; 1139-1152.

Nielsen P (1992). Coastal Bottom Boundary Layers and Sediment Transport. World Scientific.

Nielsen P & Kang H-Y (1995). Groundwater dynamics in beaches and coastal barriers. *Coastal Dynamics '95*, American Society of Civil Engineers; 521-532.

Nielsen P, Davis G A, Winterbourne J M & Elias G (1988). Wave setup and the water table in sandy beaches. Public Works Department of New South Wales, Coastal Branch, Techincal Momorandum TM 88/1.

Nordstrom K F & Jackson N L (1993). Distribution of surface pebbles with changes in wave energy on a sandy estuarine beach. *Journal of Sedimentary Petrology*, 63; 1152-1159.

O'Connor B A (1996). CSTAB Handbook and Final Report (Editor). Department of Civil Engineering, University of Liverpool.

Ogden M R & Weisman R N (1991). Beach stabilization using drains - an experimental model study. *Coastal Sediments '91*, American Society of Civil Engineers; 1955-1969.

Oh T-M & Dean R L (1994). Effects of controlled water table on beach profile dynamics. *Proceedings of the 24th International Conference on Coastal Engineering*, American Society of Civil Engineers; 2449-2460.

Orford J D (1975). Discrimination of particle size zonation on a pebble beach. *Sedimentology*, 22; 441-463.

Orford J D & Carter R W G (1982). Crestal overtop and washover sedimentation on a fringing, sandy gravel barrier coast, Carnsore Point, Southeast Ireland. *Journal of Sedimentary Petrology*, 52; 265-278.

Orford J D & Carter R W G (1985). Storm-generated dune armouring on a sand-gravel barrier system, southeastern Ireland. *Sedimentary Geology*, 42; 65-82.

Orford J D, Carter R W G & Forbes D L (1991*a*). Gravel barrier migration and sea level rise: some observations from Story Head, Nova Scotia, Canada. *Journal of Coastal Research*, 7; 477-488.

Orford J D, Carter R W g & Jennings S C (1991*b*). Coarse clastic barrier environments: evolution and implications for Quaternary sea-level interpretation. *Quaternary International*, 9; 87-104.

Orford J D, Carter R W G, McKenna J & Jennings S C (1995). The relationship between the rate of mesoscale sea-level rise and the rate of retreat of swash-aligned gravel-dominated barriers. *Marine Geology*, 124; 177-186.

Packwood A R (1983). The influence of beach porosity on wave uprush and backwash. *Coastal Engineering*, 7; 29-40.

Parks J M (1989). Beachface dewatering: a new approach to beach stabilization. *Compass of Sigma Gamma Epsilon*, 66; 65-72.

Parlange J-Y & Brutsaert W (1987). A capillary correction for free surface flow of groundwater. *Water Resources Research*, 23; 805-808.

Postmar G M (1989). Wave reflection from rock slopes under random wave attack. Unpubl. Msc thesis, Delft University of Technology (quoted in Bird *et al.* 1996).

Pawka S S (1982). Island shadows in wave directional spectra. Journal of Geophysical Research, 84 (C4); 2579-2591.

Pontee N I (1995). The morphodynamics and sedimentary architecture of mixed sand and gravel beaches, Suffolk, UK. Unpubl. PhD thesis, Department of Sedimentology, University of Reading.

Powell K A (1986). The hydraulic behaviour of shingle beaches under regular waves of normal incidence. Unpublished PhD thesis, Department of Civil Engineering, University of Southampton.

Powell K A (1988). The dynamic response of shingle beaches to random waves. *Proceedings of the 21st International Conference on Coastal Engineering*, American Society of Civil Engineers; 1763-1773.

Powell K A (1990). Predicting short term profile response for shingle beaches. Hydraulics Research, Wallingford, Report SR 219.

Powell K (1996). Study of complex coastal processes for a shoreline management plan. *Proceedings of the Institution of Civil Engineers; Municipal Engineer* , 115; 28-36.

Powell K A, Quinn P A & Greated C A (1992). Shingle beach profiles and wave kinematics. *Proceedings of the 23rd International Conference on Coastal Engineering*, American Society of Civil Engineers; 2358-2369.

Quick M C (1991). Onshore-offshore sediment transport on beaches. *Coastal Engineering*, 15; 313-332.

Quick M C & Dyksterhuis P (1994). Cross-shore transport for beaches of mixed sand and gravel. *International Symposium: Waves - physical and numerical modelling*. Canadian Society of Civil Engineers; 1443-1452.

Raubenheimer B & Guza R T (1996*a*). Observations and predictions of run-up. *Journal of Geophysical Research,* 101 (C10); 25575-25587.

Raubenheimer B & Guza R T (1996*b*). Wave transformation across the inner surf zone. *Journal of Geophysical Research,* 101 (C10); 25589-25597.

Raubenheimer B, Guza R T, Elgar S & Kobayashi N (1995). Swash on a gently sloping beach. *Journal of Geophysical Research,* 100 (C5); 8751-8760.

Remson I, Hornberger G M & Molz F J (1971). Numerical Methods in subsurface Hydrology. Wiley-Interscience, New York.

Roelvink J A & Stive M J F (1989). Bar-generating cross-shore flow mechanisms on a beach. *Journal of Geophysical Research*, 94 (C4); 4785-4800.

Russell P, Davidson M, Huntley D, Cramp A, Hardisty J & Lloyd G (1991). The British Beach and Nearshore Dynamics (B-BAND) programme. *Proceedings of Coastal Sediments '91*, American Society of Civil Engineers; 371-384.

Sakakiyama T & Kajima R (1992). Numerical simulation of nonlinear wave interaction with permeable breakwaters. *Proceedings of the 23rd International Conference on Coastal Engineering*, American Society of Civil Engineers; 1517-1530.

Sato M, Hata S & Fukushima M (1994). An experimental study on beach transformation due to waves under operation of coastal drain system. *Proceedings of the 24th International Conference on Coastal Engineering*, American Society of Civil Engineers; 2571-2582.

Schoonees J S & Theron A K (1993). Review of the field-data base for longshore sediment transport. *Coastal Engineering*, 19; 1-25.

Scott K A, Thornton E B & Birkemeier W (1991). Mean currents and sediment transport at DELILAH. *Proceedings of Coastal Sediments '91*, American Society of Civil Engineers; 477-488.

Seelig W N (1983). Wave reflection from coastal structures. *Proceedings of the International Conference on Coastal Structures*, American Society of Civil Engineers;

Shaw E M (1988). Hydrology in Practice Chapman & Hall.

Southgate H N & Nairn R B (1993). Deterministic profile modelling of nearshore processes. Part 1. *Coastal Engineering,* 19; 27-56

Strahler A N (1966). Tidal cycle of changes in an equilibrium beach, Sandy Hook, New Jersey. *Journal of Geology*, 74; 247-268.

Svendsen Ib A (1984). Wave attenuation and set-up on a beach. *Proceedings of the 19th International Conference on Coastal Engineering*, American Society of Civil Engineers; 54-69.

Symonds G, Huntley D A & Bowen A J (1982). Two dimensional surf beat: long wave generation by a time-varying breakpoint. *Journal of Geophysical Research*, 87; 492-498.

Takezawa M, Kubota S & Nakamura N (1990). A field study of swash oscillation on a steep beach face. *4th Pacific Conference on Marine Science and Technology*; 282-289.

Takezawa M, Mizuguchi M, Hotta S & Kubota S (1988). Wave run-up on a natural beach. *Proceedings of the 21st International Conference on Coastal Engineering*, American Society of Civil Engineers; 151-165.

Tappin D R, Chadwick R A, Jackson A A, Wingfield R T R & Smith N J P (1994). UK Offshore Regional Report: The geology of Cardigan Bay and the Bristol Channel HMSO (for British Geological Survey).

Tatavarti R V S N (1989). The reflection of waves on natural beaches. Unpublished PhD thesis, Dalhousie University, Halifax, Nova Scotia.

Tatavarti R V S N, Huntley D A & Bowen A J (1988). Incoming and outgoing wave interactions on beaches. *Proceedings of the 21st International Conference on Coastal Engineering,* American Society of Civil Engineers; 136-150.

Terchunian A V (1990). Performance of the STABEACH@ System at Hutchinson Island, Florida. *Proceedings of the National Conference on Beach Preservation Technology*; 185-201.

Thornton E B, Humiston R T & Birkemeier W (1996). Bar/trough generation on a natural beach. *Journal of Geophysical Research,* 101 (C5); 12097-12110.

Timco G W, Mansard E P D & Ploeg J (1984). Stability of breakwaters with variation in core permeability. *Proceedings of the 19th International Conference on Coastal Engineering,* American Society of Civil Engineers; 2487-2499.

Turner I L (1993*a*). The total water content of sandy beaches. *Journal of Coastal Research*, Special Issue 15; 11-26.

Turner I L (1993*b*). Water table outcropping on macro-tidal beaches: a simulation model. *Marine Geology*, 115; 227-238.

Turner I L (1993*c*). Beachface permeability, the groundwater effluent zone and intertidal profiles of macro-tidal beaches - a conceptual model. University of Sydney, Departmental monograph.

Turner I L (1995*a*). Simulating the influence of groundwater seepage on sediment transport by the sweep of the swash zone across macro-tidal beaches. *Marine Geology*, 125; 153-174.

Turner I L (1995*b*). Modelling the time-varying extent of groundwater seepage on tidal beaches. *Earth Surface Processes and Landforms*, 20, Technical & Software Bulletin, 4; 833-843.

Turner I L & Leatherman S P (1997). Beach dewatering as a "soft" engineering solution to coastal erosion - a history and critical review. *Journal of Coastal Research*, 13; 1050-1063.

Turner I L & Nielsen P (1997). Rapid watertable fluctuations within the beachface: implications for swash zone sediment mobility? *Coastal Engineering* (submitted).

Turner I L, Coates B P & Acworth R I (1997). Tides, waves and the super-elevation of groundwater at the coast. *Journal of Coastal Research*, 13; 46-60.

van Gent M R A (1994). The modelling of wave action on and in coastal structures. *Coastal Engineering,* 22; 311-339.

Van Wellen E, Chadwick A J, Bird P A D, Bray M, Lee M & Morfett J C (1997). Coastal sediment transport on shingle beaches. *Proceedings of Coastal Dynamics'97*, American Society of Civil Engineers (in press).

Vanek V (1991). Comment on "Tidal dynamics of the water table in beaches" by P Nielsen. *Water Resources Research*, 27; 2799-2801.

Voulgaris G (1992). Suspended sediment transport in the littoral zone. Unpubl. PhD thesis, Department of Oceanography, University of Southampton.

Voulgaris G (1996). Bailard modelling. *In*: BA O'Connor (Editor), Circulation and Sediment Transport Around Banks (CSTAB) Handbook, Department of Civil Engineering, University of Liverpool; 192-201.

Voulgaris G & Collins M B (1994). Storm damage - south coast shingle study. Department of Oceanography, University of Southampton, Technical Report TEC/94a/6/C.

Voulgaris G & Collins M B (1996). Suspended sediment fluxes. *In*: BA O'Connor (Editor), Circulation and Sediment Transport Around Banks (CSTAB) Handbook, Department of Civil Engineering, University of Liverpool; 495-547.

Voulgaris G, Wilkin M P & Collins M B (1995). The *in situ* passive acoustic measurement of shingle under waves and currents: instrument (TOSCA) development and preliminary results. *Continental Shelf Research*, 15; 1195-

1211.

Voulgaris G, Simmonds D, Michel D, Howa H, Collins M B & Huntley D A (1997). Measurements of sediment transport on a macrotidal ridge and runnel beach. *Journal of Coastal Research* (in press).

Waddell E (1976). Swash-groundwater-beach profile interactions. Beach and Nearshore Sedimentation eds R A Davis & R L Hetherington, Society of Economic and Palaeontological Mineralogists, Special Publication 24; 115-125.

Waddell E (1980). Wave forcing of beach groundwater. *Proceedings of the 17th International Conference on Coastal Engineering*, American Society of Civil Engineers; 1436-1452.

Walker J R, Everts C H, Schmelig S & Demirel V (1991). Observations of a tidal inlet on a shingle beach. *Proceedings of Coastal Sediments '91*, American Society of Civil Engineers; 975-989.

Walton T L (1992*a*). Wave reflection from natural beaches. *Ocean Engineering*, 19; 239-258.

Walton T L (1992*b*). Interim guidance for prediction of wave run-up on beaches. *Ocean Engineering*, 19; 199-207.

Walton T L (1993). Ocean City, Maryland, wave runup study. *Journal of Coastal Research*, 9; 1-10.

Ward R C & Robinson M (1990). Principles of Hydrology McGraw-Hill, UK.

Weisman R N, Seidel G S & Ogden M R (1995). Effect of water table manipulation on beach profiles. *Journal of Waterway, Port, Coastal and Ocean Engineering*, 121; 134-142.

Whitcombe L J (1995). Sediment transport processes, with particular reference to Hayling Island. Unpubl. PhD thesis, Department of Oceanography, University of Southampton.

Wiberg P & Harris (1994). Ripple geometry in wave-dominated environments. *Journal of Geophysical Research*, 99 (C1); 775-777.

Wilkinson R H (1980). Foreshore sediment movement and its relation to observed tidal currents and wave climate. Swansea Bay (Sker) Project Topic Report: 7, Institute of Oceanographic Sciences Report No 98 (unpubl.).

WMO (1988). Guide to wave analysis and forecasting. World Meteorological Organization No 702, Secretariat of the WMO, Geneva, Switzerland.

Wright L D & Short A D (1984). Morphodynamic variability of surfzones and beaches: a synthesis. *Marine Geology*, 56; 93-118.

Wright L D, Nielsen P, Short A D & Green M O (1982). Morphodynamics of a macrotidal beach. *Marine Geology*, 50; 97-128.

Zenkovich V P (1967). Processes of Coastal Development Oliver & Boyd, Edinburgh.

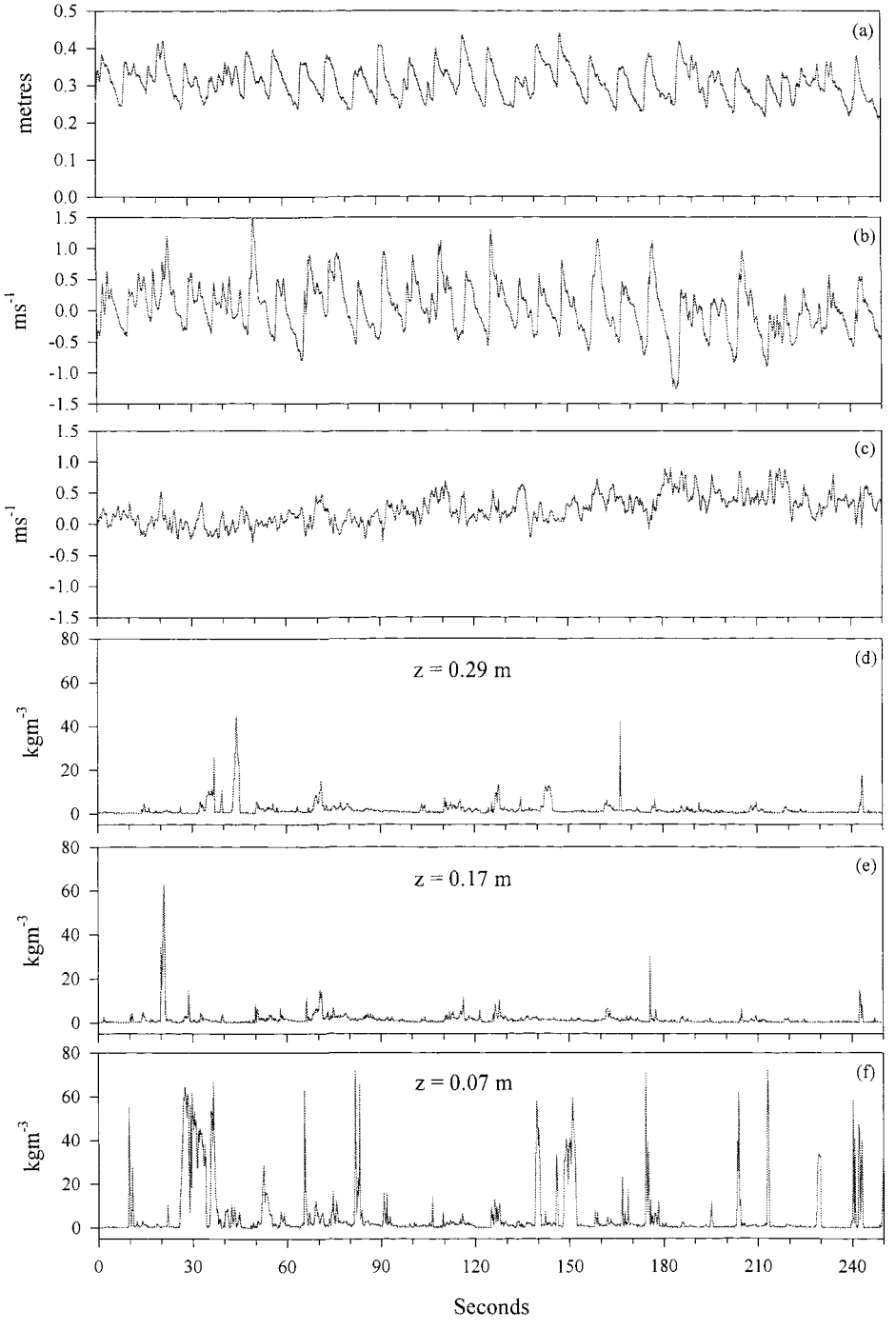

Sample time series from Tide 26, Low Water (ebb tide) of : (a) sea surface elevation; (b) and (c) cross-shore and longshore velocity respectively, at 0.12 m from the seabed; (d) (e) and (f) suspended sediment concentration at 0.29 m, 0.17 m and 0.07 m from the seabed respectively.